

**Towards electrically conductive and interleaf-
toughened carbon black-epoxy-carbon fiber
laminates with enhanced lightning strike resistance**

von der Fakultät für Ingenieurwissenschaften
der Universität Bayreuth
genehmigte Dissertation
zur Erlangung des Grades

Doktor-Ingenieur

vorgelegt von:

Gökhan Bakis, M.Sc.(hons)

Fachgutachter:

Professor Dr.-Ing. Volker Altstädt

Professor Dipl.-Ing. Dr.mont. Reinhold W. Lang

Für die Nutzung dieser Dissertation gelten folgende rechtliche Bestimmungen

- Die vorliegende Dissertation darf von der Universität Bayreuth frei im Internet angeboten werden. Eine weitere Verbreitung oder öffentliche Wiedergabe ist nicht gestattet und kann nur mit ausdrücklicher Genehmigung des Autors (Promovierten) geschehen.
- Die Vervielfältigung ist nur im Rahmen des privaten und eigenen wissenschaftlichen Gebrauchs (§ 53 UrhG) erlaubt.
- Die Publikation darf nicht bearbeitet oder in anderer Weise verändert werden.
- Der Autor hat das Recht, sein Werk, auch auszugsweise, anderweitig verfügbar zu machen und zu verbreiten.
- Für den Inhalt des Dokuments ist allein der Autor verantwortlich.
- Die Dissertation wird vertrieben durch TuTech Innovation GmbH

This publication (dissertation) is subject to the following terms of use:

- The University of Bayreuth is entitled to give open access to this publication. Further publication or public broadcasting needs explicit authorization of the copyright owner (doctor).
- Copying is permitted only for private or the own scientific purposes of the person who performs copying (according to § 53 of the German Copyright Act). The copyright owner grants production of complete single copies of this publication by means of a print on demand service.
- This publication may not be edited or changed otherwise.
- The copyright owner has got the right to publish or broadcast this publication as a whole or parts thereof elsewhere.
- The author is exclusively responsible for the content of this publication.
- The dissertation is sold by TuTech Innovation GmbH

Acknowledgements

I would first like to express my deepest appreciation to Prof. Dr.-Ing. Volker Altstädt for giving me the chance to complete my doctoral thesis in the Department of Polymer Engineering at the University of Bayreuth.

I believe that the environment in which one works has an impact on the quality of the scientific research that is produced. Therefore, I'd like to thank my colleagues Dr.-Ing. Martin Kothmann, Dipl.-Ing. Rico Zeiler, Dr.-Ing. Thomas Neumeyer, Dr.-Ing. Edin Njuhovic, Christin Pawelski-Höll, Simon Bard, Martin Demleitner, Markus Häublein, Fabian Hübner, Tobias Standau, Merve and Alper Aksit for fruitful discussions in the field of polymers and providing a creative and enjoyable workplace atmosphere. It was also a pleasure to work together with Dipl.-Ing. Ute Kuhn, Mrs. Anneliese Lang, Dipl.-Ing. Alexander Brückner, Dipl.-Ing. Andreas Mainz, Annika Pfaffenberger, M.Sc. Jacqueline Uhm, and Marko Weniger during material characterization studies. Finally, for his friendship and impressive work regarding the prepreg production trials, I thank Mr. Christian Bauer, from whom I learned a great deal about working with passion.

Special thanks to all of my students; Markus Häublein, Alper Aksit, Corinna Fischer, Felix Wendel, Zilin Wang, Andreas Frank, Christian Hils, Holger Deutges, Kunguang Zhou, Paulo Takobaro, Theresa Menzel, and Yana Wang. This work would not exist without the valuable contributions especially from Markus Häublein, Alper Aksit, and Corinna Fischer.

I would also like to thank Prof. Dr. Jingshen Wu for XPS measurements at Hong Kong University of Science and Technology and to Dipl.-Ing. Frank Nothnagel from TU Ilmenau for lightning strike experiments. In addition, I thank specially to Dr.-Ing. Hauke Lengsfeld from HEXCEL for his valuable supervision regarding the prepreg production and mechanics. Finally, I thank very much to Prof. Dr. mont. Raynold W. Lang for the scientific evaluation of this work as the second supervisor.

On a more personal note, I would like to acknowledge my family, Isa, Gülnihal, and Engin Bakis, and finally my wife, Müge, for their understanding and endless support during my doctoral studies.

Kurzfassung

Epoxid-Kohlenstofffaser-Prepregs finden in der zivilen Luft- und Raumfahrtindustrie aufgrund ihrer hervorragenden mechanischen, thermo-mechanischen und thermischen Eigenschaften zunehmend Anwendung zur Herstellung von Strukturverbundbauteilen. Obwohl Kohlenstofffasern elektrisch leitfähig sind, weisen aus Epoxid-Kohlenstofffaser-Prepreg hergestellte Bauteile aufgrund der isolierenden Natur der Epoxidmatrix oft nur sehr geringe elektrische Leitfähigkeiten in z-Richtung auf. Die verbesserte elektrische Leitfähigkeit in z-Richtung ist jedoch für moderne Verbundanwendungen notwendig, bei denen ein gewisses Maß an elektrostatischer Ableitung, elektromagnetischer Abschirmung oder eine verbesserte Widerstandsfähigkeit gegen Blitzeinschläge erforderlich ist.

Die vorliegende Arbeit beschäftigt sich hauptsächlich mit der Untersuchung des Einflusses leitfähiger Rußnanopartikel auf die elektrische Leitfähigkeit und die Bruchzähigkeit eines für die Luft- und Raumfahrt relevanten Epoxidharzes und seiner unidirektionalen Kohlenstofffaser Prepreg-Lamine. Die Beziehung zwischen dem Faservolumengehalt und der elektrischen Leitfähigkeit der reinen Lamine wurde umfassend charakterisiert. Darüber hinaus wurde der Einfluss eines PA6.6-Vlieses auf die elektrischen und mechanischen Eigenschaften der Lamine detailliert erforscht. Schließlich wurde die Korrelation zwischen der elektrischen Leitfähigkeit (in z-Richtung) und der Beständigkeit gegen Blitzschlag von mit PA6.6-Vlies modifizierten Laminen untersucht.

Obwohl Kohlenstoffnanoröhren und Graphen eine höhere elektrische Leitfähigkeit als einzelne Nanopartikel versprechen, zeigten laut ausführlicher Literaturrecherche Rußnanopartikel auch ein großes Potenzial, um leitfähige Verbundwerkstoffe bei einem niedrigen Nanopartikelgehalt zu erzielen. Die Zugabe von bis zu 2 Gew.-% Ruß im Epoxidharzsystem führte zu einem Übergang von einem isolierenden ($\approx 7 \cdot 10^{-12}$ S/m) hin zu einem ausreichend elektrisch leitfähig Verhalten (10^{-4} S/m).

Bei den Laminen ohne das PA6.6-Vlies und die Rußnanopartikel wurde die elektrische Leitfähigkeit hauptsächlich durch die Kohlenstofffaserkontakte realisiert ($\approx 10^{-1}$ S/m bei 54 vol.% Faservolumengehalt). Erstmals wurde eine exponentielle Beziehung zwischen dem Faservolumengehalt und der elektrischen Leitfähigkeit von Laminen (in z-Richtung) aufgezeigt.

Obwohl das PA6.6 Vlies als Interleaf die Bruchzähigkeit fast verdoppelte, reduzierte es die elektrische Leitfähigkeit in z-Richtung deutlich (von $\approx 10^{-1}$ S/m bis 10^{-4} S/m). Rußnanopartikel erhöhten die elektrische Leitfähigkeit der mit PA6.6-Vlies modifizierten Lamine erheblich (von 10^{-4} S/m auf 1 S/m bei 2 Gew.-% Nanopartikelgehalt in der Matrix), indem sie als leitende Brücke in den harzreichen interlaminaeren Bereichen wirken. Neben der erhöhten Leitfähigkeit beeinträchtigen Rußnanopartikel weder die Verarbeitbarkeit der Prepregs noch die thermo- mechanischen und mechanischen Eigenschaften der konsolidierten Prepreg Lamine.

Eine durch erhöhte z-Richtung elektrische Leitfähigkeit von Laminen reduziert die Schädigung nach 20 kA Blitzschlag deutlich. Folglich zeigen Lamine, die aus PA6.6 Vlies zusammen mit Rußnanopartikeln (2 Gew.-%) bestehen, eine ausgezeichnete Kombination der interlaminaeren Bruchzähigkeit und der elektrischen Leitfähigkeit. Daher eröffnen die rußnanopartikelmodifizierten Epoxid-Kohlenstofffaser Prepregs neue Anwendungen für Kompositbauteile, bei denen Widerstandserwärmung, elektrostatische Ableitung, elektromagnetische Abschirmung oder ein verstärkter Blitzschlagwiderstand erwartet werden.

Abstract

Epoxy-carbon fiber prepregs have been used increasingly by civil aerospace industry to manufacture the structural composite parts due to their excellent mechanical, thermo-mechanical and thermal properties at the cured state. Although carbon fibers are electrically conductive, due to the insulating nature of the epoxy matrix, epoxy-carbon fiber prepreg laminates mostly act as a semi-conductor in the through-thickness direction. Nowadays, an enhanced through-thickness electrical conductivity is as well desired for modern composite applications, where a certain level of electro-static dissipation, electromagnetic shielding or an enhanced lightning strike resistance is necessary.

The scientific scope of this work based mainly on the understanding of the effect of the conductive carbon black nanoparticles on the electrical conductivity and the fracture toughness of an aerospace relevant epoxy resin and its unidirectional carbon fiber prepreg laminates. The relationship between the carbon fiber volume content and the through-thickness electrical conductivity of the neat laminates received a particular attention. Furthermore, the influence of a PA6.6 interleaf fleece on the electrical and mechanical properties of the laminates was studied in a detail. Finally, the correlation between the through-thickness electrical conductivity and the lightning strike resistance of PA 6.6 interleaf fleece modified laminates was investigated.

According to the extensive literature survey, although carbon nanotubes and graphene promise a high electrical conductivity as single nanoparticles, carbon black nanoparticles showed as well a great potential to realize conductive composites at a low nanoparticle content. The addition up to 2 wt.% carbon black in epoxy enhanced the conductivity of the epoxy system already from approximately $7 \cdot 10^{-12}$ S/m to 10^{-4} S/m.

In the prepreg laminates without the PA6.6 interleaf fleece, the through-thickness electrical conduction was realized mainly by the carbon fiber contacts ($\approx 10^{-1}$ S/m at 54 vol.% carbon fiber content). An exponential relationship in between the carbon fiber volume content and the through-thickness electrical conductivity of laminates was shown for the first time.

Although the incorporation of the interleaf fleece in laminates almost doubled their fracture toughness, it deteriorated the electrical conductivity in z-direction strongly (from 10^{-1} S/m to 10^{-4} S/m). Carbon black nanoparticles however enhanced the electrical conductivity of the interleaf fleece modified laminate tremendously (from 10^{-4} S/m to 1 S/m at 2 wt.% additive content) by acting as a conductive bridge in the resin rich interlaminar regions. In addition to the enhanced conductivity, carbon black nanoparticles neither deteriorate the processability of the prepregs nor the thermo - mechanical and mechanical properties of the consolidated prepreg laminates.

Increased through thickness electrical conductivity of laminates reduced the damage after 20 kA strike distinguishably. Consequently, laminates consisting of PA6.6 interleaf fleece together with carbon black nanoparticles (2 wt.%) show an excellent combination of the interlaminar fracture toughness and electrical conductivity. Therefore, carbon black nanoparticle modified epoxy-carbon fiber prepregs open up new composite applications where resistive heating, electro-static dissipation, electro-magnetic shielding or an enhanced lightning strike resistance is desired.

Table of contents

Kurzfassung	I
Abstract	IV
Graphical abstract	VI
Acknowledgements	VII
Table of contents	VIII
Abbreviations	XI
Symbols	XII
1. Introduction	1
2. State of the art	4
2.1. Desired functionality for composites: “Electrical conductivity”	4
2.2. Composites incorporated with conductive particles	7
2.2.1. Carbon-based conductive particles.....	8
2.2.1.1. Effect of nanoparticles on electrical conductivity of epoxy resins and FRPCs.....	11
2.2.2. Dynamics of conductive network formation.....	17
2.2.3. Parameters affecting the conductivity of nanoparticle-epoxy composites....	20
2.2.3.1. Effect of particle type, alignment and aspect ratio	20
2.2.3.2. Effect of processing conditions	22
2.2.3.3. Effect of ion concentration of the resin system.....	26
2.2.3.4. Effect of external electromagnetic field	29
2.2.3.5. Effect of the inclusion of a second phase.....	31
2.3. Conductivity of carbon nanoparticle modified CF laminates	35
2.4. FRPCs modified with conductive layers	37
2.5. Behavior of composites under lightning strike	39
2.6. Summary of the state of the art	46
3. Aims of the work	49
4. Materials and methods	51
4.1. Materials	51
4.2. Processing	53
4.2.1. Manufacturing of neat resin plates and nanocomposites	53
4.2.2. Prepreg processing	55

4.2.3. Hand lay-up and laminate curing	57
4.3. Experimental methods	60
4.3.1. Viscosity measurements of uncured resins.....	60
4.3.2. Dynamical mechanical thermal analysis	60
4.3.3. Non-destructive ultrasound testing of cured laminates.....	60
4.3.4. Fracture toughness testing	61
4.3.5. Scanning and transmission electron microscopy	62
4.3.6. Electrical conductivity measurements	62
4.3.7. Image analysis	63
4.3.8. Simulated lightning strike testing	64
5. Results and discussions	68
5.1. Resin studies	68
5.1.1. Neat resin	68
5.1.2. Carbon black-epoxy nanocomposites	71
5.1.2.1. Dispersion of carbon black via various processing methods	71
5.1.2.2. Effect of carbon black content on viscosity of epoxy resin.....	74
5.1.2.3. Effect of carbon black on T_g of epoxy resin	76
5.1.2.4. Effect of carbon black on electrical conductivity of epoxy resin	78
5.1.2.5. Effect of carbon black on mechanical properties of epoxy resin	81
5.1.3. Summary.....	83
5.2. Electrical and mechanical properties of laminates	84
5.2.1. Prepreg properties	84
5.2.2. Electrical properties of prepreg laminates.....	85
5.2.2.1. Effect of only FVC on electrical conductivity of neat laminates.....	85
5.2.2.2. Effect of CB on electrical conductivity of laminates	89
5.2.2.3. Effect of only interleaf fleece on the conductivity of laminates.....	96
5.2.2.4. Effect of CB on conductivity of interleaf fleece modified laminates.....	101
5.2.3. Mechanical properties of laminates.....	103
5.2.3.1. Mode-I loading.....	104
5.2.3.2. Mode-II loading.....	111
5.2.4. Summary.....	118
5.3. Lightning strike resistance of prepreg laminates	121
6. Conclusions.....	125
7. Outlook and future work.....	129

7.1. Carbon black with various organic tougheners	129
7.2. Metal coated carbon fibers	133
8. References.....	136
9. Supporting information.....	150
10. Publications.....	155
11. Curriculum Vitae.....	159

Abbreviations

FRPC:	fiber-reinforced polymer composites
CB:	carbon black
CNTs:	carbon nanotubes
SWCNTs:	single-walled carbon nanotubes
DWCNTs:	di-walled carbon nanotubes
MWCNTs:	multi-walled carbon nanotubes
GNPs:	graphene
FVC:	fiber volume content
EMI:	electro-magnetic interference
AIF:	aluminum flakes
AgNP:	silver nanoparticles
AgNW:	silver nanowires
NiNS:	nickel nanostrands
CuNP:	copper nanoparticles
DMTA:	dynamical mechanical thermal analysis
SEM:	scanning electron microscopy
TEM:	transmission electron microscopy
Micro-CT:	micro-computer tomography
C-Scan:	ultrasound laminate scans
TGMDA:	tetraglycidyl methylene dianiline
DGEBA:	diglycidylether of bisphenol A
4,4'-DDS:	4,4'-diamino diphenyl sulfone
PA6.6:	polyamide 6.6
CF:	carbon fibers
THF:	tetrahydrofuran
COD:	crack-opening displacement
PANI:	polyaniline
3RM:	three-roll mill
ILSS:	interlaminar shear strength

Symbols

T_g :	glass transition temperature
$T_{g\text{-dry}}$:	glass transition temperature (no sample conditioning)
$T_{g\text{-wet}}$:	glass transition temperature (conditioned in hot-wet conditions)
T_m :	melting temperature
ϕ_c :	critical content of additive at threshold
ϕ_f :	fiber volume content
K_{Ic} :	critical stress intensity factor under mode-I loading
G_{Ic} :	strain energy release rate under mode-I loading
G_{IIc} :	strain energy release rate under mode-II loading
a :	crack length
ε_b :	strain at break
σ_y :	tensile strength
E_t :	elastic modulus
G_{dc} :	electrical conductance measured with direct current
R_g :	initial resistance of electrodes
E_{dc} :	electrical conductivity measured with direct current
F_{max} :	maximum force required to propagate the crack
E_{SH} :	elastic modulus calculated to Saxena and Hudak
w :	CT sample length from loading point
d :	sample thickness

1 Introduction

The civil aircraft industry increasingly uses fiber reinforced polymer composites (FRPCs) because of their excellent mechanical, chemical and thermo-mechanical properties for manufacturing of lightweight structural parts [1] [2]. More than 50 wt.% of the structural parts of Boeing 787 and Airbus A350 XWB have been produced with fiber-reinforced polymer composites (Figure 1), which is today the still state of the art.

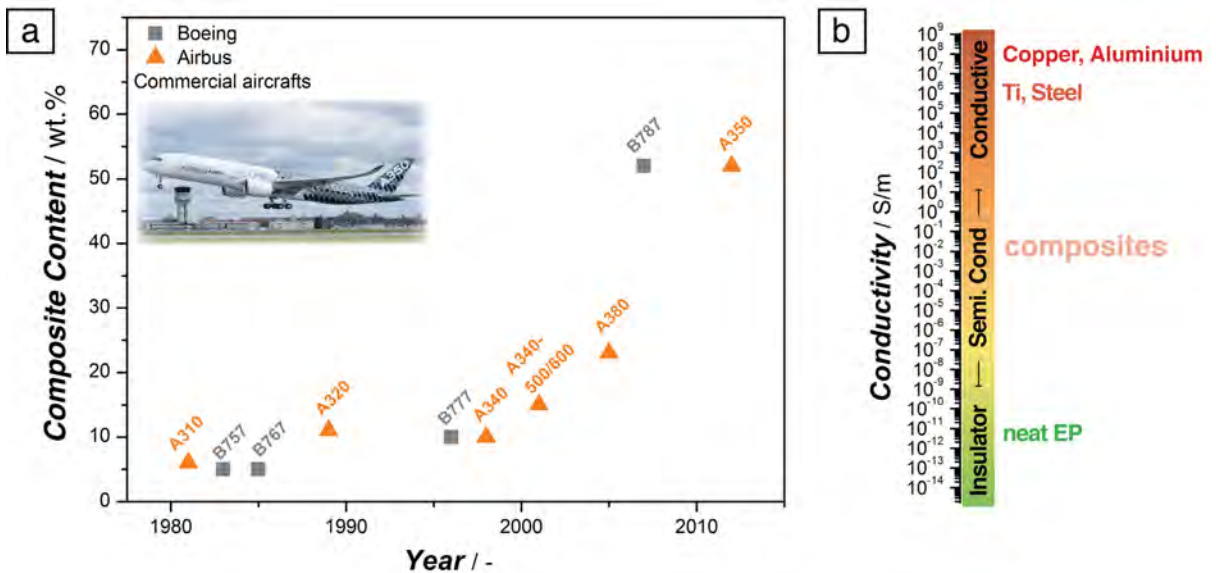


Figure 1. a) Structural composite part content in civil aircrafts, b) The scale of electrical conductivity with various relevant materials for structural aerospace parts [2]–[5].

Peters et al. [1] define the mechanical (e.g., stiffness, strength, damage tolerance) and physical properties (e.g., glass transition temperature, density, corrosion resistance) as key factors for structural aerospace materials. A certain level of electrical conductivity is also highly desired to achieve functionalities such as electrostatic dissipation, magnetic shielding, or lightning strike resistance. Previous studies have reported that fiber reinforced composites behave as semiconductors in the z-direction

(i. e., thickness direction) because the matrix polymer, which is mostly epoxy, is highly insulating [5] (Figure 1.b). Low composite conductivity is critical in the case of the electro-static loads, electromagnetic interference, or in the worst case a lightning strike during a flight.

Manufacturing with preregs (**pre-impregnated** fibers with a desired amount of reactive resin) remains as the main production route for structural parts in the civil aerospace industry [6]. There are presently four types of classified prepreg generations. The first generation preregs consist only of a neat impregnated resin system, whereas second-generation preregs include a dissolved toughener in resin. Third-generation prepreg laminates have an additional resin rich “interleaf” region responsible for enhanced fracture toughness and impact resistance [7]. Figure 2 demonstrates the differences in the laminate morphology from cross-sections [6].

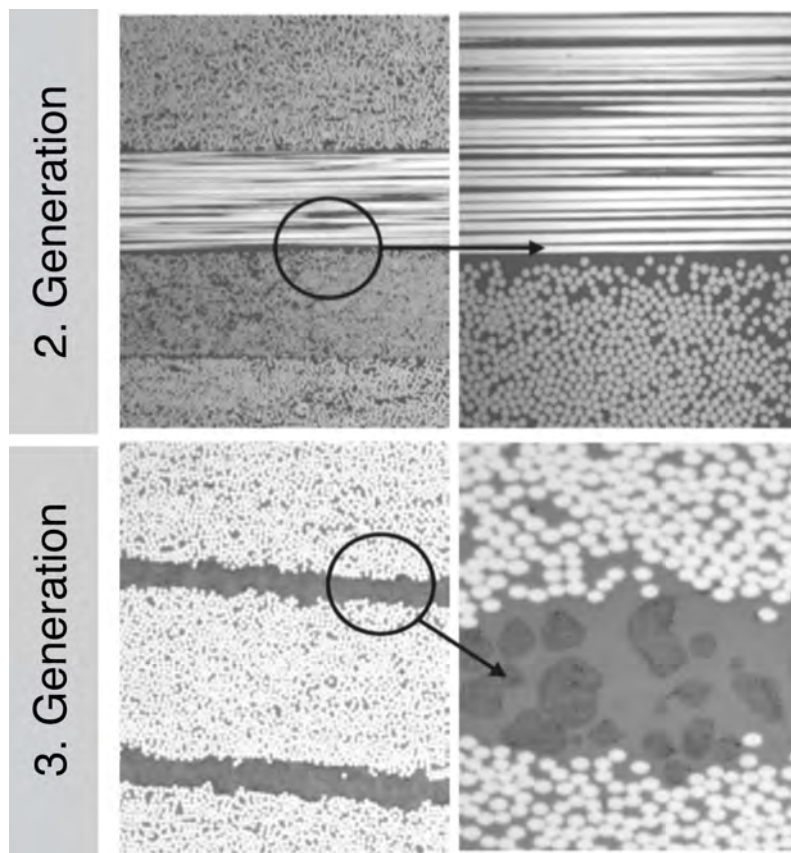


Figure 2. Laminates made of second and third-generation preregs [6].

As described previously, laminates made of second-generation prepregs act as a semiconductor with conductivities in the range of 10^{-2} S/m [5], whereas interleaf toughening lowers the conductivity to 10^{-6} S/m, which is detrimental for the dissipation of electrical energy [8]. Finally, the fourth-generation prepreg laminates theoretically promises both optimized conductivity and high toughness, of which developments are ongoing and driven largely by the industry.

There are two main approaches to electrically conductive polymer matrix fiber-reinforced composites, known as 2D and 3D approaches. The first (2D) is based on incorporating conductive lightweight meshes, fleeces, or coatings on the surface of the laminate before or after the final curing step. On the other hand, the latter strategy (3D) includes modification of the polymer matrix with conducting particulate additives to build a conducting aggregated particle network. Carbon-based conducting additives such as carbon black [9], carbon nanotubes [10] and graphene [11] are mostly used by academia to produce conductive composites.

Conductive network formation of carbon or metal based particles in epoxy resins have been studied extensively. However, the structure-property relationships of conductive nanoparticle modified epoxy-carbon fiber laminates with and without interleaf spacing remain poorly understood. The overall electrical conductivity of fiber reinforced composites is affected by multiple parameters such as fiber volume content, composite laminate quality, through-thickness microstructure (inclusion of interleaf), and the existence of second phases (tougheners), all of which hinders the ease of analysis.

The presented research offers a systematic approach towards understanding the microstructure-property relationships of the carbon black nanoparticle modified epoxy resin and their carbon fiber laminates. The effect of electrical conductivity on the extensive electrical energy dissipation of laminates is investigated and discussed. As an attempt for future outlook, multifunctional bimodal resin formulations and copper coated carbon fibers with a self-developed sizing are presented and discussed in a detail.

2 State of the art

2.1. Desired functionality for composites: “Electrical conductivity”

Epoxies are well known to be highly insulating polymers that can be used for insulation applications [12]. Although carbon fibers theoretically conduct very well parallel (2 to $3 \cdot 10^5$ S/m) and perpendicular (330 S/m) to the graphitic basal plane [13], their epoxy composites behave as semiconductors owing to the insulating nature of the matrix polymer [5]. The semiconducting behavior of composites, as reported by Lonjon et al. [5], limits various modern applications of carbon fiber-reinforced polymer composites. In addition to enhanced lightning strike resistance, high electrical conductivity leads to composite functionalities such as electrostatic dissipation, resistive curability, or electro-magnetic interference shielding (EMI) (Figure 3).

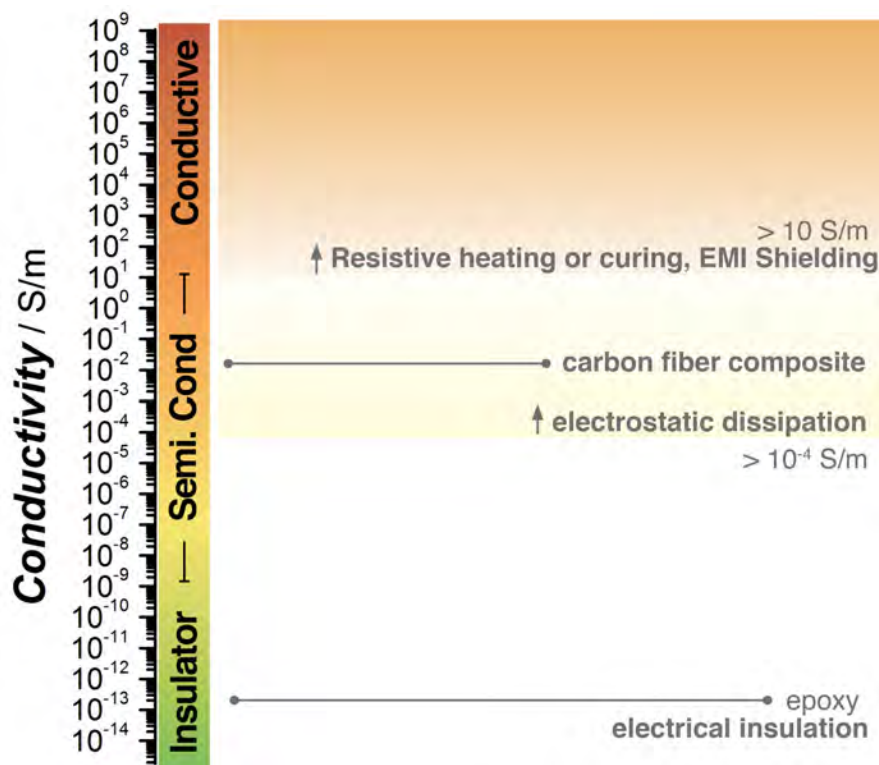


Figure 3. Expected minimum electrical conductivity ranges for new applications of fiber-reinforced composites.

Dissipation of electrostatic loading can be very helpful for applications such as composite pipes for explosive gas transport. For a fiber reinforced composite to dissipate the electrostatic charges, an electrical conductivity above 10^{-4} S/m is required.

Resistive heating can be used for composites having an electrical conductivity in the range of 10 S/m [14], which offers high energy savings during curing process compared with autoclave or hot-press curing [15] [16]. However, the composite part size remains a limiting factor for the utilization of resistive curing processes.

Electromagnetic interference shielding is another possible application of electrically conductive fiber reinforced composites [17]. Electromagnetic interference (EMI) is defined as undesired electrical disturbances or effects by external sources. A US patent issued by King et al. [18] suggests that a Faraday cage (an electrically conductive cage that dissipates electrical energy only at the outer surface) manufactured with compact metal sheets or meshes and metallized polymers can be used as shielding material, which dissipates undesired electrical currents generated from an external electromagnetic field. It is important to point out that compact solid shields generally attenuate broader electromagnetic fields compared to meshes. Conductive composites can also be used as electromagnetic interference shield material by reducing the electromagnetic disturbances in a target space [19]. Park et al. [19] reported that the MWCNT modified polymer nanocomposites with 0.1 S/m conductivity already shows an highly enhanced EMI shielding properties.

Self-damage sensing is an attractive application of electrically conductive fiber reinforced composites. Immediate changes in the electrical resistance of a conductive composite can be successfully correlated to the strain and the damage, allowing the development of self-sensing structural composites [20], [21].

Polymer matrix composites with enhanced resistance to lightning strikes belong to one of the most investigated material classes in the last decade [22], [23]. A lightning strike can carry up to 400 kA peak current with hundreds of MJ energy [24], which severely

threatens the structural integrity of airplanes and can result in burning, resistive heating, electromagnetic interference, sparking at joints, or even vapor ignition in the fuel tanks [22]. The low and anisotropic electrical conductivity of carbon fiber-reinforced epoxy composites lead to a high susceptibility to lightning strikes. To overcome this issue, composite constructions behaving like a Faraday cage are employed as lightning strike protection in modern aircrafts. A schematic illustration of a patented composite structure with a conductive mesh is shown in Figure 4.

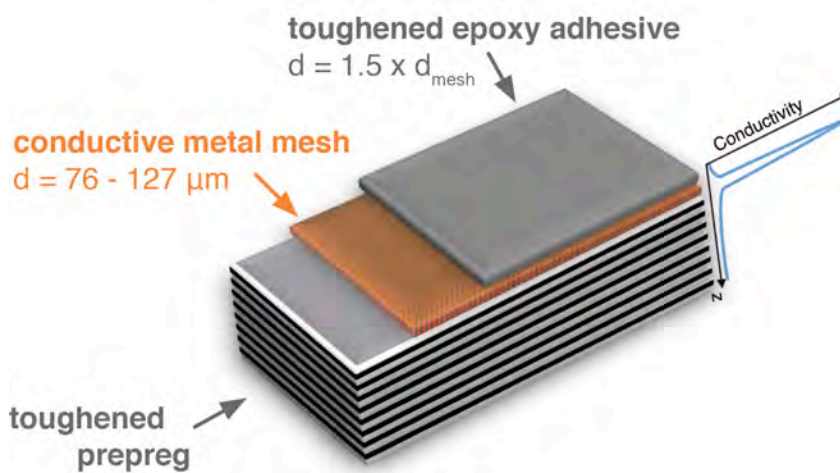


Figure 4. A laminate construction for lightning strike protection according to US005225265A from BASF [25]. Illustrated according to the patent. d is thickness.

A very thin copper mesh provides the electrical conductivity only at the outer surface of the composite structure. Therefore, there is an exceptional potential for electrically conductive composites with isotropic conductivity to replace this structure as a multifunctional composite.

Consequently, carbon fiber reinforced epoxy composites show anisotropic electrical conductivity with semi-conducting behavior in z-direction. Composites with increased conductivity can promise new applications and broaden the range of composite usage in various industries.

2.2. Composites incorporated with conductive particles

Epoxy resins are strong insulators. Contrary to electrically conductive polymers such as polyaniline [26] or polyacetylene [27] with conjugated p-orbitals and mobile electrons, epoxies (before and after curing) contain valence electrons that are bound in sp^3 hybridized covalent bonds, preventing conduction at the molecular level.

The addition of conductive particles in epoxies has been one of the most promising and widely used strategies to produce conducting composites. Mostly carbon-based additives such as carbon black [9], [28]–[32], carbon nanotubes [29], [33]–[35], and graphene [11] have been incorporated in the resin to produce conductive composites.

To achieve a leap on electrical conductivity of an insulating polymer, the conductive particles are expected to form an aggregate network. The quantity of an additive at which the composite undergoes a transition from an insulator to a conductor is called the percolation threshold [36], [37] (Figure 5).

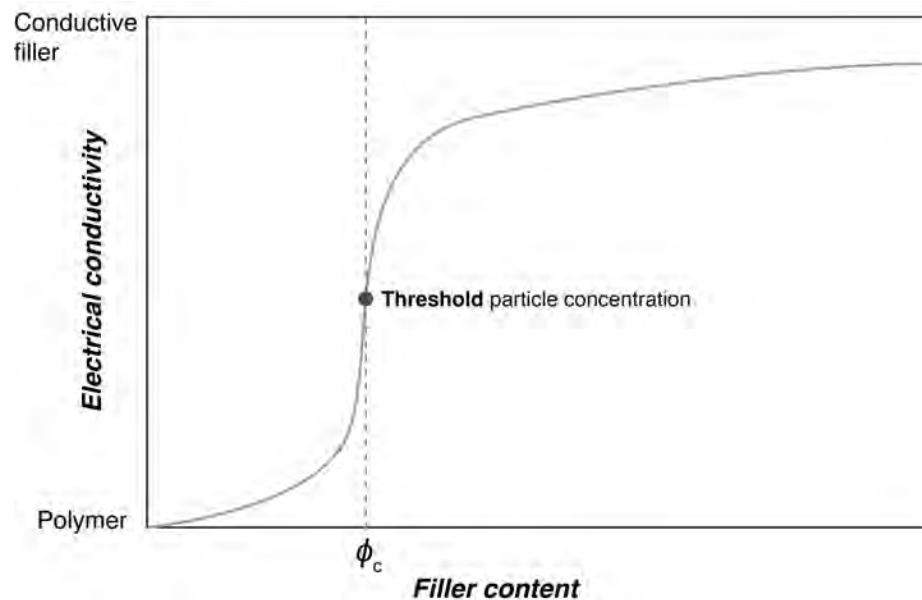


Figure 5. Graphical illustration of threshold in a conductive filler modified polymer. Illustrated according to [36], [37].

Below the critical additive content (ϕ_c), particles do not form a network by interparticle contacts, whereas above the threshold concentration, a continuous conducting network is formed, resulting in an abrupt increase in the mesoscale conductive behavior of the composite. The addition of more filler generally leads to a minor increase of the overall composite conductivity by creating additional conductive pathways.

2.2.1. Carbon-based conductive particles

As mentioned, carbon black (CB), carbon nanotubes (CNTs), graphite, and graphenes (GNPs) are often used in the literature to enhance the electrical conductivity of insulating polymers.

Carbon black, an amorphous carbon particle consisting mainly of sp^2 and sp^3 hybridized bonds, has a moderate but isotropic electrical conductivity in the range of 1.25 to $2 \cdot 10^3$ S/m [3] with a very low density of 1.8 to 2.1 g/cm³. Although single CB particles are quasi-spherical with a very low aspect ratio, their aggregates with a branched structure are expected to be useful for the formation of a conducting network (Figure 6.a).

Carbon nanotubes, having a curved atomic lattice with sp^2 hybridized bonds, received considerable attention after their discovery by Iijima in 1991 [38]. Although an exceptional electrical conductivity levels above 10^5 S/m are reported for single nanotubes [5], the overall conductivity of a CNT depends on its helicity, twisting angle, defect density, and the number of tubes within a single particle [39]. A transmission electron microscope (TEM) image (Figure 6.b) of multi-walled carbon nanotubes (MWCNTs) in epoxy resin provides insight on nanotube morphology in resin, and also reveals imperfections in the particle structure, such as strong bending points or remaining catalysts (darker spots in the micrograph).

Graphene, the youngest allotrope of carbon with a single layer of hexagonal sp^2 hybridized bonds, shows exceptional electrical properties owing to high mobility charge

carriers. Surprisingly, single, double, and additional layered (up to 10) graphenes show different electronic spectra owing to varying valence and conduction bands [40]. In general, few-layer graphenes produced via top-down approaches [41] are incorporated in polymers because of cost-related issues. A representative TEM micrograph of a few-layer graphene modified epoxy nanocomposite in Figure 6.c, highlights the thin 2D structure of this additive.

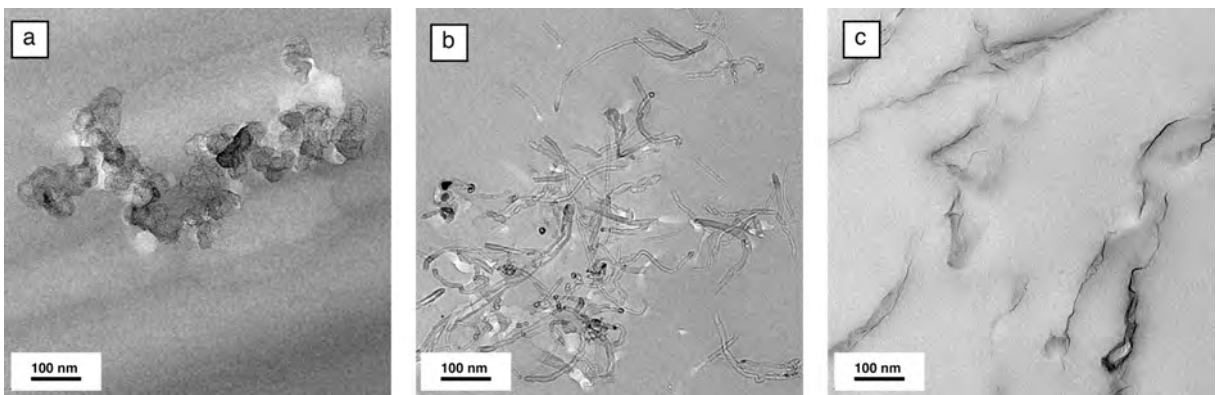


Figure 6. TEM micrographs of a) 1.5 wt.% CB, b) 0.5 wt.% NWCNTs, and c) 0.5 wt.% GNPs nanoplatelets in epoxy resin. Micrographs were taken at the Department of Polymer Engineering, University of Bayreuth.

It is important to mention that the electrical conductivity of a single nanoparticle, as described above, differs strongly from the conductivity of its powder form, which is speculated to be due to contact resistance between particles [42]. Marinho et al. [42] studied the conductivities of powders consisting of graphite, CB, CNT, and GNP. Figure 7 demonstrates that the powder conductivity is much lower regardless of the additive type compared to the conductivity of single nanoparticles, as defined above. Although the electrical response of the powders increases with pressure, the electrical conductivity of GNP, MWCNT, and CB powders are comparable and below 500 S/m at 5 MPa.

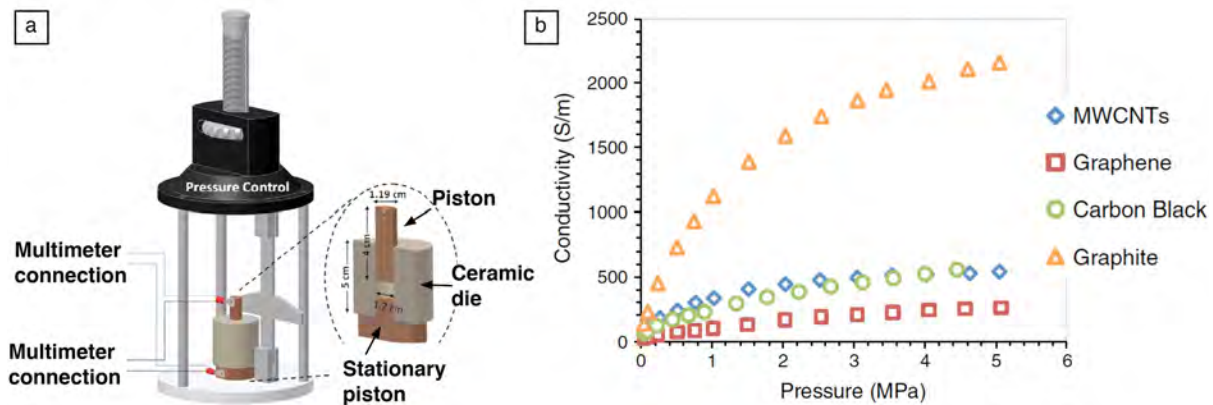


Figure 7. Electrical conductivity measurements of carbon-based powders. a) experimental set-up, b) conductivity of nanoparticle powders as a function of pressure. Reworked [42].

In summary, different types of carbon allotropes have been incorporated in polymeric nanocomposites in recent decades to enhance electrical conductivity, including the carbon black, carbon nanotubes and graphene. Carbon nanotubes and graphene promise extreme electrical conductivities above 10^5 S/m as single nanoparticles, whereas amorphous carbon black nanoparticles, mainly owing to limited conductivity of the sp^3 hybridization of the amorphous structure, shows relatively lower intrinsic conductivities. Particle-particle contact resistance is a limitation for all carbon-based nanoparticles to transform single particle conductivity into a macro-scale property of their composites. Powdered carbon black particles therefore conduct relatively similarly to carbon nanotube or graphene powders. Because of the very large price difference between carbon black and carbon nanotubes or graphene, carbon black is more attractive as a conductive additive for industrial applications.

2.2.1.1. Effect of nanoparticles on electrical conductivity of epoxy resins and FRPCs

There is considerable scientific interest in the correlation between single-nanoparticle conductivity and the transfer of particle conductivity to their epoxy nanocomposites. Academic data reported by more than 20 relevant publications summarized in Figure 8 provides a realistic overview about the potential of carbon-based nanoparticles at their threshold additive content.

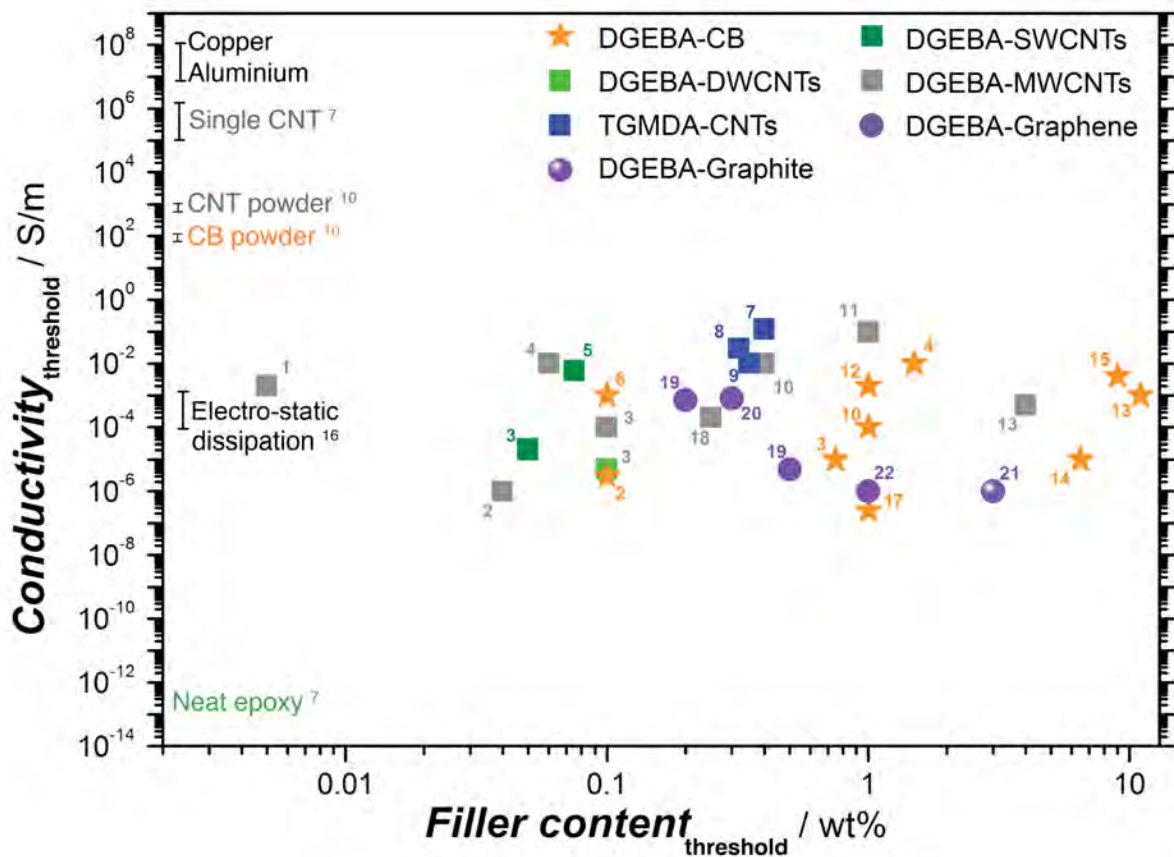


Figure 8. Summary of filler concentration versus conductivity of carbon nanoparticle modified epoxy nanocomposites at the threshold. *Only neat resin studies are shown.* The data presented are extracted from 22 publications. Data points: 1 [43], 2 [44], 3 [45], 4 [46], 5 [35], 6 [47], 7 [5], 8 [48], 9 [49], 10 [29], 11 [50], 12 [32], 13 [51], 14 [52], 15 [9], 16 [53], 17 [54], 18 [55], 19 [56], 20 [57], 21 [58], 22 [59].

Electrical conductivities of neat epoxy, bulk CB and CNT particles as powder, CNT as a single particle, metals such as aluminum and copper are shown on the y-axis, as well as the level of electrical conductivity required for electrostatic dissipation. In general, the addition of all types of carbon-based nanoparticles lead to the semi-conducting behavior of their epoxy nanocomposites at the threshold because measured conductivities are below 1 S/m. In previous studies, CNTs showed a broad range in the filler content data at threshold, varying from 0.005 wt.% [43] to 3 wt.% [51]. In the case of GNPs, the threshold value can be reached by the addition of 0.2 wt.% [56] to 1 wt.% [59] additive content. Slightly higher amounts of CB are necessary to form a conducting network. Threshold concentrations from 0.1 wt.% [44] up to 10 wt.% [51] have been reported for CB modified epoxy nanocomposites.

A simplification based on the above mentioned correlations of additive concentration at threshold and electrical conductivity is done. Figure 9 emphasizes the effectiveness of various carbon-based nanoparticles regarding their threshold concentration, where an abrupt increase of conductivity is first observed. It is obvious that CNTs are more effective compared with graphene and CB. This behavior is attributed to the high aspect ratios of CNT, compared to the other two nanoparticles.

Due to price limitations of CNTs and GNPs, nano CB remains the most suitable additive for this work because its low density, relatively low additive content at the threshold (0.1 wt.% as lowest threshold content from the literature [47]), and the price.

Only carbon-based nanoparticles in epoxy resins are summarized at their threshold content in Figure 8 and Figure 9. Research groups have performed detailed investigations into the effects of additive content on the electrical conductivity of carbon nanoparticle modified epoxy composites and chosen a single additive concentration for subsequent studies in their composites. To best of our knowledge, there are only a few systematic studies in the literature that focus on the correlation between the achieved conductivity of the modified epoxy resins and their laminates manufactured with these nanoparticle modified resins.

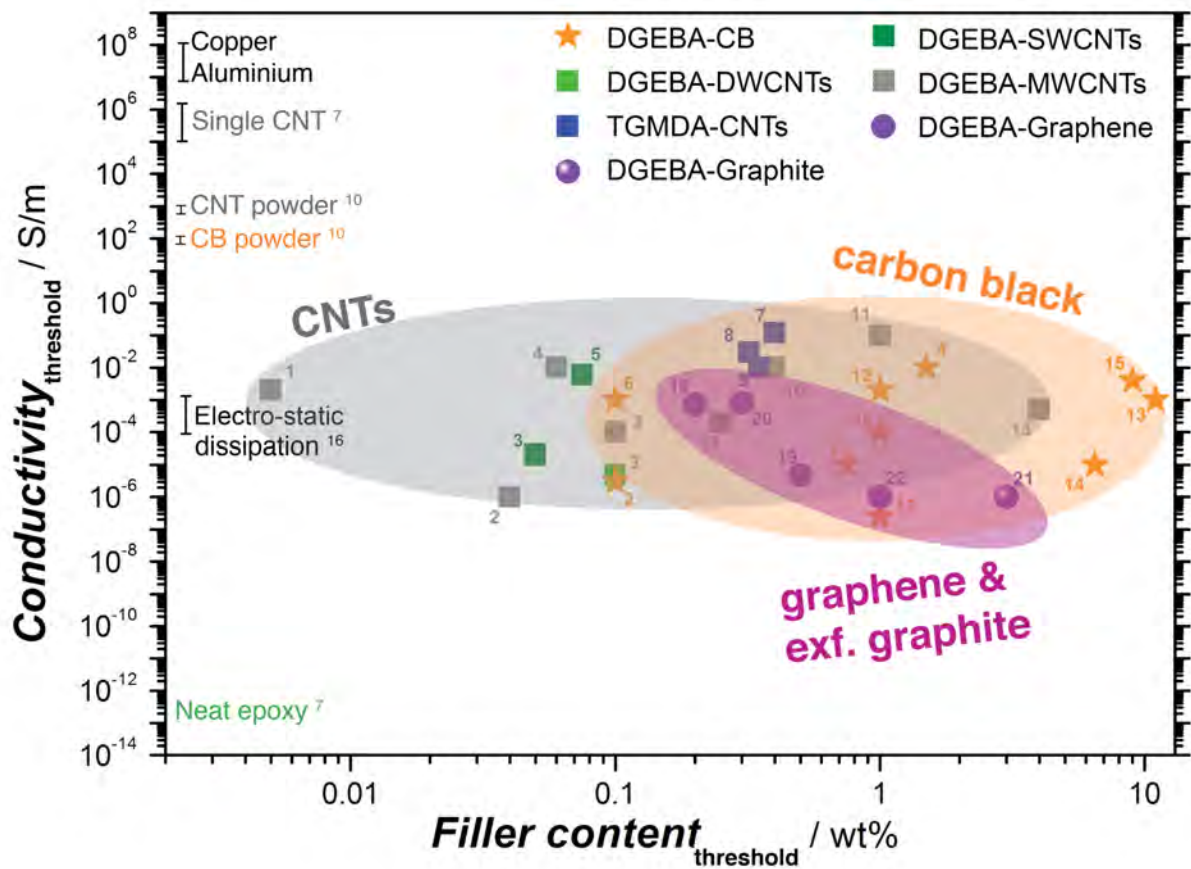


Figure 9. Summary of filler concentration and conductivity of carbon nanoparticle modified epoxy nanocomposites at threshold. The data presented here are from 22 publications. Data points: 1 [43], 2 [44], 3 [45], 4 [46], 5 [35], 6 [47], 7 [5], 8 [48], 9 [49], 10 [29], 11 [50], 12 [32], 13 [51], 14 [52], 15 [9], 16 [53], 17 [54], 18 [55], 19 [56], 20 [57], 21 [58], 22 [59].

With regards to final applications, the maximum conductivities achieved by carbon nanoparticles in neat resin and their fiber reinforced composites are important to discuss. The reported maximum achieved electrical conductivities at the highest additive concentration for carbon nanoparticle modified epoxy resins and their fiber reinforced composites are summarized in Figure 10.

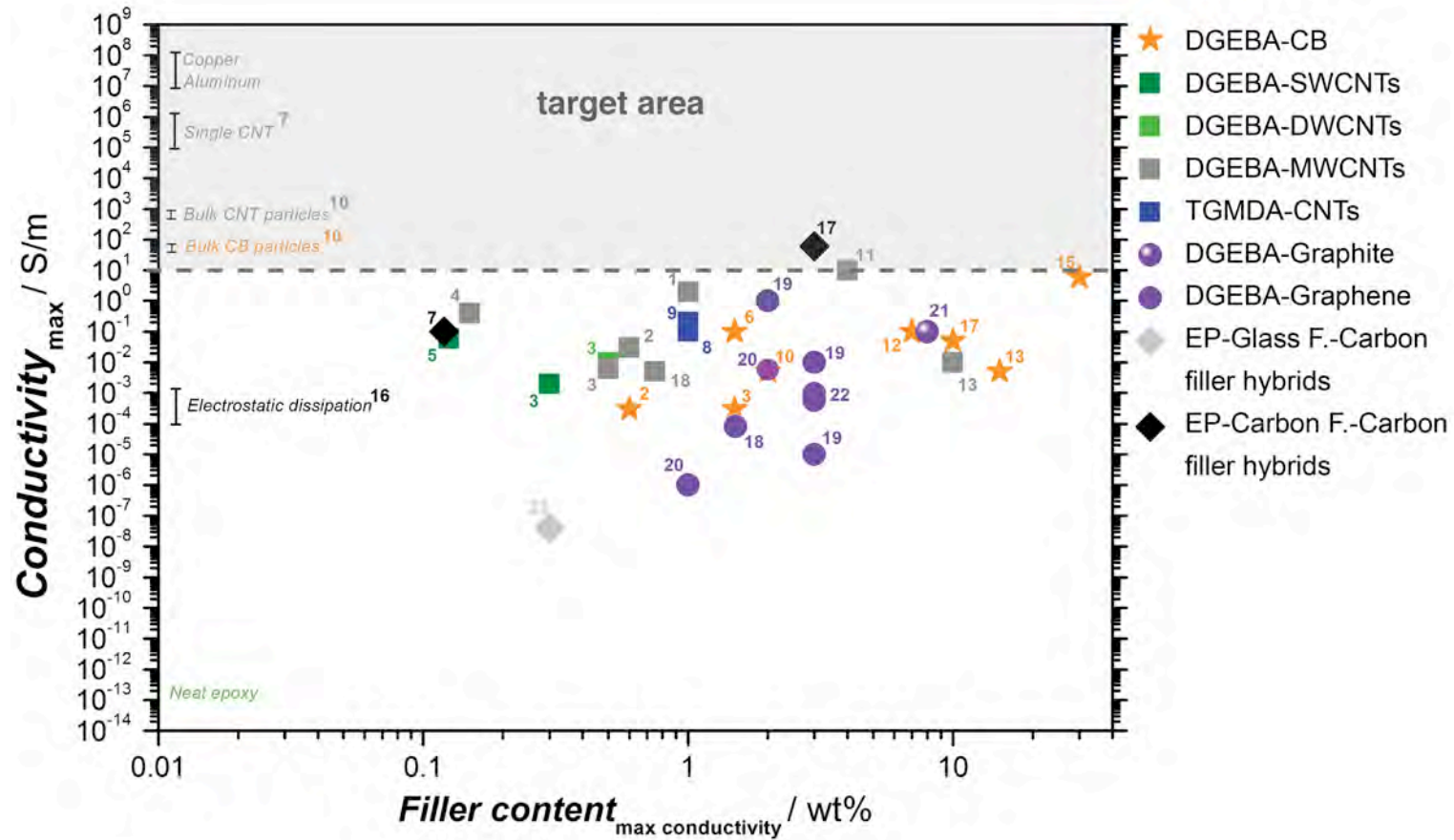


Figure 10. Filler concentration versus maximum achieved conductivity of carbon nanoparticle modified epoxy nanocomposites and their FRPCs. Data presented here are from 23 publications. Data points: 1 [43], 2 [44], 3 [45], 4 [46], 5 [35], 6 [47], 7 [5], 8 [48], 9 [49], 10 [29], 11 [50], 12 [32], 13 [51], 14 [52], 15 [9], 16 [53], 17 [54], 18 [55], 19 [56], 20 [57], 21 [58], 22 [59], 23 [33].

In the case of nanoparticle modified resins, the maximum achieved conductivities reported in the literature show that the addition of CNTs, graphene, and CB mostly transforms the epoxy resin in a semiconducting nanocomposites with conductivities ranging from 10^{-5} to 1 S/m. The maximum electrical conductivities achieved by the addition of CB, CNT, graphene or graphites are comparable. However, almost an order of magnitude higher CB or graphene were necessary to reach the same level of conductivity compared to CNT modified nanocomposites.

Zhang et al. [54] (data point 17 in Figure 10) studied the electrical conductivity of CB-modified carbon fiber (CF) epoxy composite with up to 3 wt.% CB content, and reported an electrical conductivity of ~ 60 S/m in the z-direction at this maximum CB content. However, the through-thickness electrical conductivity of the studied laminates was not dominated by the CB particles but rather the carbon fiber contacts. Because CF are also electrical conductors, it is difficult to distinguish between contributions exclusively from CF or carbon nanoparticles with regards to the overall composite conductivity. The transfer of electrical conductivity of nanoparticle modified resins to their fiber-reinforced composites is examined in a detail in this work.

Although the reported data regarding the maximum achieved conductivities by carbon nanoparticles in resins and their composites are highly variable, it is clear that carbon-based nanoparticles show great potential to produce conductive epoxy systems and composites.

The modification of epoxy resins with metal based micro or nanoparticles to obtain highly conductive composites or adhesives has also been investigated. Figure 11 summarizes the relevant scientific work using metal particles and compares the conductivity range achieved at maximum carbon nanoparticle content in epoxy composites (gray zone) with maximum conductivities achieved with metals.

Copper nanoparticles (CuNP), aluminum flakes (AlF), silver nanoparticles (AgNP) or nanowires (AgNW), and nickel nanostrands (NiNS) have been reported to produce a substantial enhancement of the electrical conductivity of epoxy resins. Except for AlF and micron-size milled copper particles, all metal based particles increase the

maximum conductivity in the composite above that achieved using carbon-based nanoparticles, as depicted by Figure 11. However, very high amounts of these additives are necessary and densities of the metal based particles are much higher compared to the carbon-based nanoparticles. High densities of the metal particles lead to instability of the uncured formulations because of sedimentation of dispersed particles in resin prior to curing. In addition, metal particles offer only a lower potential for weight reduction of composite parts compared to carbon-based nanoparticles.

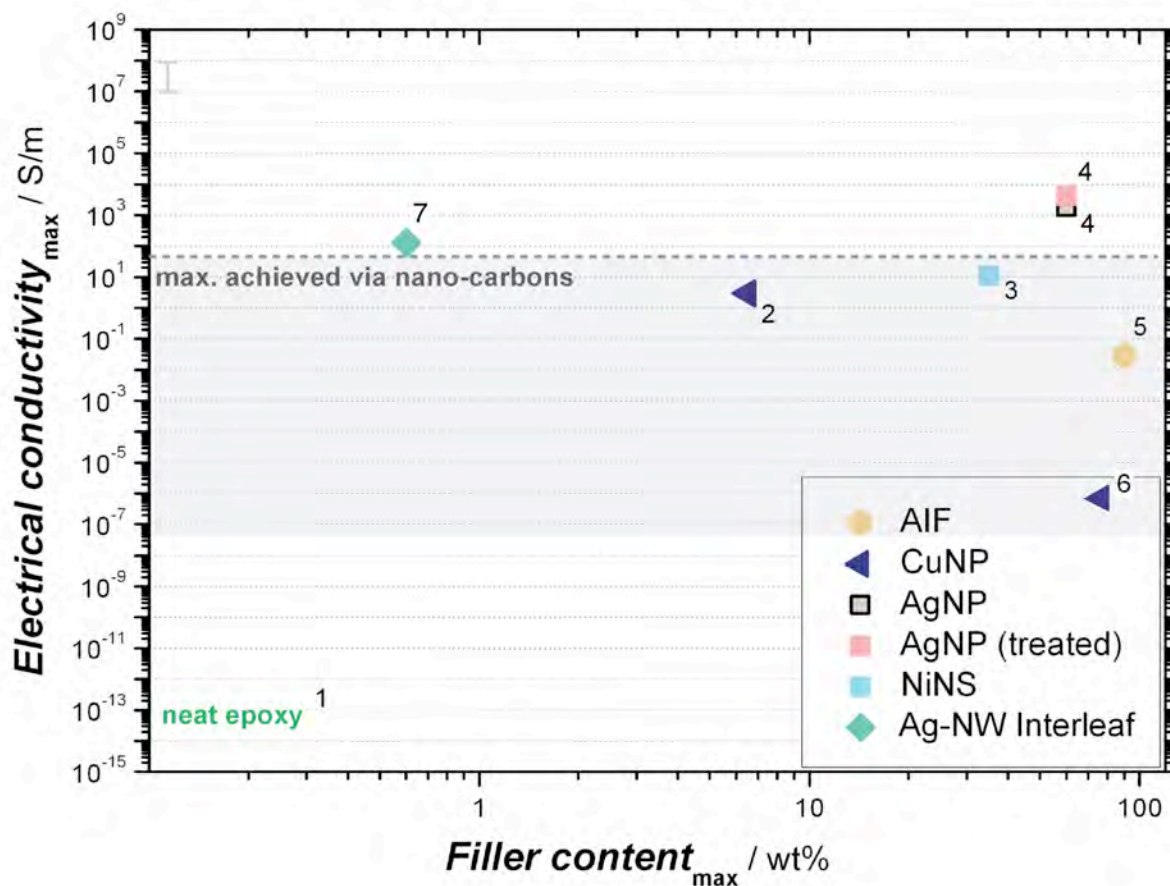


Figure 11. Summary of filler concentration and conductivity of metal based additive-modified composites and CFRPs at maximum achieved conductivity. The data presented here are extracted from six relevant publications. Data points: 1 [5], 2 [60], 3 [61], 4 [62], 5 [63], 6 [64], 7 [8].

In conclusion, carbon as well as metal based particles enhance the conductivity of epoxy resin to a certain extent. Due to very high required additive contents and risk of sedimentation (high densities), metal particles are not as effective as carbon-based nanoparticles to achieve electrically conductive composites with low additive content. Metal based conductive nanoparticles are not investigated in this work.

As Figure 8 and 9 depict, a slightly higher additive concentration is necessary to achieve electrically conductive epoxy composites with CB, however, because of its low density, price, and relatively low additive content at threshold, this additive is used in this study to improve the conductivity. Previous studies have verified that highly enhanced through-thickness conductivity can be achieved by the addition of CB, which opens up new applications for composites, as previously discussed in chapter 2.1.

2.2.2. Dynamics of conductive network formation

A discussion of collision dynamics and relevant forces acting upon particles is required for understanding the dynamics of network formation. Figure 12 shows the governing forces and their dependence on particle size, as well as theoretical particle distance.

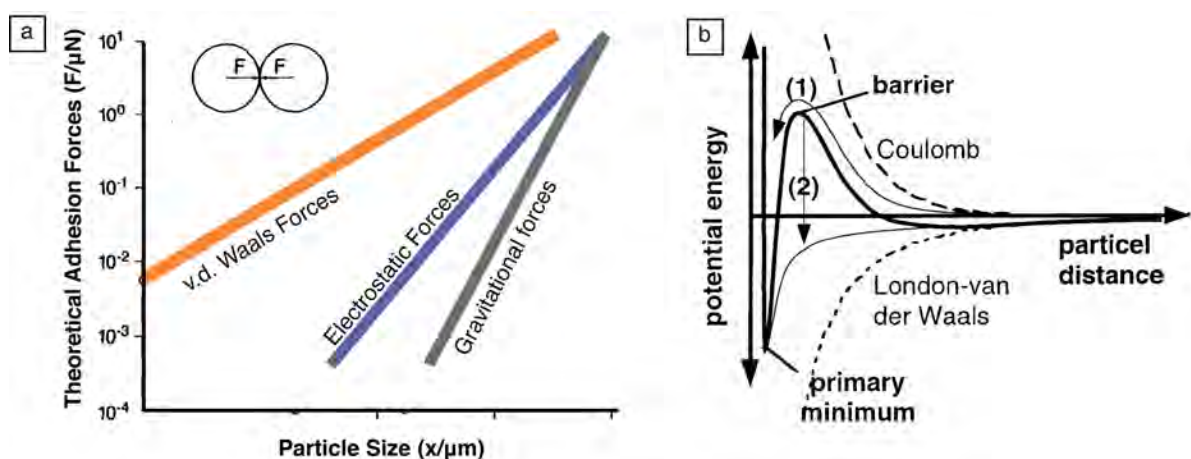


Figure 12. a) Theoretical adhesion forces acting between two spherical particles, modified [65]. b) Potential energy curve between two colloidal particles [66]. Reworked.

By excluding the external forces applied, between two perfectly spherical particles various attractive and repulsive forces act. Van der Waals, electrostatic, and gravitational forces govern the particle interactions (Figure 12), where each type gains variable importance depending on the particle size.

Van der Waals force is an anisotropic force that results from fluctuating polarizations in the molecules. Mainly these forces act on particles at the nanometer scale. Electrostatic forces, on the other hand, are due to the accumulation of ions on the surface of particles resulting in either particle adhesion or repulsion. Consequently, the governing factor of van der Waals forces increases as particle size decreases into the nanometer range, compared with electrostatic or gravitational forces [65].

Liang et al. [66] summarizes that van der Waals forces are adhesive, whereas electrostatic forces are repulsive forces, in the case of two identical nanoparticles dispersed in a liquid. Particles dispersed in a liquid tend to form persistent aggregates by means of Brownian motion. Potential energy curves of two colloidal particles (Figure 12.b) suggest that as particles approach one another because of van der Waals forces, the higher the electrostatic barrier repulses. External shear forces or reduction of repulsive forces by optimizing the ionic concentration of the polymer can accelerate the agglomeration process [47]. Additionally, particle shape, surface roughness, and mechanical locking of two particles play a role in affecting agglomerate structure and stability [65].

Battisti et al. [67] studied the dynamic nature of the network development by MWCNTs in a thermosetting matrix using electrical impedance spectroscopy and morphological studies (Figure 13).

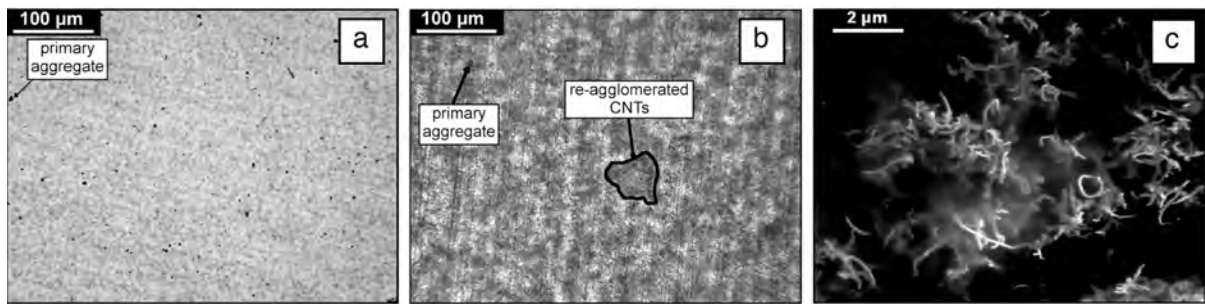


Figure 13. Micrographs of 0.1 wt.% MWCNT modified polyester resin. Transmission light microscopy of a) uncured, b) cured, and c) SEM (charge-contrast imaging) of a cured system [67]. Reworked.

Figure 13 shows the morphologies of an MWCNT modified unsaturated polyester resin before (Figure 13.a) and after curing (Figure 13.b). MWCNTs are claimed to disperse well with few primary aggregates before the curing process, and that re-aggregation of the initially well-dispersed nanotubes occurs during the curing process. Figure 13.a and Figure 13.b shed light on the re-aggregation of MWCNTs. Figure 13.c shows a charge contrast micrograph taken with a scanning electron microscope (SEM), which points out MWCNT agglomeration after curing. Consequently, the strong agglomeration of MWCNTs takes place during curing when the mobility of the particles is higher owing to the lowered viscosity of the suspension during curing.

Above the glass transition temperature (T_g) of the polymer, such particle networks remain dynamic and changing, where the particle network persists below the T_g and therefore maintains its agglomerated state. Zeiler et al. [68] also point out that a percolating network is a time-dependent structure that is affected by the host polymer properties and the temperature during and after its formation.

In summary, the formation of a three-dimensional conductive particle network is a dynamic process governed by various forces, which can be manipulated either by external shear forces or the ionic strength of the matrix. In the best case scenario, conductive particles should be dispersed as primary particles before curing and without any agglomeration, which agglomerate in sub-micron scale during curing process.

Re-aggregation due to attractive interparticle interactions is responsible for the formation of conductive network during final curing processes of the resin system.

2.2.3. Parameters affecting the conductivity of nanoparticle-epoxy composites

Deep insight into the parameters that influence nanoparticle agglomeration and network formation is critical to understand the electrical conductivity behavior of carbon-based nanoparticle modified composites. This section summarizes mainly the relevant studies that have discussed these important parameters.

2.2.3.1. Effect of particle type, alignment and aspect ratio

Gojny et al. [45] studied the effect of various nanoparticles such as CB, single (SWCNTs), di-walled (DWCNT), and multi-walled carbon nanotubes (MWCNT) with and without surface modification on the electrical behavior of epoxy resins cured with an aliphatic amine hardener (Figure 14). Sonication followed by the solvent casting method was used to disperse the nanoparticles in the resin.

Figure 14.a shows that 0.1 wt.% SWCNT was sufficient to achieve conductivity above 10^{-4} S/m, whereas 0.75 wt.% CB was needed for the same level of conductivity. The CNTs showed a generally lower threshold content compared to CB, owing to the higher aspect ratio of these particles. Surface modification with primary amines is concluded to have led to aggregation deterioration because of enhanced particle-matrix adhesion, which is documented by SEM micrographs shown in Figure 14.b and Figure 14.c. Nanocomposites containing primary amine modified MWCNTs show a lower conductivity compared with composites containing non-functionalized MWCNTs.

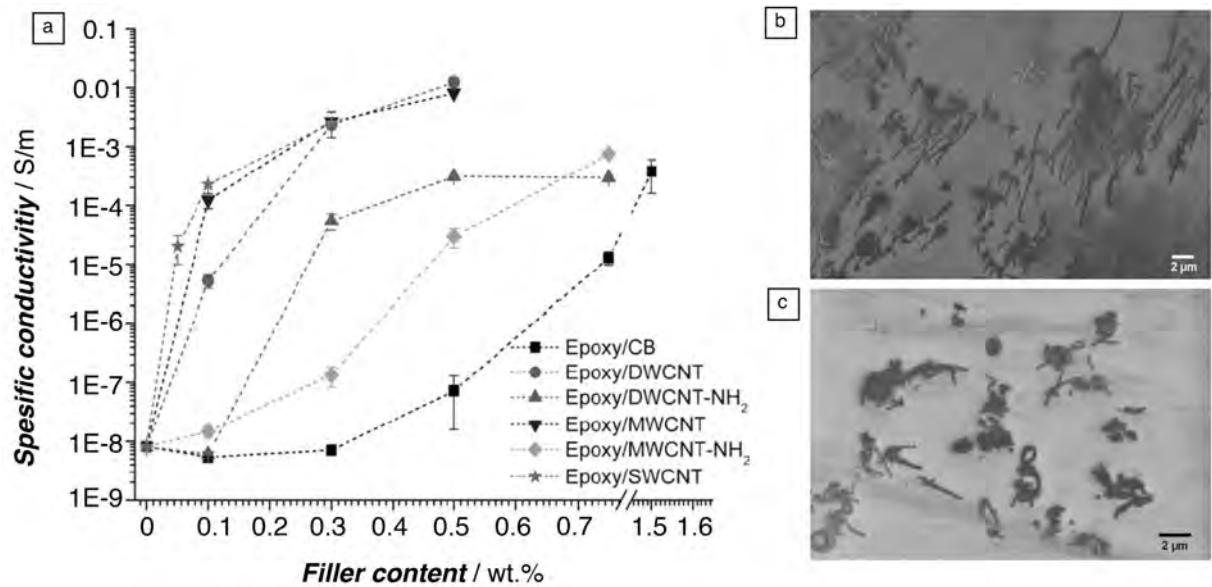


Figure 14. a) Specific conductivity of nanocomposites with various CNTs compared to CB as reference. SEM micrographs of b) 0.1 wt.% MWCNT, and c) 0.1 wt.% MWCNT-NH₂ modified epoxy nanocomposites [45]. Reworked.

Guo and Pötschke et al. [69] incorporated two types of MWCNTs in a polycarbonate matrix using a twin screw conical micro compounder. MWCNTs with high aspect ratios (313 and 474) are compared with nanotubes having aspect ratio of ~ 100 . It is concluded that the high aspect ratio of nanotubes was favorable for electrical conductivity and the storage modulus of the polycarbonate, compared to MWCNTs with lower aspect ratio.

Sandler et al. [43] studied the percolating network formation of CB and two types of MWCNTs in an amine-cured two functional diglycidylether of bisphenol A (DGEBA) system. Two types of MWCNTs were employed, which were produced via chemical vapor deposition (CVD). During CVD production, one type of nanotubes grew as entangled MWCNTs, whereas other type of nanotubes were aligned (not entangled) during CVD processing. Shear mixing was used to disperse the nanoparticles in the epoxy matrix. Figure 15 presents the evolution of the electrical conductivity of epoxy resins upon the addition of CB and various nanotubes.

An ultra-low percolation threshold with 0.0025 wt.% CNT loading was found for aligned (during CNT production) nanotube-reinforced nanocomposites, which is much lower compared to entangled MWCNTs or CB nanoparticles. Aligning of the nanotubes is suggested to be beneficial for perfect dispersion and distribution of nanoparticles in matrix prior to curing. As a conclusion, not entangled MWCNTs were suggested to be beneficial forming a conducting path of nanotubes at the lowest reported nanotube content to date.

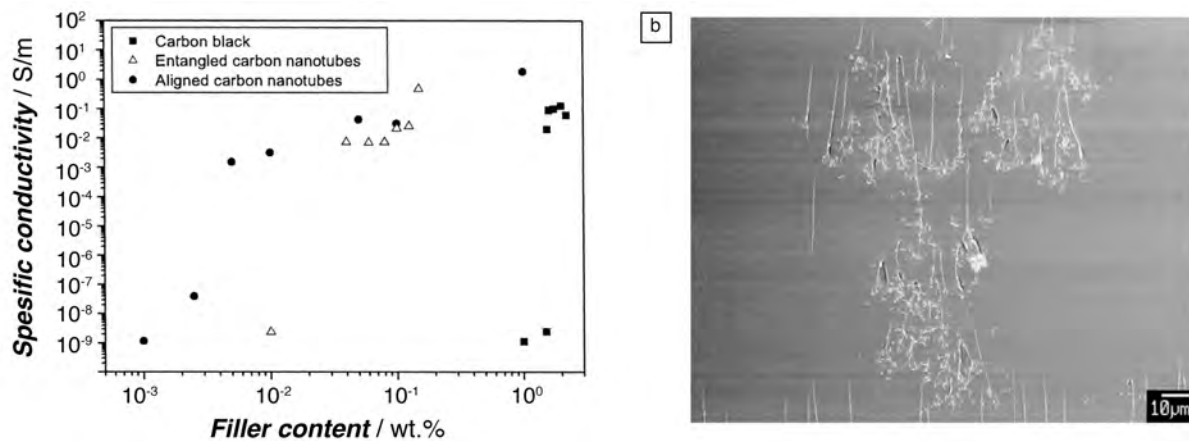


Figure 15. a) Conductivity as a function of filler content for various conductive particles. b) SEM micrograph of cured 0.0025 wt.% aligned carbon nanotube-epoxy nanocomposite [43]. Reworked.

Consequently, the high aspect ratio and low entanglement of conductive particles (prior to curing) are favorable to achieve conductivity at low additive content.

2.2.3.2. Effect of processing conditions

Because the final electrical conductivity of a nanocomposite is largely dependent on the conductive particle dispersion and distribution, the potential effects of processing conditions on nanocomposite morphology must be discussed.

Kulkarni et al. [70] studied the effect of processing parameters during manufacturing of CB-epoxy nanocomposites using a twin screw extruder. They reported that the decreased processing temperature and an increased number of passes (qualitatively higher dispersive shear forces) enhanced the final electrical conductivity of the nanocomposites. The study also showed that the variation of the screw speed did not influence the final conductivity of the nanocomposites.

Monti et al. [59] studied the effect of two different methods to process graphene-modified epoxy nanocomposites (Figure 16).

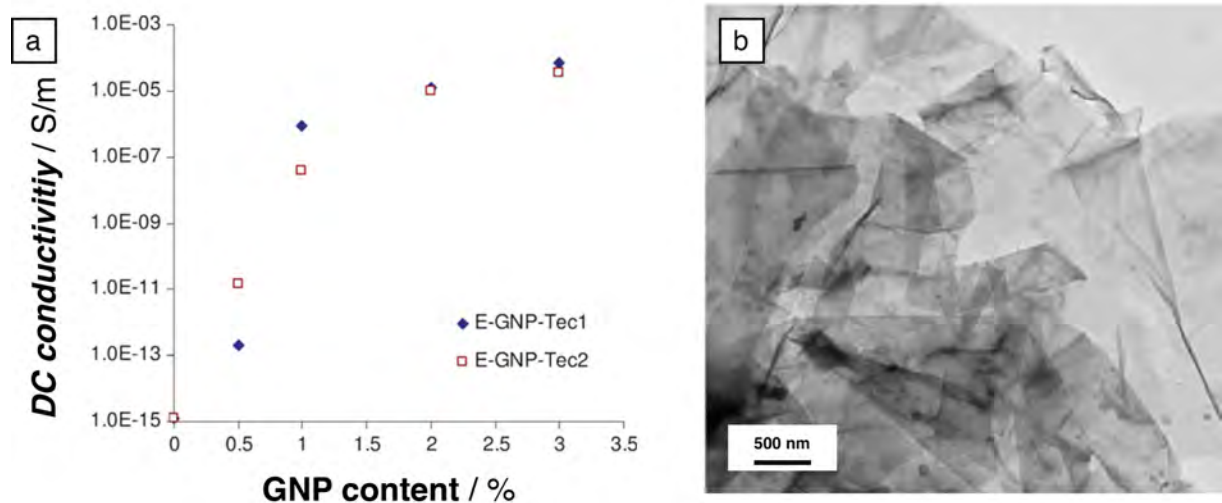


Figure 16. a) Direct current (DC) volume conductivities of graphene modified epoxy nanocomposites. b) a TEM micrograph of the graphene used in this study [59].

The first method (Tec1) includes mixing of graphenes with resin in chloroform, followed by a stoichiometric amount of hardener. The second method (Tec2) first consists of dispersing graphene in a tetrahydrofuran (THF)-hardener solution, followed by mixing with a stoichiometric amount of resin. The electrical conductivity results obtained by the two different processing methods and a representative TEM micrograph of the used graphene particles are shown in Figure 16.

The enhancement in the electrical conductivity of the nanocomposites obtained by the first method was slightly sharper. Mixing the conductive additive first with the resin or hardener did not substantially affect the final nanocomposite conductivity.

Chandrasekaran et al. [57] dispersed graphite nano-platelets in a DGEBA-anhydride system via a three-roll mill (3RM) and sonication combined with high-speed shear mixing technique (Soni_hsm). The electrical conductivity of the nanocomposites produced by these two different processing methods as a function of the filler content is shown in Figure 17, together with a representative SEM micrograph of dispersed particles prior to the processing.

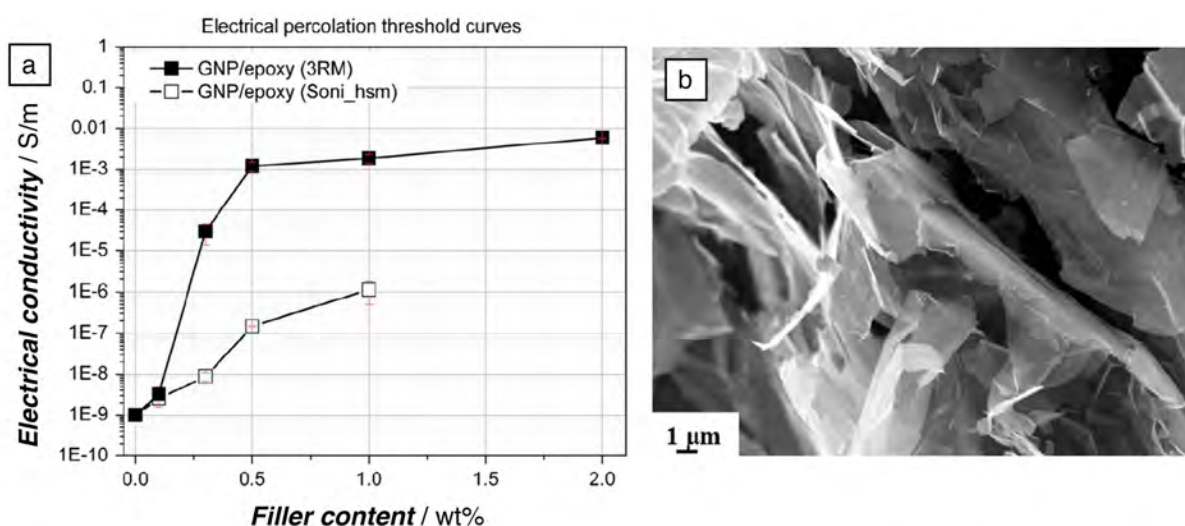


Figure 17. a) Volume conductivity of graphite nano-platelets-epoxy nanocomposites dispersed with 3RM and Soni_hsm techniques. b) SEM micrograph of graphite nanoparticles used in this study [57]. Reworked.

The SEM micrograph of used particles reveals the sheet-like structure of the graphite nano-platelets. As it can be seen, the chosen processing route substantially affects the final conductivity development of nanocomposites because the dispersive energy input by mixing techniques can vary significantly. At 0.5 wt.% nano-platelet content, four

orders of magnitude higher electrical conductivity was measured for nanocomposites processed via 3RM compared to sonication combined with shear mixing.

The morphologies of nanocomposites processed via these different production methods are shown in Figure 18. The 3RM technique dispersed the graphite nanoparticles qualitatively finer compared to the sonication with shear mixing method. It is evident from these optical micrographs that finer dispersed graphite nano-platelets formed a lower-dimensional network with higher branching, resulting in a higher electrical conductivity of their composites.

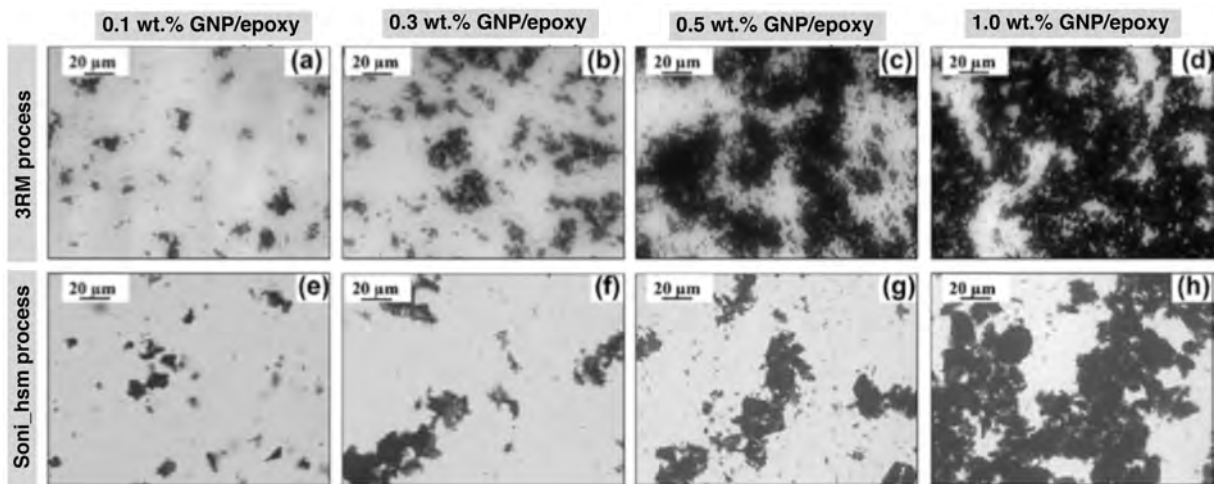


Figure 18. Transmission light micrographs of graphite nano-platelet modified epoxy suspensions (uncured) produced via 3RM (a to d) and Soni_hsm (e to h) [57]. Reworked.

Poetschke and Villmow et al. [71] studied the effect of processing conditions during the twin screw extrusion process on the dispersion and distribution of MWCNTs in a poly (lactic acid) matrix. As parameters, MWCNT loading, processing temperature, screw profile and rotation speed were investigated. Applied shear stress on the MWCNT agglomerates via increasing the rotation speed was concluded to be the most important parameter enhancing the MWCNT dispersion and distribution in the polymer matrix.

In conclusion, the choice of the nanocomposite processing method and the parameters have a critical influence on the final morphology and the final electrical conductivity. The processing temperature and number of passes or applied shear stress affect the conductive network formation of nano carbon modified epoxy resins. The three-roll mill technique obtains the best particle dispersion prior to curing, which promises a finer particle agglomeration during curing. This method is therefore considered as the best method to process the conductive composites. As an additional parameter, the dispersion of nanoparticles either first in the resin or in hardener component, was reported to have negligible effects. Hence, this parameter is not taken into account during this work.

2.2.3.3. Effect of ion concentration of the resin system

As described previously, among particles dispersed in polymers, attractive (van der Waals) and repulsive (Coulomb forces at the particle surface) forces govern the agglomeration behavior. Coulomb repulsive forces can cause an energy barrier hindering the formation of the conductive network by preventing particle agglomeration. In the case of carbon-based nanoparticle modified epoxy systems, this repulsive energy barrier can be surmounted by adjusting the ionic strength of the reactive resin-hardener system before curing which lowers the repulsive forces on the surfaces of the conductive inorganic particles [47]. Schueler and Schulte et al. [47] studied the effect of shearing (or mixing) before curing, as well as the addition of anhydrous copper chloride salts (CuCl_2) on the agglomeration behavior of CB in an aromatic amine-cured DGEBA resin system. The results are shown in Figure 19.

Copper chloride salt is expected to decrease the repulsion between CB particles by increasing the ionic concentration in the uncured resin, resulting in a higher agglomeration of CB with increased conductivity. CB was dispersed using a dissolver disc in an epoxy resin.

CB-epoxy nanocomposites cured immediately after mixing showed an abrupt enhancement in the electrical conductivity at 0.9 vol.% CB, whereas slight shearing before curing decreased the critical CB concentration to 0.3 vol.%. On the other hand, the addition of $3 \cdot 10^{-6}$ mol/gr CuCl_2 in the resin mixture decreased the critical CB concentration to 0.06 vol.%.

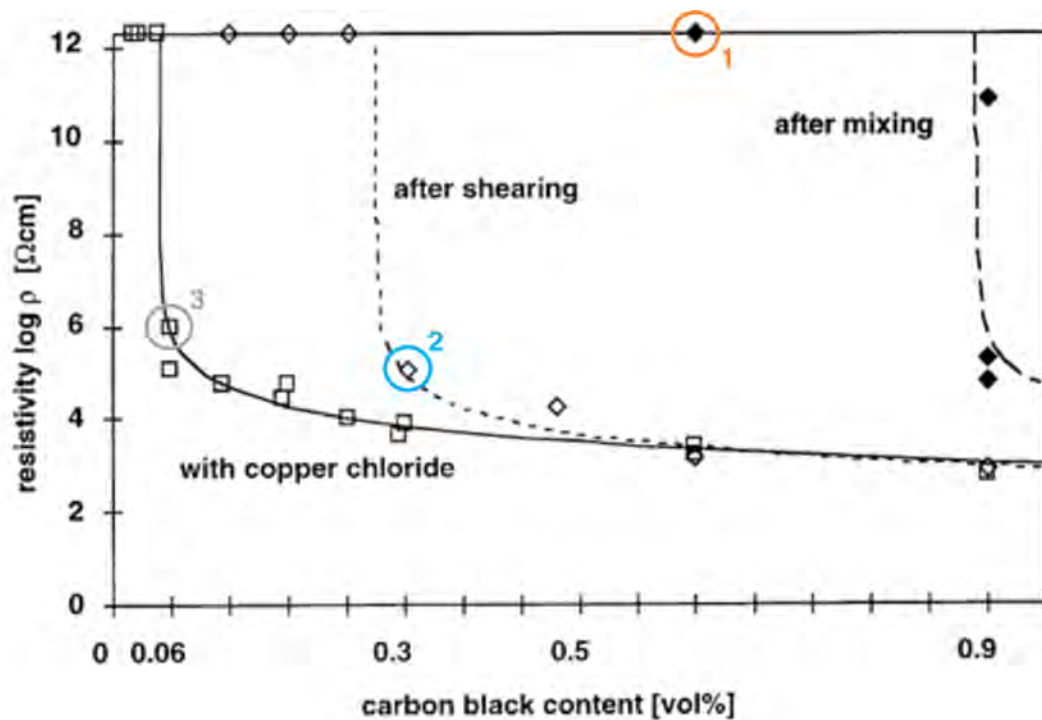


Figure 19. Volume resistivity of CB-epoxy nanocomposites reported by Schulte [47].

Epoxy nanocomposite morphologies are shown in Figure 20, which are connected via colours to Figure 19.

Both treatments, light shearing and addition of CuCl_2 , dramatically influence the morphology of the CB network. Light shearing (Figure 20.b, blue data point, 2, in Figure 19) enhances particle agglomeration by increasing particle mobility.



Figure 20. a) 0.6 vol.% CB-epoxy nanocomposite cured after mixing, b) 0.3 vol.% CB-epoxy nanocomposite cured after mixing with light shearing before curing, and c) 0.06 vol.% CB-epoxy nanocomposite with CuCl_2 [47].

On the other hand, increasing the ionic concentration of the resin system by the CuCl_2 salt assisted the CB to further reach the potential minimum and agglomerate as very thin veins (Figure 20.c, gray data point, 3, in Figure 19) by demolishing the repulsive coulomb forces [47].

The same trend was observed by Flandin et al [31]. CB nanoparticles were added to an epoxy resin with and without CuCl_2 salt. The electrical conductivity of the corresponding nanocomposites was studied and compared to composite morphology (Figure 21).

The same amount of copper chloride salt, as in the case of the study of Schulte [47], was added to the carbon black-epoxy suspension before curing. The addition of CB to above 1 vol.% with and without CuCl_2 substantially enhanced the conductivity of the resin (Figure 21.a). For the CB-epoxy nanocomposites without CuCl_2 , the critical CB concentration was identified to be 0.9 vol.%. The agglomeration of the particles in the resin was not strong (Figure 21.b). However, additional CuCl_2 decreased the critical concentration, forming a conducting network below 0.1 vol.% CB content, owing to stronger agglomeration and previous network formation (Figure 21.c).

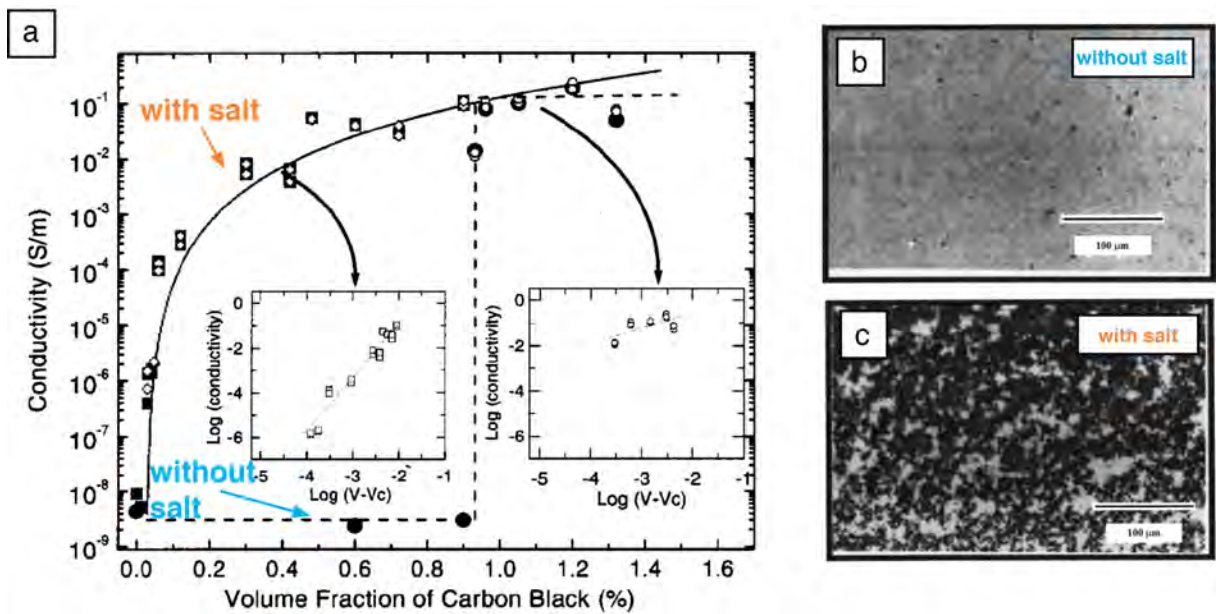


Figure 21. a) Electrical conductivity of CB-epoxy nanocomposites with (empty circles) and without (filled circles) CuCl_2 salt. Transmission optical micrographs of cured b) 0.9 vol.% CB-epoxy, c) 0.9 vol.% CB-epoxy nanocomposite with CuCl_2 [31] Modified.

Consequently, previously studies report that manipulation of a conducting particle network by lowering repulsive interparticle forces via CuCl_2 salts is a highly efficient strategy towards obtaining conductive nanocomposites.

2.2.3.4. Effect of external electromagnetic field

Previous studies have reported that the morphology of a particle network in epoxy resin can be manipulated by applying an external electromagnetic field [72], [73].

Yakovenko et al. [73] studied the electric field-induced alignment of MWCNTs in an epoxy resin and found that the extent of the particle alignment is strongly influenced by the applied field. Figure 22 presents the morphology development of an MWCNT-epoxy nanocomposite at four points in time.

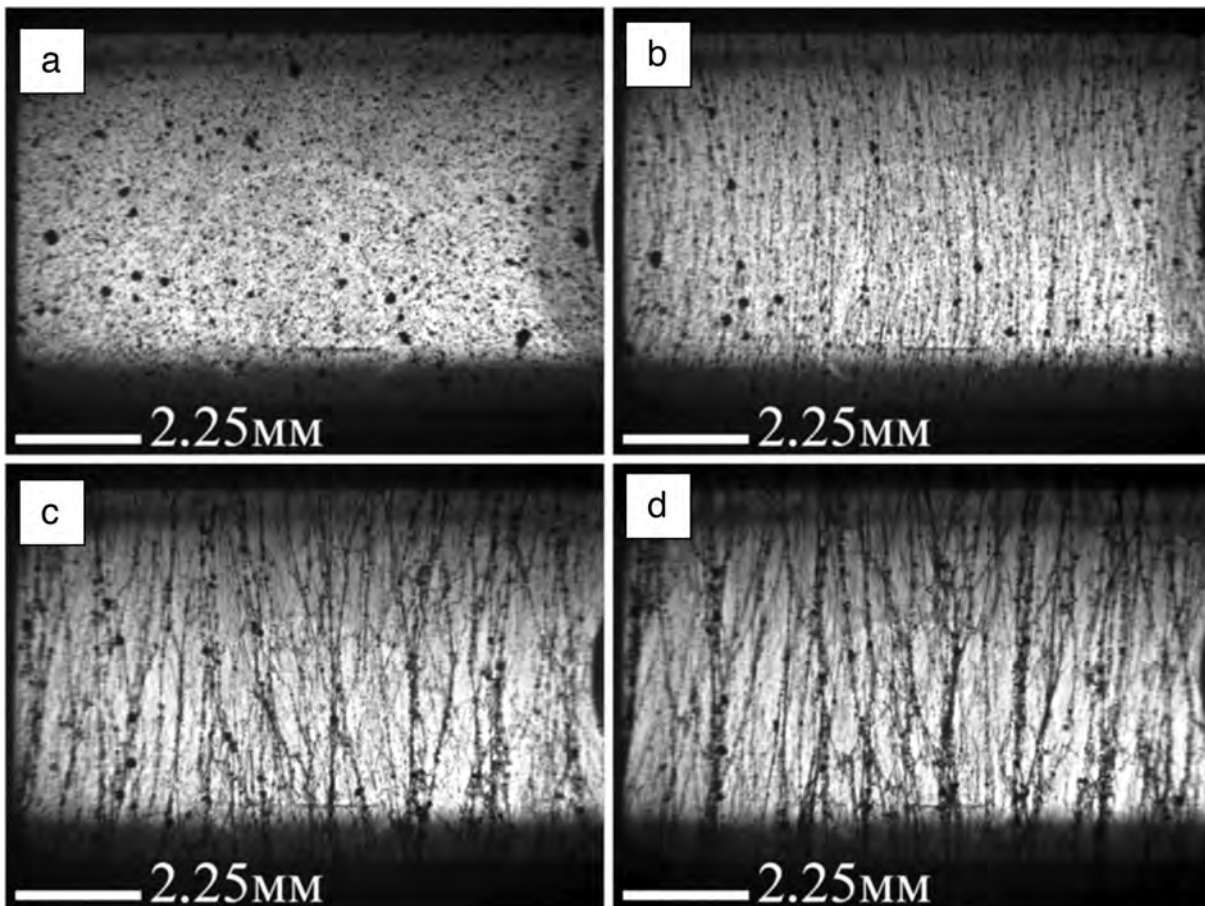


Figure 22. Optical micrographs of 0.05 wt.% MWCNT-epoxy nanocomposite under an 83.3 kV/m electric field with a frequency of 15 kHz. a) Before the electric field action, b) 12 min after c) 26 min after, and d) 60 min after [73].

Before the application of an external electric field (Figure 22.a), particles are distributed homogeneously in the resin. Electrical field is applied at room temperature and the low viscosity epoxy system (600 to 900 mPas at 23 °C) was chosen for experiments. Thermal curing is applied just after the application of the electromagnetic field. After 12 min (Figure 22.b), branching and orientation are observable. After 26 min (Figure 22.c) and up to 60 min (Figure 22.d) of electromagnetic field exposure, there is a strong orientation of the MWCNT particles in the resin. This experiment demonstrates that an external electromagnetic field can strongly influence epoxy nanocomposite morphology development when in an uncured state.

2.2.3.5. Effect of the inclusion of a second phase

The electrical conductivity of a composite largely depends on the morphology of the conducting particle network in the polymer. Formation of the conductive network is not only affected by the processing, temperature or electromagnetic field, but also by the presence of an another particle phase in the resin together with conductive particles. This additional phase can be conductive [44], [74], [75] or an insulator [28], [76], [77].

Sumfleth et al. [44] studied the structure-property relationships of simultaneously CB and MWCNT modified epoxy resins (Figure 23).

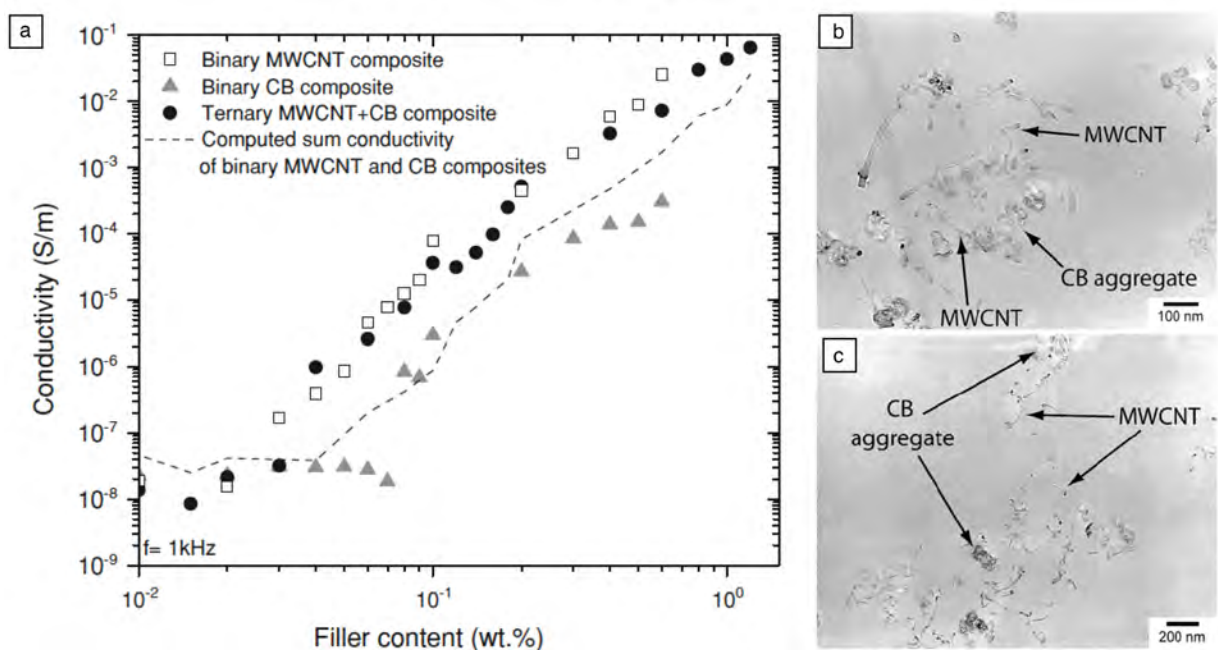


Figure 23. a) Electrical conductivity of CB, MWCNT, and CB-MWCNT modified epoxy nanocomposites. b) and c) TEM micrographs of 0.2 wt.% MWCNT with 0.2 wt.% CB modified resin under 60 kX and 28kX magnification, respectively [44]. Reworked.

CB and MWCNTs were dispersed in an anhydride-cured DGEBA resin via 3RM. Composites contained only CB, only CNTs, and as ternary composites, a combination of CB and MWCNTs. In ternary composites, only a 1:1 ratio of CB and MWCNTs was

investigated. The electrical conductivity of these nanocomposites was measured by applying an alternating current (frequency: 1 kHz). Together with conductivity results, relevant TEM micrographs are shown in Figure 23.b and Figure 23.c.

Binary CB-epoxy nanocomposites exhibit a higher percolation threshold compared to binary MWCNT-epoxy nanocomposites (Figure 23). The binary CB-epoxy system also exhibits almost two orders of magnitude lower electrical conductivity compared to nanocomposites with MWCNTs. However, a 1:1 combination of CB and MWCNT in ternary nanocomposites demonstrates almost the same electrical behavior as binary MWCNT-epoxy nanocomposites. The TEM micrographs shown in Figure 23.b and Figure 23.c depict a ternary nanocomposite comprised of 0.2/0.2 wt.% CB-MWCNTs and expose the co-supporting networks of particles. Co-supporting networks of nanoparticles with similar surface characteristics have also been reported as well by other research groups [78], [79].

Tang et al. [77] studied the effect of nano-silica and sub-micron rubber additions on the network formation of MWCNTs at a concentration of 1 wt.% in an anhydride-cured DGEBA resin system. 10 wt.% nano-silica and sub-micron rubber particles were added to the already MWCNT modified epoxy nanocomposite. Figure 24 shows TEM micrographs of the binary and ternary nanocomposites.

The incorporation of 1 wt.% MWCNT in the epoxy system enhances the conductivity of the epoxy resin by almost seven orders of magnitude from 10^{-9} S/m to 10^{-2} S/m. The addition of 10 wt.% nano-silica and 10 wt.% sub-micron rubber increase the electrical conductivity, although these additives are intrinsic insulators.

It is speculated that the inclusion of an inorganic second phase, especially nano-silica, may prohibit the formation of excessive agglomeration of MWCNTs and result in a nano-scale formation of the conducting network (Figure 24.f).

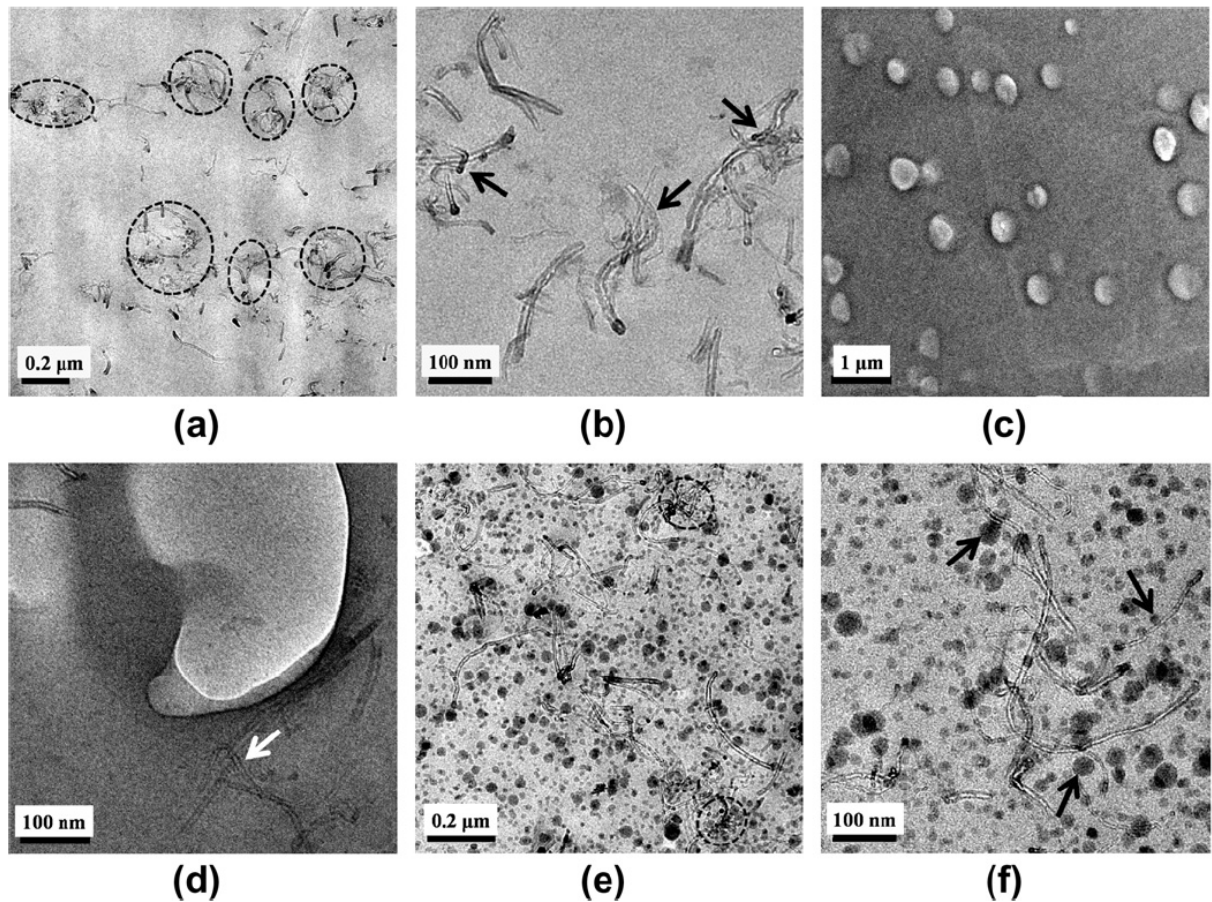


Figure 24. TEM micrographs of a) and b) 1 wt.% MWCNTs, c) and d) 1 wt.% MWCNTs with 10 wt.% submicron rubber particles, e) and f) 1 wt.% MWCNTs with 10 wt.% nano-silica [77].

Peliskova et al. [28] investigated the effect of silicone rubber particles on the conductive network formation of CB in an amine-cured epoxy system. Silicone rubber and CB were dispersed via an ultrasound disperser in the resin and the electrical conductivity of nanocomposites consisting of up to 25 wt.% CB was studied. In ternary composites, together with the CB nanoparticles, up to 50 wt.% rubber is added to the epoxy matrix.

The percolation threshold was found to be 3.5 wt.% for CB modified epoxy binary nanocomposites. Figure 25.a and 25.b indicate that the conductivity is clearly affected by the presence of the rubber phase in addition to CB. The addition of rubber

decreases the percolation threshold (Figure 25.a) and enhances the overall electrical conductivity even at high CB contents (Figure 25.b).

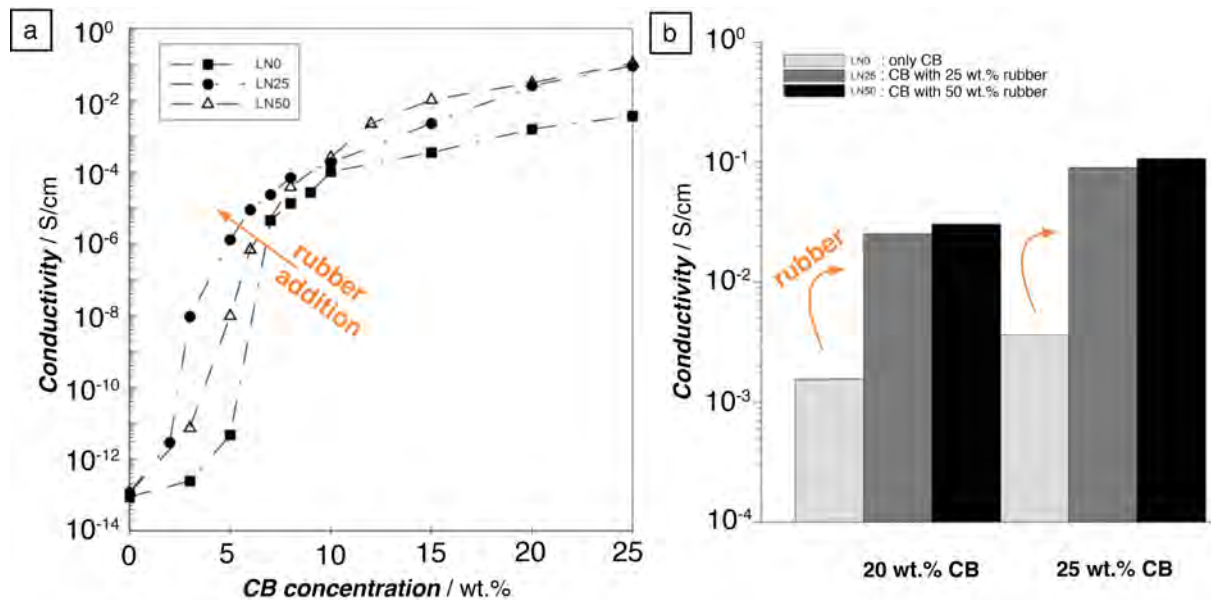


Figure 25. a) Percolation concentrations of binary CB-epoxy and ternary CB-silicone modified epoxy nanocomposites. b) Electrical conductivity of nanocomposites with 20 wt.% and 25 wt.% CB, and with (gray column 25 wt.%, black column 50 wt.% rubber) and without additional silicone rubber (light gray column) [28]. Reworked.

Figure 26 shows the microstructure of the ternary CB-silicone rubber epoxy nanocomposites from Peliskova et al. [28]. Droplet-like silicone domains of up to $8\ \mu\text{m}$ are visible. Energy dispersive X-ray (EDX) mapping suggests that the phase-separated structure of silicone rubber in epoxy affects the distribution of CB particles and limits their localization at either the surface or in interparticle regions of the silicone. The interpretation of this finding is that CB particles only gather in between these silicone particles and that this morphology enhances electrical conductivity, even though silicone rubber is naturally insulating.

The existence of the second particulate phase in the composite has been shown to potentially influence the dispersion and the distribution of conducting particles.

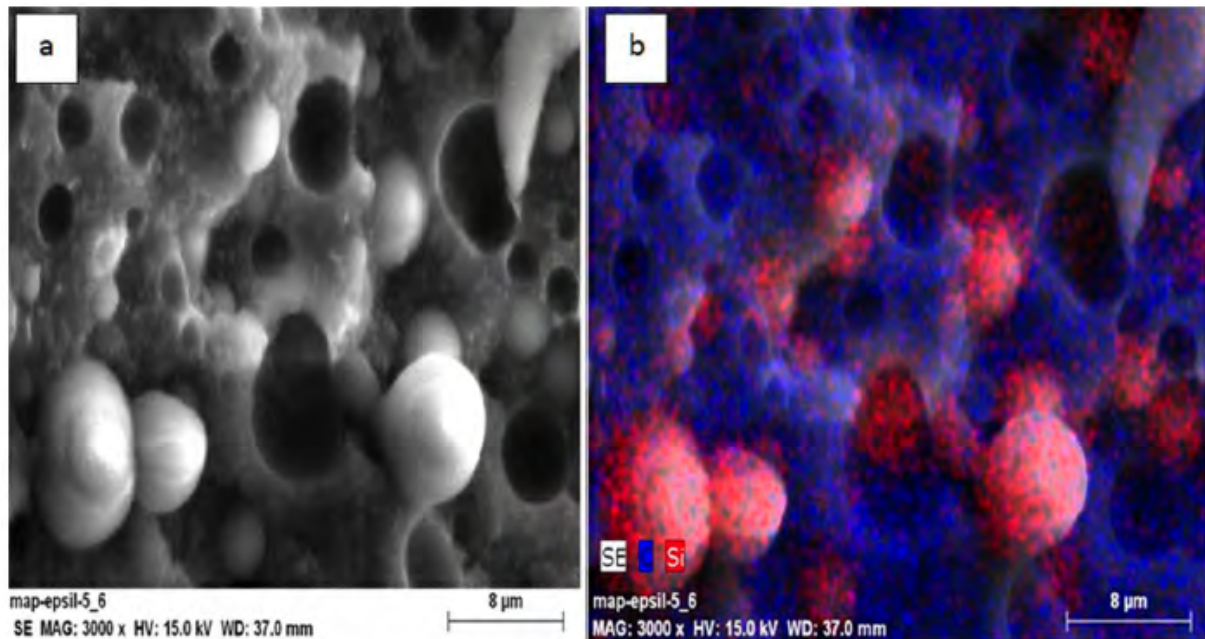


Figure 26. a) SEM micrograph of ternary 5 wt.% CB-50 wt.% silicone-epoxy system, b) EDX mapping of the same fracture surface. Blue corresponds to carbon and red corresponds to silicon atoms [28].

2.3. Conductivity of carbon nanoparticle modified CF laminates

To the best of our knowledge, Zhang et al. [54] reported the highest measured electrical conductivity for carbon black modified fiber-reinforced composites (Figure 10, data point 17) with a 3 wt.% CB modification of epoxy-carbon fiber composite. Carbon black nanoparticles were dispersed in the epoxy resin via ball milling. With and without copper chloride, an ionic strength modifier, CB decreases the resistivity of the system as shown in Figure 27.a. The 3 wt.% loading of CB already results in a plateau region for electrical conductivity. Further addition of CB shows only a minor increase. A TEM micrograph of 3 wt.% CB modified epoxy (without CuCl_2 , Figure 27.b) reveals a network of conducting nanoparticles. Although most of the CB aggregates are in contact with each other, there is an epoxy-rich insulating area with a width below 100 nm in between some aggregates.

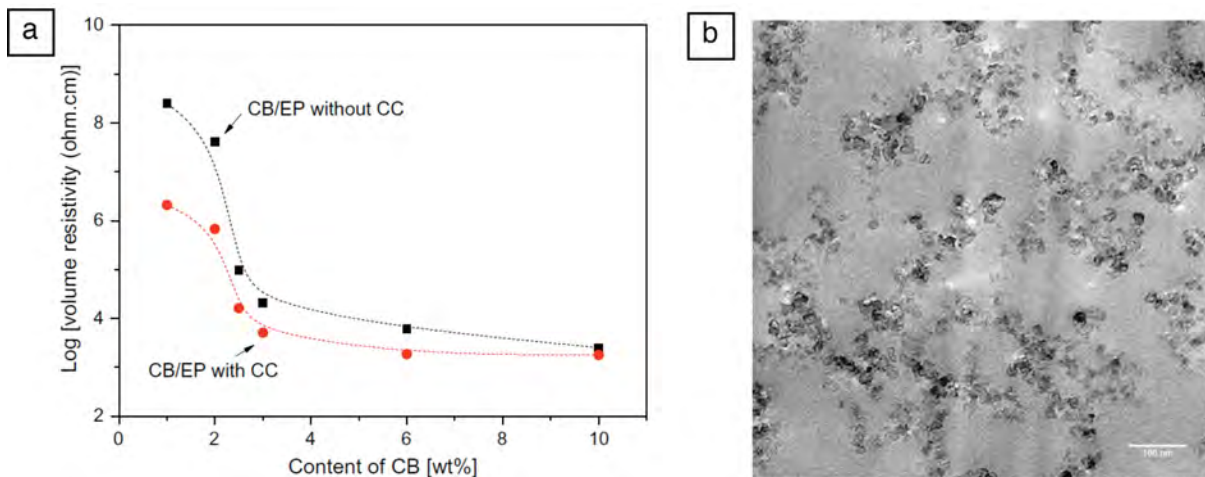


Figure 27. a) Logarithmic volume resistivity of an CB modified epoxy resin. b) TEM micrograph of a CB-epoxy nanocomposite with 3 wt.% CB loading. CC is copper chloride (CuCl_2) [54].

The CB modified epoxy resin was processed via RTM to carbon fiber (CF) reinforced epoxy composites. The fiber volume contents of neat and 3 wt.% CB modified (with CuCl_2 salt) carbon fiber-epoxy composites were 65.9 and 65.4 vol.%, respectively.

Although a considerable increment of electrical conductivity was measured in epoxy resin by CB addition, only a two-fold enhancement of through-thickness electrical conductivity was observed in the case of its 3 wt.% CB modified epoxy-carbon fiber composites (Figure 28.a). The CF dominated the conduction by fiber-fiber contacts.

Figure 28.b shows that the CB agglomerates in epoxy-rich regions and thickly covers the fiber surfaces, resulting in a further enhancement of the electrical conductivity of FRPC. Mechanical properties did not deteriorate when CB was added in the epoxy resin or in its carbon fiber RTM laminates.

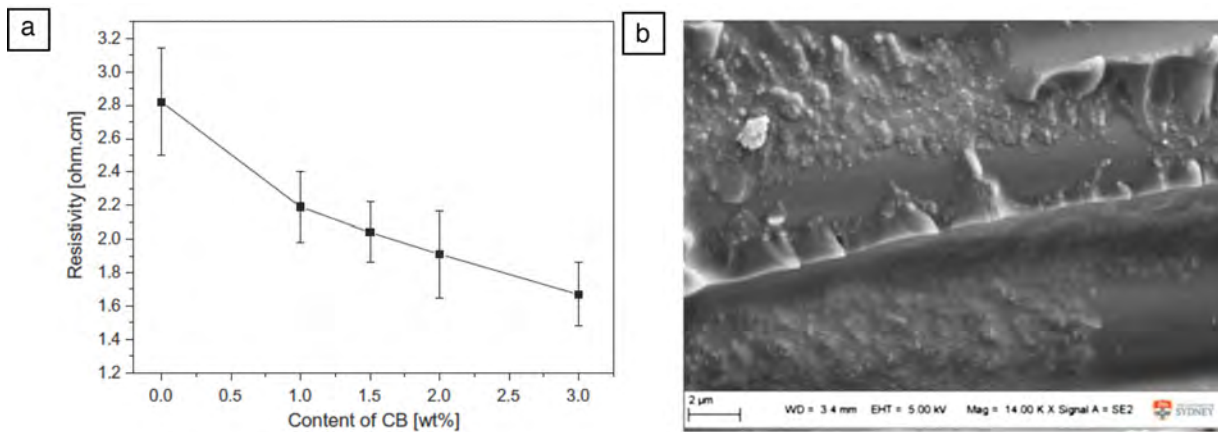


Figure 28. a) Linear volume resistivity of CB modified epoxy-carbon fiber RTM laminate. b) SEM micrograph of a CB-epoxy CF laminate with 3 wt.% CB loading and copper chloride [54].

The addition of carbon nanoparticles in carbon fiber reinforced composites results in enhanced electrical conductivity by bridging the non-contacting carbon fibers. However, in the carbon fiber epoxy composites, the through-thickness electrical conductivity is mainly dominated by carbon fiber contacts. It is important to note that there is a lack of information regarding the effect of carbon fiber volume content on the through-thickness electrical conductivity of composites, which justifies its inclusion in this work.

2.4. FRPCs modified with conductive layers

One of the main strategies used to create conductive composite structures is the incorporation of 2D conductive layers. Guo et al. [8] incorporated silver nanowires (AgNW) dip-coated polyamide 6.6 (PA6.6) fleece material as an interleaf in the carbon fiber-epoxy prepreg laminates to enhance the electrical conductivity. Figure 29 shows the microstructure of uncoated and AgNW coated fleece, as well as a cross-sectional micrograph of the AgNW coated fleece modified epoxy carbon fiber prepreg laminate.

In Figure 29.a, silver nanowires cover the polyamide interleaf fleece and act as a conductive outer layer at the polyamide fiber surface.

Laminate without an interleaf exhibited conductive behavior in the z-direction with conductivity slightly above 1 S/m, which is very high for a neat carbon fiber-epoxy composite. Incorporation of an uncoated PA6.6 fleece deteriorated the through-thickness conductivity of the prepreg laminate by a six orders of magnitude and resulted in a conductivity below 10^{-6} S/m. In contrast, it is claimed that AgNW coated fleece (Figure 29.a) established a conductive path in each prepreg layer, increasing the through-thickness conductivity above 100 S/m.

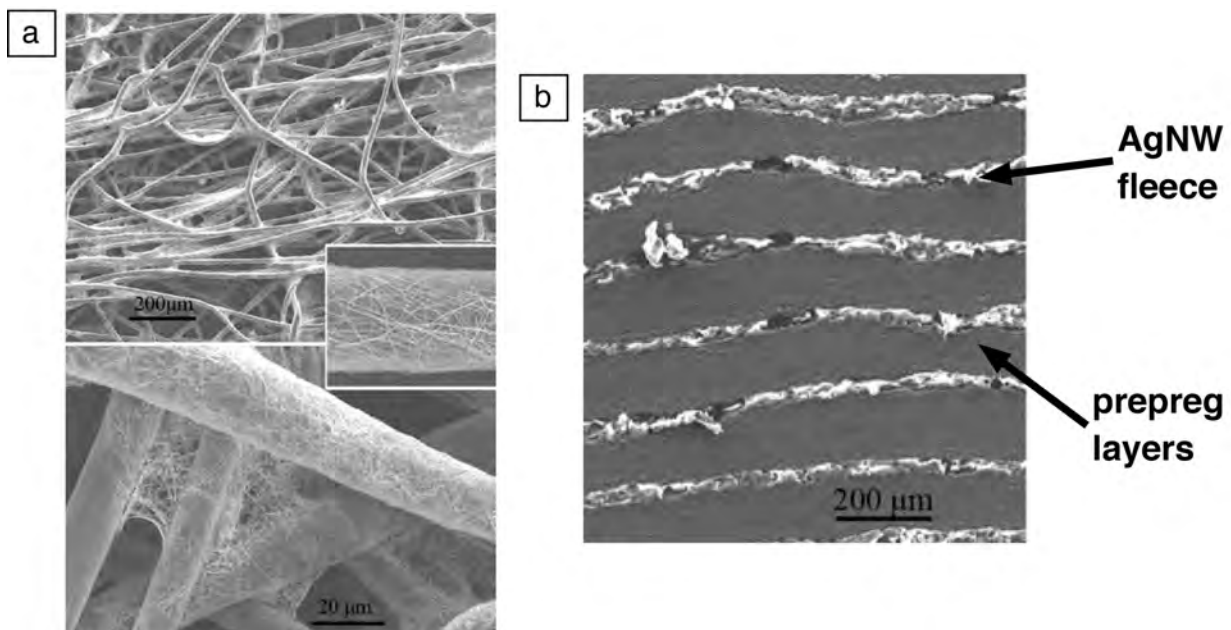


Figure 29. a) AgNW-coated PA.6.6 fleece material. B) AgNW-coated PA6.6 fleece as interleaf in carbon fiber prepreg laminates [8].

In summary, the use of thermoplastic interleaf fleeces is highly detrimental for electrical conductivity of composites. However, coating of these fleeces with a conductive additive can inhibit the diminishing effect of the insulating fleeces and result in enhanced composite conductivity.

2.5. Behavior of composites under lightning strike

Most lightning strikes hitting to airplanes are triggered by flights through heavily charged clouds. A commercial aircraft is exposed to a lightning strike statistically once per year [80]. A lightning event has extreme currents and voltage, and can be very detrimental to the structural integrity of airplanes owing to possible ignition of fire due to Joule heating, electromagnetic disturbances, sparking at joints, and ignition of vapors in the fuel tanks. Wu et al. [81] emphasized that lightning strikes are one of the primary causes of all plane crashes.

Compared to aerospace grade metal alloys, carbon fiber-reinforced epoxy composites lack the high level of electrical and thermal conductivity, which makes these lightweight structures susceptible to lightning strikes. At present, there exist lightning strike protection strategies, which include the use of copper mesh on the outermost surface of the composite. This mesh increases the structural weight, the production and maintenance costs of aircrafts [82].

Vivo et al. [83] investigated the temperature development in an aluminum alloy and carbon fiber reinforced composite after a 100-kA lightning strike via simulation (Figure 30). The aluminium laminate shows three orders of magnitude higher thermal conductivity and six orders of magnitude higher electrical conductivity compared to composite laminate.

In the case of aluminium, a peak temperature of 540 K was observed at the strike area and the produced heat was well dissipated. However, in the case of the carbon fiber laminate (Figure 30.b), temperatures up to $5.3 \cdot 10^6$ K were observed in the laminate center and the generated heat was not effectively dissipated in the in-plane or the through-thickness direction of the laminate owing to a lack of electrical and thermal conductivity.

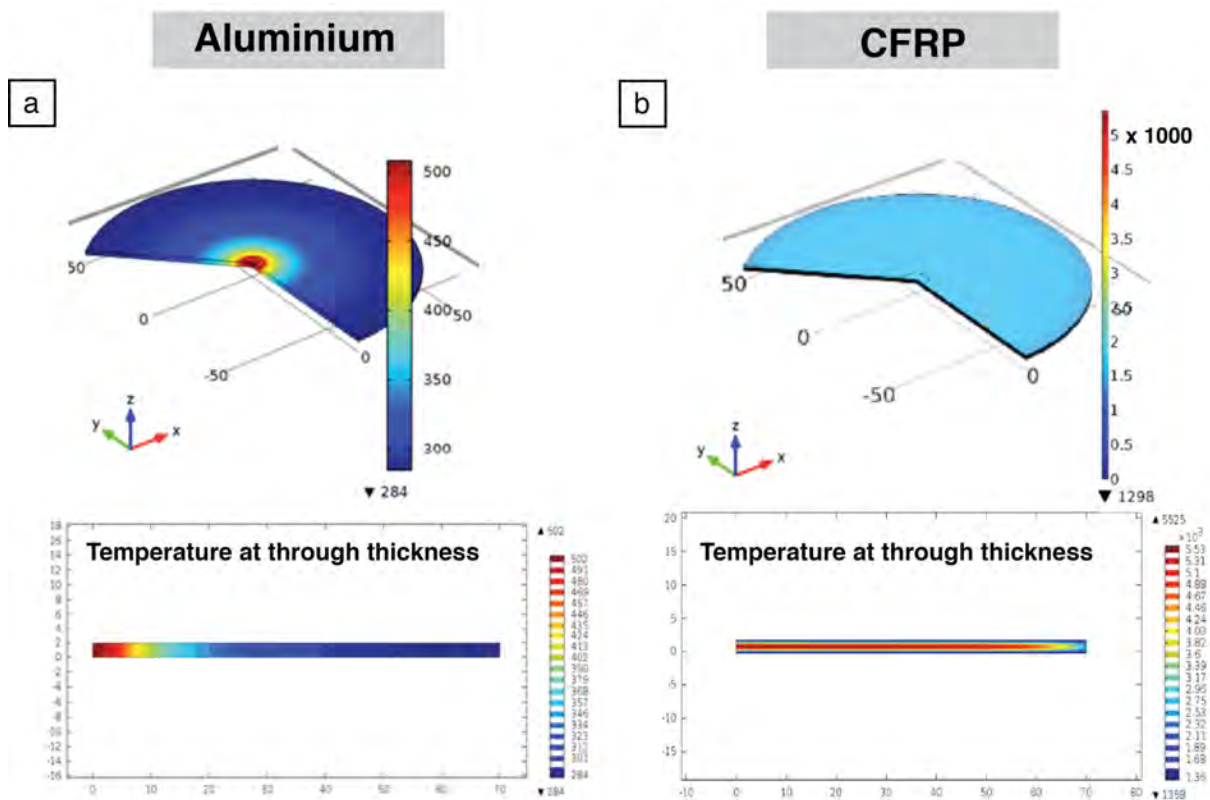


Figure 30. Heat development in a) aluminum laminate and b) CFRP laminate after a 100 kA lightning strike [83]. Temperature scale in aluminum part is up to 500 K (red), whereas in the composite part, the scale is up to 5000 K (red). Modified.

Various research groups have examined the behavior of composites under simulated lightning strike scenarios with various peak currents [83]–[89]. In addition to scholarly efforts to better understand lightning strike resistive composites, studies by industry towards processing and material development towards lightning strike resistive composites were conducted [90], [91]. During the event of a lightning strike on a composite structure, an extreme amount of energy is delivered in micro-seconds, resulting in an expansion of the ionized channel at a supersonic speed. The exceedingly high energy of the lightning transforms itself into kinetic and thermal energy in the laminate, resulting in delaminations and decomposition of the matrix. The thermo-mechanical response of composites under lightning strike depends on various parameters such as lightning peak current, electrical and thermal conductivity, matrix

properties (thermal decomposition temperature), char yield, and the interlaminar fracture toughness of the laminate [87].

Hirano and Kamiyama et al. [82] investigated the effect of the intrinsic electrical conductivity of the polymer matrix on the lightning strike resistance of biaxial CF reinforced polymer composites by comparing epoxy with a polyaniline (PANI) based polymer as the matrix system. The electrical conductivities of PANI based composites were 14800 S/m in-plane and 73 S/m in the z-direction, which are almost 6 and 30 times higher compared to the epoxy based composite, respectively. Although the epoxy CF composite showed much higher mechanical properties with comparable thermal conductivity and thermal decomposition temperature, PANI based composites resulted in substantial improvements in lightning strike resistance (Figure 31). The epoxy CF composite underwent an extensive fiber breakage and matrix decomposition after a lightning strike of 40 kA. On the other hand, the PANI based biaxial CF composite shows minor damage even after impact of a lightning strike of 100 kA. The overall electrical conductivity of the composite showed a critical impact on the lightning strike resistance, although the PANI-based composite is more susceptible to the delaminations compared to the conventional epoxy CF composite.

It is important to note that the interlaminar shear strength (ILSS) of PANI based composites is in the range of 20 MPa (before strike). This makes the usage of this particular composite problematic as a structural composite for aerospace applications. Certified resin systems for aerospace applications show ILSS above 80 MPa (M18, with 55 vol.% CF, Hexcel, USA).

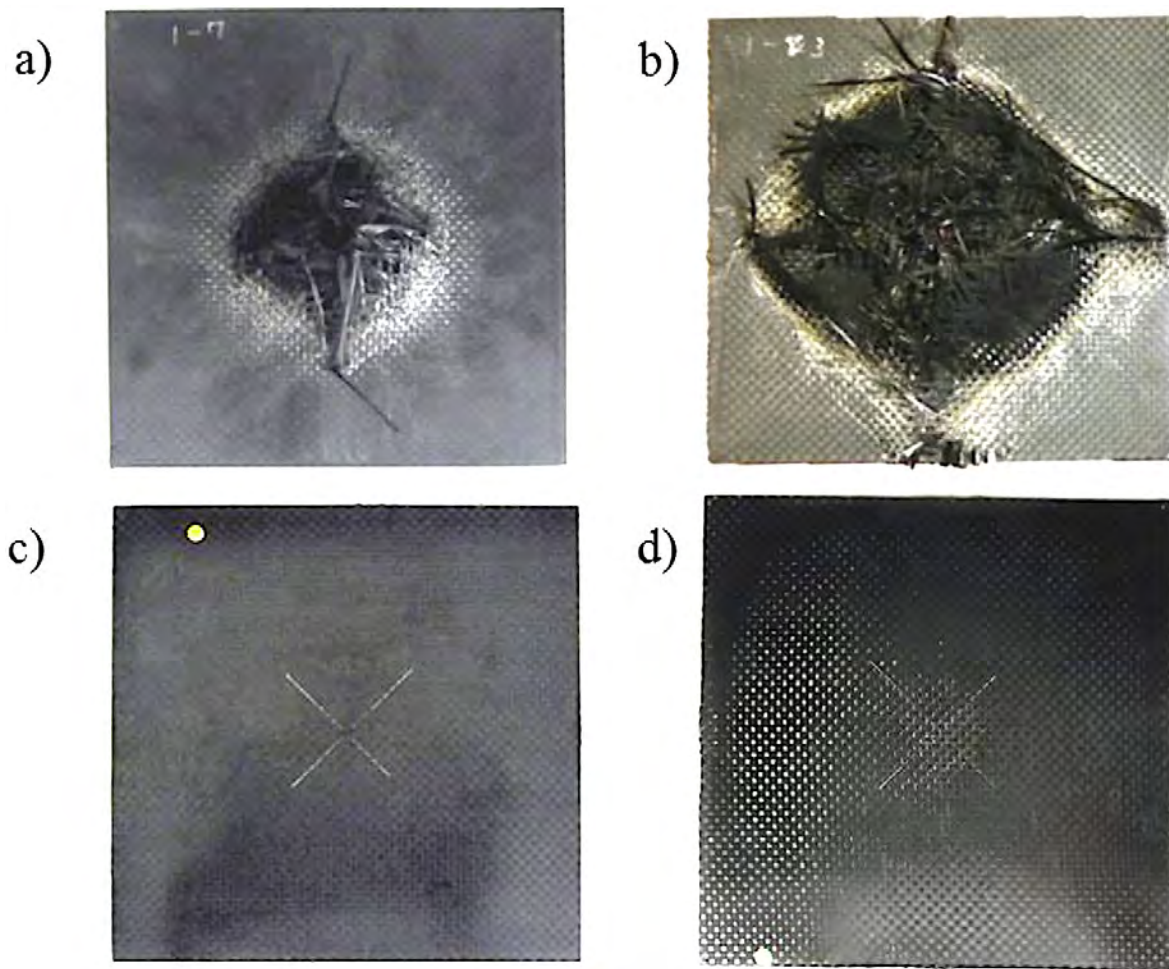


Figure 31. Epoxy-CF laminates after a a) 40 kA strike, b) 100 kA strike, PANI-CF laminates, c) 40 kA strike, and d) 100 kA strike. Laminate dimensions are 15 × 15 cm² [82].

In 2018, Kamiyama et al. [87] studied the effect of matrix properties such as thermal degradation temperature and toughness on the lightning strike resistance of composites. Biaxial CF prepregs of epoxy, bismaleimide (BMI) and polyetheretherketone (PEEK) were processed by an autoclave. 40 kA and 100 kA simulated lightning strikes were applied in accordance with SAE ARP 5412B to the center of each laminate using an impulse current generator. Arc attachment surfaces of each composite after lightning strike testing are shown in Figure 32.

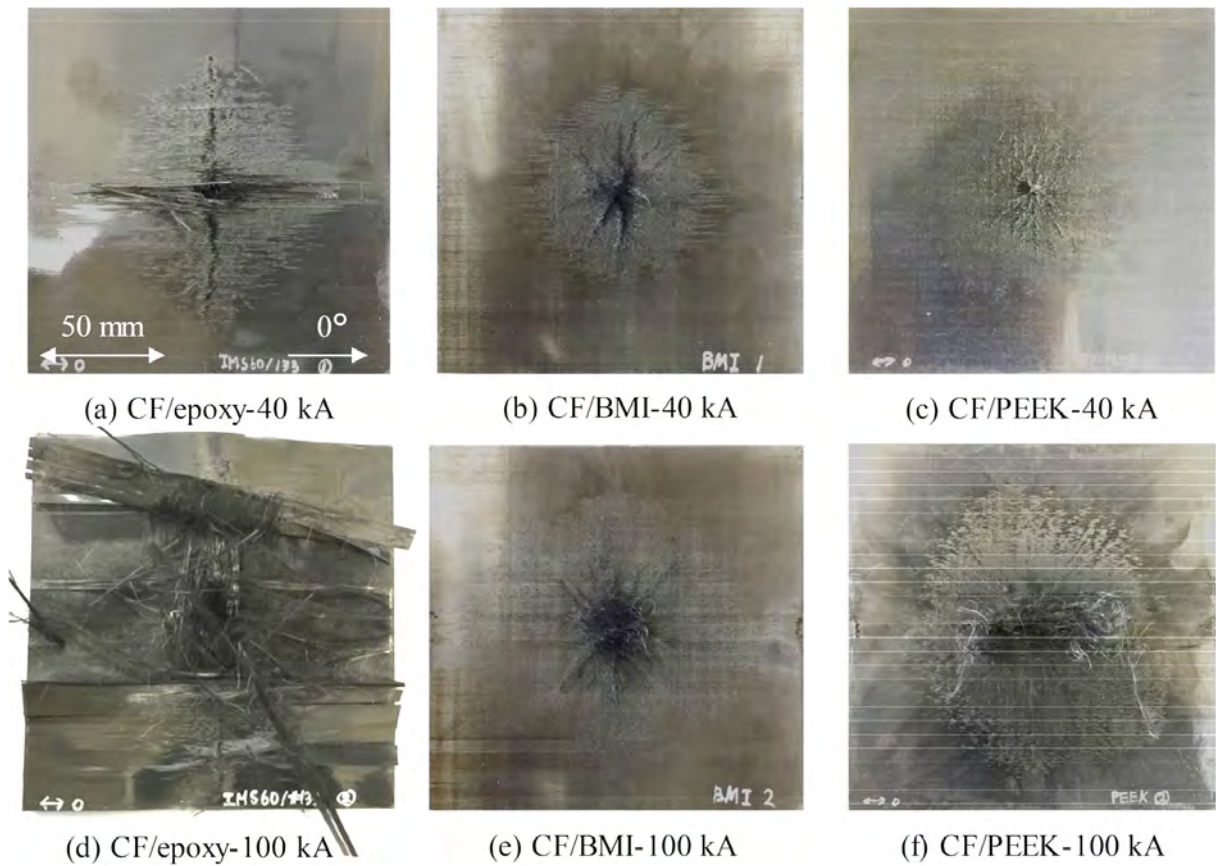


Figure 32. Arc attachment surfaces of a) and d) epoxy based, b) and e) BMI based, c) and f) PEEK based composites after 40 and 100 kA strikes [87].

The BMI-CF composite with higher heat deflection temperature (Figure 32.b and Figure 32.e) and the PEEK-CF composite with higher mode-I interlaminar fracture toughness (Figure 32.c and Figure 32.f) show increased lightning strike resistance compared to the epoxy-based composite. Results suggest that not only the electrical conductivity, but also the matrix relevant properties such as toughness and thermal degradation temperature influence the lightning strike resistance of fiber reinforced composites.

Incorporation of nanoparticles or compact films of nanoparticles is reported to be beneficial as well for the enhancement of lightning strike resistance of composites. This is primarily achieved by enhancing the dissipation of the extreme energy of lightning strike [23], [80], [81], [92], [93].

Zhang et al. [23] incorporated a bucky paper (BP) with the thickness lower than 100 μm as a compacted MWCNTs sheet only at the outer surface of a carbon fiber-epoxy laminate with the help of a heat conductive adhesive. The microstructures of the BP and the produced novel composite laminate are shown in Figure 33.

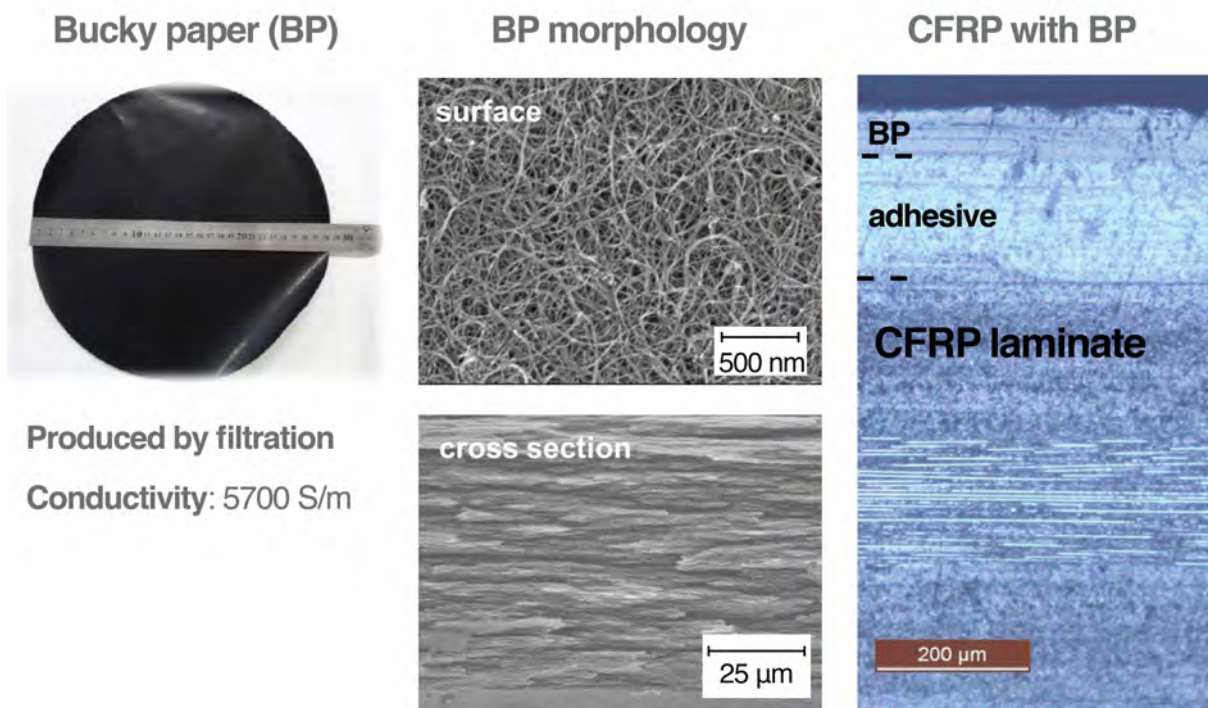


Figure 33. Microstructures of bucky paper (BP) and BP incorporated CFRP [23]. Reworked.

The BP showed an in-plane electrical conductivity of a 5700 S/m. The morphology of the BP shows no orientation of MWCNTs which were highly packed in through-thickness direction (cross sectional morphology, Figure 33). With a thickness of less than 100 μm , BP was bonded to the laminate via an adhesive that was approximately 200 μm thick. This novel composite laminate was then tested under a simulated lightning strike with a 100 kA current flow (Figure 34). Although the copper mesh with $6 \cdot 10^7$ S/m conductivity locally evaporated with a mass loss of 5.65 g after testing, C and B-scans showed only slight surface damage on the mesh, not in the laminate. In the

case of BP modified laminate, in addition to the local evaporation of the BP, only a slight fiber damage in the laminate structure was measured. However, the rest of the composite laminate remained intact. It is worth to note that the incorporation of BP rather than a copper mesh resulted in an overall part weight reduction of 35 % together with an excellent lightning strike resistance.

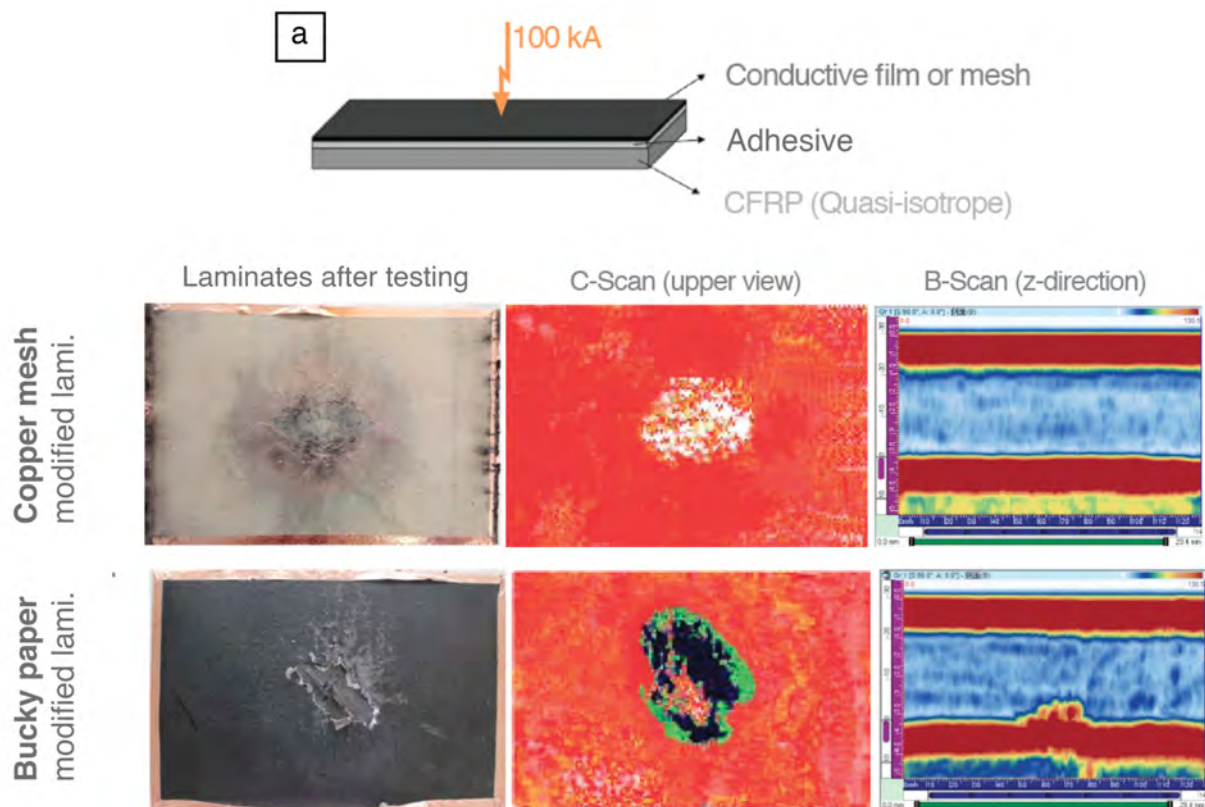


Figure 34. a) Illustration of test set-up, b) Optical pictures and C and B-scans of laminates after lightning strike testing, reworked [23].

Logakis et al. [93] studied the effect of MWCNTs on the lightning strike resistance of an epoxy-CF composite produced via infusion. An aerospace certified resin system (RTM6, Hexcel, USA) was modified with 0.1 wt.% MWCNTs by shear mixing. The study claimed that the MWCNTs were mostly filtered by the CFs and located at the outermost surface of the laminate. The enhancement of the local conductivity at the

outermost surface via nanotubes led to a broader distribution of the strike energy (100 kA), resulting in 40 % higher resistance to lightning strike.

In conclusion, the electrical conductivity is the most important parameter for lightning strike resistance, however, enhanced interlaminar fracture toughness, thermal conductivity, and thermal properties of the resin are also beneficial.

2.6. Summary of the state of the art

Epoxy carbon fiber composites are often used in structural aerospace applications. In addition to excellent mechanical and thermo-mechanical performance, a certain degree of electrical conductivity is desired for electro-static dissipation and lightning strike resistance. Composites having electrical conductivity above 10^{-4} S/m can already dissipate the electrostatic loading, where higher conductivities are necessary for enhanced lightning strike, EMI shielding ($> 10^{-1}$ S/m) and resistive heating ($> 10^1$ S/m). Although CFs are anisotropic conductors to a certain extent, the highly insulating nature of the epoxy resins reduces the conductivity of the composite and leads to semiconducting behavior in the z-direction. Interleaf toughened laminates have epoxy-rich interlayers, which further diminishes the z-direction conductivity.

There are two main strategies reported in the literature leading to an increased conductivity of epoxy and its fiber reinforced composites. The first strategy is mainly based on the dispersion of conducting nanoparticles in an insulating polymer matrix. According to percolation theory, an extreme conductivity change of the host polymer is observed, where conductive particles form a three-dimensional network. Carbon nanoparticles are excellent candidates for conductive epoxy nanocomposites due to their high intrinsic electrical conductivity and their low density which prevents the particle sedimentation compared to metal particles. The CNTs form a conductive network at the lowest additive content in various epoxy resins, followed by CB and GNPs.

Although CB has comparatively lower intrinsic electrical conductivity due to its amorphous nature with sp^3 hybridized bonds, it shows a great potential for electrically conductive resins because of percolating network formation with comparably low additive contents (as low as 0.1 wt.%). Additionally, CB is cheaper compared to the other nanoparticles. *Consequently, CB is chosen as the conductive additive for this work due to the affordable price and performance balance.*

The other main strategy involves the incorporation of two-dimensional conductive layers or coated fleeces into fiber-reinforced composites either at the outermost layer or as interleaf in between each fiber-rich layer. *This strategy does not necessarily follow the percolation theory and mostly results in a two-dimensional enhancement of conductivity, therefore is not considered in this work.*

The electrical conductivity of carbon nanoparticle modified epoxy nanocomposites and their laminates is dependent on various parameters, including particle type and aspect ratio, processing conditions, ionic strength of the resin, external applied electrical field, and a dispersed second phase in the resin (e.g., tougheners).

The excellent pre-dispersion of the conductive nanoparticles enhances the electrical conductivity because the additives agglomerate mostly in a sub-micron level if they are dispersed as primary particles prior to curing. *In the literature, three-roll milling was suggested to be the most suitable dispersion method for the conductive additives. That method is also investigated in this work.*

The addition of $CuCl_2$ salt leads to decreased repulsive Coulomb forces in between CB particles. According to the literature, this results in a high number of finer agglomerates and thus a highly conductive epoxy-CB composites at low particle content. *However, due to the lack of information regarding the effect of this salt on the mechanical properties and the environmental stability of the fiber reinforced composites, the effect of $CuCl_2$ salt is not studied in this work.*

The network formation of conductive particles is strongly influenced by the presence of a second phase in the resin. The second phase might be conductive particles or insulating tougheners. However, the morphology development and intermolecular interactions between these two phases in epoxy remain poorly understood. *Because of this knowledge deficit, the effect of various tougheners on the network formation of the CB is addressed in this study.*

In the case of fiber reinforced epoxy composites, the through-thickness electrical conductivity largely depends on the type of the fibers (glass or carbon), in addition to the parameters discussed above. It was reported that CFs dominate the conduction by fiber to fiber contacts, where the carbon nanoparticles increase the conductivity only to a small degree by bridging the non-contacting fibers. *However, there is a lack of information regarding the effect of fiber volume content on the electrical conductivity of the carbon fiber epoxy laminates and resulting composite morphology. Consequently, this aspect is investigated during this work.*

Some studies have reported that the addition of interleaf fleeces in laminates substantially decreases the through-thickness electrical conductivity. *However, a systematic study investigating the effect of carbon-based nanoparticles on the conductivity of interleaf toughened composites by varying the additive content remains unreported in the literature and is therefore investigated in a detail in this work.*

Lightning strike resistance of a composite depends on various material properties, mainly electrical conductivity, thermal conductivity, interlaminar fracture toughness of the composite, finally thermo-mechanical properties and thermal degradation temperature of the matrix polymer. Among these parameters, enhanced electrical conductivity either at the outermost surface or in the z-direction is crucial for higher lightning strike resistance. *Thus, the effect of increased electrical conductivity on the lightning strike resistance of the prepreg laminates is addressed briefly in this work.*

3 Aims of the work

The main scientific aim of this study was focused on the understanding of the impact of amorphous carbon black nanoparticles on the electrical and mechanical properties of epoxy carbon fiber prepreg laminates without and with interleaf regions. The relationship between the carbon fiber volume content and the electrical conductivity of neat prepreg laminates gained a particular attention. Finally, efforts were done to correlate the through-thickness electrical conductivity with the lightning strike resistance of the laminates.

The main technical focus on the other hand is to develop interleaf toughened and electrically conductive prepreg laminates having the properties of;

- Excellent thermo-mechanical properties of the resin system; $T_{g-dry} > 200\text{ }^{\circ}\text{C}$ together with $T_{g-wet} > 160\text{ }^{\circ}\text{C}$
- High through-thickness (z-direction) electrical conductivity; $E_{dc} > 10\text{ S/m}$
- Enhanced interlaminar fracture toughness under different loading modes; $G_{Ic} > 400\text{ J/m}^2$ together with $G_{IIc} > 1000\text{ J/m}^2$

Figure 35 is a schematic representation of the main experimental routes used to reach the scientific and technical aims of this thesis.

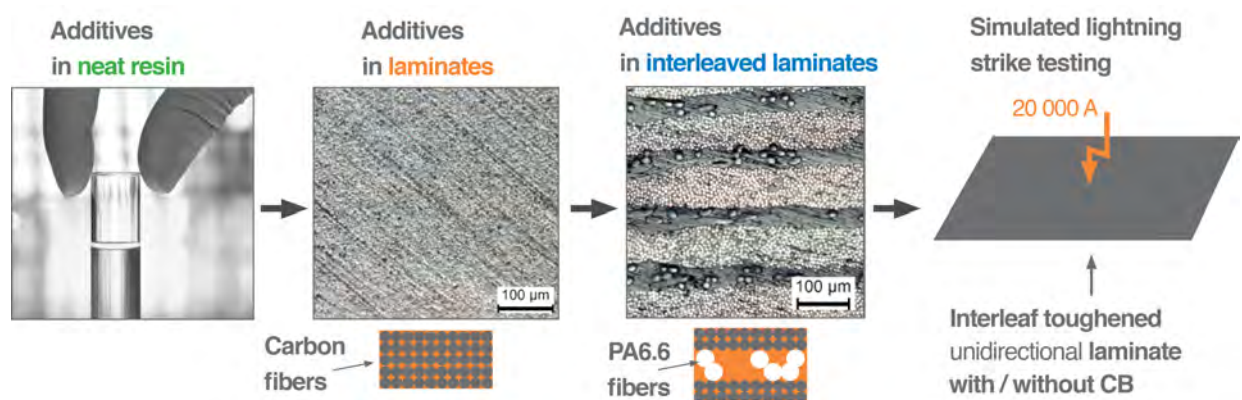


Figure 35. Schematic illustration of the structure of the work.

Various sub-aims are defined to reach the overarching goals of the thesis. At first, an epoxy resin system consisting of multifunctional epoxy resins is formulated to achieve excellent thermo-mechanical properties. As shown in Figure 35, the scientific interest was then focused on understanding the effect of CB nanoparticles on the viscosity of uncured resin and thermo-mechanical, mechanical, and electrical properties of the cured nanocomposite. Efforts were made to refine a suitable processing method to disperse CB nanoparticles perfectly prior to curing. The experimental results are discussed together with the optical, scanning and transmission electron microscopical analysis.

Focus was as well laid on the understanding of the network formation of carbon black in the presence of unidirectional CFs. The effect of CB under the constraint of the carbon fibers is important to analyze because the inter-fiber distance in CF-epoxy prepreg laminate is very low. Prior to adding CB to the matrix resin in prepreps, understanding the relationship between CF volume content and electrical conductivity of the neat laminates has to be established. The effect of CB nanoparticles on the through-thickness conductivity and the mechanical properties of the prepreg laminates are investigated and correlated to the composite morphology.

As discussed previously, resin rich interleaf areas diminishes the through-thickness electrical conductivity of composites further. Therefore, focus is laid strongly on the investigations of the impact of the PA6.6 fleece in neat epoxy-CF laminates. The effect of CB on the conductivity of the laminates with interleaf fleece is especially noteworthy because the CFs do not dominate the through-thickness electrical conduction due to the insulating resin-rich interlaminar areas. Besides electrical properties, mechanical properties of these laminates are investigated as well.

The last sub-goal is related to the correlation of through-thickness electrical conductivity with the lightning strike resistance of interleaved laminates with and without CB nanoparticles. To reach this goal, laminates were tested under a current impulse with a 20 kA peak current.

4 Materials and methods

4.1. Materials

Resins for primary structures in the aerospace industry require proven mechanical properties, high thermal and chemical resistance, low moisture uptake, and hot-wet performance. The epoxy resin used in this study is a blend of diglycidylether of bisphenol A, DGEBA resin, Baxxores 2200[®] (epoxy equivalent weight: 182 g mol⁻¹, provided by BASF, Germany, price ≈ 4 €/kg), and tetraglycidyl methylene dianiline (TGMDA) resin, Epikote[™] 496 (epoxy equivalent weight: 115 g mol⁻¹, provided by HEXION, Germany, price ≈ 40 €/kg). As the hardener, 4,4'-diaminodiphenyl sulfone (4,4'-DDS) ORGANICA[®] (amine equivalent weight: 62 g mol⁻¹ provided by Feinchemie GmbH, Germany, price ≈ 80 €/kg) was chosen because of its latency and stiff molecular structure. No accelerator was used in the resin system. TGMDA and 4,4'-DDS are common reactive molecules for aerospace-grade resins because of their high functionality and stiff aromatic groups in the molecules.

The chemical structures of the mentioned molecules are presented in Figure 36.

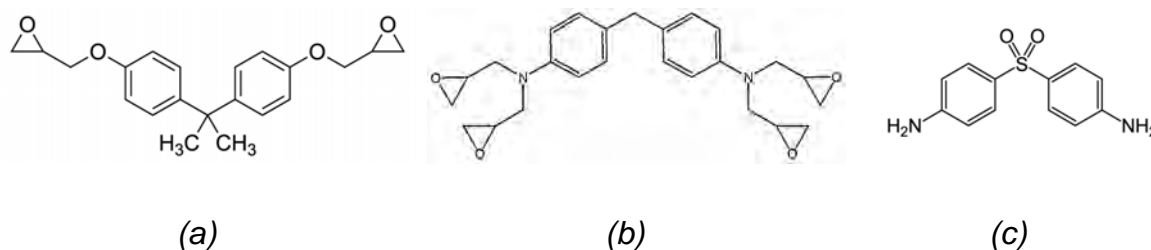


Figure 36. a) DGEBA resin, b) TGMDA resin, c) 4,4'-DDS hardener

Carbon black (CB, Printex XE-2B, 1000 m²/g BET surface area, Orion Engineered Carbons GmbH, Germany) was chosen as the conductive nanoparticle. Orion Engineered Carbon GmbH offers as the market leader various other CB products with much lower BET surface area, which are mostly used for coating and coloring applications (Printex U, V, etc.). The high surface area of the conductive nano-additive is beneficial to achieve conductive polymer nanocomposites. Printex XE-2B is sold as micron-sized aggregated particles promoting a safe handling of the powder. Scanning electron micrographs of the as-purchased CB powder reveal the size of aggregates and single CB nanoparticles (Figure 37). Quasi-spherical single CB nanoparticles have a particle diameter of 30 nm (measured by SEM).

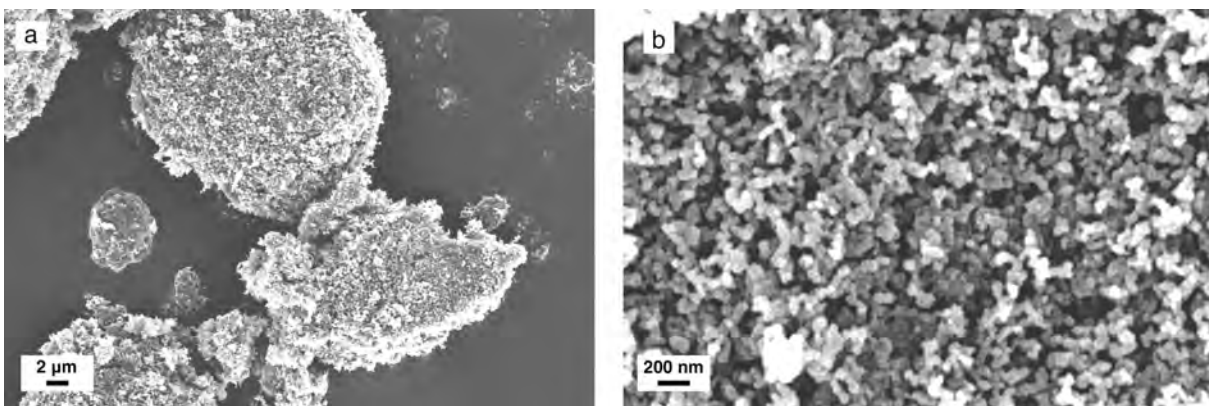


Figure 37. SEM micrographs of CB aggregates as purchased. a) single aggregates up to 50 μm, b) single particles of CB, strongly aggregated.

As *organic tougheners*, insoluble spherical core-shell particles (CS, Albidur 2240-A, EVONIK AG, Germany) and soluble polyethersulfone with a minimum of 50 % -OH termination (PESU, Ultrason E-2020P SR, BASF, Germany) were used.

As *carbon fibers*, the polyacrylonitrile based 12K high-tenacity unidirectional carbon fiber rovings (HTS40 F13-12K, Toho Tenax Europa GmbH, Germany) were used. Each fiber roving consists of 12 000 single filaments with an average diameter of 7 μm. The fiber surface contains a polyurethane-based sizing. Fibers do not involve any

stitching and were spread by the prepreg machinery during prepreg processing.

A polyamide 6.6 non-woven fleece (PA6.6 fleece, provided by TFP Global, United Kingdom) was chosen as *the interleaf spacer*. The areal weight of the PA6.6 fleece is 10 gr/m², and the melting temperature of the PA 6.6 is approximately 270 °C (via DSC). This melting point ensures the stability of the interleaf fleece during the curing of the resin system, which reaches a maximum temperature of 200 °C. Thermogravimetric analysis results indicated that water content of as purchased PA6.6 fleece was approximately 1 wt.%. The PA6.6 fleeces were therefore dried in a vacuum oven at 70 °C for a minimum of 24 h before the prepreg hand-lay up process. Dynamical mechanical thermal analysis results indicated that PA6.6 fleece did not influence the hot-wet T_g of the laminates and hot-wet properties of the laminate were still dominated by the epoxy resin (hot-wet conditioned T_g of neat resin and PA6.6 fleece modified laminate are measured to be 201 and 200 °C, respectively).

4.2. Processing

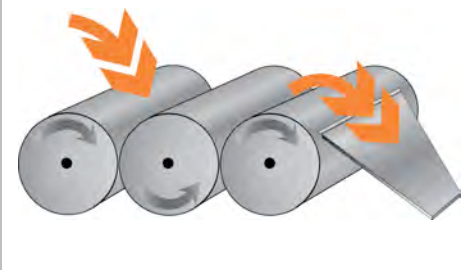
4.2.1. Manufacturing of neat resin plates and nanocomposites

For neat resin plates, the calculated amount of TGMDA and DGEBA was first mixed at 60 °C in an oil bath with a laboratory stirrer (\approx 500 rpm, 20 min). The temperature of the resin mixture was then increased to 140 °C and a stoichiometric amount of the 4,4'-DDS component was added. The hardener was dissolved for 25 to 30 min at 140 °C under precise temperature control. The reactive mixture was immediately degassed (at 10-20 mbar for minimum 10 minutes) after dissolving the hardener and poured into a steel mold for final curing of the plates. The resin plates were cured at 180 °C for 150 min and post cured at 200 °C for an additional 60 min in a convection oven.

In case of CB modified epoxy nanocomposites, the processing route includes additional steps. Lindner et al. [94] pointed out that CB nanoparticles can be toxic because of their high specific surface area and absorbed detrimental polycyclic aromatic hydrocarbons at their surface during their production. To reduce the risk of

human exposure to these caustic fumes, CB pre-dispersion in the DGEBA-TGMDA resin blend was completed in a laboratory stirrer at 60 °C under a fume hood using a respiratory mask. After the nanoparticles were dispersed in the resin, the three-roll milling technique (3RM, EXAKT 120 EH-450 mill, EXAKT, Germany) was utilized before adding the hardener to the resin-CB mixtures. Parameters for dispersion are listed in table 1. The processing procedure was applied two times at a speed of 300 rpm.

Table 1. Parameters used during 3-roll milling of carbon black-epoxy resin mixtures

	Temperature of rolls	50 ± 5 °C
	1 st gap distance	60 μm
	2 nd gap distance	40 μm

After three-roll milling processes, a stoichiometric amount of 4,4'-DDS hardener was added to the CB modified epoxy resins at 140 °C for 30 min by using a laboratory stirrer. To produce CB modified epoxy nanocomposite plates, the reactive mixture was degassed and poured into a steel mold. The curing procedure is similar to the neat resin processing, as described previously.

In the case of resin systems mixed additionally with organic tougheners, a calculated amount of toughener was added at 140 °C during the blending of the TGMDA and DGEBA and mixed with the laboratory mixer for one hour.

The uncured neat and CB modified epoxy resin systems were stored at -18 °C until prepreg processing. To produce 100 m of unidirectional epoxy-carbon fiber prepregs, minimum 2 kg of resin was prepared.

4.2.2. Prepreg processing

The unidirectional prepregs were produced via hot-melt processing in the laboratory scale prepreg impregnation machinery of the University of Bayreuth (EHA Composite Machinery GmbH, Germany). Figure 38 shows the prepreg machinery used.



Figure 38. Laboratory-scale prepreg impregnation machine at the Department of Polymer Engineering. Below, left to right: roving organization, fiber pre-spreading, resin coating, and a final prepreg.

The important parameters during prepreg production are listed in table 2. The unidirectional 12K CF rovings were organized and spread on the pre-spreading unit (Figure 38, below, second from the left). The resin film was coated at 70 °C using a siliconized carrier paper on the coating unit of the prepreg machinery. Heating zones and the impregnating calendar were set to 100 °C.

Table 2. Prepreg production parameters

Materials	
Fibers	HTS 40 F13 12K CF rovings (16 rovings)
Resin (neat)	TGMDA-DGEBA-4,4'-DDS
Carrier paper*	Low siliconized Mondi GL wh G02J1
Cover paper*	Highly siliconized Mondi GL wh G02J1
Machinery parameters	
Gap at coating unit	180 μm
Machinery speed	1 to 5 m/min
Resin film coating type	Direct coating**
<i>Temperatures</i>	
Coating unit (rolls and resin container)	70 °C
Infrared heater (for fibers)	Off
Heating zone 1 and 2	100 °C and 30 °C, respectively
Heated calendar	100 °C
Cooling table	15 °C
<i>Tensional forces</i>	
Cover paper (rewinder)	50 N
Carbon fiber	850 to 1000 N
<i>Pressures</i>	
Heated calendar	6 bar
Pulling calendar unit	5 bar
<i>Prepreg properties</i>	
Target areal weight of prepreg	$\approx 140 \text{ g/m}^2$
Target resin content of prepreg	$\approx 42 \text{ wt.}\%$, 50 vol.%
Prepreg width	$\approx 160 \text{ mm}$

* Carrier and cover papers are provided by Mondi, Austria.

** Direct coating: coating of the resin system directly on the siliconized carrier paper through the resin container and first calendar roll.

Pre-spread fibers were impregnated by the epoxy resin to the final prepreg after passing the first heating zone and the heated calendar. The quality of the produced prepregs is very sensitive to deviations of the production parameters. Therefore, the

prepreg production was monitored continuously by a self-written application called “Prepreg Data Tracker” (University of Bayreuth, Germany). This program is designed to simultaneously trace all changes of the chosen parameters during the production.

4.2.3. Hand lay-up and laminate curing

Unidirectional prepreg laminates were produced via hand-lay up and autoclave curing. Figure 39 shows the hand-lay up of a standard 3 mm prepreg laminate with images of the reference prepreg and cured prepreg laminate. In total, 26 prepreg layers were hand-layed up to achieve 3 mm thick laminates. Only the 2nd and 25th prepreg layer were chosen along the 90° fiber direction to optimize the handling of the unidirectional structure. In the center plane, a perforated 50 mm thick teflon film was inserted as a crack initiator for the interlaminar fracture toughness testing.

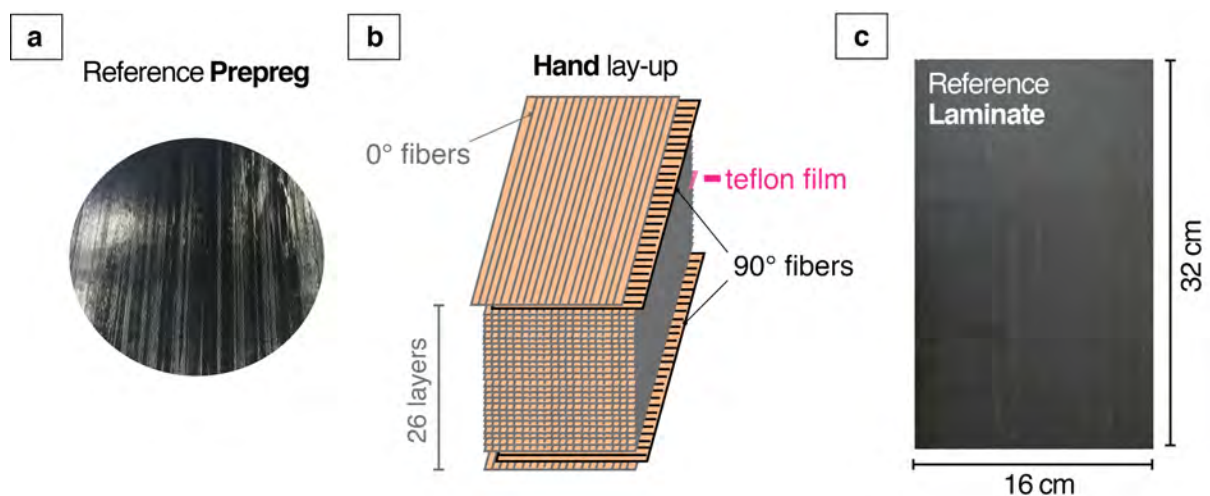


Figure 39. a) reference prepreg, b) structure of the hand-layed up prepreg laminate and c) cured laminate.

The prepreg stacks were then cured and consolidated under vacuum and external air pressure in a self-built autoclave (Figure 40). A self-built steel form with 40 mm thickness was pressed in a hydraulic press (LZT 110L, Langzauner, Austria).

Dimensions of the pressurized volume produced in the autoclave were $400 \times 400 \times 30 \text{ mm}^3$, which is enough to produce prepreg laminates. The steel form was pressurized by pumping the external air into the mold with a maximum air pressure of 8 bar. The vacuum was created by a pump and applied only to the non-consolidated laminate. The pressurized chamber was heated by the hydraulic press from the top and bottom.

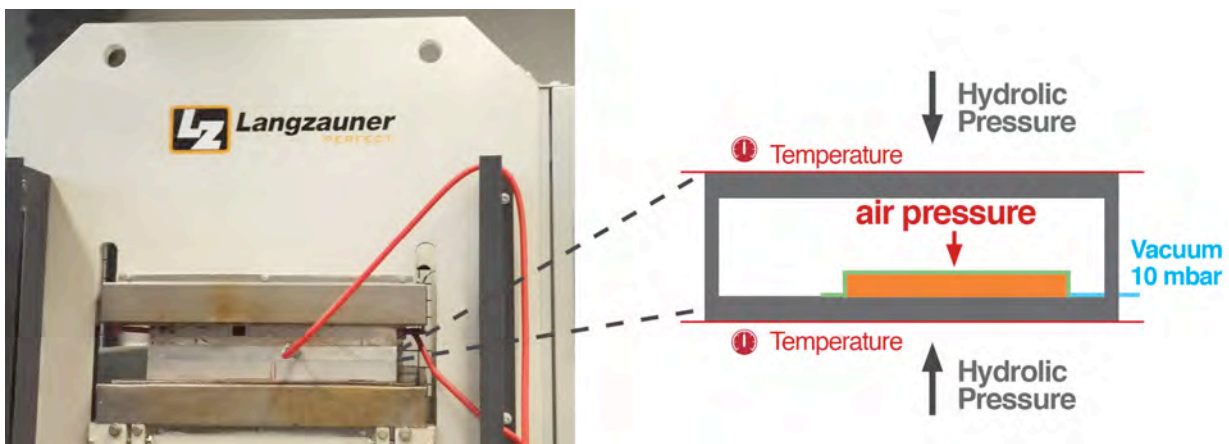


Figure 40. Self-built autoclave system for curing the prepreg laminates

Figure 41.a shows the optimum curing cycle during production for both temperature and the pressure, where the Figure 41.b shows the viscosity of the neat resin during production. The temperature profile applied to cure the prepreg laminates is the same profile used to cure the resin plates.

Figure 41 indicates that curing takes place in three isothermal steps. During the first heating step up to $140 \text{ }^\circ\text{C}$, the viscosity drops to 100 mPas (see Figure 41.b), and then starts to increase during the isothermal step at $140 \text{ }^\circ\text{C}$. Up to this point, a vacuum of 10-20 mbar was applied to the laminate. The vacuum was closed after 10 minutes at $140 \text{ }^\circ\text{C}$. The degassing and the primary consolidation of the laminate take place within this first isothermal step. During the second isothermal step, the autoclave temperature reaches to $180 \text{ }^\circ\text{C}$ and remains at this temperature for 150 minutes while the laminate

cures further. Post-curing of the laminates then occurs at 200 °C for 1 hour. Following, the autoclave is cooled down to 30 °C.

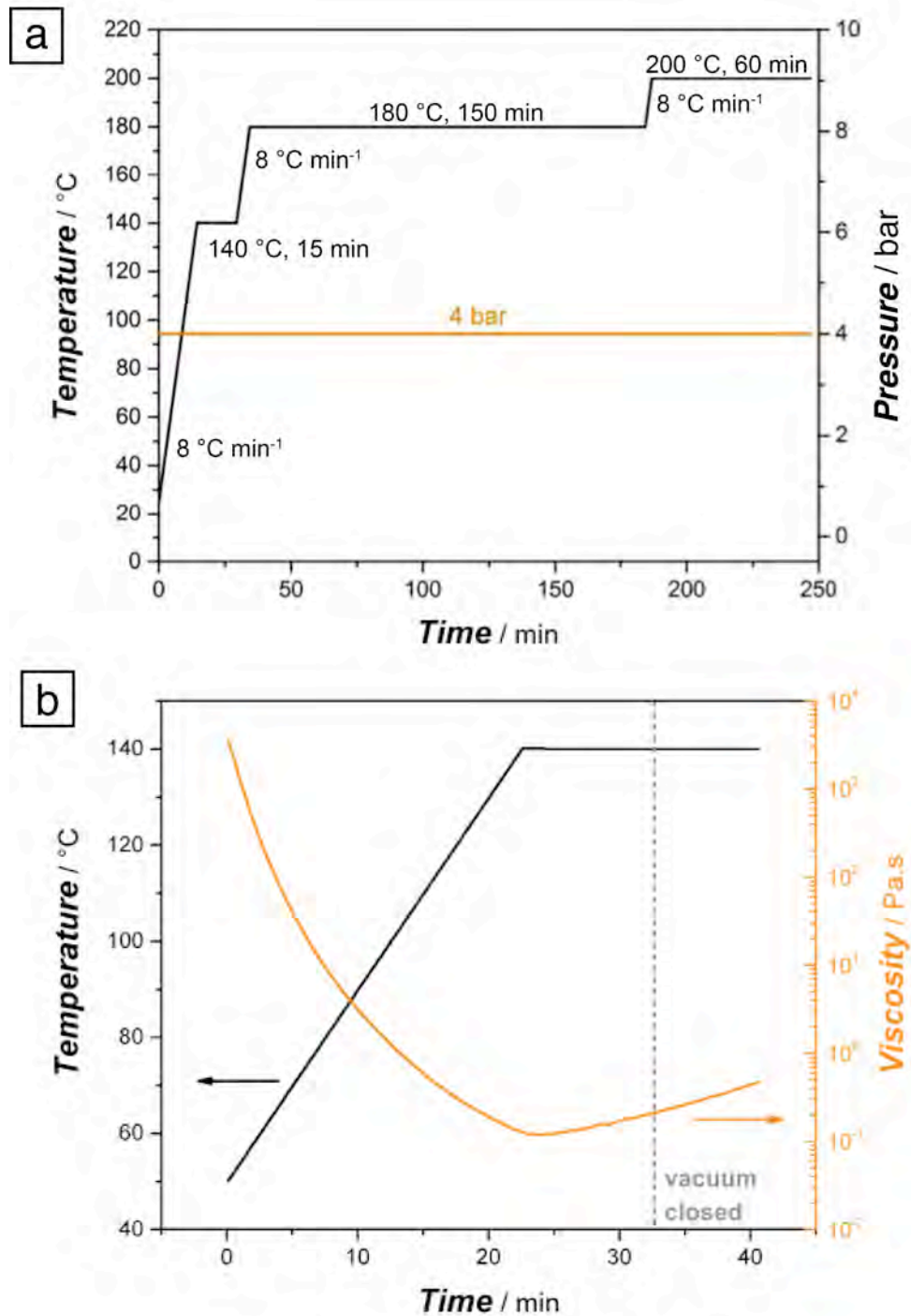


Figure 41. a) Temperature and pressure profile of the autoclave during curing, b) temperature and viscosity profile of the resin at processing conditions.

4.3. Experimental methods

4.3.1. Viscosity measurements of uncured resins

Viscosity of the resins was measured under oscillation mode with a Rheoplus MCR 301 rheometer (Anton Paar, Austria). The heating rate and distance between two plates was set to 2 K/min and 1 mm, respectively. Deformation amplitude (γ) was 15 % with an angular frequency (ω) of 1 rad/s. The analysis was aborted when the Moment stepped over the threshold of 150 mNm.

4.3.2. Dynamical mechanical thermal analysis

Dynamical mechanical thermal analyses (DMTA) were performed according to DIN EN ISO 6721-7 using an advanced rheometric expansion system (ARES RDAIII, Rheometrics Scientific) in torsional mode. A deformation of 0.1 % was chosen with a frequency of 1 Hz from 25 to 250 °C. The heating rate was set to 3 K/min. According to the standard, rectangular samples were used (50 × 10 mm²) for cured resin samples as well as prepreg laminates. The glass transition temperature (T_g) of the cured resin plates and their prepreps was then carefully evaluated from the G' onset. To measure the wet T_g , DMTA samples were conditioned for 14 days in water at 70 °C prior to testing. Only slight surface drying was applied to samples prior to DMTA testing after immersion in hot water.

4.3.3. Non-destructive ultrasound testing of cured laminates

To investigate the quality of the overall cured unidirectional CF-epoxy prepreg laminates as well as the damaged area after the lightning strike testing, non-destructive ultrasound tests were performed using a HFUS 2400 (Air Tech, Dr. Hillger Ingeniurburo, Germany) test machine. The tests were done in distilled water.

4.3.4. Fracture toughness testing

The critical stress intensity factor (K_{Ic}) was determined according to ISO 13586 using CT specimens. The overall specimen length was 41.25 mm while the specimen length from the loading point (w) was 33 mm and the specimen thickness (d) was 4 mm. For each sample, a sharp crack was generated by tapping a new razor blade into the machined V-notch. The tests were carried out using a universal testing machine Zwick BZ2.5/TN1S (Zwick GmbH & Co. KG, Ulm, Germany). The crack opening displacement (COD) was measured using a clip extensometer (632.29F-30, MTS, Germany).

The K_{Ic} of the neat epoxy and nanocomposites were calculated according to Equation (1). F_{max} is the maximum force required to propagate the crack, d is the sample thickness, w is the specimen length from the loading point, a is crack length, and $f(a/w)$ is a geometrical factor.

$$K_{Ic} = \frac{F_{max}}{d\sqrt{w}} f\left(\frac{a}{w}\right) \quad (1)$$

Critical strain energy release rate (G_{Ic}) is calculated according to Equation (2). E_{SH} is the elastic modulus calculated according to the theory of Saxena and Hudak from the material compliance during unstable crack propagation.

$$G_{Ic} = \frac{K_{Ic}^2}{E_{SH}} \quad (2)$$

The interlaminar fracture toughness of the cured prepreg laminates under modes I and II loading were tested according to the DIN EN 6033 and 6034 standards, respectively, using a universal testing machine (Zwick Z050, Zwick-Roell, Germany). The samples have a rectangular geometry of $250 \times 25 \times 3 \text{ mm}^3$. At the cracked side of the samples, aluminum blocks were glued to be able to apply the mode-I force. The initial load was 2 N, followed with a testing speed of 10 mm/min. A minimum of five samples per laminate were tested.

4.3.5. Scanning and transmission electron microscopy

Fracture surfaces of nanocomposites and prepreg laminates were examined with a Zeiss 1530 (Carl Zeiss AG, Oberkochen, Germany) scanning electron microscope having a field emission cathode. The acceleration voltage was set to 1.5 kV. The morphologies of nanocomposites were characterized using a LEO 922 A EFTEM transmission electron microscope (Carl Zeiss AG, Oberkochen, Germany) with an acceleration voltage of 200 kV. Thin sections of 50 nm were cut on a Leica Ultracut microtome (Leica Biosystems GmbH, Nussloch, Germany) equipped with a glass knife.

4.3.6. Electrical conductivity measurements

The electrical conductivity of the nanocomposites and prepreg laminates were measured *only in the solid state* according to ASTM D257 using a Keithley 2100 multimeter or Keithley 6517A high-resistance meter (for neat resin) applying the direct current (DC). Volume electrical conductivity (E_{dc}) was calculated from measured volume conductance (G_{dc}) using Equation (3), where d is the sample thickness and A is the area of the measuring electrode. The ground resistance (R_g) of the measuring system was 0.3Ω , which is taken into account during calculations.

$$E_{dc} = \frac{d}{A} G_{dc} \quad (3)$$

In case of epoxy resins and CB modified epoxy nanocomposites, the samples were cured in a rheometer in between two round brass electrodes at the fixed electrode distance. Controlled curing the samples with the electrodes led to an excellent contact between the resin and electrodes. During curing, a 1 mm sample thickness was held constant. The effective electrode diameter was 4 cm. Samples are schematically shown in Figure 42.

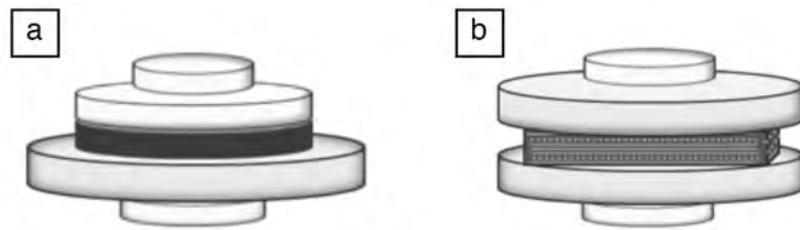


Figure 42. Electrode-sample configurations of a) neat resin and CB-epoxy nanocomposites, and b) prepreg laminates with or without CB modification.

In the case of cured prepreg laminates with or without CB, samples were first carefully polished to remove the first insulating epoxy layer on the sample surface. Samples were then measured with the same type of the round brass electrodes.

4.3.7. Image analysis

ImageJ was used to calculate the fiber to fiber distances in prepreg laminates without PA6.6 interleaf fleece. This method allows to achieve a very rough estimation regarding the fiber to fiber distances in fiber rich zones of the consolidated laminates. Figure 43 shows the calculation method schematically.

More than 140 fiber to fiber distances were calculated from SEM micrographs (cross-section) of the neat consolidated laminate. Since the produced 3 mm thick neat laminate contains approximately 5 million single carbon fibers, it is not possible to run the analysis for the complete laminate. Therefore, only fiber rich zones in the laminates were focused for the analysis to achieve a rough estimation of fiber distribution in the fiber rich zones of the laminates.

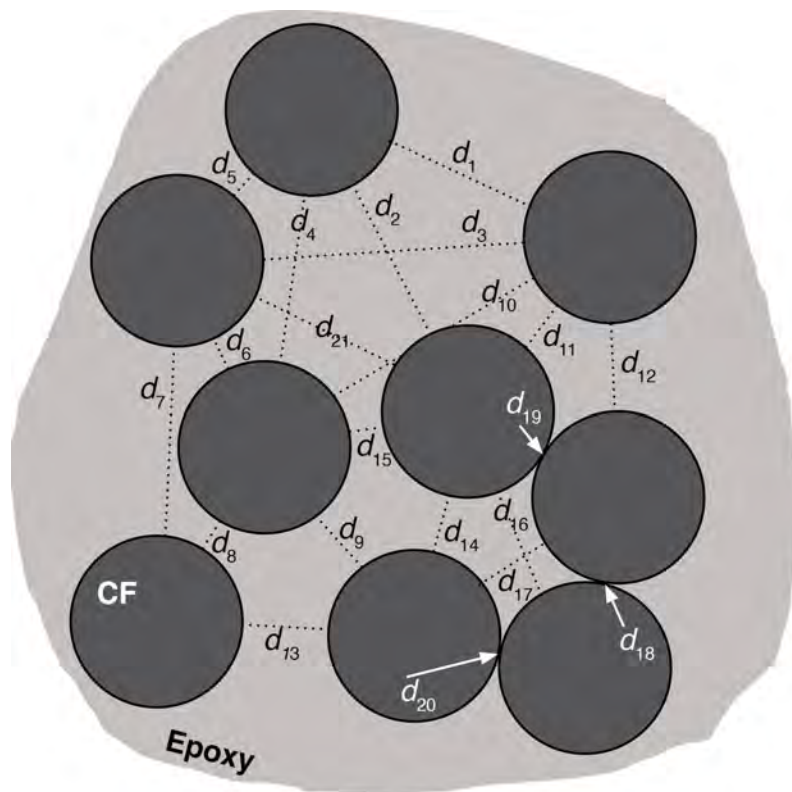


Figure 43. Illustration of calculation of the fiber to fiber distances in the neat consolidated laminate via ImageJ.

4.3.8. Simulated lightning strike testing

The SAE ARP 5412 standard written by the Society of Automotive Engineers (SAE) defines three different lightning zones for a commercial aircraft [95]. Figure 44 presents the lightning strike zones schematically.

Zone 1 refers to the regions of an airplane that are most likely to attract the lightning strikes. Zone 2 represents the regions likely to experience the subsequent swept strokes. A lightning strike might enter from the radome portions of an airplane (Zone 1A), however, it might be pushed back to spread over the fuselage (Zone 2A) until the exit. Zone 3 consists of the areas that are highly unlikely to experience an initial lightning strike.

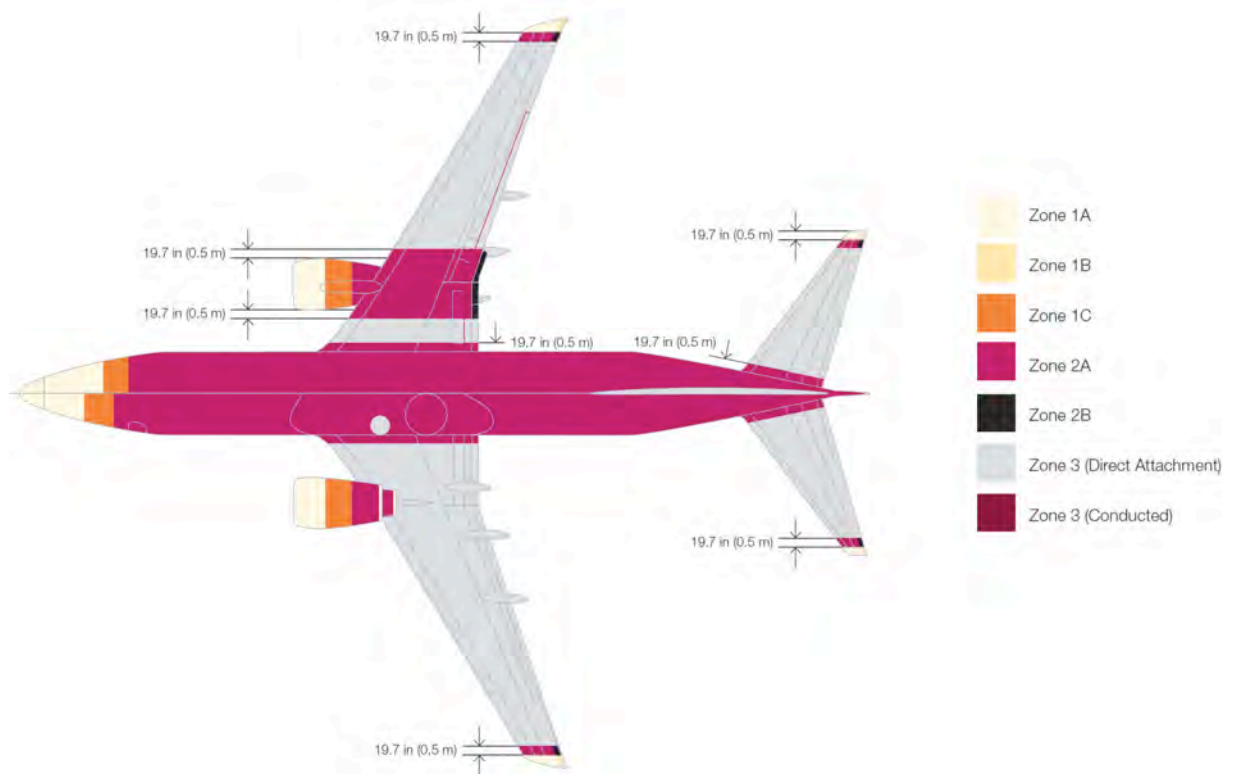


Figure 44. Lightning zone divisions of a commercial airplane [96].

The standard SAE ARP 5412 divides the lightning strike current waveforms into four different components (Figure 45, waveforms A to D). Although the current waveform consists of all four component types, A and D are mostly used as reference waveforms to simulate lightning strikes. Zone 1 likely experiences the initial stroke with component A, other zones are likely to be subjected to intermediate current (component B) and continuing currents (component C), as well as a restrike (component D). Previous studies published in literature [82], [95] have used a current waveform similar to component A with peak currents varying from 10 to 100 kA to characterize the composite's ability to dissipate the extremely high energy of a stimulated lightning strike.

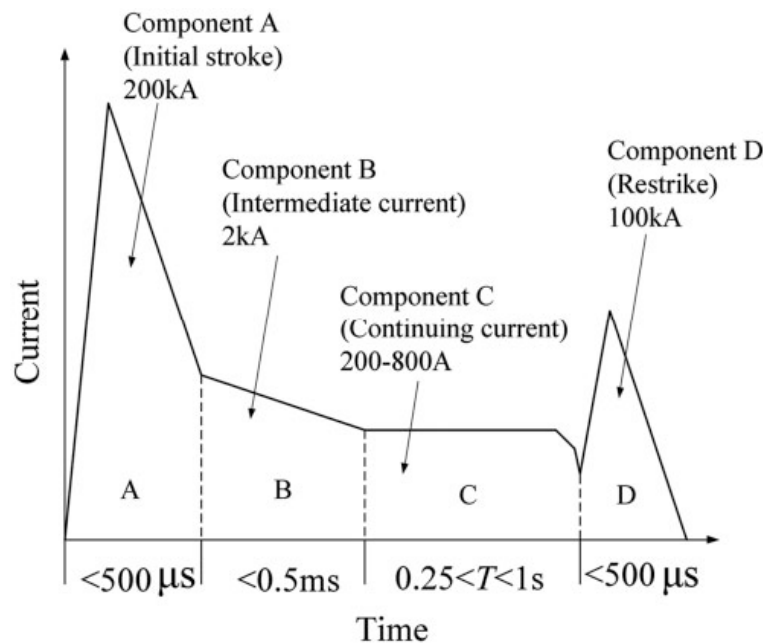


Figure 45. Simulated normative lightning strike current waveforms according to SAE ARP 5412 [95].

An impulse generator at the Technical University, Ilmenau, with a maximum capacity of 50 kA was used for the strike testing (Figure 46). In this work, a peak current of 20 kA was chosen as the peak current for the lightning strike experiments.

Tested samples were fixed with a picture frame-type copper jig, as shown in Figure 46.b. The impulse current was conducted to the center of the tested laminates via a spherical discharge electrode located approximately 20 mm above the laminate (Figure 46.b). In addition, the applied current was measured simultaneously during testing by a digital oscilloscope.

Due to the fact that the capacity of the generator can not reach to the 200 kA and the waveform generated may slightly vary to the SAE ARP 5412 standard, the lightning strike testing performed in this work is only used for comparison reasons.

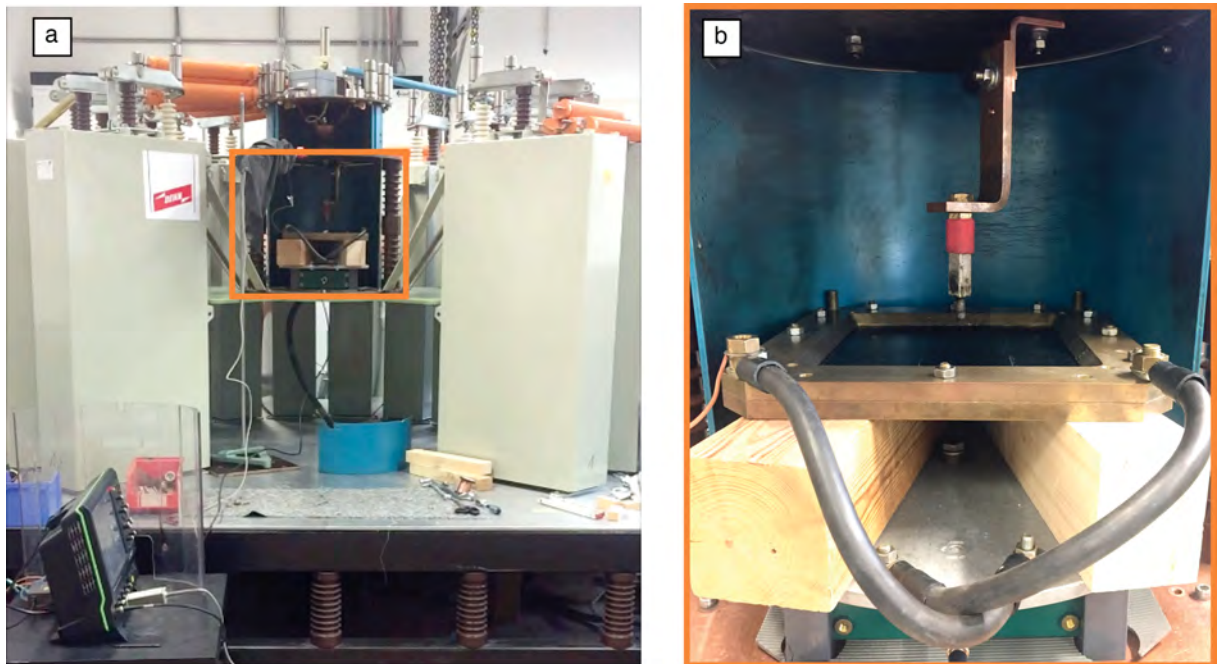


Figure 46. a) Impulse generator at TU Ilmenau (max. 50 kA). Colored area shows the location of the sample b) Sample placed in copper jig. The discharge electrode can be seen in the picture.

5 Results and discussions

5.1. Resin studies

5.1.1. Neat resin

As the first step, it is aimed to formulate a resin system with excellent thermo-mechanical properties in the both dry (target $T_{g\text{-dry}}$: 200 °C) and wet conditions (target $T_{g\text{-wet}} > 160$ °C), together with an optimal price and performance balance. The DGEBA resin was blended with different ratios of TGMDA and cured stoichiometrically with 4,4'-DDS. The glass transition temperatures of these various blends were then investigated via DMTA, in dry condition. Results are summarized in Figure 47.

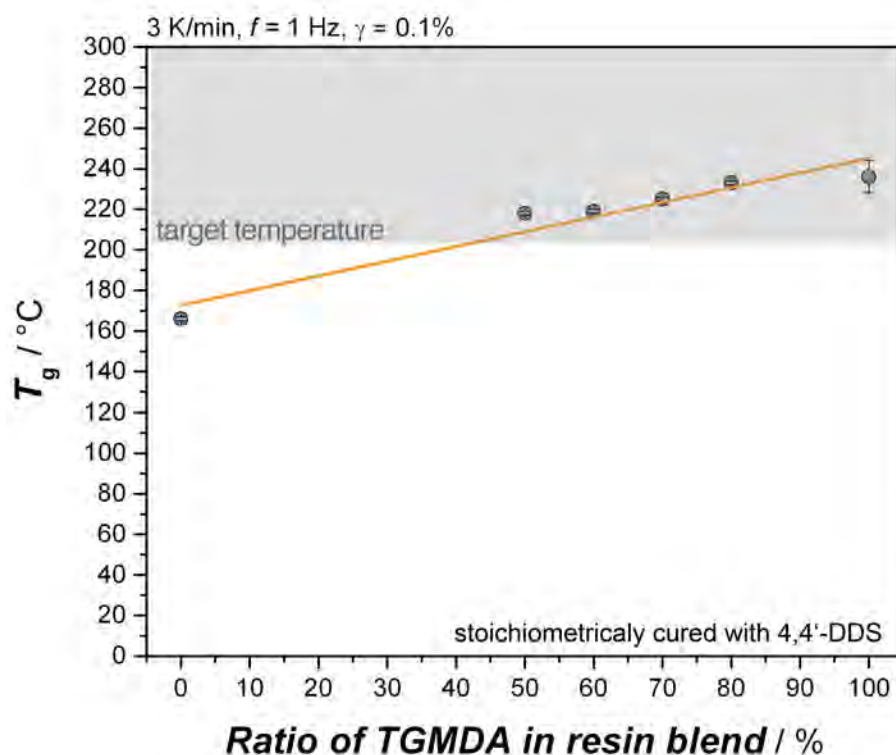


Figure 47. Glass transition temperatures of different resin blends of TGMDA and DGEBA cured stoichiometrically with 4,4'-DDS.

The DGEBA-4,4'-DDS system has a T_g of 166 °C, whereas the T_g of neat TGMDA-4,4'-DDS system is 236 °C. Because the target T_{g-dry} was set to 200 °C, only blends with a minimum of 50 % TGMDA in the resin component were studied. A 60 / 40 blend of TGMDA-DGEBA cured with 4,4'-DDS with a T_g of 219 °C was chosen as a reference resin blend and tested further with DMTA after hot-wet conditioning of the sample according to the AIRBUS internal standard. Figure 48 shows the storage modulus (G') of the dry and wet conditioned samples of 60 / 40 TGMDA-DGEBA blend cured with 4,4'-DDS.

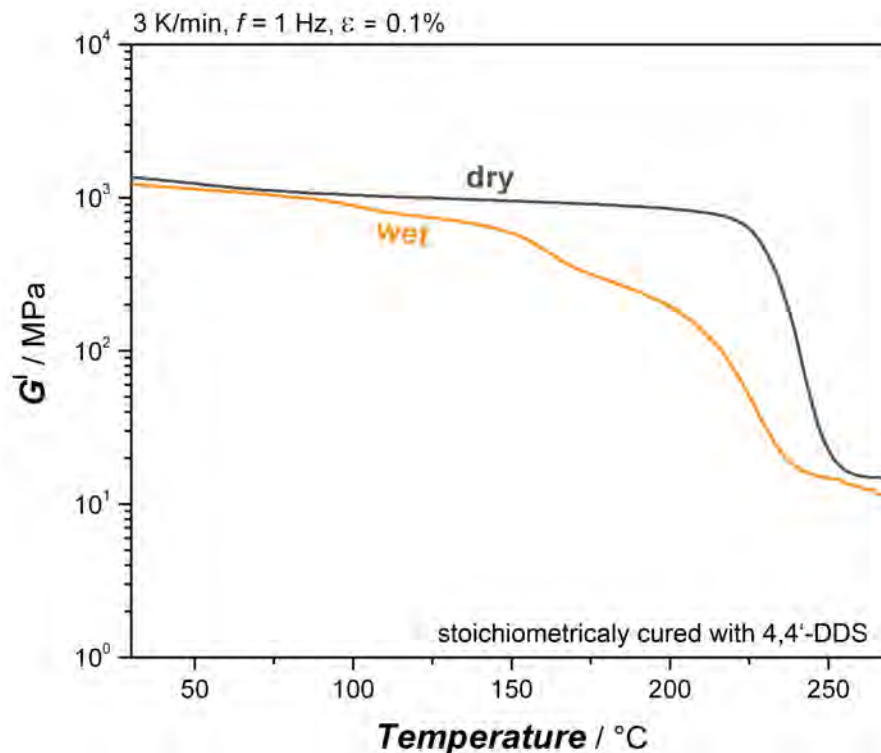


Figure 48. G' as a function of temperature for neat resin at dry and hot-wet conditions. Hot-wet conditioning was performed according to the AIRBUS internal standard, 14 days immersed in 70 °C distilled water.

The dry neat resin sample shows a T_g of 219 °C, while the hot-wet conditioned neat resin sample shows a continuous decay of the storage modulus with a major drop at

201 °C. The slight increase of storage modulus (or shoulder) observed around 150 °C for the hot-wet conditioned epoxy is attributed to the evaporation of the absorbed water, which is not captured in the crosslinked network. Consequently, the 60 / 40 TGMDA-DGEBA resin blend cured with 4,4'-DDS is chosen as a reference resin system because it meets the targeted dry and wet thermo-mechanical properties.

The main mechanical and thermo-mechanical properties of the neat resin system consisting of a 60 / 40 TGMDA-DGEBA resin blend are summarized in Table 3.

Table 3. Main properties of the neat resin system with a 60 / 40 TGMDA-DGEBA blend

$T_{g,dry}$ °C	$T_{g,wet}^*$ °C	K_{Ic} MPa. \sqrt{m}	G_{Ic} J/m ²	E_t GPa	σ_y MPa	ϵ_b %	E_{dc} S/m
219	201	0.48 ± 0.04	71 ± 11	3.6 ± 0.2	57 ± 5	1.9 ± 0.2	$7.7 \cdot 10^{-12} \pm 6 \cdot 10^{-12}$

* $T_{g,wet}$ is measured after immersion of samples in 70°C distilled water for 14 days.

The measured critical stress intensity factor (K_{Ic}) of the neat resin is 0.48 ± 0.04 MPa \sqrt{m} , which is slightly lower compared to most of the amine-cured resin systems. The brittle nature of the resin system is reflected by low strain at break (ϵ_b) and ultimate tensile strength (σ_y) under loading. The use of a tetra-functional epoxy and aromatic hardener consisting of stiff phenol rings lead to a high thermo-mechanical performance under wet conditions but low fracture toughness of the resin.

The electrical conductivity of the neat resin is measured as $7.7 \cdot 10^{-12}$ S/m under direct current (DC), which reflects the highly insulating nature of the neat epoxy. It is well known in the literature that epoxy resins are insulating polymers. Table 4 lists the conductivity of resins measured by five independent research groups.

Table 4. Electrical conductivity (E_{dc}) data of various neat epoxy resins

Research Group	Conductivity (S/m)	Resin chemistry	Measurement unit
-	-	-	-
Chekanov et al. [97]	$\approx 10^{-11}$	Epoxy (no further details)	Impedance meter
Tantawy et al. [98]	$\approx 10^{-12}$	Epoxy (no further details)	Two electrode tech.
Lonjon et al. [5]	$7 \cdot 10^{-12}$	Epoxy, M21 (Hexcel)	AC, Impedance spectrometer
Aal et al. [9]	10^{-13}	DGEBA, aromatic hardener	DC, electrometer
Ma et al. [29]	$\approx 6 \cdot 10^{-13}$	DGEBA, amine hardener	DC and AC

Electrical conductivity of neat epoxy systems depends on several parameters, including the molecular structure and the purity of the reactive components. The conductivity of unfilled epoxy systems mostly falls in the range of 10^{-13} to 10^{-11} S/m. The electrical conductivity of the neat resin system measured in this work ($7.7 \cdot 10^{-12}$ S/m) agrees with reported values in the literature.

5.1.2. Carbon black-epoxy nanocomposites

5.1.2.1. Dispersion of carbon black via various processing methods

As Chandrasekaran et al. [57] reported, the processing route is one of the most important factors affecting the pre-dispersion of conducting particles in the matrix, and therefore strongly influences the final composite morphology. The method chosen for nanocomposite processing should transfer sufficient dispersive energy to reduce the nanoparticle agglomerate size prior to curing. Re-agglomeration occurs during curing at elevated temperatures owing to the increased mobility of the conductive particles in the uncured resin. Therefore, a percolation network can be achieved at very low additive contents only if conductive additives are dispersed effectively prior to curing and re-agglomerate well during curing reaction.

In this work, two processing routes are first compared in terms of their efficiency for particle dispersion. Figure 49 shows the viscosity and optical micrographs of 1.5 wt.% CB modified epoxy processed via laboratory mixer and 3RM. The amount of CB was fixed to 1.5 wt.% to study the effectiveness of various dispersion processes.

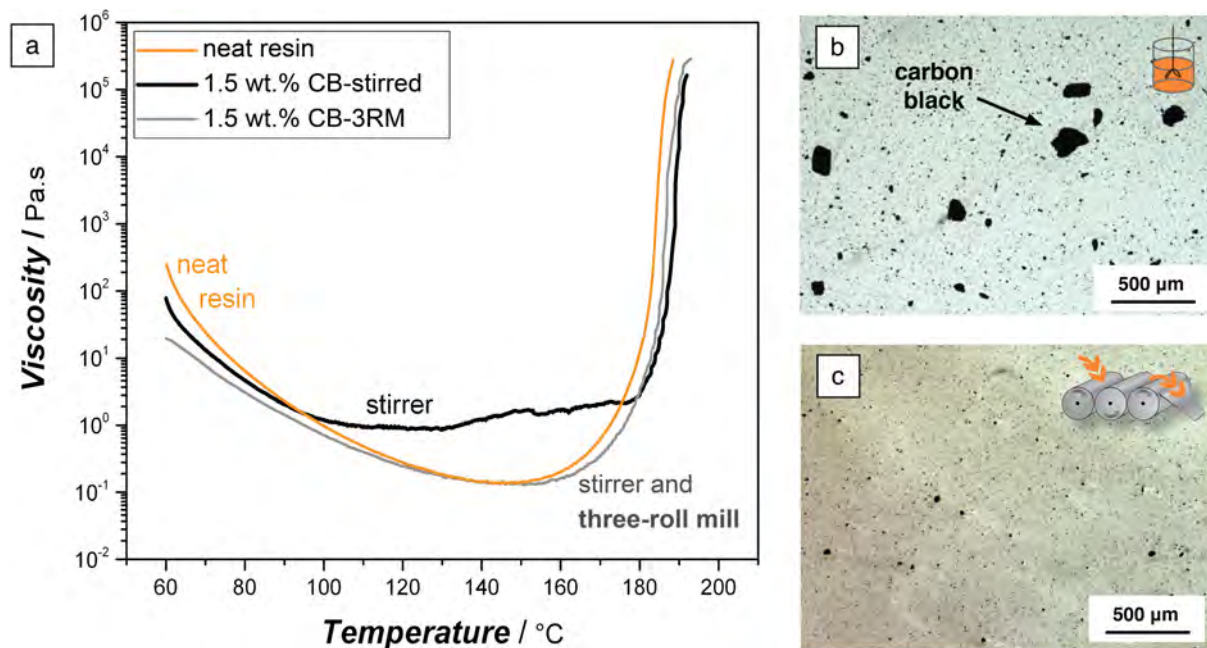


Figure 49. a) Viscosity of neat resin and 1.5 wt.% CB containing nanocomposites produced via stirring and 3RM. Optical micrographs of uncured 1.5 wt.% CB modified epoxy processed via b) laboratory mixer, and c) three-roll mill.

The neat epoxy resin shows the typical rheological behavior of a reactive system, including a decrease of viscosity with increasing temperature until the cross-linking reaction starts to dominate the rheological behaviour of the resin. A minimum viscosity of approximately 100 mPas was observed at 150 °C for neat resin. The incorporation of CB dispersed via 3RM does not strongly influence the viscosity of neat resin system, as presented in Figure 49.a. The suspension processed via stirrer (or laboratory mixer) showed no further decrease of viscosity after 100 °C, which is mostly owing to agglomerates dominating the rheological response of the suspension. Godara et

al. [99] observed this unusual viscosity behavior in a pristine MWCNT modified epoxy system and proposed a correlation with large agglomerates dominating the measurement because of friction of these agglomerates with the plates.

Micrographs of uncured CB-epoxy suspensions under the transmitted light reveal the difference between the mixer and 3RM methods regarding the quality of the nanoparticle dispersion (Figure 49.b and c). Prior to dispersion, CB particles are strongly aggregated as a powder product. Dispersion of CB nanoparticles with the laboratory mixer leads to a good distribution of the particles in resin but with agglomerates up to 250 μm in lateral dimension (Figure 49.b). On the other hand, processing of the 1.5 wt.% CB in epoxy resin with 3RM results in a perfect dispersion and distribution of CB nanoparticles (Figure 49.c), where the observable agglomerates show a maximum diameter of 40 μm .

A reduction of the agglomerate size by increasing the applied shear forces on nanoparticles is expected, and the same trend was observed by Chandrasekaran [57] and Kulkarni et al. [70]. It is reasonable to conclude that this processing technology is more suitable for manufacturing of conductive epoxy systems compared to standard mixing at low additive content due to the fact that the 3RM decreases the maximum agglomerate size to 40 μm prior to the curing reaction. Therefore, 3RM is the standard dispersion technique used during following production processes in this work.

Finally, a dispersion quality of up to 2 wt.% CB modified epoxy systems prior to curing was studied to ensure sufficient dispersion of the particles prior to gelation and curing of the resin. Figure 50 presents optical micrographs of uncured epoxy with up to 2 wt.% CB.

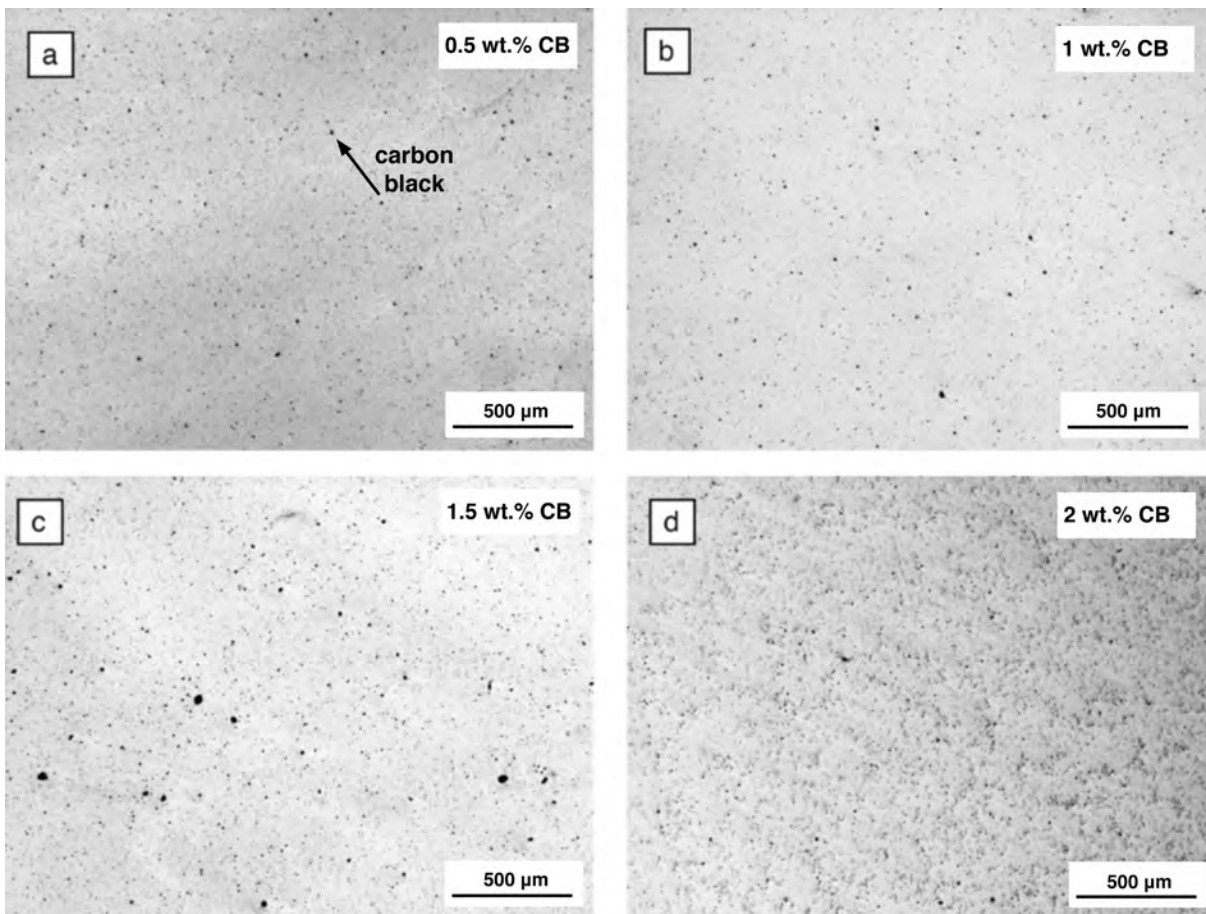


Figure 50. Optical micrographs of a) 0.5 wt.% CB, b) 1 wt.% CB, c) 1.5 wt.% CB, and d) 2 wt.% CB dispersed in epoxy system via 3RM. Resins are uncured, investigated at 23 °C.

The micrographs indicate that regardless of the CB content in the resin, excellent CB dispersion and distribution can be achieved prior to curing using the 3RM process. The maximum agglomerate size observed was 40 µm for each CB content.

5.1.2.2. Effect of carbon black content on viscosity of epoxy resin

The aim of this section is to investigate the influence of CB particle content on the viscosity of the neat resin system. The viscosity of the neat and modified resins is important because the resin viscosity at coating unit of the prepreg machine must be between 200 mPas and 50 Pas for a successful prepreg production. Too low resin

viscosity results in droplet formation of resin film on the carrier paper, while too high resin viscosity prohibits complete coating of the resin on the carrier paper. The effect of CB content on the viscosity of the neat resin is shown in Figure 51 with an indication of a processable viscosity window by the prepreg machine.

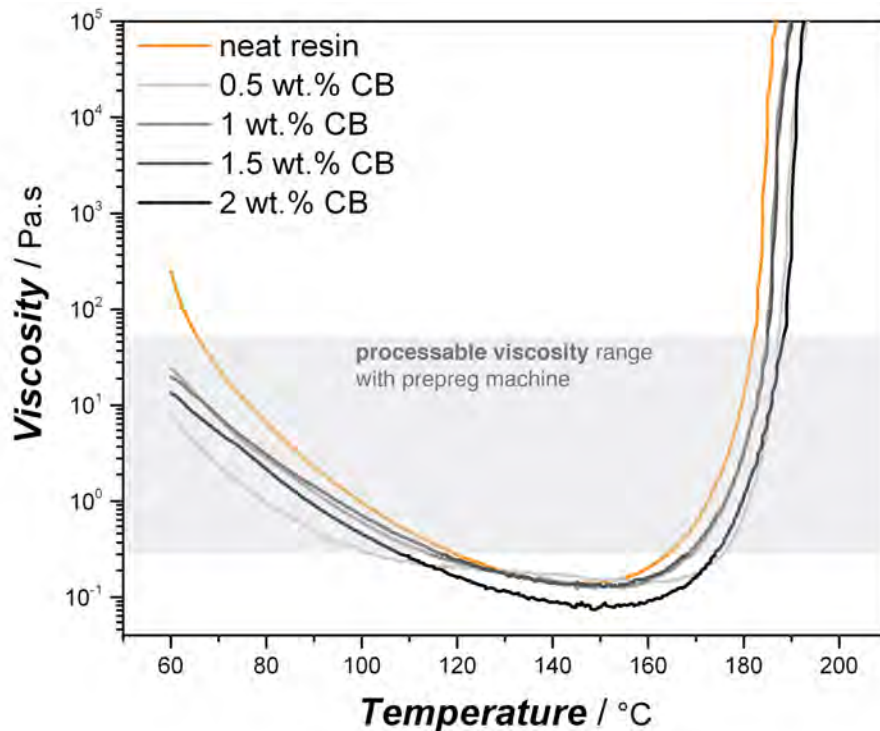


Figure 51. Viscosity measurements of neat resin and up to 2 wt.% CB modified epoxy under oscillation. Heating rate is 2 K/min.

The introduction of CB nanoparticles in epoxy via 3RM up to 2 wt.% does not significantly influence the viscosity of the epoxy system. The deviations of the measured viscosity of different systems can be attributed to the varying stirring times of resin-hardener components during mixing of the reactive components. The viscosity minimum for all materials is observed at approximately 150 °C. In addition, the incorporation of CB up to 2 wt.% does not change the onset of the viscosity increment which is due to a cross-linking reaction. Because resins with a maximum viscosity of 50 Pas can be processed with the prepreg machinery, from a rheological point of view,

it is possible to process neat epoxy and all CB modified epoxy resins at the coating unit within the temperature range of 70 to 100 °C.

Godara et al. [99] studied the effect of various carbon nanotubes on the processability and mechanical properties of CNT modified epoxy prepregs. No major influence of nanotube addition on the resin viscosity was observed for most types of nanotubes. Il'in et al. [100] indicate that dispersion, the distribution of particles and interfacial affinity in between particles and resin have an influence on the final viscosity of the nanocomposite. According to the literature, the addition of inorganic particles into resin systems mostly increases the viscosity by limiting molecular mobility [101]–[104] of the resin. Yearsley et al. [101] studied the effect of carbon-based nanoparticles (CB and CNTs) in an epoxy matrix and highlighted that nanoparticles increase the viscosity and induce shear thickening behavior, although the neat epoxy behaved as a Newtonian fluid.

Consequently, the minor impact of CB on the viscosity of DGEBA-TGMDA-4,4'-DDS system is attributed to effective pre-dispersion of CB in the resin, as well as very low particle-matrix interfacial affinity. The observed deviations in the viscosity are attributed to the slight differences in the mixing times of hardener in the resin. However, due to problems with degassing, it was not possible to reach additive contents above 2 wt.% in the resin.

5.1.2.3. Effect of carbon black on T_g of epoxy resin

The glass transition of an epoxy resin is the temperature range at which the amorphous polymer experiences a transformation from a glassy to a rubbery state. In addition to the molecular structure of reactive molecules and cross-linking density, the existence of inorganic additives as a second phase can influence the T_g of the matrix [105]–[108]. As stated by Kosmidou et al. [105], the addition of inorganic particles into a polymeric matrix can influence the T_g by constraining the mobility of neighboring polymer chains

or by influencing the free volume of the matrix. The T_g of the neat and CB modified epoxy nanocomposites are shown in Figure 52.

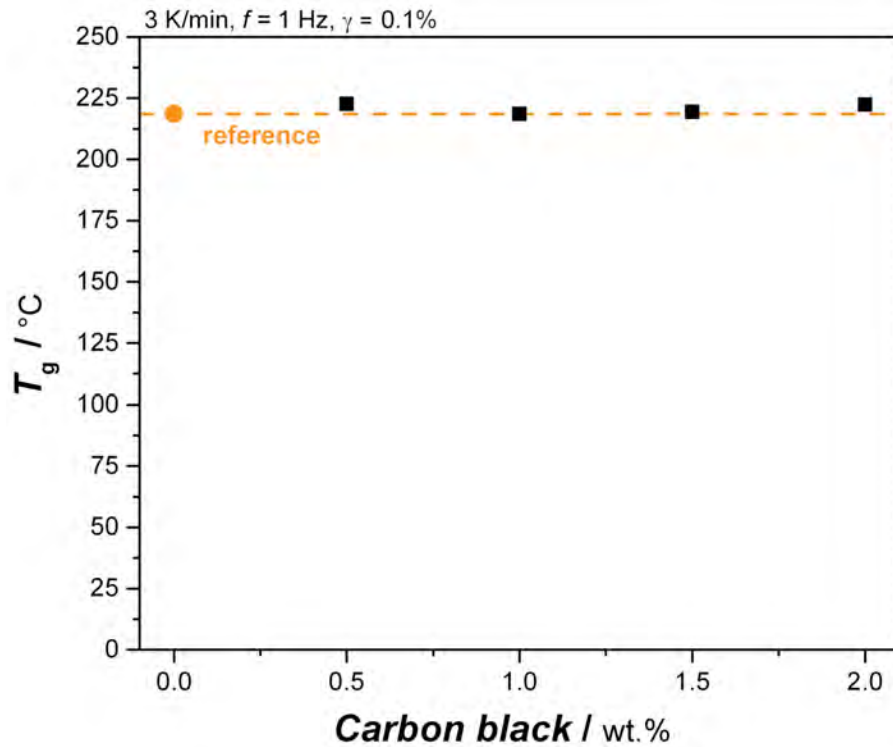


Figure 52. T_g of neat and CB modified epoxy nanocomposites.

The neat DGEBA-TGMDA-4,4'-DDS epoxy resin system has a T_g of 219 °C, measured with a standard deviation of less than 1 °C. As seen in Figure 52, the addition of up to 2 wt.% CB does not significantly influence the T_g of the epoxy. There are contradictory reports in the literature regarding the effect of CB on the T_g of epoxy resin system. Etika et al. [76] argued that the addition of CB into an amine-cured epoxy system decreases T_g due to low interfacial adhesion between CB particles and the epoxy matrix. However, Kosmidou [105] reported that incorporation of CB leads to higher T_g because of limited mobility of the polymer chains at the particle-matrix interphase. The minor effect of CB on the T_g of epoxy resin observed in this study is attributed to the

very low CB contents, as well as the very low interfacial affinity between CB and the epoxy matrix.

5.1.2.4. Effect of carbon black on electrical conductivity of epoxy resin

The electrical conductivity of CB modified epoxy nanocomposites is investigated under direct current. The neat epoxy shows a highly insulating behavior with measured electrical conductivity in the range of 10^{-12} S/m (Figure 53). The addition of up to 2 wt.% CB increases the electrical conductivity progressively, while the addition of only 0.5 wt.% CB leads already to an insulator to semiconductor transition. An electrical conductivity above 10^{-4} S/m can be achieved with the addition of only 2 wt.% CB in the resin. This level of conductivity promises the ability of electro-static dissipation for a nanocomposite, as described in the chapter 2 (state of the art).

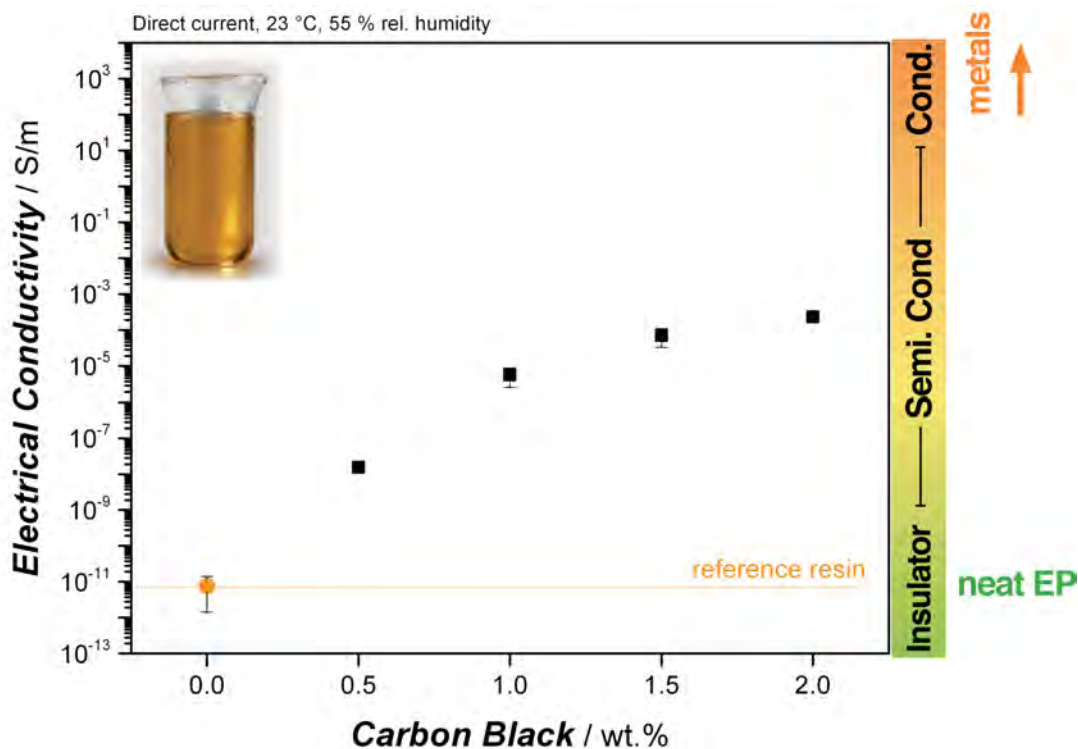


Figure 53. DC electrical conductivity of neat epoxy and epoxy-CB nanocomposites in the solid state.

The threshold concentration in a polymeric composite is defined as the critical concentration where an abrupt increase of electrical conductivity is observed. The threshold concentration for this particular system is in the range of 0.5 wt.%, although the electrical conductivity does not particularly follow the theoretical S-curve. The literature suggests a broad range for the CB threshold concentration in epoxy systems, which varies from 0.1 wt.% to 10 wt.% (Figure 9). This variation in threshold concentration is attributed to use of different resin systems, processing methods and different CB particles (chemistry, size, aspect ratio) employed. Nevertheless, the maximum conductivity ($\approx 10^{-4}$ S/m at 2 wt.% CB loading) measured in this work agrees well with the literature. It is worth noting that Gojny et al. [45] stated the semi-conducting behavior of CB epoxy nanocomposites at a comparable CB content and obtained similar results ($\approx 10^{-4}$ S/m).

Microstructure of carbon black-epoxy nanocomposites

Transmission electron microscopy (TEM) is mostly used in academia to study the morphology of the conductive polymer nanocomposites because of the very high image resolution. However, it is crucial to emphasize that the TEM analysis provides information from only a small portion of the sample and in a two-dimensional orientation of a three-dimensional structure. 1.5 wt.% CB modified epoxy resin (above threshold) was chosen for the morphology investigations (Figure 54).

There are lines observed especially in Figure 54.a and Figure 54.b, which are artefacts of cutting process with the ultra-microtome, and are not relevant to the microstructure of the nanocomposite.

The CB particles formed highly branched agglomerations (Figure 54.a). Aside from the direct particle contacts in these agglomerates, interparticle distances extend up to 50 nm. Smaller agglomerates with lateral extensions of up to 500 nm were also detected (Figure 54.b). Higher interparticle distances were observed around these smaller particle agglomerates.

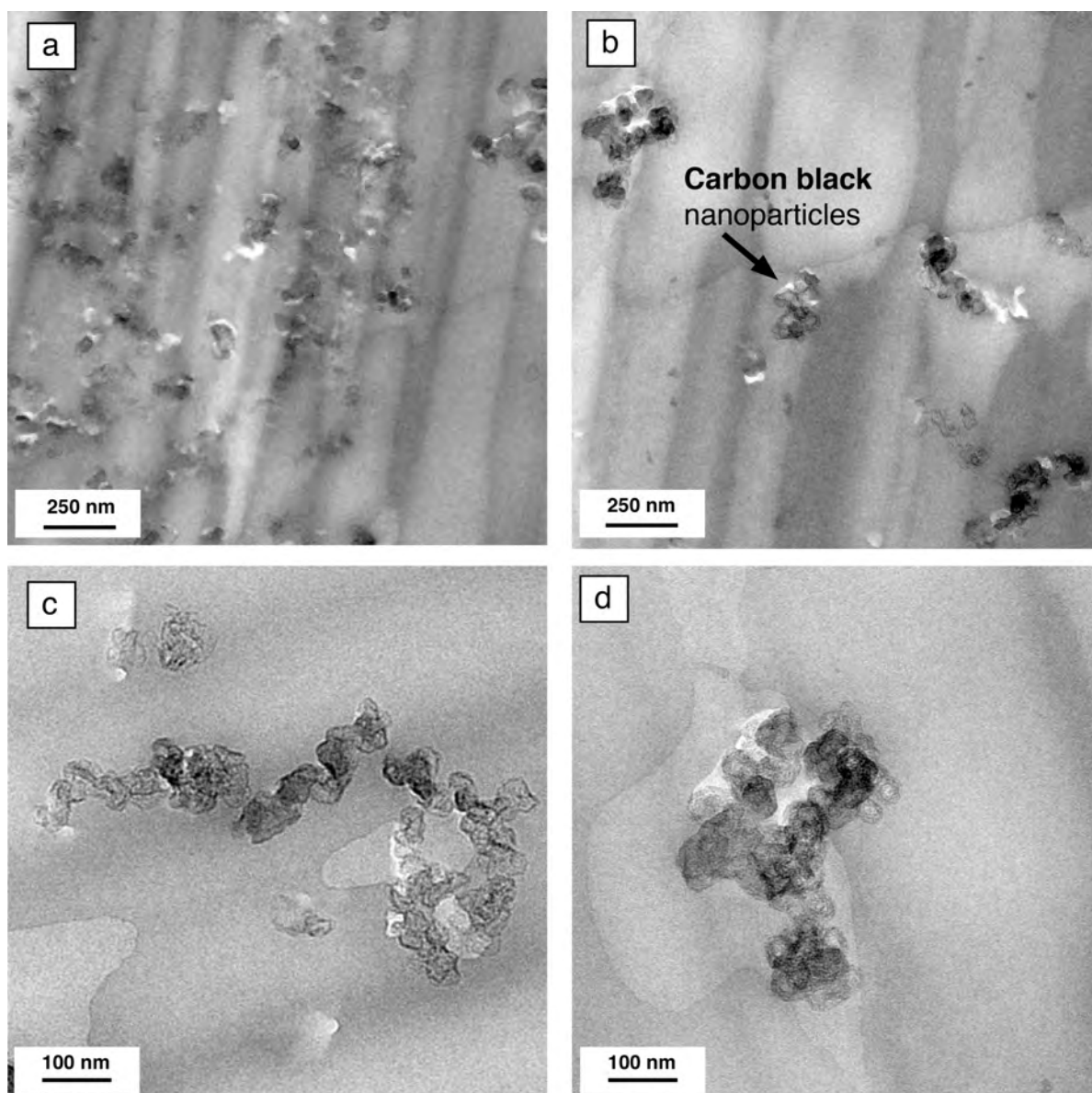


Figure 54. TEM micrographs of the 1.5 wt.% CB-epoxy nanocomposite.

The TEM micrographs in Figure 54.c and Figure 54.d show the aggregated structure of the CB at higher magnifications. Although the aspect ratio of a single CB particle is theoretically 1 (due to the spherical primary particle geometry), these branched aggregation of particles, called superstructures, possess higher aspect ratios. The superstructures of CB (Figure 54.c) are thought to be responsible for the semi-conducting behaviour of their epoxy nanocomposites at very low additive contents.

5.1.2.5. Effect of carbon black on mechanical properties of epoxy resin

While the addition of nanoparticles can enhance the property of one material, it can simultaneously deteriorate others. Although the electrical conductivity of CB-epoxy nanocomposites is the main focus of this chapter, the effect of CB on the mechanical properties of the resin was investigated as well. Figure 55 shows the quasi-static fracture toughness of neat and CB modified epoxy nanocomposites.

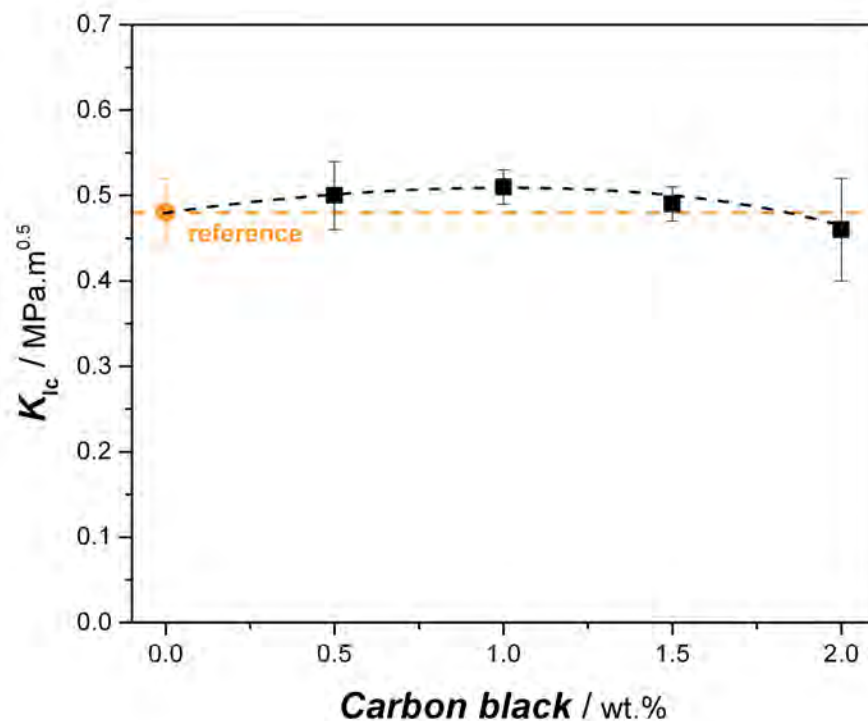


Figure 55. Fracture toughness of the neat and CB modified epoxy nanocomposites.

The neat epoxy resin system has a critical stress intensity factor (K_{Ic}) of 0.48 ± 0.02 MPa \sqrt{m} , which illustrates the brittle nature of the neat resin. The fracture toughness of the neat resin system is slightly lower compared to standard two-functional resins cured with various amine hardeners [109]–[111], but found to be comparable to the resins cured with anhydrides [112], [113]. This is attributed to the blending of TGMDA in the neat resin formulation because TGMDA resin consists of

four reactive epoxide groups that increase the network density, which can lead to further brittleness of the resin system.

The addition of CB increases the fracture toughness up to 1 wt.% CB, which is then followed by a reduction of fracture toughness at higher CB contents. While the addition of 1 wt.% CB results in a 6 % higher K_{Ic} ($0.51 \pm 0.02 \text{ MPa}\cdot\sqrt{\text{m}}$), further addition up to 2 wt.% decreases the toughness by 16 % ($0.40 \pm 0.07 \text{ MPa}\cdot\sqrt{\text{m}}$) compared to the neat system. It is widely accepted that the introduction of nanoparticles in epoxy resins typically increases the toughness of the system by interacting with the crack tip during crack propagation [114]–[120], whereas the extensive agglomeration of inorganic particles in resin can be deteriorative for the fracture toughness.

Analysis of fracture surfaces of CB-epoxy nanocomposites

To understand the micro-mechanical toughening mechanisms, the fracture surfaces of the CB modified nanocomposites were investigated via SEM (Figure 56). As indicated by its low K_{Ic} , neat epoxy resin has a very smooth fracture surface without any topographical features (Figure 56.a and b).

CB particles are typically dispersed as small aggregates (mostly below 2 μm) but as well formed branched agglomerates (above 10 μm) in the cured resin system (Figure 56.c to Figure 56.f). Higher CB content leads to an enhancement of agglomeration. The enhancement of the quasi-static fracture toughness up to 1 wt.% CB content is attributed to the void formation and debonding of individual CB particles in addition to the crack pinning around CB agglomerates above 500 nm (Figure 56.d).

However, extensive agglomeration of CB particles at 2 wt.% (Figure 56.f) results in a qualitatively lower number of the crack tip-CB interactions. Therefore, increasing the CB content does not enhance the toughness of the resin further.

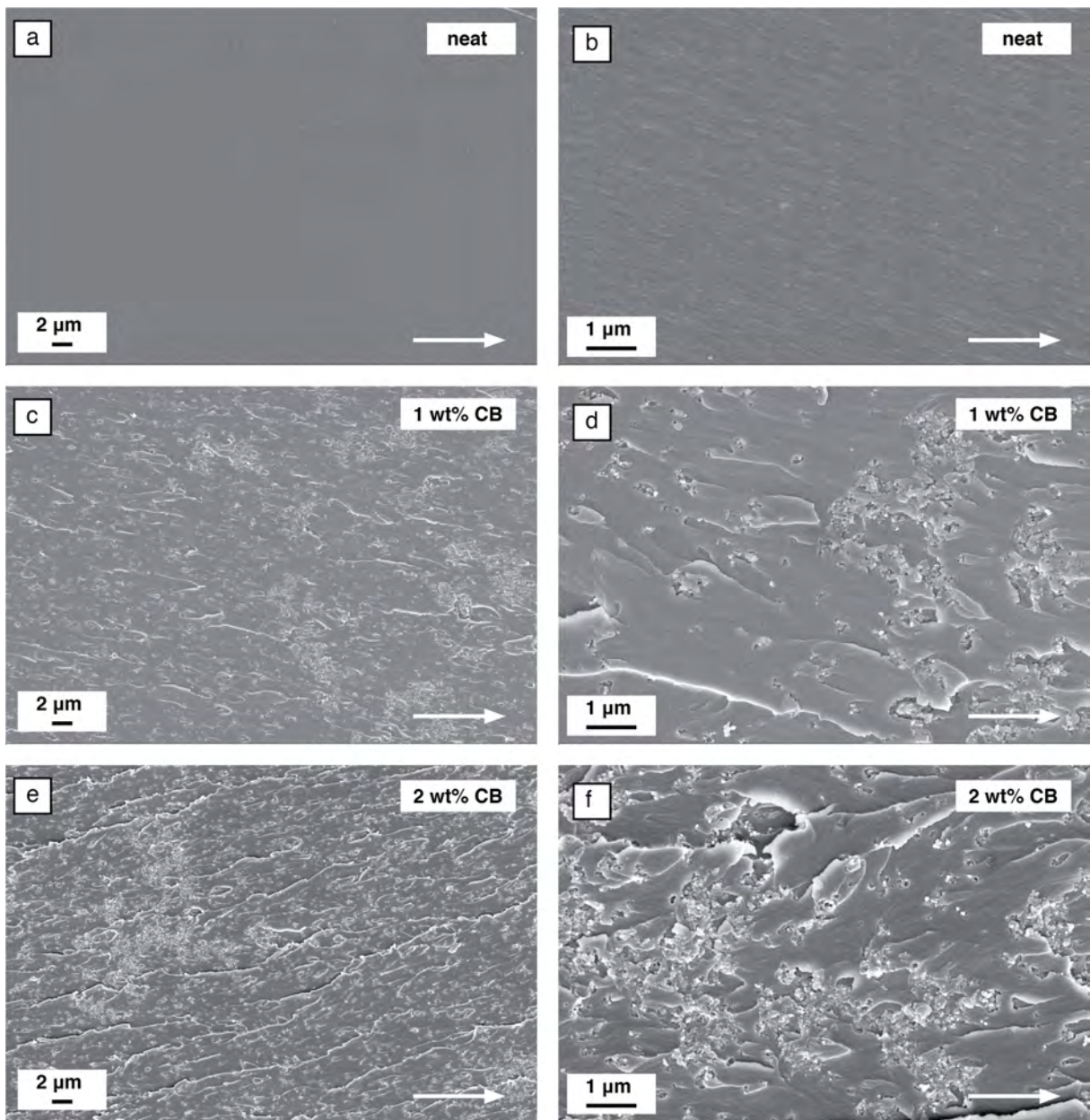


Figure 56. SEM micrographs of a) and b) neat epoxy, c) and d) 1 wt.% CB, and e) and f) 2 wt.% CB modified epoxy nanocomposites. Direction of the crack propagation is from right to the left, indicated by the white arrows.

5.1.3. Summary

The neat resin system shows a highly insulating behavior with an electrical conductivity of $7.7 \cdot 10^{-12}$ S/m. The addition of carbon black up to 2 wt.% does not influence the

thermo-mechanical properties and the viscosity of the neat epoxy resin, but increases the electrical conductivity to 10^{-4} S/m resulting in semi-conductor behavior. The percolation threshold is estimated to be in the range of 0.5 wt.% CB content. Micrographs reveal that CB nanoparticles are dispersed in the resin system as branched agglomerates as well as single particles. The addition of CB increases the fracture toughness of the resin up to 1 wt.% by activating the crack pinning around the agglomerates and particle debonding of single CB particles. However, the higher CB contents up to 2 wt.% does not necessarily contribute to the fracture toughness of the resin, due to extensive particle agglomeration.

5.2. Electrical and mechanical properties of laminates

5.2.1. Prepreg properties

Prepreg impregnation quality and areal weights are crucial parameters to achieve consistent fiber volume contents in laminates. Comparable laminate quality and fiber volume content make it possible to study the effects of CB on the electrical and mechanical properties of the prepreg laminates.

The target areal weight of 145 to 150 g/m² was set prior to prepreg processing, which is 47 wt.% (slightly above 50 vol.%) resin in the uncured prepreg (Figure 57). This prepreg areal weight was set because of the expected high resin-flow during the curing process. The neat epoxy-CF prepreg had an areal weight of 155 g/m² with a narrow areal weight distribution. (Figure 57.a). Although the 1.5 wt.% CB modified prepreg show slightly lower areal weight, comparable prepreg qualities were achieved for all types of prepregs. Measured areal weight deviations were higher for the 1 wt.% CB modified prepregs, which is attributed to deviation in the coated resin content in the coating unit during the production of this particular prepreg material.

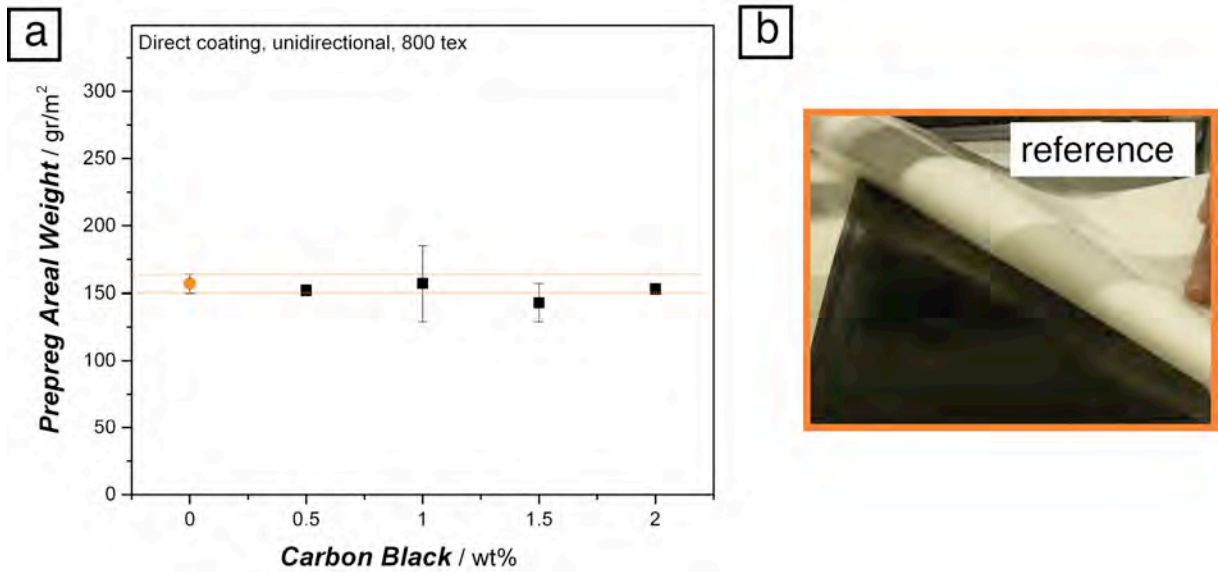


Figure 57. a) Areal weights of neat and CB-modified prepregs measured during production. b) reference unidirectional prepreg with an areal weight of 155 g/m², corresponding to approximately 48 wt.% resin.

The viscosity profile of the resin system was ideal for prepreg production, which is 30 Pas at coating unit (70 °C) and approximately 1 Pas before calendaring (100 °C). Excellent prepreg quality was achieved during prepreg production with the hot-melt prepreg impregnation route (Figure 57.b). Fiber spreading and homogeneity were optimal because no fiber-free spots or fiber knicking was observed with the naked eye on produced prepregs.

5.2.2. Electrical properties of prepreg laminates

5.2.2.1. Effect of only FVC on electrical conductivity of neat laminates

Although the epoxy resin is a strong insulator, the carbon fibers result in a transformation of the laminates from insulator to semiconductor or conductor in the z-direction, owing to high conductivity of fibers in parallel ($\sim 10^5$ S/m) [121] and perpendicular (330 S/m) to the graphitic basal plane [13]. To calculate the influence of

CB particles alone, it is essential to understand first the effect of the CFs on the electrical conductivity of composites. The dependence of through-thickness electrical conductivity on CF volume content for this material system is shown in Figure 58.

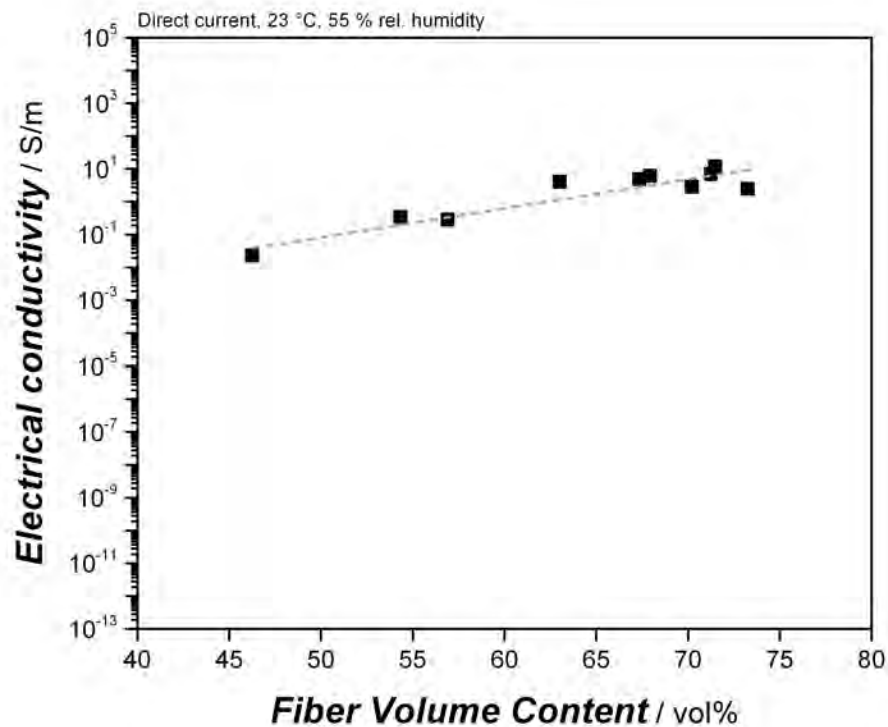


Figure 58. Through-thickness electrical conductivity of laminates as a function of CF volume content.

It was possible to cover a broad range of fiber volume content varying from approximately 46 to 73 vol.%. The neat epoxy-CF UD prepreg laminate with 46 vol.% fibers showed $2.3 \cdot 10^{-2}$ S/m electrical conductivity, whereas laminates with FVC in the range of 55 to 57 vol.% have a conductivity of $2.8 \cdot 10^{-1}$ S/m. The laminates having FVC of 67-70 vol.% show electrical conductivities varying from 2.8 to 6.2 S/m. A conductivity of 12 S/m was measured for a neat prepreg laminate with approximately 72 vol.% CF content. The relationship between FVC and through-thickness electrical conductivity

followed the exponential equation (4) very well, in which ϕ_f represents the fiber volume content.

$$E_{dc} = 10^{0.08769 \cdot \phi_f - 5.4627} \quad (4)$$

This relation allows an estimation of the through-thickness electrical conductivity for this particular composite system with a desired carbon fiber volume content.

Electrical conductivity of epoxy-CF composites is a very attractive area of scientific research. Most studies in literature, however, do not contain a detailed information about the fiber volume content of the laminates [5], [122]–[126]. The measured data in this work are compared with the available values reported in the literature in Figure 59.

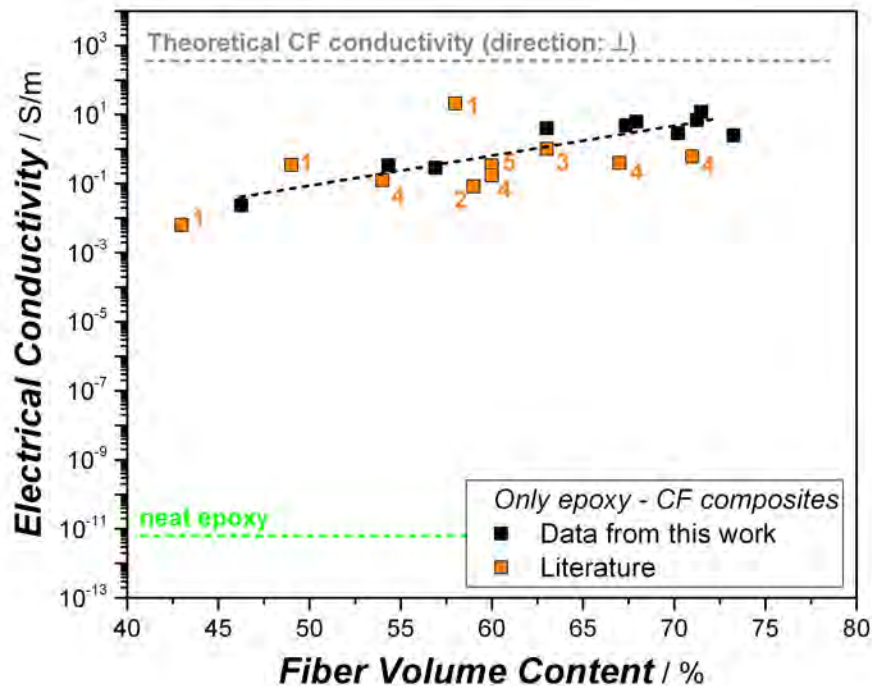


Figure 59. Through-thickness electrical conductivity as a function of CF volume content compared with literature values. Only neat epoxy-unidirectional CF composites are summarized. Data points: 1-[127], 2-[87], 3-[54], 4-[128], 5-[129].

Chippendale et al. [130] modeled the electrical conductivity of an epoxy-CF composite system based on Monte Carlo simulations with randomly distributed fibers in the matrix, and report that percolation was achieved at 40 vol.% of the CFs. Above this percolation threshold for carbon fibers in epoxy matrix, there is agreement with Equation (4) and with previously published data (Figure 59). Variations between different studies are attributed to different laminate qualities and measurement methods used for the determination of FVC and electrical conductivity.

Optical micrographs were taken from the polished cross-section surfaces of the laminates to investigate the underlying mechanisms responsible for the increment of through-thickness electrical conductivity of laminates with increasing FVC. Figure 60 shows representative cross-sectional micrographs of laminates with 46 vol.% and 70 vol.% FVC.

The packing density of the fibers in the z-direction is strongly affected by the FVC. Although the neat epoxy-CF prepreg laminate with 46 vol.% fibers (Figure 60.a and Figure 60.c as filtered) already has conducting pathways consisting of carbon fiber contacts, the distribution of fibers are highly random. On the other hand, the laminate with 70 vol.% fibers shows a much higher packing density of fibers (Figure 60.b and Figure 60.d) with a higher number of conducting pathways. The maximum observed fiber to fiber distance is 10 μm for this laminate.

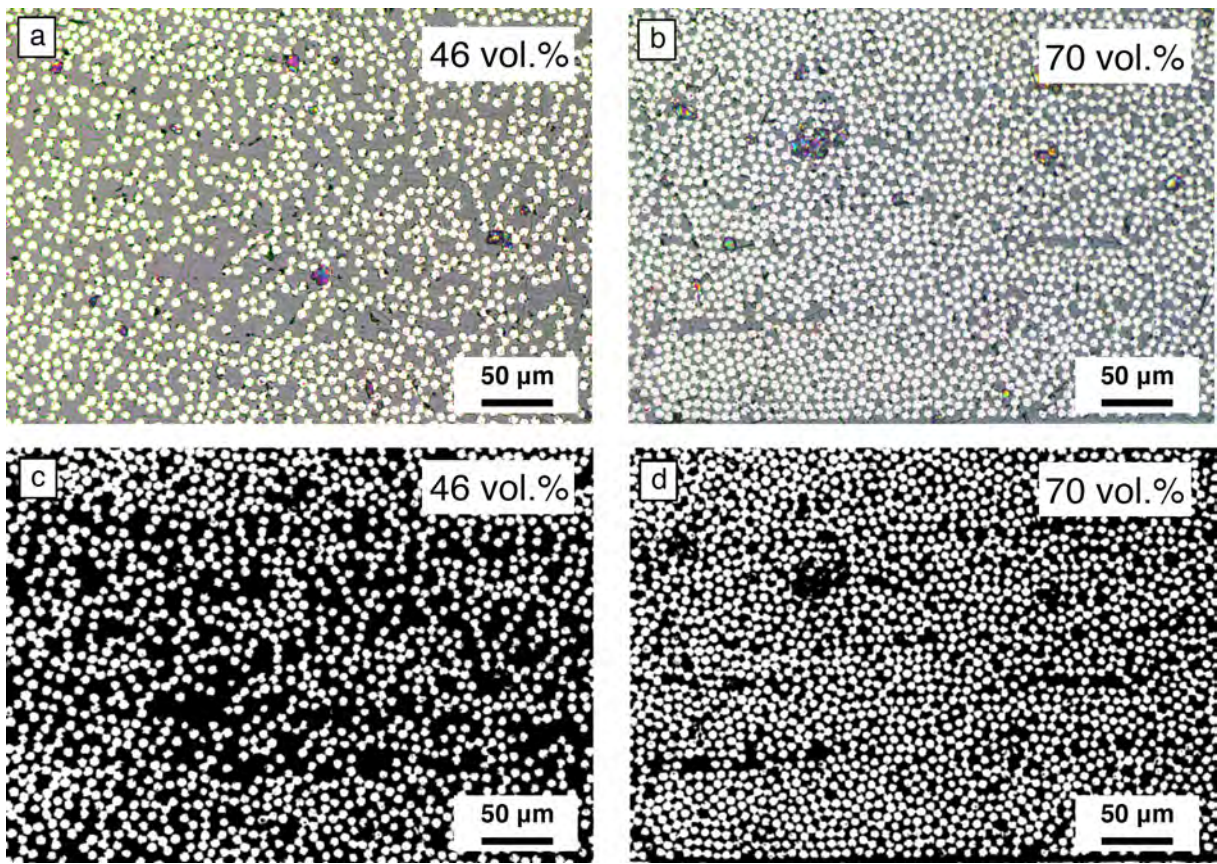


Figure 60. Cross-sectional micrographs of prepreg laminates with a and c) 46 vol.%, b and d) 70 vol.% CF content. Micrographs of c) and d) are filtered as black and white.

5.2.2.2. Effect of CB on electrical conductivity of laminates

To study the effect of CB nanoparticles on the electrical conductivity of the laminates, epoxy-CF prepreg laminates containing up to 2 wt.% CB nanoparticles (in resin) were produced and tested. In this section, their structure-property relationships are presented and discussed. The electrical conductivity of the neat and CB modified prepreg laminates are shown in Figure 61.

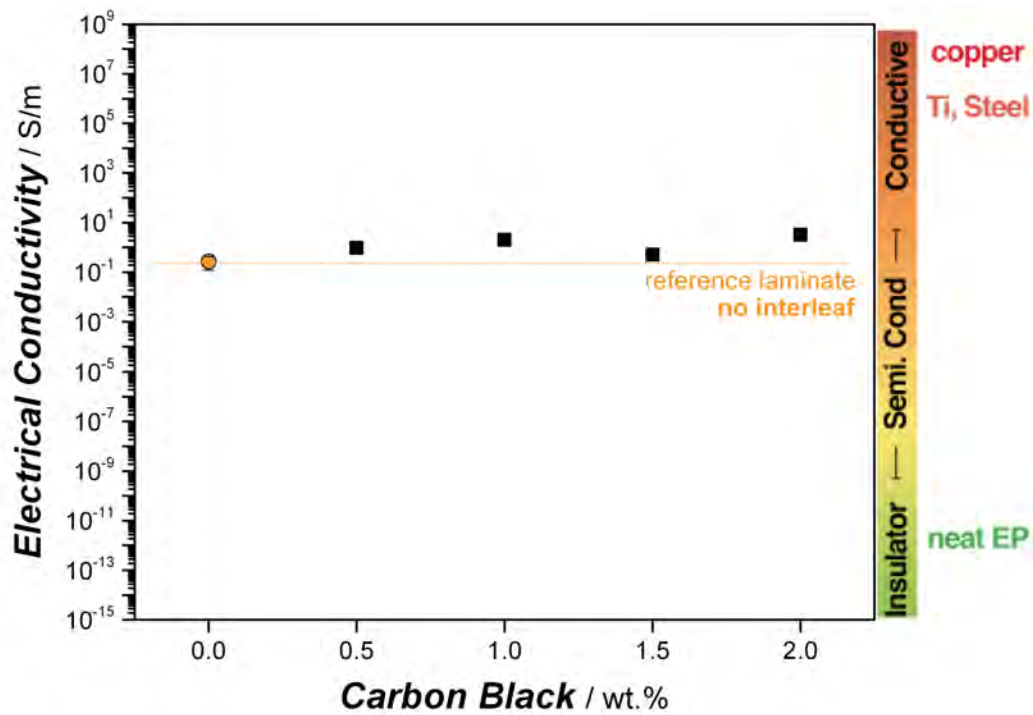


Figure 61. Through-thickness electrical conductivity of prepreg laminates as a function of CB content in resin.

The neat epoxy CF prepreg laminate with 54 vol.% FVC yields an electrical conductivity of approximately 0.2 S/m, which is consistent with previous studies for this range of fiber volume content. Incorporation of up to 2 wt.% CB nanoparticles leads to a steady increase of the conductivity up to 3.2 S/m, which is 16 times higher compared to the neat prepreg laminate. This increment is minor compared to CB modified resin studies, where the addition of 2 wt.% CB led to an above 10^7 times higher electrical conductivity of the neat epoxy resin.

To extract the effect of CB nanoparticles on the electrical conductivity of epoxy-CF laminates, the effect of the slightly varying FVC is normalized (Table 5). By using Equation (4), the through thickness electrical conductivity of laminates was calculated according to their FVC. Most of the CB modified prepreg laminates, except the 1.5 wt.% CB-modified system, show comparable fiber volume content to reference laminate with a FVC of 54 vol.%. This normalization was particularly important for the

1.5 wt.% CB-modified prepreg laminate because the FVC of this laminate was determined as 46 vol.%, which is reflected in the conductivity results (Figure 61).

Table 5. Normalisation of the effect of CFs to determine the effect of only CB particles on the electrical conductivity of the laminates.

Laminate	Measured FVC* of laminates	Calculated basis E_{dc} acc. to laminates FVC (no CB)**	Measured E_{dc} of laminates	Effect of CB particles only
-	vol.%	S/m	S/m	%
Reference	54	-	0.2 ± 0.06	-
0.5 wt.% CB	56	0.28	1.0 ± 0.03	+ 357
1 wt.% CB	55	0.23	2.0 ± 0.25	+ 870
1.5 wt.% CB	46	0.04	0.5 ± 0.05	+ 1250
2 wt.% CB	57	0.30	3.2 ± 0.16	+ 1067

* FVC is determined by TGA.

** Equation (4) in chapter 5.2.2. is used to calculate the basis conductivity of prepreg laminates dependent on the FVC of the laminates without the CB addition.

The addition of 0.5 wt.% CB particles enhances the conductivity by approximately 3.5 times compared to the reference system. The addition of up to 2 wt.% results in more than 10 times higher through-thickness electrical conductivity (3.2 S/m) compared to neat prepreg laminate, which results in a transition from semi-conducting to conducting behavior. Zhang et al. [54] incorporated a similar type of CB up to 3 wt.% in CF-epoxy composites produced via RTM (comparable FVC with this study). Although copper chloride was used to promote further agglomeration by lowering the surface charge of the particles, an increase of only a factor of two was observed at 3 wt.% CB content. Compared to this work, the lower the impact of the CB particles by Zhang et al. [54] is attributed to the possible filtration of CB particles via CF during RTM processing of the composites. The prepreg route employed in this work does not show any risk of CB filtration by CF, since no infusion necessary.

Mechanisms of electrical conductivity in neat and CB modified epoxy-CF laminates without interleaf

The CFs are distributed randomly in the z-direction of the neat epoxy-CF laminate structure, and conduction occurs due to fiber to fiber contacts. The micro-computer tomography (micro-CT) and SEM were employed to study the morphology and identify electrical conduction pathways in the neat and CB modified laminates.

Figure 62 shows the micro-CT results of the neat prepreg laminate from different angles. Rotation of the laminate is counter-clockwise.

The neat epoxy-CF prepreg laminate does not show any imperfections. No epoxy rich region is observed in the sample, which verifies that the prepreg layers (26 prepreg layers for a 3 mm laminate) were sufficiently consolidated during curing.

A polished cross-section of the reference laminate was analyzed via SEM to investigate the laminate morphology with a focus on fiber to fiber contacts (Figure 63). A random distribution of carbon fibers in the neat epoxy-CF laminate results in two building blocks for conducting CF network, which are resin-rich regions (Figure 63.a) and fiber-rich regions (Figure 63.b). As seen in Figure 63.a, the fiber-rich regions are well connected to each other via the carbon fibers, where the insulating effect of resin rich regions are therefore prevented.

Consequently, the interconnected fiber-rich regions with conduction pathways are mainly responsible for the measured through-thickness electrical conductivity for these laminates.

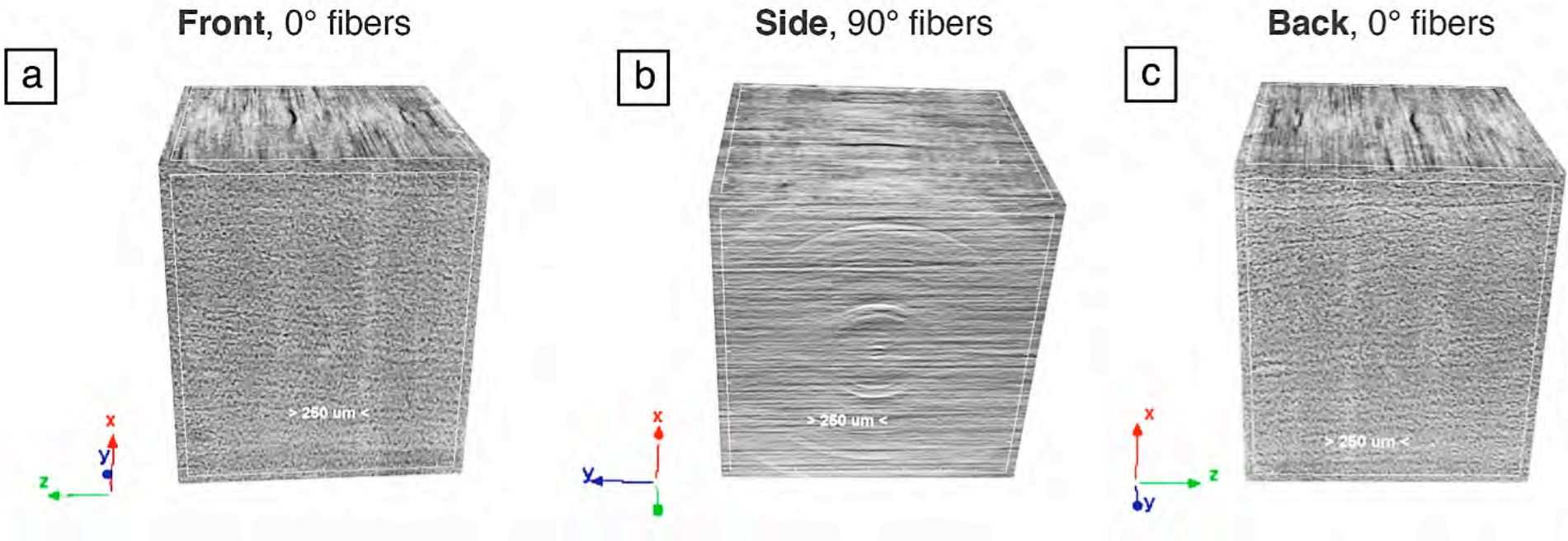


Figure 62. Micro-CT scans of the neat epoxy-CF unidirectional prepreg laminate with 54 vol.% CF content. Rotation is counter-clockwise.

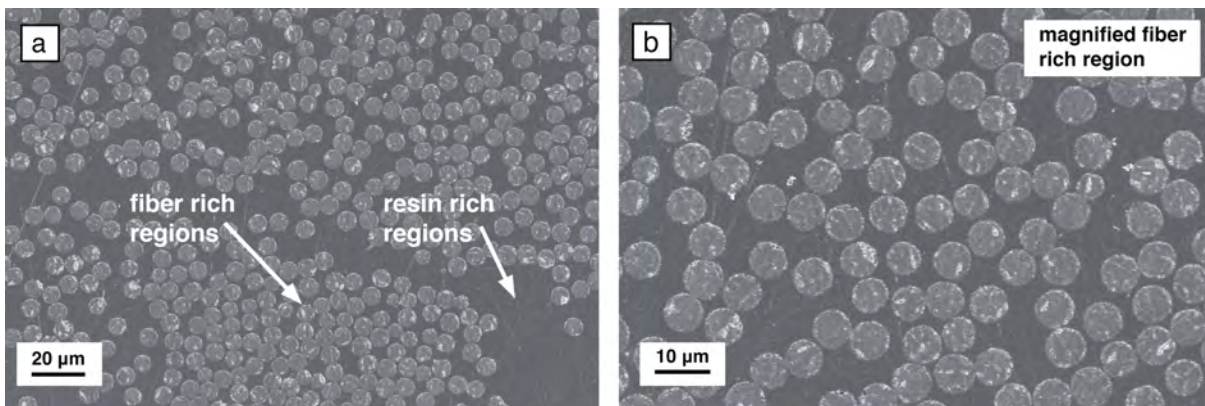


Figure 63. SEM micrographs from a polished cross-section of the neat epoxy-CF prepreg laminate without CB particles.

The fiber to fiber distances of carbon fibers in the fiber-rich zones of reference laminate were analysed further with an image analysis method (see the chapter 4.3.7). Figure 64 presents the fiber to fiber distances measured via ImageJ.

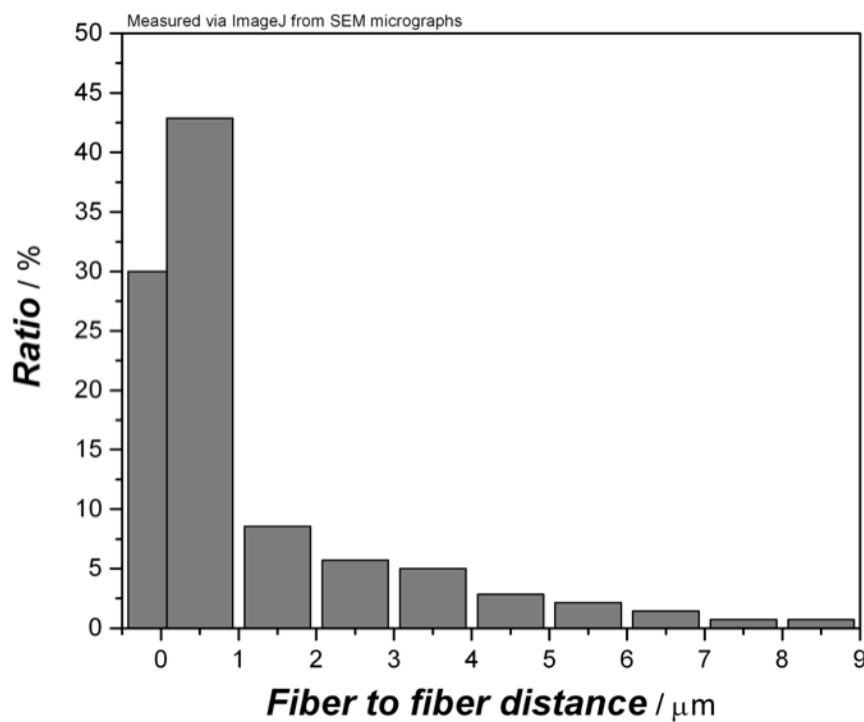


Figure 64. Cross-sectional fiber to fiber distances in fiber-rich regions of the neat epoxy-CF prepreg laminate. as explained in a detail in section 4.3.7.

Approximately 30 % of the measured fiber to fiber distances are 0 μm , indicates the fiber contact. More than 40 % of the fiber to fiber distances were up to 1 μm , and the remaining \sim 30 % of the measured fiber to fiber distances are in the range of 2 – 8 μm . As a summary, neat consolidated epoxy-CF laminate consists of fiber rich and epoxy rich domains in the cross-sectional morphology (Figure 63), where the conducting fiber rich domains are interconnected via few carbon fibers to each other. In these fiber rich domains, most of the fibers do not show a direct fiber to fiber contact, where only 30 % of the measured interfiber distances were 0 μm .

The addition of CB increases the electrical conductivity of the neat epoxy CF laminate up to 3 S/m, which is more than a ten-fold increase at the loading of 2 wt.% CB in the resin. This is however a marginal increment. SEM micrographs of 1.5 wt.% CB-epoxy-CF laminates from the in-plane direction are presented in Figure 65.

The micrographs reveal that the CB nanoparticles are located in resin-rich areas between fibers as sub-micron aggregates (Figure 65.a and Figure 65.b). Although an extensive agglomeration of these nanoparticles was not observed as in the case of the CB modified epoxy nanocomposites (Figure 54.a), a high number of CB aggregates with a diameter below 1 μm were detected in between non-contacting CFs (Figure 65.a and Figure 65.b).

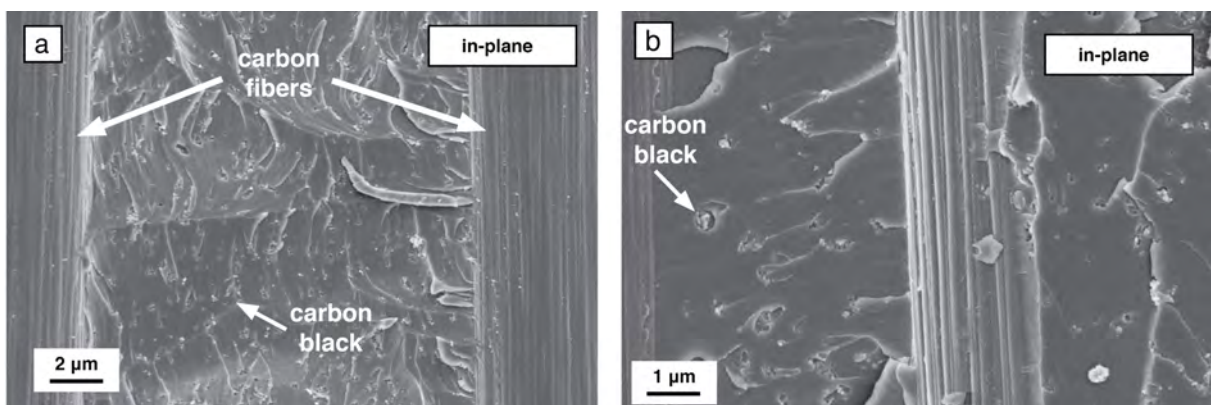


Figure 65. SEM micrographs of 1.5 wt.% CB-epoxy-CF laminates from in-plane direction.

5.2.2.3. Effect of only interleaf fleece on the conductivity of laminates

To optimize the damage resistance and tolerance of the epoxy-CF laminates, parallel to the resin toughening [131]–[133], following strategies are presented in literature:

- *interleaf structures* consisting of thermoplastic particles [134], [135],
- elastomer modified resins [136],
- thermoplastic fleeces (polyamide, polysulfone, or phenoxy based) [137]–[140],
- nanoparticle based or nanoparticle modified fleeces [141], [142],
- nanofibrous (mostly polyamide-based) fleeces [143]–[146].

Figure 66 shows the microstructure of an interleaf toughened epoxy-carbon fiber prepreg consisting of the thermoplastic particle based interlayers (TORAYCA Prepreg P2302; first material to pass the Boeing high toughness specifications). No information about the type or chemistry of the toughener is given [147].

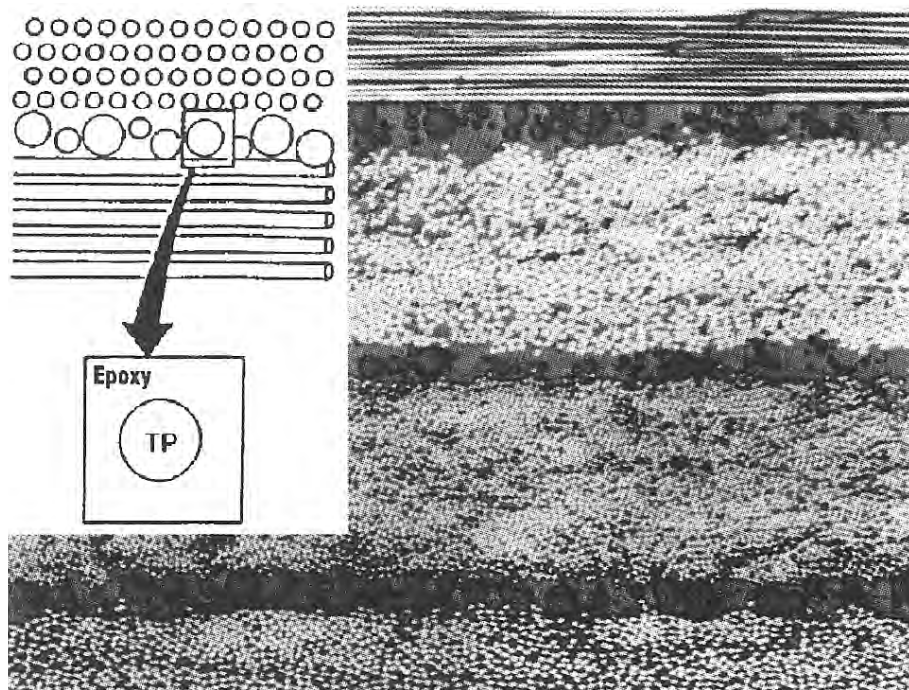


Figure 66. Cross-section of P2302 laminate from Toray. The thermoplastic particle interleaf can be seen between each prepreg layer [147].

The thermoplastic interleaf increases the fracture toughness and damage tolerance of the prepreg laminates under static and dynamic loading, because the toughened interlayer regions result in a high strain energy release during the crack propagation [135], [147]. On the other hand, interleaf toughened laminates [5], [8] show a much lower through-thickness electrical conductivity compared to laminates without the interleaf. This is attributed to the strongly insulating behavior of the resin-rich interleaf regions.

In this chapter, the effect of a polyamide 6.6 based interleaf fleece (10 g/m²) on the electrical conductivity of the laminates is presented and discussed in detail. The electrical conductivity results of neat resin, prepreg laminate without interleaf and with interleaf fleece are presented in Figure 67.

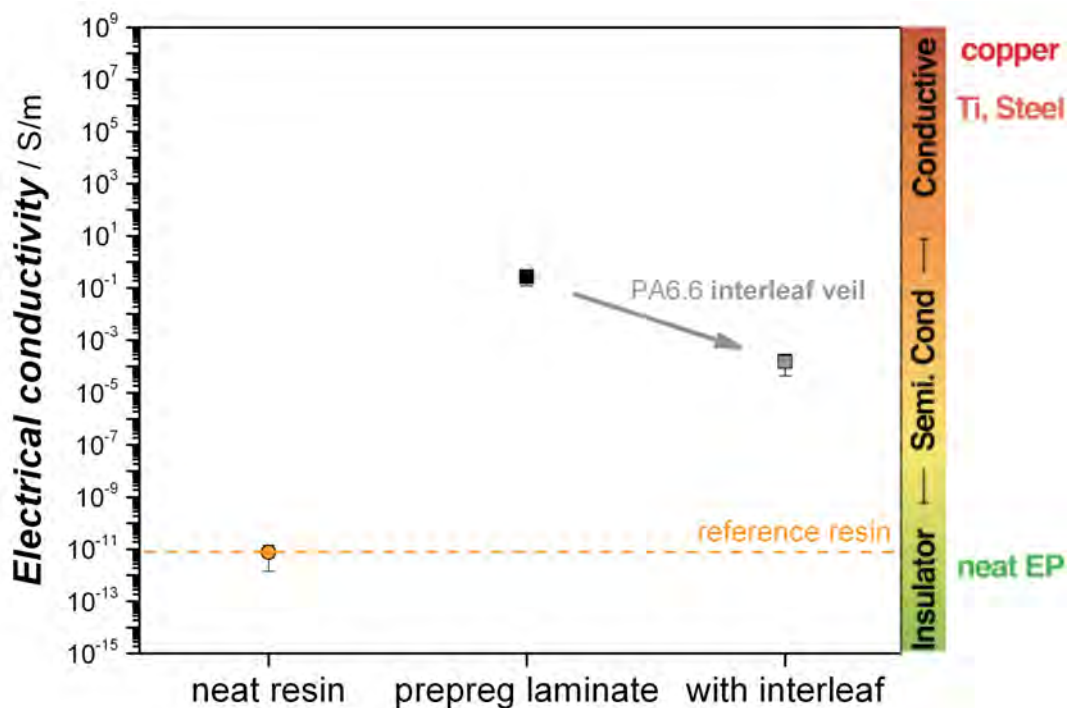


Figure 67. Electrical conductivity in z-direction of neat epoxy, neat prepreg laminate, and neat prepreg laminate with PA6.6 interleaf fleece. The thicknesses for neat laminate without and with interleaf fleece are 2.73 ± 0.1 mm (FVC: 54 vol.%) and 2.89 ± 0.2 mm (FVC: 52 vol.%), respectively.

The addition of the interleaf between each layer leads to a significant decrease of the z-direction conductivity by almost three orders of magnitude to $1.5 \cdot 10^{-4}$ S/m. The FVC of the laminates are comparable. Achieving same FVC in interleaf modified laminate is attributed to the increased compaction of carbon fibers in each prepreg layer. Therefore the reduction of conductivity is attributed only to the addition of the interleaf spacing. The detrimental effect of the interleaf fleece on the conductivity is understood and discussed previously by Guo et al. [8], where the addition of the same type of fleece (PA6.6) as the interleaf toughener lead to conductivities even lower than 10^{-6} S/m.

Mechanisms of conduction in interleaf modified neat laminates

Figure 68 shows optical micrographs of neat laminates with and without interleaf.

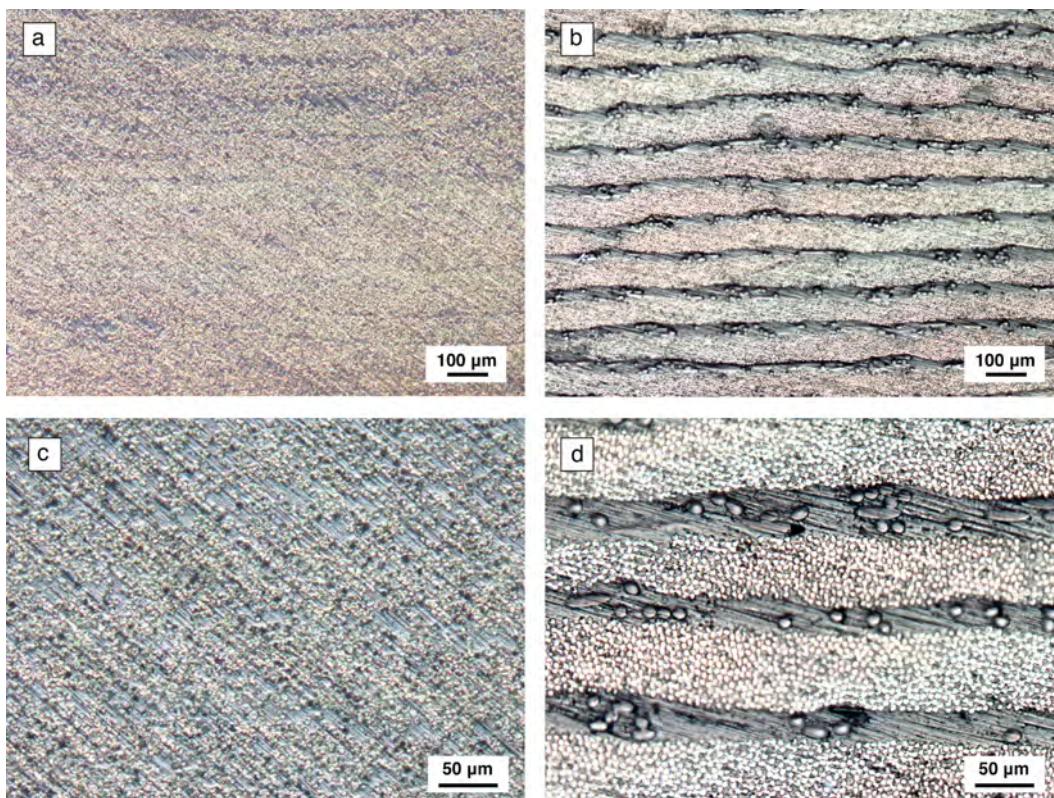


Figure 68. Cross sections of a) and c) without interleaf, b) and d) with interleaf fleece.

As previously described, the prepreg laminate without interleaf fleece contains fibers that are distributed randomly through the laminate, resulting in a semi-conductor behavior with electrical conductivity of 0.2 S/m in the z-direction (Figure 68.a and c).

The introduction of a 10 g/m² interlaminar PA6.6 fleece in the prepreg laminate results in an resin rich interlaminar spacing of $47 \pm 10 \mu\text{m}$ ($d_{\text{max}}-d_{\text{min}} \approx 20 \mu\text{m}$). Because the melting point of PA6.6 ($T_m \approx 270 \text{ }^\circ\text{C}$) is almost 70 °C higher than the post curing temperature of the laminates (200 °C), the interleaf fleece did not melt and therefore stabilized the interlaminar region during curing. Polyamide fibers are clearly observed in Figure 68.d, and have a much higher fiber diameter (approximately 20 μm) compared to the CFs.

Micro-CT scans were performed to investigate the structure of the interleaf prepreg laminate in three dimensions. The CT-scans allow for a detailed examination of the neat epoxy-carbon fiber interleaf laminate (Figure 69), and reveal the structure of the interleaf regions through the laminate from the front and back surfaces. Although incorporation of the interleaf layers provides a constant interlaminar spacing throughout the sample, as it can be seen in Figure 69.a and Figure 69.c, the interlaminar regions are not perfectly linear. From the side view (Figure 69.b), it is clear that prepreg layers and interlaminar regions are stable and separated clearly from each other through the length of the laminate.

In conclusion, these interleaf layers prohibits the contacts in between each prepreg layer and results in a strong deterioration of the z-direction electrical conductivity of the laminate.

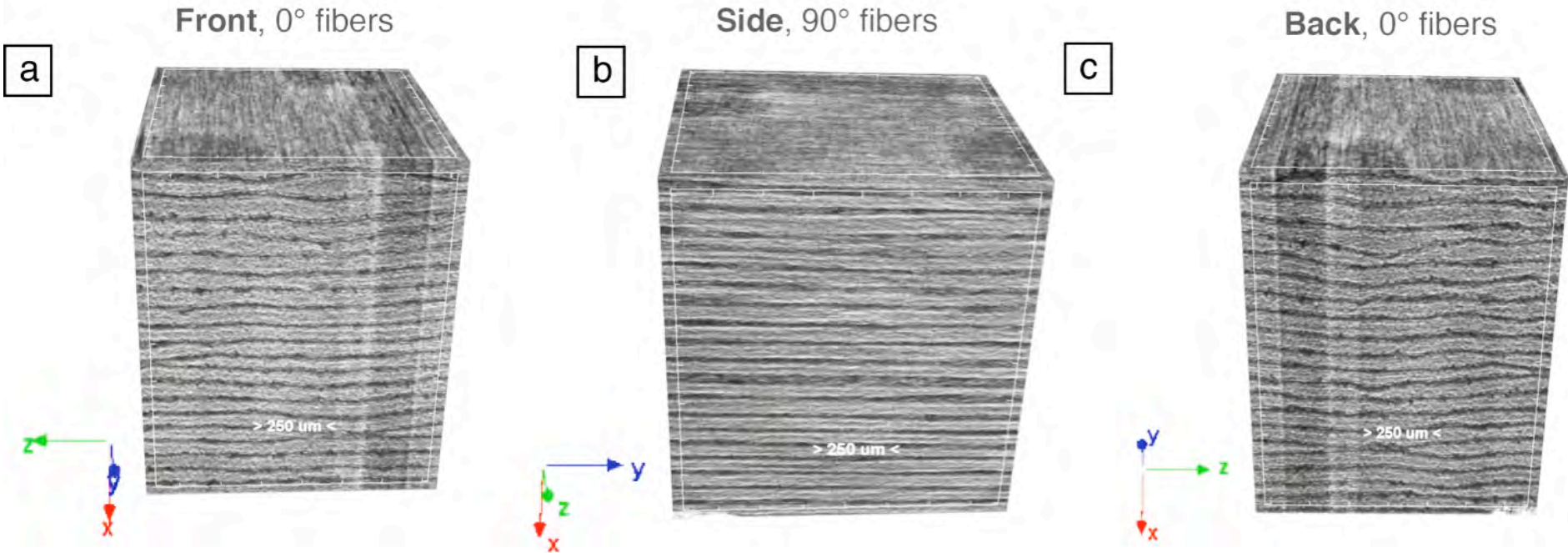


Figure 69. Micro-CT scans of the neat epoxy-CF unidirectional prepreg laminate with interleaf. Direction of rotation is counter-clockwise.

5.2.2.4. Effect of CB on conductivity of laminates with interleaf

The influence of CB nanoparticles on the through-thickness conductivity of the epoxy-CF prepreg laminates with interleaf is examined and the results are shown in Figure 70. Neat prepreg laminate with a polyamide interleaf fleece acts as a semiconductor with a conductivity of $1.5 \cdot 10^{-4}$ S/m. In contrast to prepreg laminates without interleaf, the addition of CB nanoparticles to the interleaf prepreg laminate leads to a substantial enhancement of electrical conductivity.

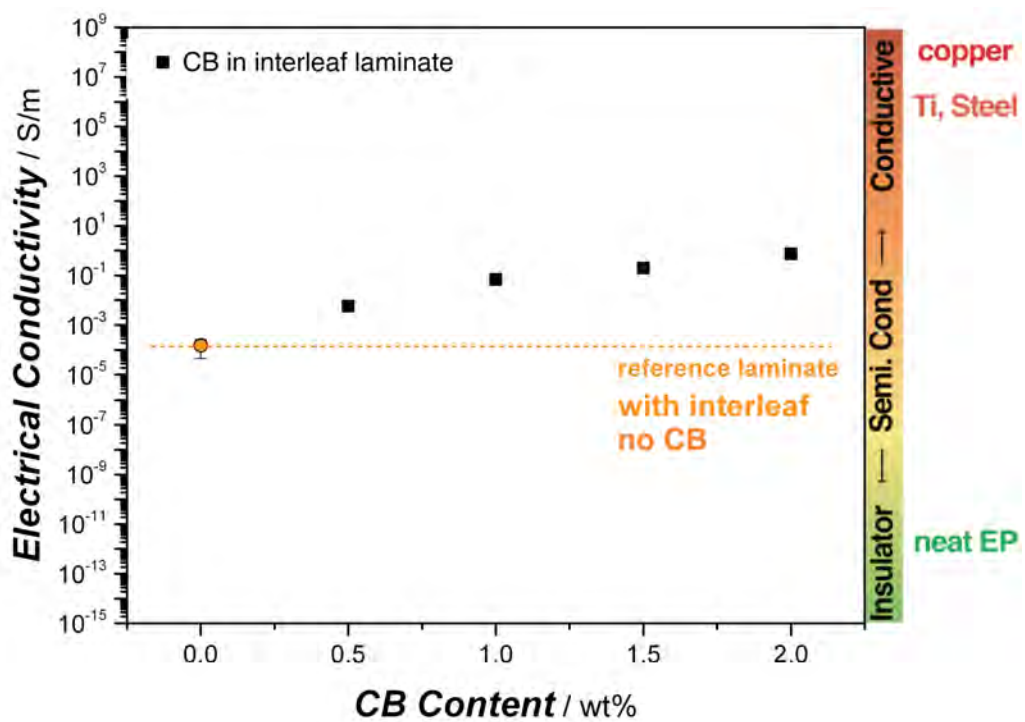


Figure 70. Electrical conductivity of interleaf toughened and CB modified prepreg laminates in z-direction as a function of CB content. Fiber volume contents of the laminates are comparable (except the laminate with 1.5 wt.% CB nanoparticles).

Fiber volume contents of all laminates are comparable and in the range of 52 to 54 vol.%. Only, 1.5 wt.% CB modified interleaf prepreg laminate (47 vol.%) shows lower FVC, which is attributed to the very low resin flow during prepreg consolidation

in the autoclave. In the interleaf toughened prepreg systems, however, the effect of FVC on conductivity is not substantial because the resin-rich interlayers prohibit the conduction in z-direction. The addition of only 0.5 wt.% CB in the resin leads to 30-times higher conductivity ($5.7 \cdot 10^{-3}$ S/m) compared to the reference interleaf laminate. The incorporation of 2 wt.% nanoparticle in the composite results in an electrical conductivity of 0.74 S/m, which is 4000 times higher compared to the neat prepreg laminate with interleaf (no CB). In addition, 2 wt.% CB modified interleaf prepreg laminate conducts better than the reference laminate without interleaf and no CB particles (0.2 S/m). The difference of conductivity in between 2 wt.% CB modified laminate without and with interleaf fleece is trivial.

Mechanisms of conduction in CB modified laminates with interleaf fleece

To investigate the agglomeration behavior of CB in prepreg laminates with interleaf fleece, SEM is used to analyze the surfaces of the neat and 1.5 wt.% CB-modified laminates. The SEM micrographs focus only on the resin rich areas to investigate the agglomeration of CB particles (Figure 71).

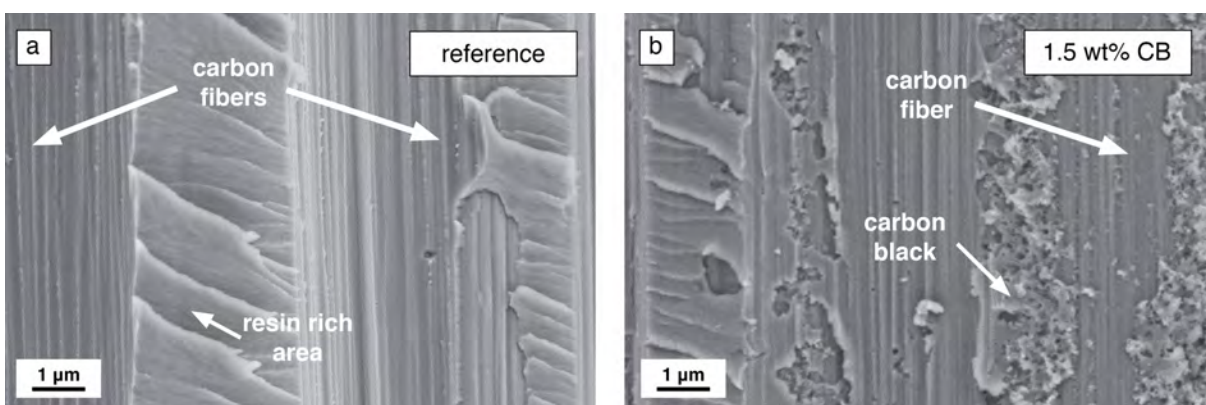


Figure 71. In-plane SEM micrographs of a) neat and b) 1.5 wt.% CB modified epoxy-CF prepreg laminates with PA6.6 interleaf fleece.

To study the morphology of CB modified epoxy-CF prepreg laminates with interleaf, 1.5 wt.% CB loading was chosen because this concentration is above the percolation threshold of CB in epoxy resin. As it can be seen, epoxy resin covers the fibers and acts as an insulator in between each CF. Figure 71.b reveals a very strong agglomeration of the CB nanoparticles in between CF. This observation in the interleaf prepreg laminate is contrary to case of prepreg laminate without interleaf, where CB does not agglomerate very strongly (Figure 65). The strong agglomeration of CB nanoparticles in prepreg laminate with interleaf is attributed to the difference in mobility of CB nanoparticles in these two different laminate structures. In prepreg laminate without interleaf, as previously discussed, 70 % of the measured fiber to fiber distances are below 2 μm , which likely constrain the mobility of the CB particles and prevent the CB agglomeration. On the other hand, laminate with PA6.6 interleaf regions consists of a high number of resin-rich areas, leaving space for CB to move and agglomerate in these resin rich zones.

5.2.3. Mechanical properties of laminates

Although the main focus of this work is to understand the through-thickness electrical conductivity of prepreg laminates modified with CB and interleaf fleece, the mechanical properties of the neat and modified laminates should also be investigated.

According to the literature, the addition of interleaf fleeces or nanoparticles to fiber reinforced epoxy composites improves interlaminar fracture toughness [148]–[150] under mode-I and mode-II loading. During the last two decades, inorganic nanoparticles including nano-silica [113], [151]–[154], carbon nanotubes [155], [156], [165]–[168], [157]–[164] carbon nanofibers [169]–[172], nanoclays [173]–[175], and nano-sized CB [54], [111] have been incorporated in epoxy resin and their fiber reinforced composites to enhance the fracture toughness.

Quasi-static interlaminar fracture toughness results of neat and CB modified laminates under mode-I and mode-II loading are presented and discussed in this chapter.

5.2.3.1. Mode-I loading

Mode-I fracture toughness of neat laminates (without CB)

The measured strain energy release rates (G_{Ic}) of the neat resin and neat laminates under mode-I loading are shown in Figure 72. In the prepreg laminates, the crack propagates parallel to the fiber direction.

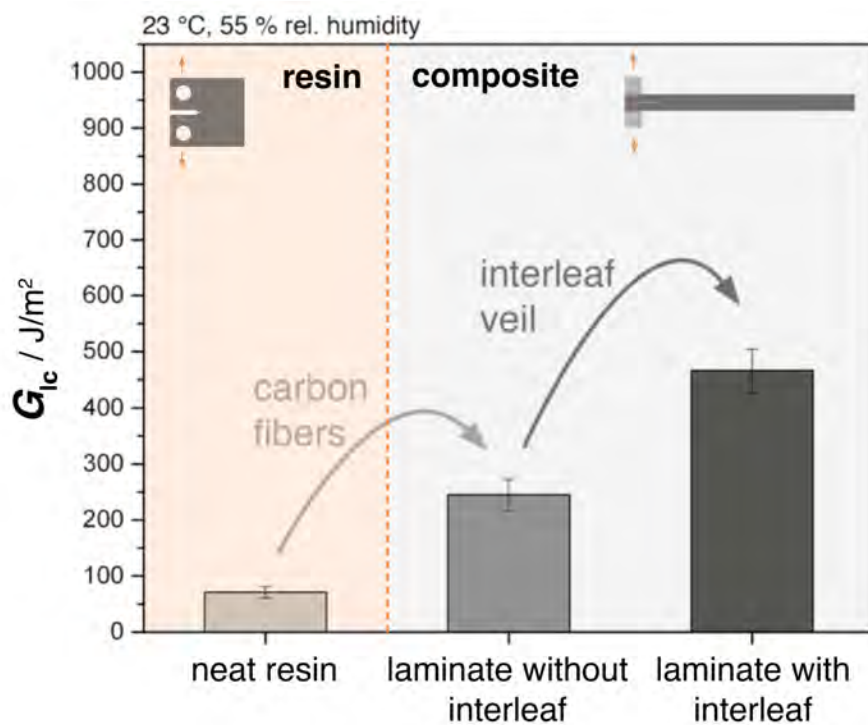


Figure 72. Quasi-static interlaminar fracture toughness of neat resin and laminates under mode-I loading.

As previously presented, the neat resin system is brittle with a strain energy release rate (G_{Ic}) of 71 J/m² under mode-I loading. Neat laminate without interleaf fleece has more than a three-fold higher toughness compared to the neat resin (250 J/m²). This increase is attributed mainly to CF bridging effects during the crack propagation [54].

In the case of interleaf fleece modified laminate, the addition of only polyamide 6.6 interleaf fleece substantially enhanced the toughness up to 466 J/m², which is 86 % higher than the laminate without interleaf toughening.

Morphologies of neat laminates-mode I

To develop an understanding regarding the failure mechanisms of the neat laminates without and with interleaf fleece, their fracture surfaces were studied in a detail. SEM micrographs are presented in Figure 73 and Figure 74. These prepreg laminates does not contain the carbon black nanoparticles.

According to Bradley [176], mode-I delamination of a fiber reinforced composite is dominated by two main parameters: resin toughness and fiber-matrix interfacial bonding strength. Figure 73 focuses first only the fracture surfaces, where only the CF and resin deformation can be investigated. In the case of the reference prepreg laminate without interleaf fleece (Figure 73.a), matrix deformation and carbon fiber pull-out are observed at the fracture surface. In addition, good fiber-matrix adhesion can be inferred from this micrograph, where a large amount of matrix fragments is found on the fiber surfaces after crack propagation. These two phenomena contribute to the energy release during crack propagation where CF crack bridging also occurs [177].

On the other hand, the fracture surface of the neat prepreg laminate with PA6.6 interleaf fleece is qualitatively more covered with the resin, as can be seen in Figure 73.b. A stronger deformation of the resin-rich areas during crack propagation is therefore evident.

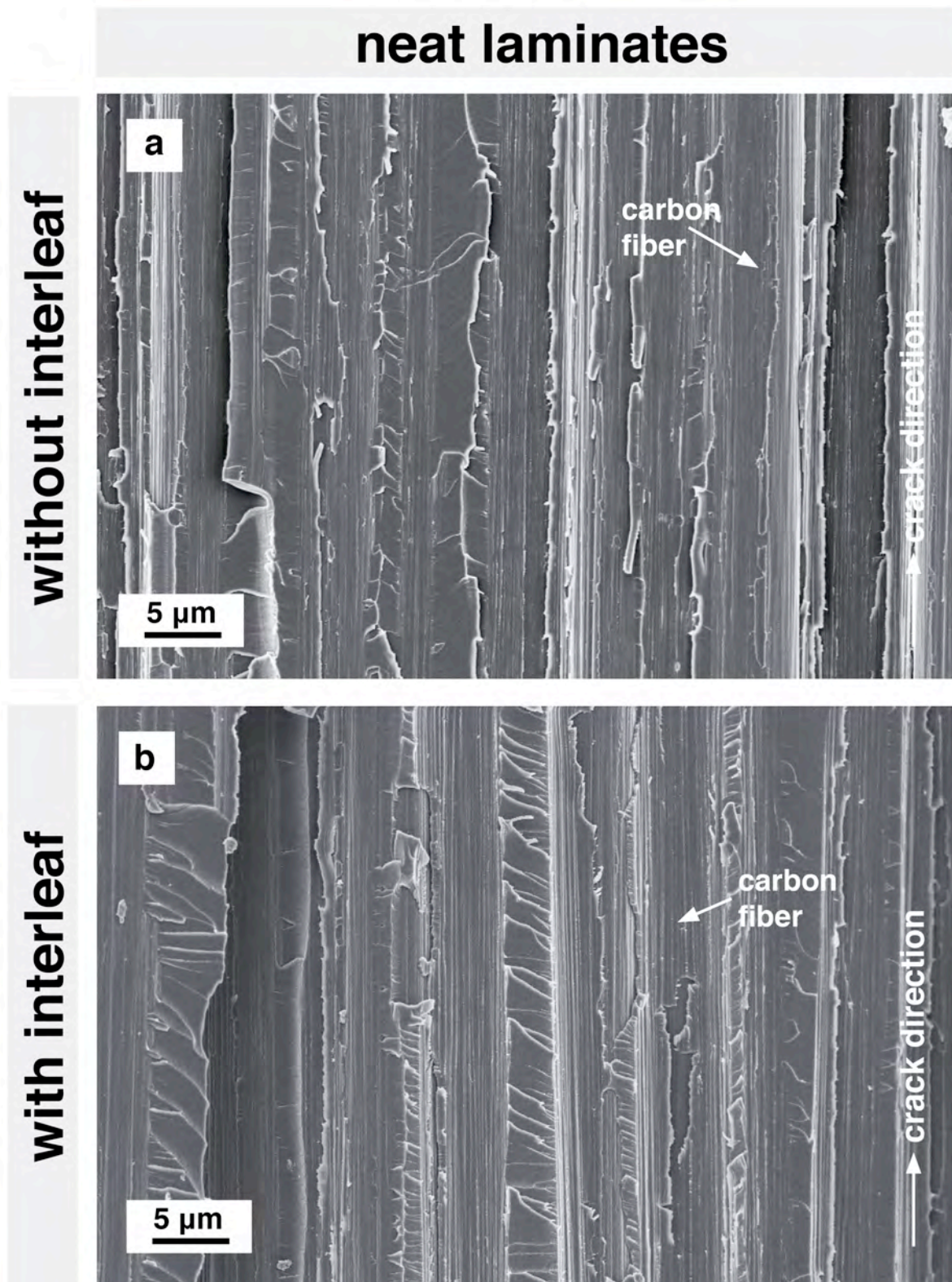


Figure 73. SEM micrographs of mode-I fracture surfaces of a) reference prepreg laminate without interleaf, b) reference laminate with PA6.6 interleaf. White arrows show the direction of crack propagation.

In addition to the deformation of resin-rich areas, pull-out and breakage of the PA6.6 interleaf fibers are also observable at the fracture surfaces of interleaf toughened laminate (Figure 74). Figure 74.a clearly shows the pulled-out polyamide fibers on the fracture surface of the laminate. A number of PA6.6 fiber breakages were also observed on the fracture surfaces, which are shown in Figure 74.b.

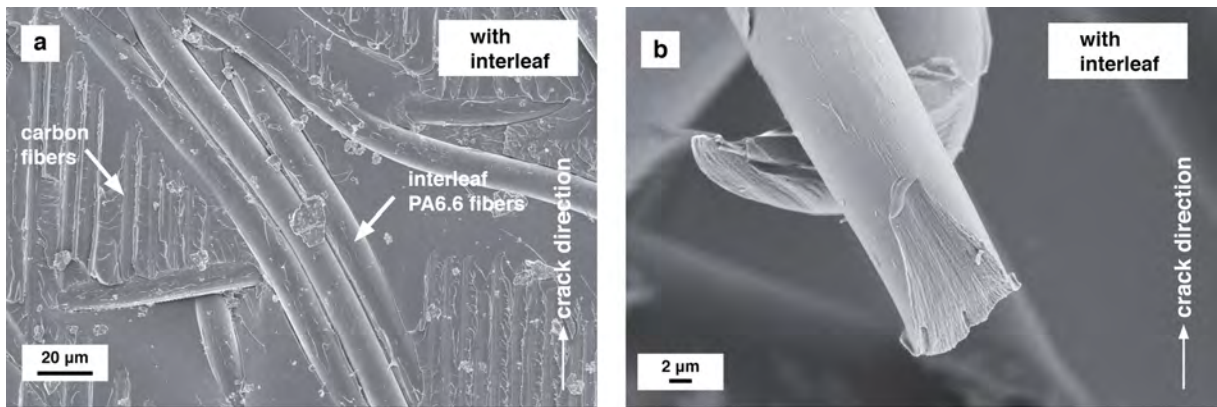


Figure 74. SEM micrographs of mode-I fracture surfaces of a) and b) reference prepreg with PA6.6 interleaf. Focus was given to the fracture mechanisms of PA6.6 interleaf fleece. White arrows show the direction of crack propagation.

Consequently, the PA6.6 interleaf fleece enhances the fracture toughness of the prepreg laminates under mode-I loading by almost 90 %, owing to increased matrix deformation and polyamide fiber pull-out and damage during crack propagation.

Mode-I fracture toughness of laminates modified with carbon black

The effect of CB on the mode-I fracture toughness of epoxy resin and its carbon fiber prepreg laminates is examined. The results are presented in Figure 75. Only 1.5 wt.% CB content is investigated since this additive content is already above the threshold concentration.

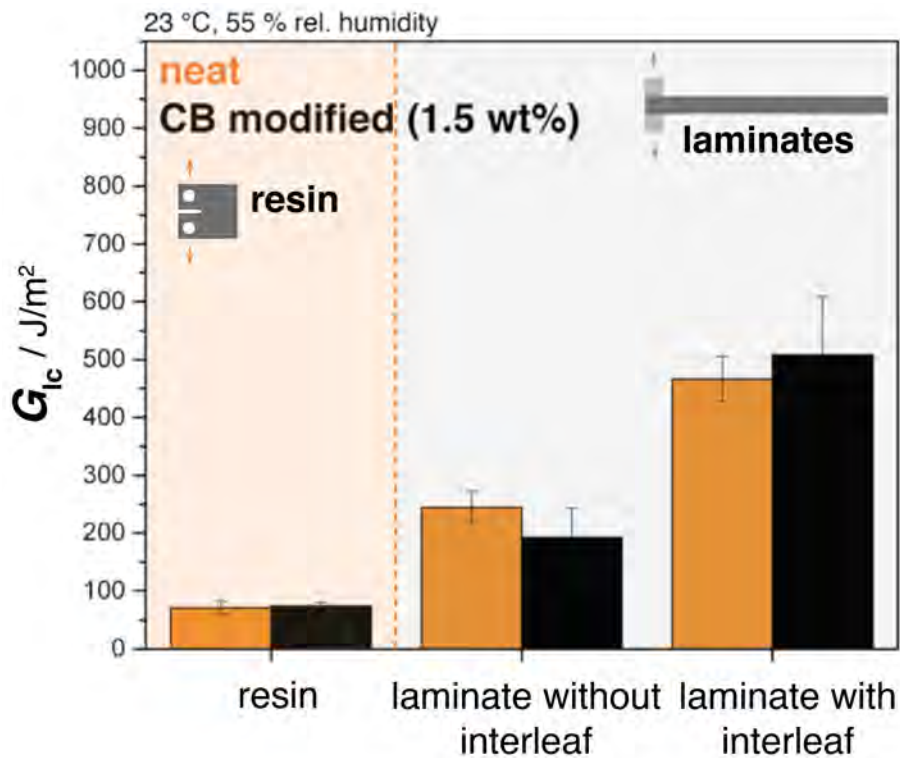


Figure 75. Quasi-static interlaminar fracture toughness of neat and 1.5 wt.% CB modified resin and their laminates under mode-I loading.

As shown by Figure 75, the addition of 1.5 wt.% CB does not dramatically affect the fracture toughness of the neat polymer and their fiber reinforced composites under mode-I loading. In the case of neat epoxy resin, 1.5 wt.% CB loading does not influence the fracture toughness (as previously discussed in chapter 5.1.2.6). In prepreg laminates without the interleaf fleece, the 1.5 wt.% CB modified laminate shows slightly lower fracture toughness (average G_{1c} of 192 J/m²) compared to the reference laminate. However, by taking the standard deviations into account, the decrement is minor. These findings are contrary to the work of Zhang et al. [54], where the addition of 3 wt.% CB (same product, Printex XE2) in a unidirectional epoxy-CF composite increased the mode-I fracture toughness under mode-I loading by 45 %.

On the other hand, the incorporation of 1.5 wt.% CB in interleaf fleece modified prepreg laminate increased the interlaminar fracture toughness under mode-I to an average of

508 J/m², which is 10 % higher compared to the reference interleaf toughened laminate, whereas this increment is negligible since the measured values with standard deviations are comparable.

Morphologies of composites with carbon black nanoparticles-mode I

The fracture surfaces of neat and 1.5 wt.% CB modified laminates (with and without interleaf fleece) are presented in Figure 76.

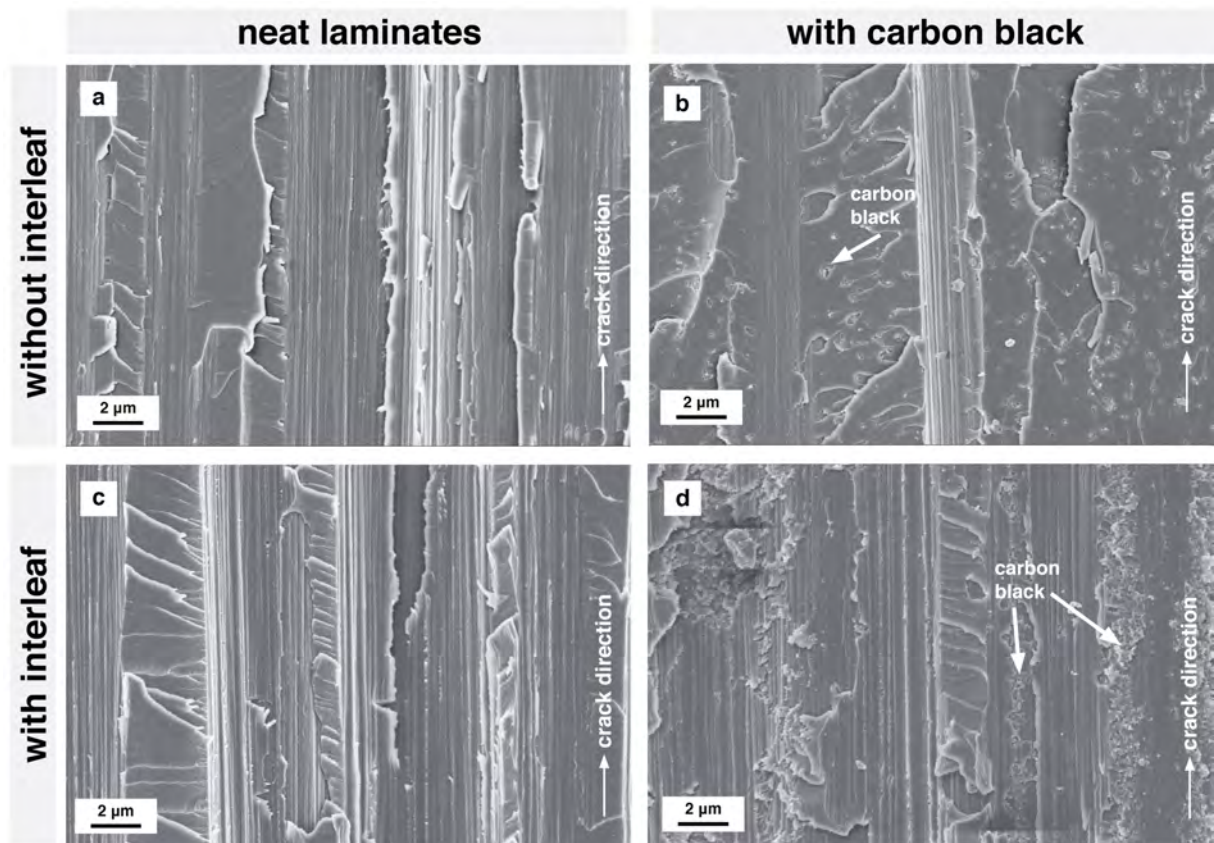


Figure 76. SEM micrographs of mode-I fracture surfaces of a) neat and b) 1.5 wt.% CB modified prepreg laminates without interleaf, c) neat and d) 1.5 wt.% CB modified laminates with PA6.6 interleaf. Arrows indicate the direction of crack propagation.

In the case of CB modified laminate without interleaf fleece (Figure 76.b), CB nanoparticles are mostly dispersed in resin-rich areas as small aggregates with an aggregate diameter below 1 μm , indicated by a white arrow. Tails of crack pinning are observed around the CB aggregates, whereas void formation is observed around the dispersed single particles.

In the case of CB modified prepreg laminates with interleaf fleece, an extensive agglomeration of CB nanoparticles in resin was detected (Figure 76.d). Although the matrix polymer is the same for both types of laminates, the stronger agglomeration of the CB is attributed to the higher mobility of CB particles in resin-rich areas of the interleaf modified prepreg laminate. As discussed previously, there is no strong inhibition of CB agglomeration in the interleaf regions, since there are no carbon fibers in resin-rich areas prohibiting the movement of the particles.

To study CB agglomeration behavior in CB modified interleaf prepreps more in a detail, backscattered electron micrographs are presented in Figure 77.

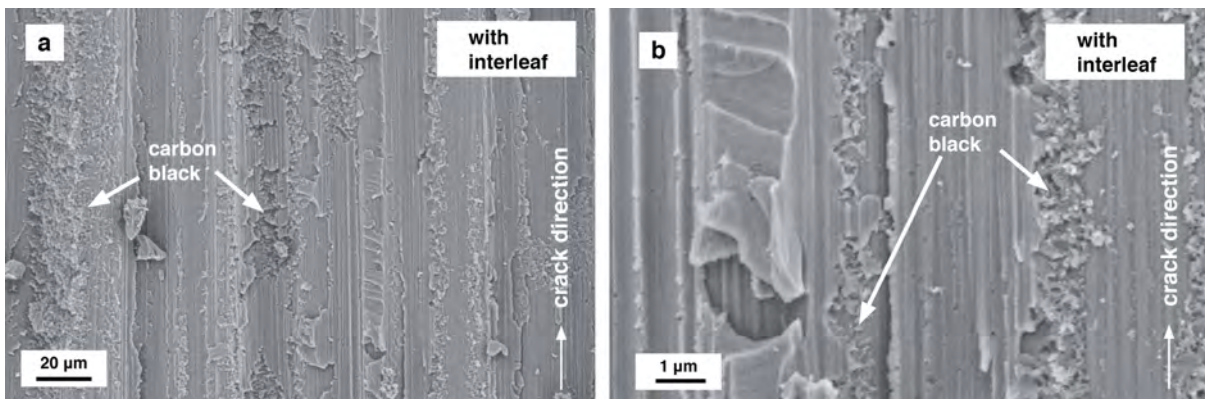


Figure 77. SEM micrographs of 1.5 wt.% CB modified laminate with PA6.6 interleaf fleece. Arrows indicate the direction of crack propagation. A backscattered electron detector was used.

Agglomerates of CB particles are mostly located in between CF. Particularly large amounts of CB containing matrix residues are detected on the CF, which are indicated with white arrows in Figure 77.

Consequently, the incorporation of CB particles in laminates without and with interleaf fleece did not deteriorate the fracture toughness under mode-I loading. In laminates without the interleaf fleece, CB nanoparticles did not show an extensive agglomeration in between CFs. Crack pinning and void formation around the CB aggregates were observed. In case of laminates with interleaf, despite the strong agglomeration of CB particles in resin rich areas, neither the fiber-matrix adhesion nor the formation of micro-cracks was influenced.

5.2.3.2. Mode-II loading

Mode-II fracture toughness of neat laminates (without carbon black)

Figure 78 presents the mode-II fracture toughness results of neat laminates with and without interleaf toughening.

Neat epoxy-carbon fiber laminate without interleaf fleece has a strain energy release rate of 750 J/m^2 under mode-II loading. According to Tang et al. [148], the G_{IIc} to G_{Ic} ratio for brittle composites lays in between 3 to 10, whereas for the tough systems this ratio is below 3 and gets closer to 1. In case of the neat epoxy-CF laminates without the interleaf fleece, the ratio of G_{IIc} to G_{Ic} is 3 which indicates the brittle nature of the laminate.

The addition of a PA6.6 interleaf fleece in between each prepreg layer led to a major enhancement of mode-II fracture toughness up to 982 J/m^2 , which is 30 % higher compared to the neat laminate without interleaf. Therefore, the incorporation of the fleece decreases the ratio of G_{IIc} to G_{Ic} down to 2, showing the toughening effect of the fleece under mode-II loading.

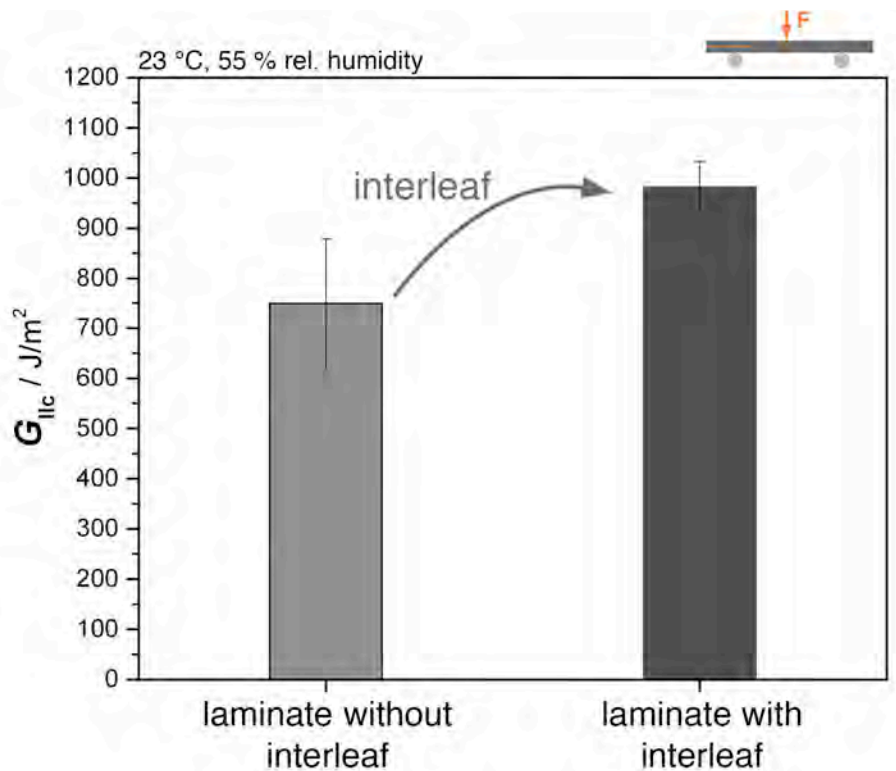


Figure 78. Mode-II interlaminar fracture toughness of neat prepreg laminates

Morphologies of neat laminates-mode II

SEM micrographs taken from mode-II fracture surfaces of neat laminates with and without interleaf toughening are shown in Figure 79. According to Altstädt et al. [7], because of the high shear loading in the resin rich zones, micro-cracking followed by micro-crack collapse and hackle formation is common for fiber reinforced epoxy composites under mode-II loading.

During crack propagation under mode-II loading, the crack tends to deviate from the propagation plane, which is however limited because of CF constraints. The hackling is therefore multiplied along the propagation plane, forming the final hackling patterns at the fracture surface. As shown in Figure 79.a and b, well-known shear-induced structures called “hackles” are clearly observable on the fracture surfaces of both laminates. CF pull-out was also observed for both types of prepreg laminates.

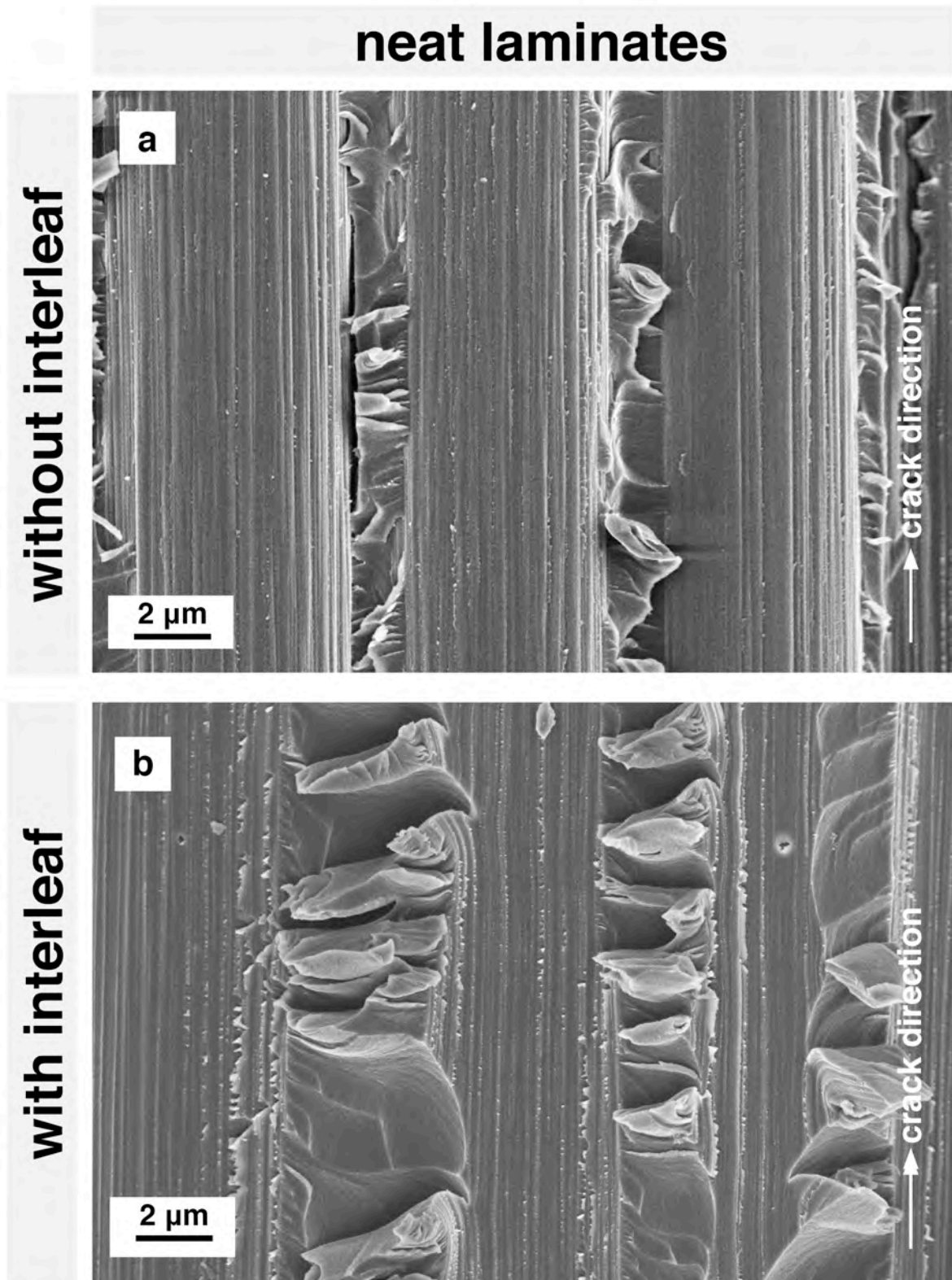


Figure 79. SEM micrographs of mode-II fracture surfaces of a) neat laminate without interleaf, b) with PA6.6 interleaf. Arrows indicate the direction of crack propagation. With these SEM micrographs, only resin deformation mechanisms are first investigated.

As previously described, the interleaf toughened laminate in this study shows 30 % higher mode-II fracture toughness compared to the laminate without the interleaf fleece. The dimensions of the hackles at the fracture surface of the interleaf modified laminate are much higher compared to the laminate without the interleaf fleece (shown in Figure 79).

Consequently, it can be concluded that the hackling is more pronounced in interleaf modified laminate compared to the laminate without interleaf.

Figure 80 reveals the deformation mechanisms of the polyamide interleaf fleece during crack propagation in the interleaf modified laminate.

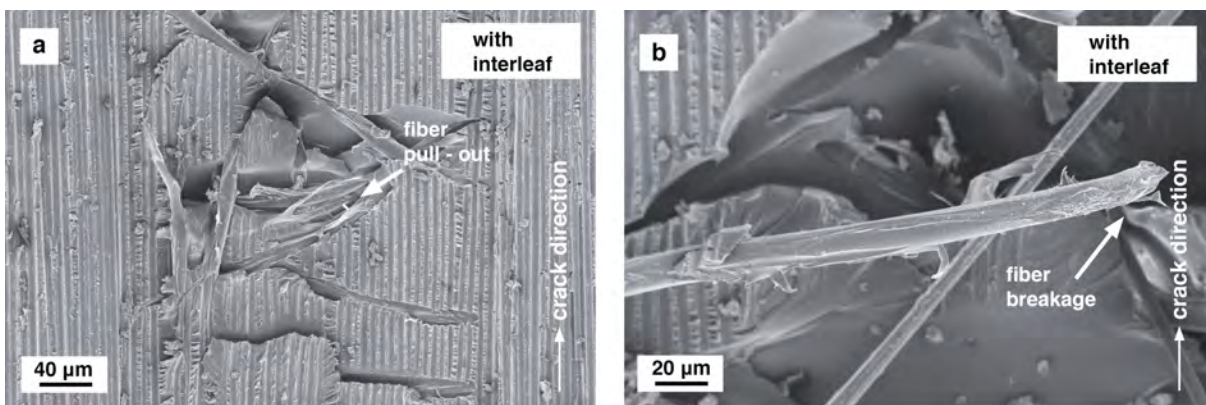


Figure 80. SEM micrographs of mode-II fracture surfaces of a) and b) neat prepreg laminate with PA6.6 interleaf fleece. Focus was given to the deformation of interleaf fleece. Arrows indicate the direction of crack propagation.

An extensive interleaf polyamide fiber pull-out (Figure 80.a) and breakage (Figure 80.b) were observed in the interleaf toughened laminate. The pull-out and damage of the interleaf fleece significantly contribute to the strain energy release rate during crack propagation under mode-II loading.

Mode-II fracture toughness of laminates with carbon black

The effect of CB on the interlaminar fracture toughness of laminates under mode-II loading is shown in Figure 81.

The addition of 1.5 wt.% CB to both types of prepreg laminates slightly increases the mode-II fracture toughness. In case of laminates without interleaf, addition of 1.5 wt.% CB yields to G_{IIc} of 788 J/m², which is 5 % higher compared to the reference laminate without interleaf. However, this increase is still minor considering the standard deviation of the measurements. The addition of the same content nanoparticle in the interleaf laminate has no effect on mode-II fracture toughness. As previously reported as well by Zhang et al. [54], the addition of CB nanoparticles in the resin component up to 3 wt.% only slightly increases the G_{IIc} of its CF-epoxy RTM laminates.

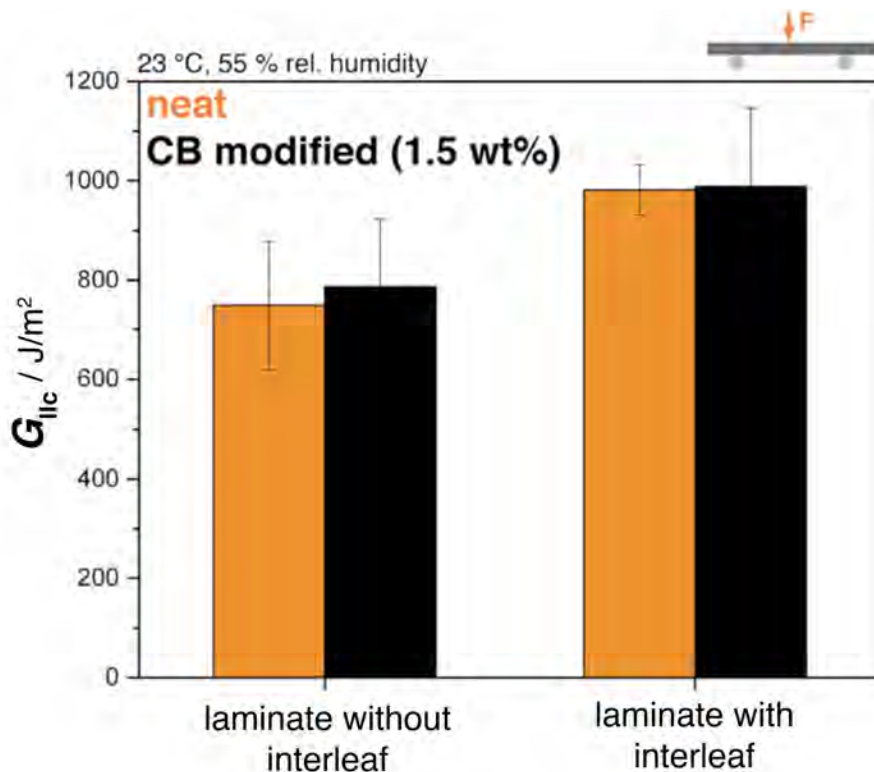


Figure 81. Mode-II interlaminar fracture toughness of neat and 1.5 wt.% CB modified prepreg laminates

Morphologies of laminates with carbon black-mode II

The addition of 1.5 wt.% CB increases the mode-II fracture toughness of the prepreg laminates slightly, which is in agreement with the previous studies [54]. The SEM micrographs taken from fracture surfaces are shown in Figure 82.

CB particles, as nanosized aggregates, were observed on the hackle structures (Figure 82), which are indicated with a white arrow. In addition, 1.5 wt.% CB modified laminate without interleaf fleece (Figure 82.a) shows locally more pronounced hackle formation compared to the neat laminate without interleaf (Figure 79.a), which is attributed to the higher resin volume content in the CB modified laminate.

Although the existence of CB agglomerates in the interleaf modified laminate does not influence toughness under mode-II loading compared to the neat laminate, CB nanoparticles influence the size and shape of the hackles as presented in Figure 82.b and Figure 79.b. In particular, the shape of hackles observed in Figure 82.b are not smooth compared to the reference laminate (Figure 79.b). Although the hackle formation was not suppressed by the CB nanoparticles, the height of the hackles were decreased in the presence of CB nanoparticles dispersed in the matrix. In addition, it is concluded that the crack mostly propagates at the interphase of the PA6.6 fleece and prepreg layers, since the fracture surfaces mostly lack the PA6.6 fibers.

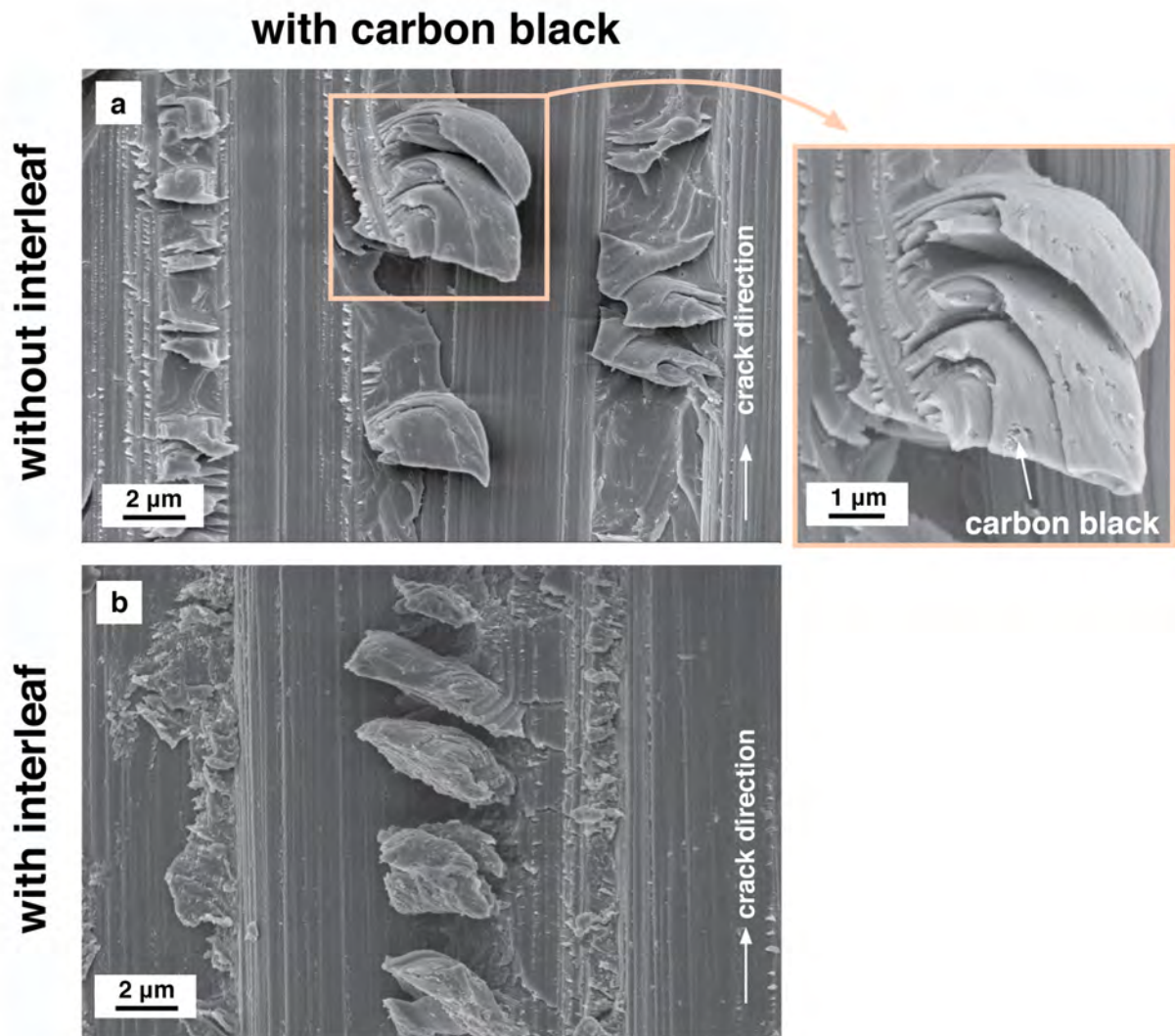


Figure 82. SEM micrographs of mode-I fracture surfaces of a) and b) 1.5 wt% CB modified laminate without interleaf, c) and d) 1.5 wt% CB modified laminate with PA6.6 interleaf. Arrows indicate the direction of crack propagation.

As in the neat interleaf modified laminate, the interleaf fleece itself contributes to the strain energy release rate in CB modified interleaf laminate (Figure 83.a and b). Micrographs clearly show the perpendicular pull-out of PA6.6 fibers from the fracture surface, and some PA6.6 fiber breakages are also observable. It is expected that the interleaf fleece peeled off from the fracture surface rather than pull-out perpendicularly. This is possibly due to the fact that a some PA6.6 fibers passed through the prepreg

layer during consolidation of the laminate, which then acted like pins in between prepreg layers during the crack propagation.

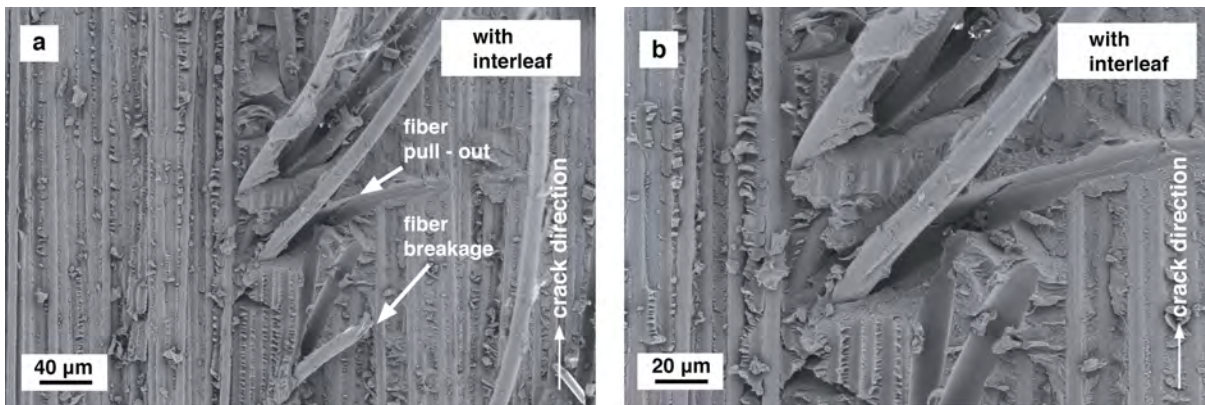


Figure 83. SEM micrographs of mode-II fracture surfaces of a) and b) 1.5 wt.% CB modified prepreg laminate with PA6.6 interleaf. Focus was given to the interleaf damage mechanisms. Arrows indicate the direction of crack propagation.

Consequently, the effect of the interleaf fleece on the mode-II interlaminar fracture toughness of laminates is very pronounced. This effect is attributed to the pull-out and breakage of the polyamide fleece during crack propagation, under mode-II loading. In addition, due to the increased resin rich regions due to the interleaf fleece, hackle formation was increased. The addition of 1.5 wt.% CB nanoparticles in laminates led to a minor increase of the interlaminar fracture toughness under mode-II loading.

5.2.4. Summary

In the case of neat epoxy-CF laminates without any interleaf, the electrical conduction in the z-direction is realized by carbon fibers that are in contact with each other. It is clearly shown in this work that the percolating network of CF in laminates without interleaf consists of two main domains: fiber-rich and resin-rich regions with few bridging CFs. In the fiber-rich regions, approximately 30 % of the measured fiber to

fiber distances indicated the direct contact, whereas the remaining 70 % of the measured interfiber distances were in the range of 1 to 8 microns.

Because most of the CFs are not in direct contact with their neighboring fibers, the through-thickness electrical conductivity of the laminate without interleaf is highly susceptible to increasing fiber volume content. To the best of our knowledge, an exponential relationship (Equation (4)) was found between the electrical conductivity and fiber volume content varying from 46 to 73 vol.% for the first time. It is possible to calculate the electrical conductivity of a neat laminate with a desired FVC using this equation, which is valid for this particular composite system.

The addition of CB in the epoxy-CF prepreg laminates leads to a higher than ten-fold enhancement at only 2 wt.% CB content in the resin. This observation agrees well with the literature [54]. Carbon black nanoparticles were dispersed as small aggregates between CFs and no filtration by the CFs was detected during prepreg production. The low agglomeration of CB during laminate consolidation (by air pressure in autoclave) is attributed to the hindering effects of fibers on the mobility of the CB nanoparticles. The increase in electrical conductivity of laminates by CB addition is due to the fact that CB nanoparticles act as a bridge between non-contacting CFs.

The incorporation of only 10 g/m² interleaf fleece in between each prepreg layer significantly reduces the through-thickness electrical conductivity of the prepreg laminates. The reduced conductivity is due to the lowered number of carbon fiber to fiber contacts, since the micro-CT results show a mostly linear and constant interleaf region through the laminate. Equation (4) is not valid for the interleaf prepreg laminates because the carbon fiber to fiber contacts are hindered by the epoxy rich interlaminar regions.

As shown systematically in this work, the addition of CB nanoparticles in the interleaf prepreg laminates substantially increases the electrical conductivity. The 2 wt.% CB modified prepreg laminate with interleaf conducted four times better when compared to the neat prepreg laminate without the interleaf fleece. This effect is attributed to the different agglomeration dynamics of the nanoparticles in prepreg laminates with and

without interleaf spacing. The CB agglomerates more effectively in the interleaf prepreg laminates because the interleaf regions provide the epoxy-rich zones for CB nanoparticles to agglomerate. These observations expand the state of the art in the field of interleaf toughened and conductive prepreg laminates.

The developed neat epoxy resin used in this study is brittle with a low G_{Ic} value of 71 J/m². The brittleness of the matrix polymer is transferred to its fiber reinforced composite, where neat epoxy-carbon fiber prepreg laminate without interleaf has a G_{Ic} of 250 J/m². Use of the PA6.6 interleaf fleece results in an almost doubled G_{Ic} due of higher deformation of resin rich regions, interleaf fiber pull-out and breakage during crack propagation.

In the case of mode-II loading, the hackle formation were observed for all laminates. The neat epoxy-CF prepreg laminate showed a G_{IIc} value of 750 J/m², which is three times higher than that under mode-I conditions. The incorporation of interleaf fleece increased the mode-II energy release rate up to 982 J/m², which is approximately 30 % higher compared to the reference laminate without interleaf. This is attributed to the interleaf fiber pull-out and breakage together with an enhanced hackle formation.

The addition 1.5 wt.% CB in the resin did not significantly influence the interlaminar fracture toughness of prepreg laminates under both loading conditions. Neither fiber-matrix adhesion nor deformation of resin-rich areas were affected by CB nanoparticles. These findings are contrary to the work of Zhang et al. [54], where the addition of 3 wt.% CB (same product, Printex XE2) in a unidirectional epoxy-CF composite increased the mode-I fracture toughness under mode-I loading by 45 %. The measured difference is attributed to the used CuCl₂ salt in the work by Zhang et al. [54] resulting in a pronounced agglomerate formation, which is expected to enhance the crack-CB particle interactions during crack propagation.

5.3. Lightning strike resistance of prepreg laminates

Increased through-thickness electrical conductivity of a composite plays a particularly crucial role in enhancing electrical energy dissipation during a strike, as recently reported by Hirano et al. [82]. To investigate the impact of the through-thickness electrical conductivity of interleaf modified laminates on the lightning strike resistance, reference and 2 wt.% CB modified interleaf laminates were tested under 20 kA impulse current. As described in chapter 2, previous studies in literature used peak currents from 10 to 100 kA. A representative curve of applied current versus time is presented in Figure 84.

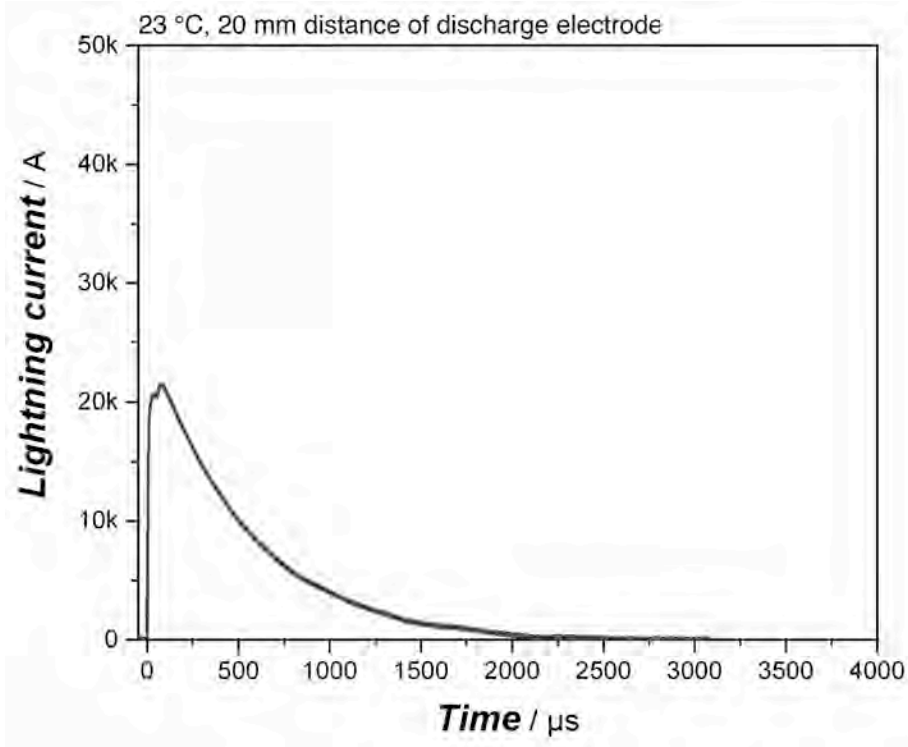


Figure 84. a) Representative curve of the current of lightning passing through test laminates.

After 70 μs , the 20 kA peak current had already passed through the composite samples. 10 kA was already dissipated within the first 500 μs , and the total energy was dissipated after 2.5 ms.

For this particular test, the reference interleaf prepreg laminate was compared to the 2 wt.% CB modified interleaf prepreg laminate, which showed the highest conductivity. Ultrasound scans (C-scan) from back-surface echo of laminates before and after testing are shown in Figure 85.

The reference interleaf laminate is a semi-conductor with a through-thickness conductivity of $1.5 \cdot 10^{-4}$ S/m, where 2 wt.% CB modified interleaf laminate is almost a conductor with a through-thickness conductivity of $7.4 \cdot 10^{-1}$ S/m (i.e., 5000 times higher). The thermo-mechanical properties of the resin and the interlaminar fracture toughness for these two systems are identical, as described previously.

From ultrasound scans (C-scans) of both laminates (Figure 85.a and Figure 85.b) it can be seen that both laminates show inhomogenities prior to testing, which are attributed to trapped air in both laminates during curing. A 20 kA lightning current resulted in major damage in the reference interleaf laminate with a semi-conductor nature, as shown in Figure 85.c. However, delaminations were more pronounced in the 0° fiber direction. The delaminated area was measured (via ImageJ) to be approximately 94.5 cm^2 for the neat interleaf laminate. The magnitude of the measured damaged area is reasonable according to the reported literature values, although the applied peak current and tested laminate conductivities vary [82], [87]. In the case of 2 wt.% CB modified interleaf laminate, the delamination was located more at the laminate center and propagated in both fiber directions of 0° and 90° , which can be seen in Figure 85.d. The delamination area was suppressed by 45 % and observed to be much more localized, which was measured to be approximately 51.7 cm^2 .

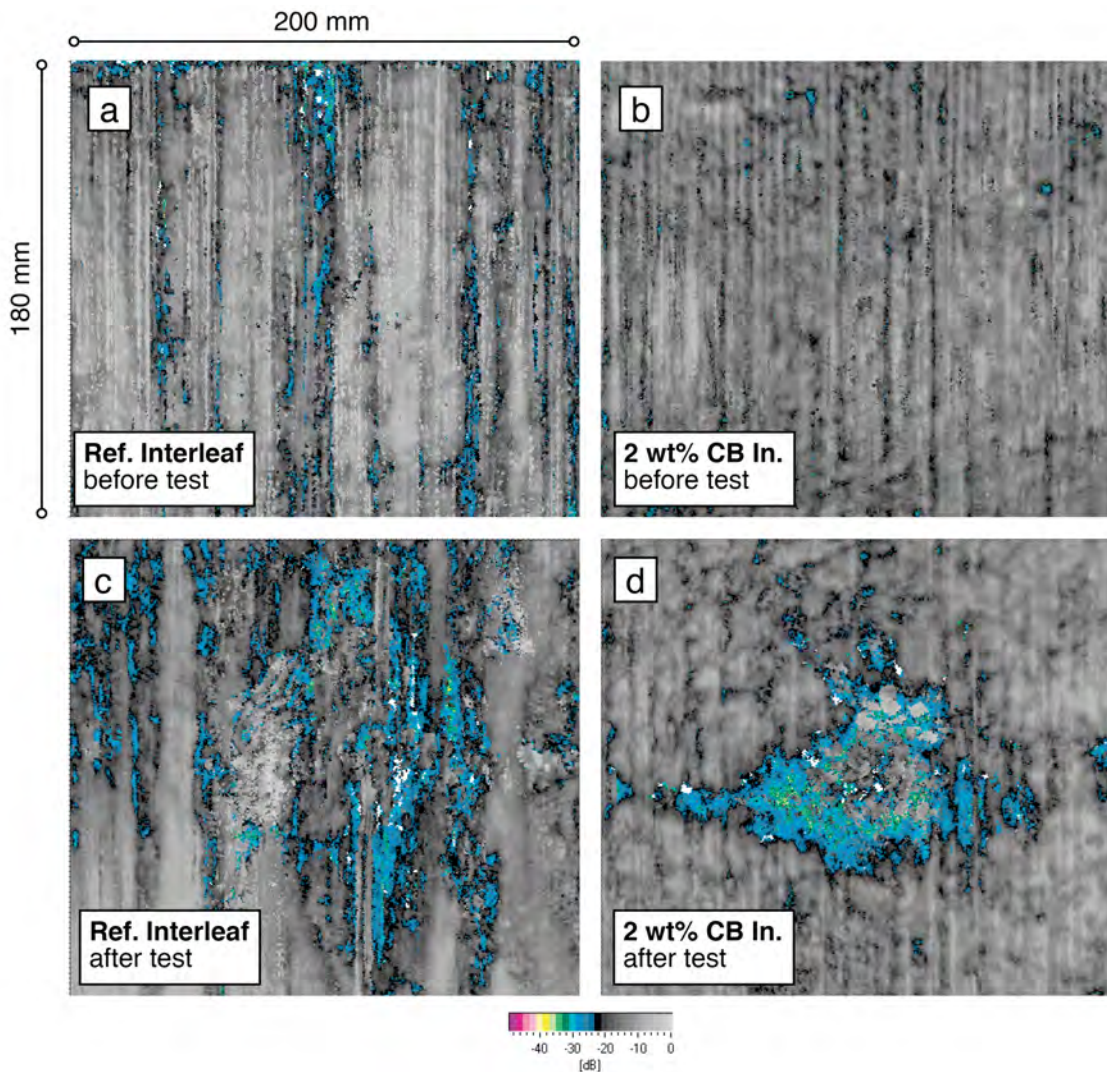


Figure 85. a) and c) Ultrasound C-scans of reference and b) and d) 2 wt.% CB modified interleaf (CB-In.) laminate before and after the lightning strike testing, respectively. 0° fiber direction for laminates is from below to above.

To evaluate the impact of the 20 kA strike through the laminate thickness, cross-sectional optical micrographs are taken from the center of both of the laminates (Figure 86).

A major laminate damage was observed for the neat laminate with interleaf, after 20 kA impulse current, as shown in Figure 86.a. The strike passed through all the prepreg layers in the laminate and resulted in a pronounced damage.

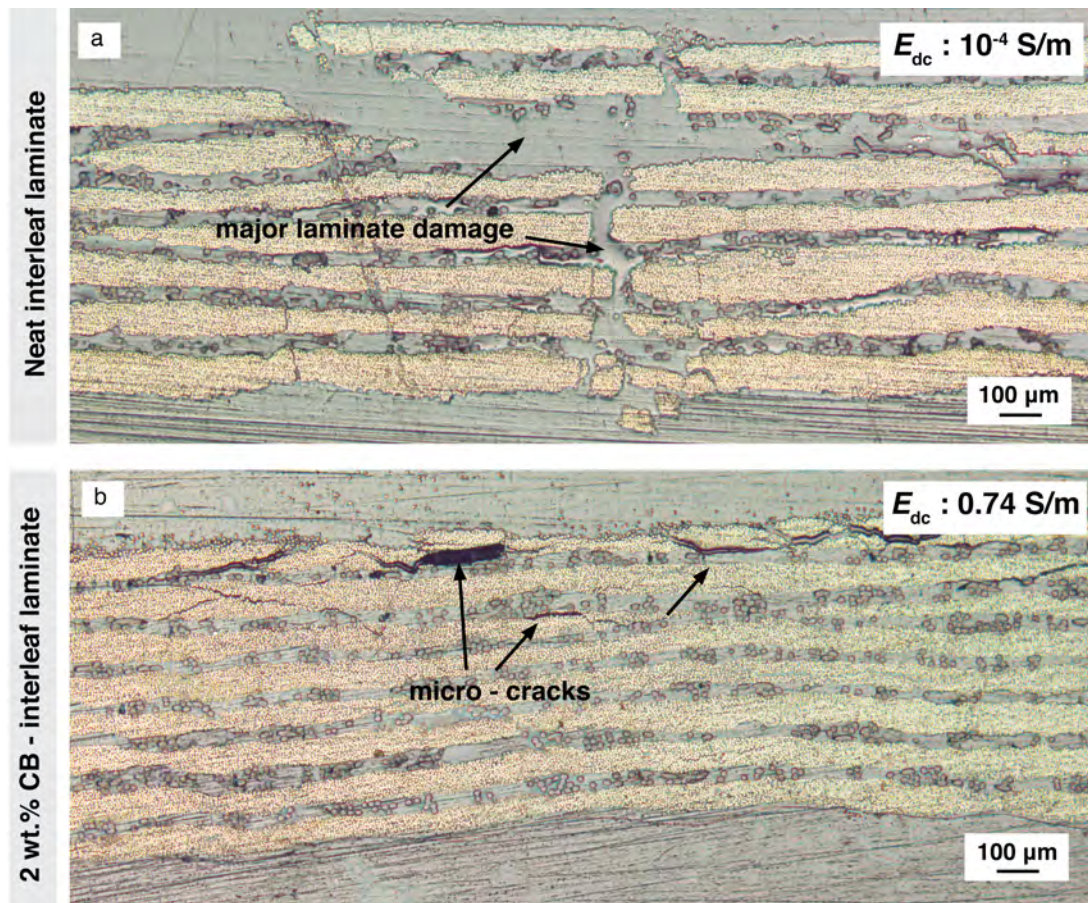


Figure 86. Cross-sectional optical micrographs of a) reference and b) 2 wt.% CB modified laminates with interleaf fleece. Images are taken after the lightning strike testing.

Only micro-crack formation in the first three prepreg layers was observed for the 2 wt.% CB modified interleaf laminate, after 20 kA strike (Figure 86.b). The deformation was more pronounced at the outermost layer. The rest of the laminate stayed intact.

In conclusion, the addition of the carbon black nanoparticles in the laminate with interleaf fleece enhanced the lightning strike resistance tremendously. The delamination area was suppressed by 45 % and the delamination depth was only limited to first three prepreg layers, whereas the neat laminate with interleaf was completely damaged after 20 kA strike. This is attributed to the enhanced through-thickness electrical conductivity due to CB particles.

6 Conclusions

The main scientific focus of this study was laid on understanding of the effect of amorphous carbon black nanoparticles on the electrical and mechanical properties of epoxy carbon fiber prepreg laminates with and without interleaf toughening. The relationship between the carbon fiber volume content and the electrical conductivity of prepreg laminates was also studied in detail. Finally, the effect of carbon black on the lightning strike resistance of the interleaf prepreg laminates was investigated.

Blending the DGEBA resin with TGMDA increased the dry T_g (G^1 -onset) almost linearly. The DGEBA-4,4'-DDS resin system showed a dry T_g of 166 °C, whereas the TGMDA-4,4'-DDS system had a T_g of 236 °C. To achieve the dry T_g over 200 °C, a 60 phr TGMDA and 40 phr DGEBA resin blend cured with 4,4'-DDS was used in this work as reference epoxy resin system. This resin system showed excellent thermo-mechanical properties with 219 °C dry T_g and 201 °C wet T_g .

As expected, the selected epoxy resin mixture in this study is a highly insulating polymer with an electrical conductivity of $7.7 \cdot 10^{-12}$ S/m. The 3-roll milling technique was investigated to be the most suitable processing route due to excellent pre-dispersion of the carbon black in uncured resin. Up to 2 wt.% of CB in the resin results in an insulator to semiconductor transition with 10^{-4} S/m volume conductivity. The percolation threshold was found to be roughly at 0.5 wt.% carbon black loading in the cured state. TEM micrographs reveal a conducting network consisting of branched carbon black agglomerates as well as single CB particles.

The neat TGMDA-DGEBA (60 : 40)-4,4'-DDS resin system showed a K_{Ic} of 0.48 MPa. \sqrt{m} . Carbon black particles led to an increase of the fracture toughness of the neat resin up to 1 wt.%, whereas a diminishing effect of CB at 2 wt.% additive content was observed, which is attributed to particle agglomeration.

The through-thickness electrical conductivity of the prepreg laminates without interleaf is highly susceptible to slight changes in the fiber volume content since the conductivity was mostly dominated by CF. The neat prepreg laminate with 46 vol.% FVC showed a through thickness conductivity of $2.3 \cdot 10^{-2}$ S/m. On the other hand, the laminate with 72 vol.% fibers had already conductive behaviour with 12 S/m conductivity. For this particular composite system, an exponential relationship (equation 4, chapter 5.2.2.1) was found that correlates the electrical conductivity and the fiber volume content, which can be used to estimate the through-thickness conductivity of a carbon fiber-epoxy composite at a desired carbon fiber volume content. The conducting network of CF consists of two main domains: a fiber-rich and a resin-rich. Measurements of fiber to fiber distances allow a rough estimation of the fiber distribution in the fiber rich domains. 30 % of the measured fiber to fiber distances indicate the interfiber contact, whereas the remaining 70 % show an interfiber distance in the range of 1 to 8 μm .

The addition of carbon black leads to a more than ten-fold conductivity enhancement at maximum additive content of 2 wt.%. It is suggested that the carbon black nanoparticles create a bridge between non-contacting CF. 2 wt.% CB modified laminate without interleaf show a conductivity of 3.2 S/m, which is a conductor.

The incorporation of only 10 g/m² interleaf fleece in between each prepreg layer hinders the carbon fiber contacts and lowers the conductivity significantly (10^{-4} S/m), which is almost three orders of magnitude lower compared to the reference laminate without interleaf fleece. In contrast, carbon black nanoparticles substantially increase the electrical conductivity of interleaf prepreg laminates. 2 wt.% CB modified interleaf prepreg laminate show a conductivity of nearly 1 S/m, which is a conductor. Carbon black agglomerates much stronger during the laminate consolidation in the interleaf prepreg laminates because epoxy-rich interleaf regions do not consist of highly packed carbon fibers, which constrain the mobility of carbon black in the resin.

It is therefore possible to adjust the electrical conductivity of the prepreg laminates (without interleaf) with the resin content. However, such an adjustment is not possible

for laminates with an interleaf. Therefore, CB particles play a major role for enhanced conductivity in the laminates with interleaf fleece.

Finally, Figure 87 compares the achieved maximum electrical conductivities in this work with the values reported in the literature.

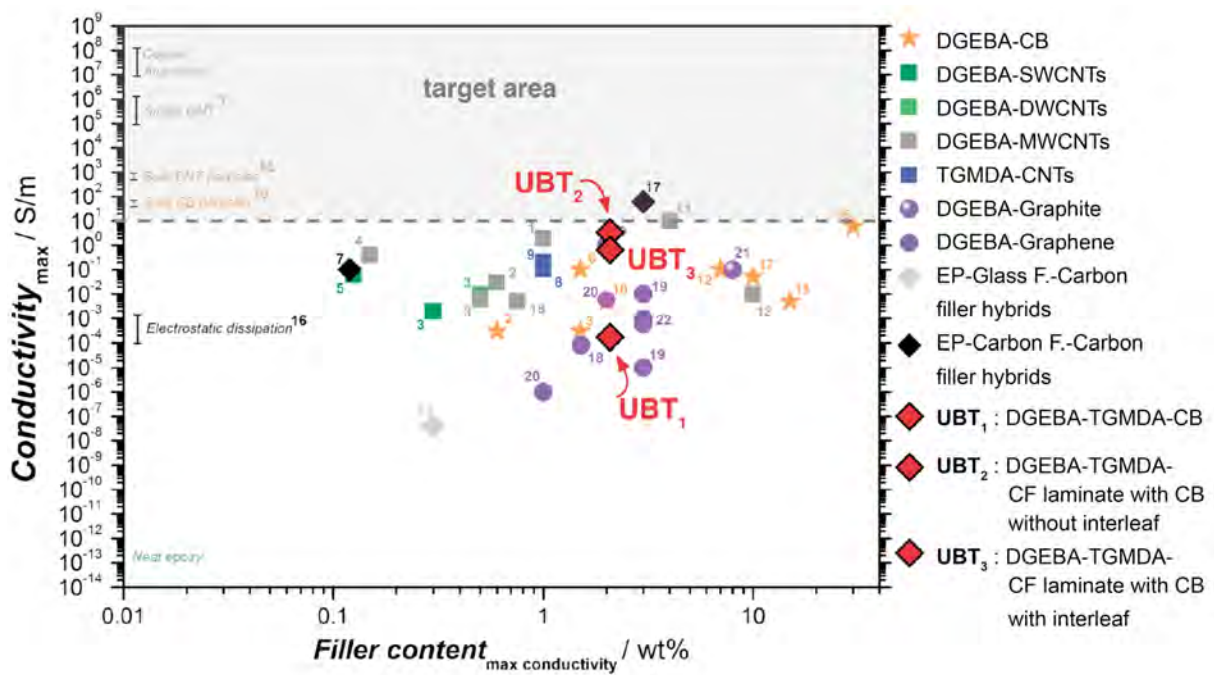


Figure 87. Comparison of maximum achieved conductivities in this work with published data in literature in the field of epoxy nanocomposites and laminates. Data points: 1 [43], 2 [44], 3 [45], 4 [46], 5 [35], 6 [47], 7 [5], 8 [48], 9 [49], 10 [29], 11 [50], 12 [32], 13 [51], 14 [52], 15 [9], 16 [53], 17 [54], 18 [55], 19 [56], 20 [57], 21 [58], 22 [59], 23 [33].

Data point UBT₁ indicates the epoxy-CB nanocomposite with 2. wt.% CB content, where the UBT₂ and UBT₃ are laminates containing 2 wt.% CB without and with interleaf fleece, respectively. Firstly, the measured data in this work agrees very well with the data published in literature. In case of epoxy-CB nanocomposite, achieved maximum conductivity of 10⁻⁴ S/m at 2 wt.% CB loading is relatively lower compared to the literature. This is attributed to the high viscosity of the used resin system in this

work, since mostly two functional DGEBA resin was used in literature. Laminates with 2 wt.% CB on the other hand, almost reached to the targeted area of 10^1 S/m.

Strain energy release rates of 250 and 750 J/m² were measured under mode-I and mode-II loading, respectively, for the neat laminate without interleaf. The incorporation of PA6.6 interleaf toughening doubles the G_{Ic} and results in a 30 % higher G_{IIc} compared to the reference laminate without interleaf. Under mode-I loading, higher resin deformation, polyamide fiber pull-out, and breakage are responsible for the increased toughness for interleaf toughened laminates. On the other hand, pronounced hackle formation and fiber pull-out are responsible for the higher mode-II strain energy release rate after interleaf toughening. The addition of carbon black does not significantly influence the interlaminar fracture toughness of the laminates under both loading conditions. Fiber-matrix adhesion and deformation of the matrix or fibers are not affected by carbon black nanoparticles.

To correlate the electrical conductivity with the lightning strike resistance, the reference and 2 wt.% CB modified laminates with interleaf were studied using a 20 kA peak impulse current. In the case of the reference interleaf laminate with semiconducting behavior (10^{-4} S/m conductivity), the delaminated area after the strike was 94.5 cm², which is in agreement with the literature [82], [87]. In the 2 wt.% CB modified interleaf laminate with a conducting behavior (approximately 1 S/m conductivity), only the laminate center was damaged and the delamination area was suppressed by 45 % compared to reference laminate. Optical micrographs from the cross-sections were taken from the center of the laminates after the strike. A 20 kA current impulse resulted in a major damage in the reference laminate by destroying all the prepreg layers in the through-thickness direction. 2 wt.% CB modified laminate, however, showed only micro-cracking in the first three prepreg layers, where most of the laminate was still intact after a 20 kA current impulse. This is attributed to the high through-thickness electrical conductivity of the composite, which is crucial for dissipating the extremely high energy of a lightning strike. By means of these investigations, a fourth-generation prepreg system with highly enhanced mechanical and electrical properties was developed which can be used for various new composite applications.

7 Outlook and future work

In this final chapter, two new promising approaches towards electrically conductive composites are presented and discussed in detail as an outlook and future work.

7.1. Carbon black with various organic tougheners

As previously described in chapter 2.2.4.4, the inclusion of a second phase (e.g., tougheners or inorganic nanoparticles) in addition to the conducting additives can tailor the dispersion and distribution state of conductive particles, which leads to a different level of the overall conductivity. The effect of core-shell particles (insoluble in resin) and OH-terminated polyether sulfone (PESU) tougheners (soluble in resin, no phase separation during curing) on the electrical conductivity of already CB modified epoxy resins and its prepreg laminates is therefore worthy of further study. To explore this possibility, 5 wt.% core-shell or PESU was added to an already 1.5 wt% CB containing epoxy nanocomposite. The final electrical conductivity of these binary composites is compared to neat epoxy and a only 1.5 wt.% CB modified nanocomposite (Figure 88).

As discussed, the addition of only 1.5 wt.% CB in the neat epoxy results in a semiconductor nanocomposite with a conductivity of $7 \cdot 10^{-5}$ S/m. The further addition of 5 wt.% soluble OH-terminated polyethersulfone (PESU) to this nanocomposite decreases the conductivity by more than one order of magnitude ($6.1 \cdot 10^{-6}$ S/m). In contrast to PESU, the addition of the same content of core-shell particles to already 1.5 wt.% CB containing epoxy nanocomposite leads to almost 500 times higher electrical conductivity compared to the CB modified system ($3.6 \cdot 10^{-2}$). It is expected for an insulating soluble organic toughener to decrease the electrical conductivity of CB modified epoxy nanocomposite because the viscosity of the formulation increases dramatically, which reduces the mobility and therefore the agglomeration of the CB particles in resin during curing.

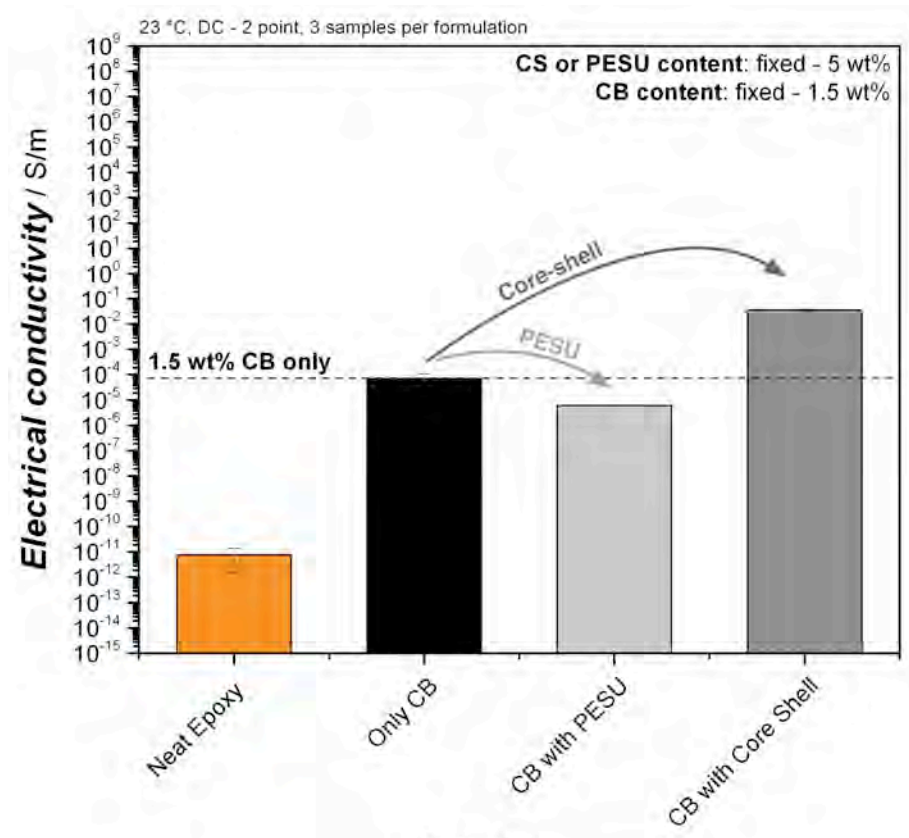


Figure 88. Electrical conductivity of neat epoxy and 1.5 wt.% CB-epoxy nanocomposite compared with binary mixtures of 1.5 wt.% CB with additional 5 wt.% core-shell or PESU tougheners.

An enhancement of electrical conductivity by further addition of non-soluble tougheners, was previously reported by Peliskova et al. [28], where the addition of rubber particles to already CB modified epoxy resin resulted in a higher electrical conductivity. The underlying mechanism for this change was concluded to be that CB agglomeration was much more localized and constrained by the existence of the rubber phase.

To study the structure-property relationships of the binary systems investigated in this work, TEM micrographs of the binary nanocomposites are compared to the epoxy nanocomposite with only 1.5 wt.% CB (Figure 89).

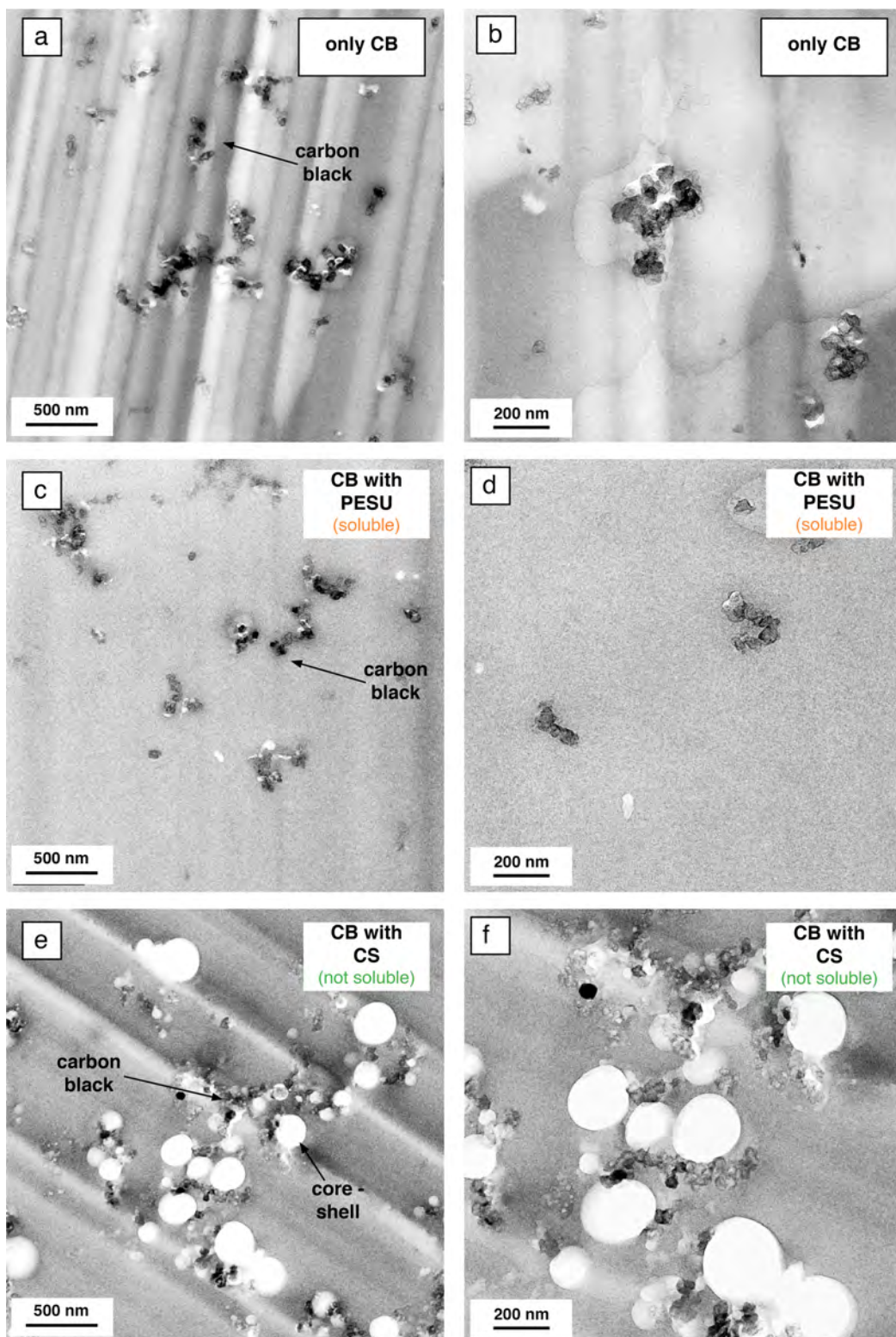


Figure 89. TEM micrographs of a) and b) only 1.5 wt.% CB modified epoxy, c) and d) 1.5 wt.% CB with 5 wt.% PESU and e) and f) 1.5 wt.% CB with 5 wt.% CS mod. epoxy nanocomposites.

As described previously, CB nanoparticles are dispersed in an epoxy resin as aggregates and single particles (Figure 89.a and b). Since OH-terminated PESU is soluble in the resin (as well during curing), no polyethersulfone phase is observed in PESU modified CB-epoxy binary nanocomposites (Figure 89.c). This results in a slightly similar appearance of the morphology in comparison to the only CB modified epoxy nanocomposite. It is important to note that the addition of 5 wt.% polyethersulfone (PESU) appears to slightly decrease CB aggregation and increase the interparticle distance of CB particles (Figure 89.d).

In contrast, the core-shell particles are not soluble and are dispersed as single particles in the resin. As presented in Figure 89.e and Figure 89.f, TEM micrographs of CS and CB modified binary nanocomposite reveal an extensive agglomeration of CB nanoparticles with core-shell particles. Carbon black nanoparticles are localized at the core-shell surfaces, as well in between core-shell particles, resulting in vein-like networks. Carbon black is mostly produced via the burning of hydrocarbons in a furnace reactor [178]. Therefore, a certain amount of CH, -CHO, -OH, -COOH and C=O groups can be found on the surface of these amorphous carbon-based nanoparticles [179]. Core-shell particles in this case consist of a cross-linked polysiloxane core with a stiff epoxy compatible shell. It is therefore expected that CB particles are attracted to core-shell particles due to the polarity of these functional groups, as mentioned above.

In conclusion, it is clearly shown that the addition of tougheners can affect the morphology of the conducting network given by CB nanoparticles in the epoxy resin. However, the structure-property relationships of these binary nanocomposites require further study more in a detail, and are therefore suggested as a promising strategy for future work.

7.2. Metal coated carbon fibers

Another promising strategy towards highly conductive carbon fiber composites involves the development and incorporation of coated CF or carbon-based particles with metals such as silver, nickel, zinc, and copper in the resin system [180], [181], [190]–[192], [182]–[189]. According to Lampke [181], a copper coating of CF increases the conductivity of carbon fiber rovings up to 10^6 S/m. In most cases, an electro-deposition method is used to coat CF rovings with metals [181], [182], [191]. To the best of our knowledge, fiber-matrix adhesion after metal coating of the CF has not been previously reported in the literature. A suitable sizing is not only necessary for the fiber-matrix adhesion, but for the processability of the fibers during prepreg production as well.

In collaboration between the Department of Polymer Engineering of University of Bayreuth at and the University of Applied Sciences in Hof, unidirectional carbon fiber rovings (12K, PAN-based, 800 tex) were coated with copper via the physical vapor deposition (PVD) technique. Although it is not possible to coat each fiber in the roving, this technique offers a continuous dry coating process with high coating thickness control compared to a wet electro-deposition technique. SEM micrographs of coated fibers are shown in Figure 90.

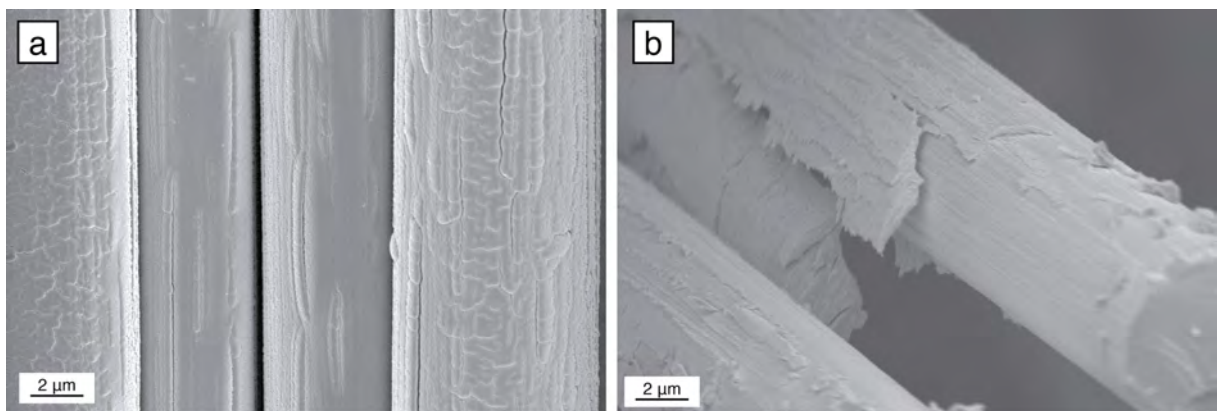


Figure 90. SEM micrographs of copper-coated PAN based high tenacity CF.

As can be seen in the SEM micrographs, a continuous, close-packed copper coating was achieved via the PVD route (Figure 90.a). The thickness of the coating was measured to be approximately 100 nm (Figure 90.b), for which the increase of the fiber weight can be neglected. According to 4 point direct current testing, the achieved copper coating results in a substantially lower surface resistivity; decreasing from approximately $1 \Omega \cdot \text{cm}^2$ for neat CF to an average of $0.015 \Omega \cdot \text{cm}^2$ for copper coated fibers via PVD technique.

Suitable sizing was still necessary for these copper-coated CF rovings. Thiol molecules are organosulfur compounds that contain a sulfhydryl group bonded to a carbon atom (C-SH), and are known for their strong adhesion with metals such as gold and copper [193]–[199]. Therefore, thiols are good candidates for sizing of a metal coated CF.

This work was performed in a close collaboration with the Hong Kong University of Science and Technology (HKUST). 50 nm copper particles were used during the experiments. The copper nanoparticles were surface-coated in an ethanol solution. Surfaces of the nanoparticles were studied via X-ray photoelectron spectroscopy (XPS) before and after surface modification. The sulfur concentration (via XPS) is shown in Figure 91 from the Cu surface coated only with the most promising modifier, 4,4'-thiobisbenzene thiol (TBBT), as a function of time.

According to the XPS results obtained at HKUST, the maximum amount of TBBT had adsorbed on the copper surface after 20 seconds. This very fast chemisorption reaction promises the possibility of continuous sizing processing on copper-coated CF rovings in a bath or via a spray coating processes. In conclusion, these pre-developments demonstrate the possibility to continuously coat CF rovings with copper and apply the desired amount of thiol sizing afterwards.

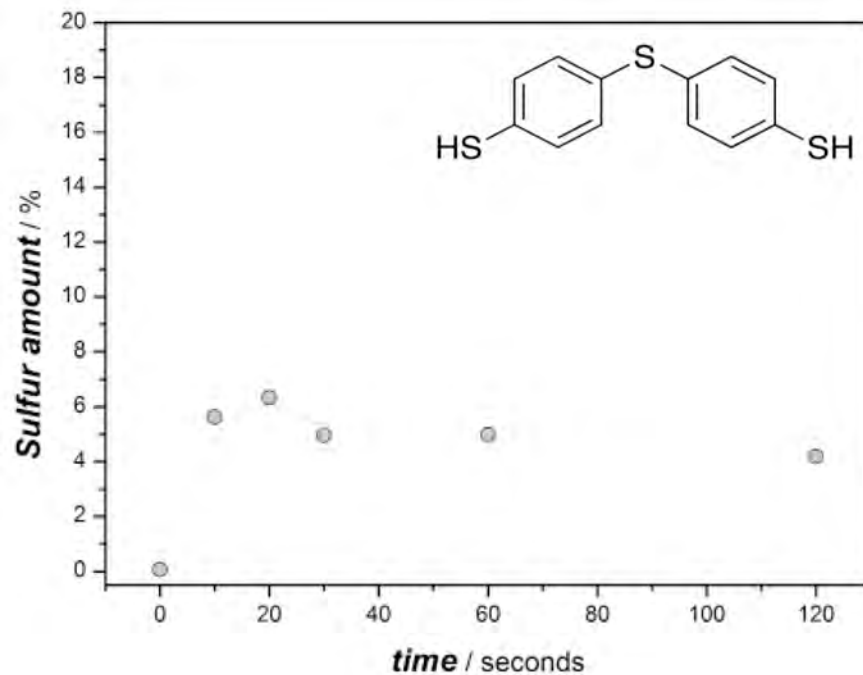


Figure 91. XPS results of the TBBT modified Cu surface measured at different times. Only the concentration of sulfur is taken into account. The solvent is ethanol and the concentration of thiol in ethanol is set to 1 mmol. Development done by Uni. Bayreuth and HKUST.

As an outlook, it is suggested to test the new copper coated CF (via CVD method) prepreg laminates with lightning strike testing (SAE ARP 5412 standard up to 200 kA). It is expected that the a micron thick copper coating can dramatically enhance the lightning strike resistance of the fiber reinforced polymer composites.

8 References

- [1] M. Peters and C. Leyens, "Aerospace and Space Materials," in *Materials Science and Engineering, vol III*, 2009.
- [2] Victor Giurgiutiu, *Structural Health Monitoring of Aerospace Composites*. Elsevier, 2015.
- [3] R. A. Serway, *Principles of Physics*, 2. Edition. Saunders College, 1998.
- [4] R. A. Matula, "Electrical resistivity of copper, gold, palladium, and silver," *J. Phys. Chem. Ref. Data*, vol. 8, no. 4, 1979.
- [5] A. Lonjon, P. Demont, E. Dantras, and C. Lacabanne, "Electrical conductivity improvement of aeronautical carbon fiber reinforced polyepoxy composites by insertion of carbon nanotubes," *J. Non. Cryst. Solids*, vol. 358, no. 15, pp. 1859–1862, 2012.
- [6] H. Lengsfeld, F. Wolff-Fabris, J. Krämer, J. Lacalle, and V. Altstädt, *Faserverbund-werkstoffe Prepregs und ihre Verarbeitung*. Hanser, 2015.
- [7] V. Altstädt, D. Gerth, M. Stangle, and H. G. Recker, "Interlaminar Crack-Growth in 3Rd-Generation Thermoset Prepreg Systems," *Polymer*, vol. 34, no. 4, pp. 907–909, 1993.
- [8] M. Guo, X. Yi, G. Liu, and L. Liu, "Simultaneously increasing the electrical conductivity and fracture toughness of carbon-fiber composites by using silver nanowires-loaded interleaves," *Compos. Sci. Technol.*, vol. 97, pp. 27–33, 2014.
- [9] N. A. Aal, F. El-tantawy, A. Al-Hajry, and M. Bououdina, "New Antistatic Charge and Electromagnetic Shielding Effectiveness from Conductive Epoxy Resin / Plasticized Carbon Black Composites," *Polym. Compos.*, pp. 125–132, 2008.
- [10] Y. X. Zhou, P. X. Wu, Z. Cheng, J. Ingram, and S. Jeelani, "Improvement in electrical , thermal and mechanical properties of epoxy by filling carbon nanotube," *eXPRESS Polym. Lett.*, vol. 2, no. 1, pp. 40–48, 2008.
- [11] M. M. Bernal, M. Hernandez, and R. Verdejo, "Comparison of filler percolation and mechanical properties in graphene and carbon nanotubes filled epoxy nanocomposites," *Eur. Polym. J.*, vol. 49, no. 6, pp. 1347–1353, 2013.
- [12] W. Zhang, A. Dehghani-Sanij, and R. S. Blackburn, "Carbon based conductive polymer composites," *J. Mater. Sci.*, vol. 42, no. 10, pp. 3408–3418, 2007.
- [13] H. O. Pierson, "Handbook of Carbon, Graphite, Diamond and Fullerenes," *Handb. Carbon, Graph. Diam. Fullerenes*, 1993.
- [14] K. Chu, D. Yun, D. Kim, H. Park, and S. Park, "Study of electric heating effects on carbon nanotube polymer composites," *Org. Electron.*, vol. 15, no. 11, pp. 2734–2741, 2014.
- [15] H. Fukuda, "Processing of carbon fiber reinforced plastics by means of Joule heating," *Adv. Compos. Mater.*, vol. 3, no. 3, pp. 153–161, 1994.

-
- [16] C. Joseph and C. Viney, "Electrical resistance curing of carbon-fibre epoxy composites," *Comp. Sci. and Tech.*, vol. 60, pp. 315–319, 2000.
- [17] R. Rohini and S. Bose, "Extraordinary Improvement in Mechanical Properties and Absorption-Driven Microwave Shielding through Epoxy-Grafted Graphene 'interconnects,'" *ACS Omega*, vol. 3, no. 3, pp. 3200–3210, 2018.
- [18] D. R. King, J. C. Rowan, D. D. Johnson, and B. E. Reis, "US005761053A, United States Patent," 1998.
- [19] S. Park, P. Theilmann, P. Asbeck, and P. R. Bandaru, "Enhanced electromagnetic interference shielding through the use of functionalized carbon nanotube-reactive polymer composites," *IEEE*, pp. 1–6, 2009.
- [20] L. Böger, M. H. G. Wichmann, L. O. Meyer, and K. Schulte, "Load and health monitoring in glass fibre reinforced composites with an electrically conductive nanocomposite epoxy matrix," *Compos. Sci. Technol.*, vol. 68, no. 7–8, pp. 1886–1894, 2008.
- [21] F. Inam, B. R. Bhat, N. Luhyna, and T. Vo, "Comparison of structural health assessment capabilities in epoxy-Carbon black and epoxy-Carbon nanotube nanocomposites," *Express Polym. Lett.*, vol. 8, no. 1, pp. 55–61, 2014.
- [22] P. Feraboli and M. Miller, "Damage resistance and tolerance of carbon/ epoxy composite coupons subjected to simulated lightning strike," in *AIAA, Structures, Structural Dynamics, and Materials Conference*, 2009.
- [23] J. H. Han, H. Zhang, M.J. Chen, D. Wang, Q. Liu, Q. Wu, Z. Zhang, "The combination of carbon nanotube buckypaper and insulating adhesive for lightning strike protection of the carbon fiber/epoxy laminates," *Carbon*, vol. 94, pp. 101–113, 2015.
- [24] V. Rakov and M. Uman, "Positive and bipolar lightning discharges to ground," *Light. Phys. Eff.*, pp. 214–240, 2003.
- [25] J. M. Prandy and Hermann Sitt, "Environmentally durable lightning strike protection materials for composite structures," US5225265A, 1993.
- [26] A. Heeger, "Nobel Lecture: Semiconducting and metallic polymers: The fourth generation of polymeric materials," *Rev. Mod. Phys.*, vol. 73, no. 3, p. 681, 2001.
- [27] C. S. Yannoni and T. C. Clarke, "Molecular Geometry of cis- and trans-Polyacetylene by Nutation NMR Spectroscopy," *Phys. Rev. Lett.*, vol. 51, no. 13, pp. 1191–1193, 1983.
- [28] P. Michaela, N. E. Kazantseva, J. Prokes, B. Hausnerova, and S. Petr, "Electrical Conductivity of Epoxy/Silicone/Carbon Black Composites: Effect of Composite Microstructure," *Polym. Compos.*, pp. 2234–2240, 2014.
- [29] P.-C. Ma *et al.*, "Enhanced electrical conductivity of nanocomposites containing hybrid fillers of carbon nanotubes and carbon black," *ACS Appl. Mater. Interfaces*, vol. 1, no. 5, pp. 1090–6, 2009.
- [30] M. E. Achour, C. Brosseau, and F. Carmona, "Dielectric relaxation in carbon black-epoxy composite materials," *J. Appl. Phys.*, vol. 103, no. 9, p. 094103, 2008.
- [31] L. Flandin, T. Prasse, R. Schueler, K. Schulte, W. Bauhofer, and J. Cavaille,

- “Anomalous percolation transition in carbon-black – epoxy composite materials,” *Phys. Rev. B*, vol. 59, no. 22, pp. 349–355, 1999.
- [32] S.-P. Rwei, F.-H. Ku, and K.-C. Cheng, “Dispersion of carbon black in a continuous phase: Electrical, rheological, and morphological studies,” *Colloid Polym. Sci.*, vol. 280, no. 12, pp. 1110–1115, Dec. 2002.
- [33] F. H. Gojny, M. H. G. Wichmann, B. Fiedler, W. Bauhofer, and K. Schulte, “Influence of nano-modification on the mechanical and electrical properties of conventional fibre-reinforced composites,” *Compos. Part A Appl. Sci. Manuf.*, vol. 36, no. 11, pp. 1525–1535, Nov. 2005.
- [34] V. A. Silva, L. D. C. Folgueras, G. M. Cândido, A. L. De Paula, M. C. Rezende, and M. L. Costa, “Nanostructured composites based on carbon nanotubes and epoxy resin for use as radar absorbing materials,” *Mater. Res.*, vol. 16, no. 6, pp. 1299–1308, 2013.
- [35] L. Liu and J. C. Grunlan, “Clay Assisted Dispersion of Carbon Nanotubes in Conductive Epoxy Nanocomposites,” *Adv. Funct. Mater.*, vol. 17, no. 14, pp. 2343–2348, Sep. 2007.
- [36] M. Rahaman, A. Aldalbahi, P. Govindasami, N.P. Khanam, S. Bhandari, P. Feng, T. Altalhi, “A new insight in determining the percolation threshold of electrical conductivity for extrinsically conducting polymer composites through different sigmoidal models,” *Polymers*, vol. 9, no. 10, pp. 1–17, 2017.
- [37] M. Rahaman, T. K. Chaki, and D. Khastgir, “Development of high performance EMI shielding material from EVA, NBR, and their blends: Effect of carbon black structure,” *J. Mater. Sci.*, vol. 46, no. 11, pp. 3989–3999, 2011.
- [38] S. Iijima, “Helical microtubules of graphitic carbon,” *Nature*, vol. 353, pp. 56–58, 1991.
- [39] M. Rahmandoust and M. R. Ayatollahi, *Characterization of Carbon Nanotube Based Composites under Consideration of Defects*. Springer, Cham, 2016.
- [40] K. N. Andre Geim, “The Rise of Graphene,” *Nat. Mater*, vol. 6, no. 183, pp. 1–14, 2007.
- [41] S. Stankovich, D.A. Dikin, G. H. B. Dommett, K.M. Kohlhaas, E. J. Zimney, E. A. Stach, R. D. Piner, S. T. Nguyen, R. S. Ruoff, “Graphene-based composite materials,” *Nature*, vol. 442, pp. 282–286, 2006.
- [42] B. Marinho, M. Ghislandi, E. Tkalya, C. E. Koning, and G. de With, “Electrical conductivity of compacts of graphene, multi-wall carbon nanotubes, carbon black, and graphite powder,” *Powder Technol.*, vol. 221, pp. 351–358, 2012.
- [43] J. K. W. Sandler, J. E. Kirk, I. a. Kinloch, M. S. P. Shaffer, and a. H. Windle, “Ultra-low electrical percolation threshold in carbon-nanotube-epoxy composites,” *Polymer*, vol. 44, no. 19, pp. 5893–5899, 2003.
- [44] J. Sumfleth, X. C. Adroher, and K. Schulte, “Synergistic effects in network formation and electrical properties of hybrid epoxy nanocomposites containing multi-wall carbon nanotubes and carbon black,” *J. Mater. Sci.*, vol. 44, no. 12, pp. 3241–3247, 2009.

-
- [45] F. H. Gojny, M. H. G. Wichmann, B. Fiedler, I. A. Kinloch, W. Bauhofer, A. H. Windle, K. Schulte, "Evaluation and identification of electrical and thermal conduction mechanisms in carbon nanotube/epoxy composites," *Polymer*, vol. 47, no. 6, pp. 2036–2045, 2006.
- [46] J. Sandler, M. S. . Shaffer, T. Prasse, W. Bauhofer, K. Schulte, and A. . Windle, "Development of a dispersion process for carbon nanotubes in an epoxy matrix and the resulting electrical properties," *Polymer*, vol. 40, no. 21, pp. 5967–5971, Oct. 1999.
- [47] R. Schueler, J. Petermann, K. Schulte, and H. Wentzel, "Agglomeration and Electrical Percolation Behavior of Carbon Black Dispersed in Epoxy Resin," pp. 1741–1746, 1996.
- [48] L. Guadagno *et al.*, "Development of epoxy mixtures for application in aeronautics and aerospace," *R. Soc. Chem.*, 2014.
- [49] B. De Vivo, L. Guadagno, P. Lamberti, M. Riamondo, G. Spinelli, V. Tucci, L. Vertuccio, V. Vittoria, "Electrical properties of multi-walled carbon nanotube/tetrafunctional epoxy-amine composites Electrical Properties of Multi-Walled Carbon Nanotube/Tetrafunctional Epoxy-Amine Composites," in *AIP Conference Proceedings*, vol. 1459, pp. 199–201, 2012.
- [50] A. Allaoui, S. Bai, H. M. Cheng, and J. B. Bai, "Mechanical and electrical properties of a MWNT/epoxy composite," *Compos. Sci. Technol.*, vol. 62, pp. 1993–1998, 2002.
- [51] J. J. Karippal, H. N. N. Murthy, K. S. Rai, M. Krishna, and M. Sreejith, "The Processing and Characterization of MWCNT/Epoxy and CB/Epoxy Nanocomposites Using Twin Screw Extrusion," *Polym. Plast. Technol. Eng.*, vol. 49, no. 12, pp. 1207–1213, 2010.
- [52] K. M. Jäger, D. H. McQueen, I. A. Tchmutin, N. G. Ryckina, and M. Klüppel, "Electron transport and ac electrical properties of carbon black polymer composites," *Phys. D Appl. Phys.*, vol. 34, pp. 2699–2707, 2001.
- [53] M. B. Bryning, M. F. Islam, J. M. Kikkawa, and a. G. Yodh, "Very Low Conductivity Threshold in Bulk Isotropic Single-Walled Carbon Nanotube-Epoxy Composites," *Adv. Mater.*, vol. 17, no. 9, pp. 1186–1191, 2005.
- [54] D. Zhang, L. Ye, S. Deng, J. Zhang, Y. Tang, and Y. Chen, "CF / EP composite laminates with carbon black and copper chloride for improved electrical conductivity and interlaminar fracture toughness," *Compos. Sci. Technol.*, vol. 72, no. 3, pp. 412–420, 2012.
- [55] M. Martin-Gallego, M. Hernández, V. Lorenzo, R. Verdejo, M. A. Lopez-Manchado, and M. Sangermano, "Cationic photocured epoxy nanocomposites filled with different carbon fillers," *Polymer*, vol. 53, no. 9, pp. 1831–1838, 2012.
- [56] T. Wei, L. Song, C. Zheng, K. Wang, J. Yan, B. Shao, Z.J. Fan, "The synergy of a three filler combination in the conductivity of epoxy composites," *Mater. Lett.*, vol. 64, no. 21, pp. 2376–2379, 2010.

-
- [57] S. Chandrasekaran, C. Seidel, and K. Schulte, "Preparation and characterization of graphite nano-platelet (GNP)/epoxy nano-composite: Mechanical, electrical and thermal properties," *Eur. Polym. J.*, vol. 49, no. 12, pp. 3878–3888, 2013.
- [58] N. Jović, D. Dudić, A. Montone, M. V. Antisari, M. Mitrić, and V. Djoković, "Temperature dependence of the electrical conductivity of epoxy/expanded graphite nanosheet composites," *Scr. Mater.*, vol. 58, no. 10, pp. 846–849, 2008.
- [59] M. Monti, M. Rallini, D. Puglia, L. Peponi, L. Torre, and J. M. Kenny, "Morphology and electrical properties of graphene-epoxy nanocomposites obtained by different solvent assisted processing methods," *Compos. Part A Appl. Sci. Manuf.*, vol. 46, no. 1, pp. 166–172, 2013.
- [60] N. H. Mohd Hirmizi, M. Abu Bakar, W. L. Tan, N. H. H. Abu Bakar, J. Ismail, and C. H. See, "Electrical and thermal behavior of copper-epoxy nanocomposites prepared via aqueous to organic phase transfer technique," *J. Nanomater.*, vol. 2012, 2012.
- [61] N. Hansen, D. O. Adams, and D. T. Fullwood, "Quantitative methods for correlating dispersion and electrical conductivity in conductor-polymer nanostrand composites," *Compos. Part A Appl. Sci. Manuf.*, vol. 43, no. 11, pp. 1939–1946, 2012.
- [62] H. Jiang, K. S. Moon, J. Lu, and C. P. Wong, "Conductivity enhancement of nano silver-filled conductive adhesives by particle surface functionalization," *J. Electron. Mater.*, vol. 34, no. 11, pp. 1432–1439, 2005.
- [63] Z. M. Elimat, A. M. Zihlif, and G. Ragosta, "Study of ac electrical properties of aluminium-epoxy composites," *J. Phys. D. Appl. Phys.*, vol. 41, no. 16, 2008.
- [64] M. N. F. Pargi, T. P. Leng, S. Husseinsyah, and C. K. Yeoh, "The Effect of Coarse Particle Size on the Properties of Recycled Copper-Filled Epoxy Composites," *Polym. Plast. Technol. Eng.*, vol. 54, no. 3, pp. 265–269, 2013.
- [65] K. Borho, R. Polke, K. Wintermantel, H. Schubert, and K. Sommer, "Produkteigenschaften und Verfahrenstechnik," *Chemie Ing. Tech.*, vol. 63, no. 8, pp. 792–808, 1991.
- [66] Y. Liang, N. Hilal, P. Langston, and V. Starov, "Interaction forces between colloidal particles in liquid: Theory and experiment," *Adv. Colloid Interface Sci.*, vol. 134–135, pp. 151–166, 2007.
- [67] A. Battisti, A. A. Skordos, and I. K. Partridge, "Dielectric monitoring of carbon nanotube network formation in curing thermosetting nanocomposites," *J. Phys. D. Appl. Phys.*, vol. 42, no. 15, 2009.
- [68] R. Zeiler, U. A. Handge, D. J. Dijkstra, H. Meyer, and V. Altstädt, "Influence of molar mass and temperature on the dynamics of network formation in polycarbonate/carbon nanotubes composites in oscillatory shear flows," *Polymer*, vol. 52, no. 2, pp. 430–442, 2011.
- [69] J. Guo *et al.*, "Aspect Ratio Effects of Multi-walled Carbon Nanotubes on Electrical, Mechanical, and Thermal Properties of Polycarbonate / MWCNT Composites," *J. Polym. Sci.*, vol. 52, no. 1, pp. 73–83, 2014.

- [70] R. M. Kulkarni, G. B. Rudrakshi, H. N. Narasimhamurthy, and A. Materials, "Processing and Characterisation of Epoxy / Carbon Black Nanocomposites by Twin Screw Extrusion," *Asian J. Eng. Appl. Technol.*, vol. 3, no. 2, pp. 55–58, 2014.
- [71] T. Villmow, S. Pegel, L. Haussler, B. Kretzschmar, and P. Poetschke, "Influence of twin-screw extrusion conditions on the dispersion of multi-walled carbon nanotubes in a poly (lactic acid) matrix," *Polymer*, vol. 49, pp. 3500–3509, 2008.
- [72] C. A. Martin *et al.*, "Electric field-induced aligned multi-wall carbon nanotube networks in epoxy composites," *Polymer*, vol. 46, no. 3, pp. 877–886, 2005.
- [73] O. Yakovenko *et al.*, "Electrical Properties of Composite Materials with Electric Field-Assisted Alignment of Nanocarbon Fillers," *Nanoscale Res. Lett.*, vol. 12, 2017.
- [74] L. Yue, G. Pircheraghi, S. A. Monemian, and I. Manas-Zloczower, "Epoxy composites with carbon nanotubes and graphene nanoplatelets-Dispersion and synergy effects," *Carbon*, vol. 78, pp. 268–278, 2014.
- [75] J. Sumfleth, X. C. Adroher, S. Buschhorn, and S. Karl, "Synergistic electrical and rheological effects in carbon nanotube/carbon black-epoxy three phase systems," *ICCM Int. Conf. Compos. Mater.*, 2009.
- [76] K. C. Etika, L. Liu, L. A. Hess, and J. C. Grunlan, "The influence of synergistic stabilization of carbon black and clay on the electrical and mechanical properties of epoxy composites," *Carbon*, vol. 47, no. 13, pp. 3128–3136, 2009.
- [77] L. C. Tang *et al.*, "Fracture toughness and electrical conductivity of epoxy composites filled with carbon nanotubes and spherical particles," *Compos. Part A Appl. Sci. Manuf.*, vol. 45, pp. 95–101, 2013.
- [78] K.-S. Kim, K.-E. Choi, and S.-J. Park, "Electrical and Mechanical Properties of Graphite Nanosheet/Carbon Nanotubes-filled Epoxy Nanocomposites," *Carbon Lett.*, vol. 10, no. 4, pp. 335–338, 2009.
- [79] Y. Sun, H. Bao, Z. Guo, and J. Yu, "Modeling of the Electrical Percolation of Mixed Carbon Fillers in Polymer-Based Composites," *Macromolecules*, vol. 42, no. 1, pp. 459–463, 2009.
- [80] J. Gou, Y. Tang, F. Liang, Z. Zhao, D. Firsich, and J. Fielding, "Carbon nanofiber paper for lightning strike protection of composite materials," *Compos. Part B Eng.*, vol. 41, no. 2, pp. 192–198, 2010.
- [81] C. Wu, H. Lu, Y. Liu, and J. Leng, "Study of carbon nanotubes/short carbon fiber nanocomposites for lightning strike protection," *Behav. Mech. Multifunct. Mater. Compos.*, 2010.
- [82] Y. Hirano *et al.*, "Lightning damage suppression in a carbon fiber-reinforced polymer with a polyaniline-based conductive thermoset matrix," *Compos. Sci. Technol.*, vol. 127, pp. 1–7, 2016.
- [83] B. De Vivo, P. Lamberti, G. Spinelli, and V. Tucci, "Evaluation of the Lightning Strikes on Carbon Fibers Panels for Aircraft Structural Parts," in *Comsol Conference*, 2015.

-
- [84] Y. Wang and O. I. Zhupanska, "Lightning strike thermal damage model for glass fiber reinforced polymer matrix composites and its application to wind turbine blades," *Compos. Struct.*, vol. 132, pp. 1182–1191, 2015.
- [85] P. Feraboli and H. Kawakami, "Damage of Carbon/Epoxy Composite Plates Subjected to Mechanical Impact and Simulated Lightning," *J. Aircr.*, vol. 47, no. 3, pp. 999–1012, 2010.
- [86] H. Kawakami and P. Feraboli, "Lightning strike damage resistance and tolerance of scarf-repaired mesh-protected carbon fiber composites," *Compos. Part A Appl. Sci. Manuf.*, vol. 42, no. 9, pp. 1247–1262, 2011.
- [87] S. Kamiyama, Y. Hirano, T. Okada, and T. Ogasawara, "Lightning strike damage behavior of carbon fiber reinforced epoxy, bismaleimide, and polyetheretherketone composites," *Compos. Sci. Technol.*, vol. 161, pp. 107–114, 2018.
- [88] J. R. Gaier, M. E. Slabe, and O. B. Norman, "Effect of Lightning Strike on Fiber Reinforced Composite Materials," Cleveland, Ohio, 1991.
- [89] S. Kamiyama, Y. Hirano, and T. Ogasawara, "Delamination analysis of CFRP laminates exposed to lightning strike considering cooling process," *Compos. Struct.*, vol. 196, pp. 55–62, 2018.
- [90] K. R. Vaidyanathan and J. Campbell, "Method for Manufacturing Lightning Strike mitigation composites," US008158045B2, 2012.
- [91] M. Simmons and J. Cawse, "Composite Materials," US20140047710A1, 2014.
- [92] O. Soykasap, S. Karakaya, and M. Colakoglu, "Simulation of lightning strike damage in carbon nanotube doped CFRP composites," *J. Reinf. Plast. Compos.*, vol. 35, no. 6, pp. 504–515, 2016.
- [93] E. Logakis and A. A. Skordos, "Lightning Strike Performance of Carbon Nanotube Loaded Aerospace Composites," in *ECCM 15-15th European Conference on Composite Materials*, 2012.
- [94] K. Lindner *et al.*, "Biological effects of carbon black nanoparticles are changed by surface coating with polycyclic aromatic hydrocarbons," *Part. Fibre Toxicol.*, vol. 14, no. 1, pp. 1–17, 2017.
- [95] L. Shulin, Y. Junjie, Y. Xueling, C. Fei, and S. Xiaopeng, "Damage analysis for carbon fiber/epoxy composite exposed to simulated lightning current," *J. Reinf. Plast. Compos.*, vol. 35, no. 15, pp. 1201–1213, 2016.
- [96] B. G. Sweers, B. Birch, and J. Gokcen, "Lightning Strikes: Protection, Inspection, and Repair," *Aero Magazine*, pp. 18–28, 2012.
- [97] Y. Chekanov, R. Ohnogi, S. Asai, and M. Sumita, "Electrical properties of epoxy resin filled with carbon fibers," *J. Mater. Sci.*, vol. 34, pp. 5589–5592, 1999.
- [98] F. El-tantawy, K. Kamada, and H. Ohnabe, "Electrical properties and stability of epoxy reinforced carbon black composites," vol. 57, pp. 242–251, 2002.
- [99] A. Godara *et al.*, "Influence of carbon nanotube reinforcement on the processing and the mechanical behaviour of carbon fiber/epoxy composites," *Carbon*, vol. 47, no. 12, pp. 2914–2923, 2009.

- [100] S. O. Il'in, I. Y. Gorbunova, E. P. Plotnikova, and M. L. Kerber, "Rheological and mechanical properties of epoxy composites modified with montmorillonite nanoparticles," *Int. Polym. Sci. Technol.*, vol. 39, no. 7, pp. 57–61, 2012.
- [101] K. M. Yearsley, M. R. Mackley, F. Chinesta, and A. Leygue, "The rheology of multiwalled carbon nanotube and carbon black suspensions," *J. Rheol.*, vol. 56, no. 6, pp. 1465–1490, 2012.
- [102] A. W. K. Ma, M. Yearsley, K. M. R. Mackley and F. Chinesta, "The microstructure and rheology of carbon nanotube suspensions," *J. Nanoeng. Nanosyst.*, pp. 71–94, 2009.
- [103] S. F. Halim, "A Study of the Effect of Al₂O₃ Nanoparticles on the Cure behavior of Bisphenol A Epoxy Resin," *NSTI-Nanotech*, vol. 1, pp. 275–278, 2014.
- [104] R. Umer, Y. Li, Y. Dong, H. J. Haroosh, and K. Liao, "The effect of graphene oxide (GO) nanoparticles on the processing of epoxy/glass fiber composites using resin infusion," *Int. J. Adv. Manuf. Technol.*, vol. 81, no. 9–12, pp. 2183–2192, 2015.
- [105] T. V. Kosmidou, A. S. Vatalis, C. G. Delides, E. Logakis, P. Pissis, and G. C. Papanicolaou, "Structural, mechanical and electrical characterization of epoxy-amine/carbon black nanocomposites," *Express Polym. Lett.*, vol. 2, no. 5, pp. 364–372, 2008.
- [106] A. Allaoui and N. El Bounia, "How carbon nanotubes affect the cure kinetics and glass transition temperature of their epoxy composites? - A review," *Express Polym. Lett.*, vol. 3, no. 9, pp. 588–594, 2009.
- [107] A. J. Ma, W. Chen, Y. Hou, and G. Zhang, "Dispersion, mechanical and thermal properties of epoxy resin composites filled with the nanometer carbon black," *Polym.-Plast. Technol. Eng.*, vol. 49, no. 9, pp. 916–920, 2010.
- [108] M. H. Kothmann, M. Ziadeh, G. Bakis, A. Rios de Anda, J. Breu, and V. Altstädt, "Analyzing the influence of particle size and stiffness state of the nanofiller on the mechanical properties of epoxy/clay nanocomposites using a novel shear-stiff nano-mica," *J. Mater. Sci.*, vol. 50, no. 14, 2015.
- [109] N. Domun, K. R. Paton, H. Hadavinia, T. Sainsbury, T. Zhang, and H. Mohamud, "Enhancement of fracture toughness of epoxy nanocomposites by combining nanotubes and nanosheets as fillers," *Materials*, vol. 10, no. 10, 2017.
- [110] X. Wang, J. Jin, and M. Song, "An investigation of the mechanism of graphene toughening epoxy," *Carbon*, vol. 65, pp. 324–333, 2013.
- [111] F. H. Gojny, M. H. G. Wichmann, B. Fiedler, and K. Schulte, "Influence of different carbon nanotubes on the mechanical properties of epoxy matrix composites - A comparative study," *Compos. Sci. Technol.*, vol. 65, pp. 2300–2313, 2005.
- [112] G. Bakis, M. H. Kothmann, R. Zeiler, A. Brückner, M. Ziadeh, J. Breu, and V. Altstädt, "Influence of size, aspect ratio and shear stiffness of nanoclays on the fatigue crack propagation behavior of their epoxy nanocomposites," *Polymer*, vol. 158, pp. 372–380, 2018.

- [113] M. H. Kothmann, G. Bakis, R. Zeiler, M. Ziadeh, J. Brey, and V. Altstädt, "Fatigue crack growth behaviour of epoxy nanocomposites," *in ISBN: 978-3-319-41879-7*, 2017.
- [114] H. R. Azimi, R. a Pearson, and R. W. Hertzberg, "Role of crack tip shielding mechanisms in fatigue of hybrid epoxy composites containing rubber and solid glass spheres," *J. Appl. Polym. Sci.*, vol. 58, no. 2, pp. 449–463, 1995.
- [115] M. Imanaka, Y. Takeuchi, Y. Nakamura, A. Nishimura, T. Iida, "Fracture toughness of spherical silica-filled epoxy adhesives," *Int. J. Adhes. Adhes.*, vol. 21, pp. 389–396, 2001.
- [116] B. Wetzel, P. Rosso, F. Hauptert, and K. Friedrich, "Epoxy nanocomposites-fracture and toughening mechanisms," *Eng. Fract. Mech.*, vol. 73, no. 16, pp. 2375–2398, 2006.
- [117] J. a. M. Ferreira, L. P. Borrego, J. D. M. Costa, and C. Capela, "Fatigue behaviour of nanoclay reinforced epoxy resin composites," *Compos. Part B Eng.*, vol. 52, pp. 286–291, 2013.
- [118] H. Y. Liu, G. Wang, and Y. W. Mai, "Cyclic fatigue crack propagation of nanoparticle modified epoxy," *Compos. Sci. Technol.*, vol. 72, no. 13, pp. 1530–1538, 2012.
- [119] M. Battistella, M. Cascione, B. Fiedler, M. H. G. Wichmann, M. Quaresimin, and K. Schulte, "Fracture behaviour of fumed silica/epoxy nanocomposites," *Compos. Part A Appl. Sci. Manuf.*, vol. 39, no. 12, pp. 1851–1858, 2008.
- [120] B. R. K. Blackman, A. J. Kinloch, J. S. Lee, A. C. Taylor, R. Agarwal, G. Schueneman, S. Sprenger, "The fracture and fatigue behaviour of nano-modified epoxy polymers," *J. Mater. Sci.*, vol. 42, no. 16, pp. 7049–7051, 2007.
- [121] L. Laffont, M. Monthieux, and V. Serin, "Plasmon as a tool for in situ evaluation of physical properties for carbon materials," *Carbon*, vol. 40, no. 5, pp. 767–780, 2002.
- [122] E. Bekyarova *et al.*, "Multiscale carbon nanotube-carbon fiber reinforcement for advanced epoxy composites," *Langmuir*, vol. 23, no. 7, pp. 3970–3974, 2007.
- [123] D. Wentzel and I. Sevostianov, "Electrical conductivity of unidirectional carbon fiber composites with epoxy-graphene matrix," *Int. J. Eng. Sci.*, vol. 130, pp. 129–135, 2018.
- [124] S. B. Lee *et al.*, "Processing and characterization of multi-scale hybrid composites reinforced with nanoscale carbon reinforcements and carbon fibers," *Compos. Part A Appl. Sci. Manuf.*, vol. 42, no. 4, pp. 337–344, 2011.
- [125] S. Wang and D. D. . Chung, "Electrical behavior of carbon fiber polymer-matrix composites in the through-thickness direction," *J. Mater. Sci.*, vol. 35, pp. 91–100, 2000.
- [126] L. Guadagno *et al.*, "Correlation between electrical conductivity and manufacturing processes of nanofilled carbon fiber reinforced composites," *Compos. Part B Eng.*, vol. 80, pp. 7–14, 2015.
- [127] J. C. Abry, S. Bochard, A. Chateauminois, M. Salvia, and G. Giraud, "In situ detection of damage in CFRP laminates by electrical resistance measurements,"

- Compos. Sci. Technol.*, vol. 59, pp. 925–935, 1999.
- [128] H. C. Kim and S. K. See, “Electrical properties of unidirectional carbon-epoxy composites in wide frequency band,” *J. Phys. D. Appl. Phys.*, vol. 23, no. 7, pp. 916–921, 1990.
- [129] S. A. Jawad *et al.*, “Electrical properties of laminated epoxy-carbon fiber composite,” *Polym. Int.*, vol. 32, no. 1, pp. 23–31, 1993.
- [130] R. D. Chippendale and I. O. Golosnoy, “Percolation effects in electrical conductivity of Carbon Fibre Composites,” in *IET 8th International Conference on Computation in Electromagnetics*, 2011.
- [131] C. B. Bucknall and I. K. Partridge, “Phase separation in epoxy resins containing polyethersulphone,” *Polymer*, vol. 24, pp. 639–644, 1983.
- [132] C. B. Bucknall and A. H. Gilbert, “Toughening tetrafunctional epoxy resins using polyetherimide,” *Polymer*, vol. 30, pp. 213–217, 1989.
- [133] N. G. Ozdemir, T. Zhang, I. Aspin, F. Scarpa, H. Hadavinia, and Y. Song, “Toughening of carbon fibre reinforced polymer composites with rubber nanoparticles for advanced industrial applications,” *Express Polym. Lett.*, vol. 10, no. 5, pp. 394–407, 2016.
- [134] F. Gao, G. Jiao, and L. Zhixian, “Mode II Delamination and Damage Resistance of Carbon/Epoxy Composite Laminates Interleaved with Thermoplastic Particles,” *Compos. Mater.*, vol. 41, no. 1, pp. 111–123, 2005.
- [135] M. Hojo, S. Matsuda, M. Tanaka, S. Ochiai, and A. Murakami, “Mode I delamination fatigue properties of interlayer-toughened CF/epoxy laminates,” *Compos. Sci. Technol.*, vol. 66, pp. 665–675, 2006.
- [136] K. R. Hirschbuehler, B. A. Stern, and R. E. Evans, “High impact strength fiber resin matrix composites,” EP0156148-A2, 1985.
- [137] D. W. Y. Wong, H. Zhang, E. Bilotti, and T. Peijs, “Interlaminar toughening of woven fabric carbon/epoxy composite laminates using hybrid aramid/phenoxy interleaves,” *Compos. Part A*, 2017.
- [138] D. W. Y. Wong, L. Lin, P. T. McGrail, T. Peijs, and P. J. Hogg, “Improved fracture toughness of carbon fibre/epoxy composite laminates using dissolvable thermoplastic fibres,” *Compos. Part A Appl. Sci. Manuf.*, vol. 41, no. 6, pp. 759–767, 2010.
- [139] I. V. Sela and O. Ishai, “Interlaminar fracture toughness and toughening of laminated composite materials: a review,” *Composites*, vol. 20, no. 5, pp. 423–435, 1989.
- [140] M. Guo and X. Yi, “Effect of Paper or Silver Nanowires-Loaded Paper Interleaves on the Electrical Conductivity and Interlaminar Fracture Toughness of Composites,” *Aerospace*, vol. 5, no. 77, 2018.
- [141] Y. Ou, C. Gonzales, and J. J. Vilatela, “Understanding interlaminar toughening mechanisms in structural carbon fiber/epoxy composites interleaved with CNT veils,” in *ECCM18-18th European Conference on Composite Materials*, 2018.
- [142] X. Du *et al.*, “Graphene/epoxy interleaves for delamination toughening and monitoring of crack damage in carbon fibre/epoxy composite laminates,”

Compos. Sci. Technol., 2017.

- [143] K. Magniez, T. Chaffraix, and B. Fox, "Toughening of a Carbon-Fibre Composite Using Electrospun Poly(Hydroxyether of Bisphenol A) Nanofibrous Membranes Through Inverse Phase Separation and Inter-Domain Etherification," *Materials*, vol. 4, pp. 1967–1984, 2011.
- [144] K. Shivakumar, S. Lingaiah, H. Chen, P. Akangah, G. Swaminathan, and L. Russell Jr., "Polymer Nanofabric Interleaved Composite Laminates," *AIAA J.*, vol. 47, no. 7, pp. 1723–1729, 2009.
- [145] M. Kuwata, H. Zhang, E. Bilotti, and T. Peijs, "Interlaminar Toughness improvement of carbon fibre/epoxy composite laminates by electrospun nanofibre interleaves," in *ECCM15-15th European Conference on Composite Materials*, 2012.
- [146] P. Akangah, S. Lingaiah, and K. Shivakumar, "Effect of Nylon-66 nano-fiber interleaving on impact damage resistance of epoxy / carbon fiber composite laminates," *Compos. Struct.*, vol. 92, no. 6, pp. 1432–1439, 2010.
- [147] N. Odagiri, H. Kishi, and M. Yamashita, "Development of TORAYCA prepreg P2302 carbon fiber reinforced plastic for aircraft primary structural materials," *Adv. Compos. Mater.*, vol. 5, no. 2, pp. 249–252, 1996.
- [148] Y. Tang, L. Ye, Z. Zhang, and K. Friedrich, "Interlaminar fracture toughness and CAI strength of fibre-reinforced composites with nanoparticles – A review," *Compos. Sci. Technol.*, vol. 86, pp. 26–37, 2013.
- [149] S. U. Khan and J. Kim, "Impact and Delamination Failure of Multiscale Carbon Nanotube-Fiber Reinforced Polymer Composites: A Review," *Int. J. Aeronaut. Sp. Sci.*, vol. 12, no. 2, pp. 115–133, 2011.
- [150] B. J. Njuguna, K. Pielichowski, and J. R. Alcock, "Epoxy-Based Fibre Reinforced Nanocomposites," *Adv. Eng. Mater.*, vol. 9, no. 10, pp. 835–847, 2007.
- [151] T. H. Hsieh, A. J. Kinloch, K. Masania, J. S. Lee, A. C. Taylor, and S. Sprenger, "The toughness of epoxy polymers and fibre composites modified with rubber microparticles and silica nanoparticles," *J. Mater. Sci.*, vol. 45, pp. 1193–1210, 2010.
- [152] J. L. Tsai, B. H. Huang, and Y. L. Cheng, "Enhancing Fracture Toughness of Glass / Epoxy Composites for Wind Blades Using Silica Nanoparticles and Rubber Particles," *Procedia Eng.*, vol. 14, pp. 1982–1987, 2011.
- [153] Y. Tang, L. Ye, D. Zhang, and S. Deng, "Characterization of transverse tensile , interlaminar shear and interlaminar fracture in CF / EP laminates with 10 wt % and 20 wt % silica nanoparticles in matrix resins," *Compos. Part A*, vol. 42, no. 12, pp. 1943–1950, 2011.
- [154] S. Sprenger, "Fiber-reinforced composites based on epoxy resins modified with elastomers and surface-modified silica nanoparticles," *J. Mater. Sci.*, vol. 49, no. 6, pp. 2391–2402, 2014.
- [155] J. L. Abot, Y. Song, M. J. Schulz, and V. N. Shanov, "Novel carbon nanotube array-reinforced laminated composite materials with higher interlaminar elastic properties," *Compos. Sci. Technol.*, vol. 68, pp. 2755–2760, 2008.

- [156] P. M. Ajayan and M. N. Ghasemi-nejhad, "Multifunctional composites using reinforced laminae with carbon-nanotube forests," vol. 5, pp. 457–462, 2006.
- [157] S. S. Wicks, W. Wang, M. R. Williams, and B. L. Wardle, "Multi-scale interlaminar fracture mechanisms in woven composite laminates reinforced with aligned carbon nanotubes," *Compos. Sci. Technol.*, vol. 100, pp. 128–135, 2014.
- [158] S. S. Wicks, R. G. de Villoria, and B. L. Wardle, "Interlaminar and intralaminar reinforcement of composite laminates with aligned carbon nanotubes," *Compos. Sci. Technol.*, 2009.
- [159] P. R. Thakre *et al.*, "Investigation of the effect of single wall carbon nanotubes on interlaminar fracture toughness of woven carbon fiber – epoxy composites," *J. Compos. Mater.*, pp. 1–17, 2011.
- [160] G. Romhány and G. Szabó, "Interlaminar crack propagation in MWCNT / fiber reinforced hybrid composites," *eXPRESS Polym. Lett.*, vol. 3, no. 3, pp. 145–151, 2009.
- [161] F. Mujika, G. Vargas, J. Ibarretxe, J. De Gracia, and A. Arrese, "Influence of the modification with MWCNT on the interlaminar fracture properties of long carbon fiber composites," *Compos. Part B*, vol. 43, no. 3, pp. 1336–1340, 2012.
- [162] H. Zhang, Y. Liu, M. Kuwata, E. Bilotti, and T. Peijs, "Improved fracture toughness and integrated damage sensing capability by spray coated CNTs on carbon fibre prepreg," *Compos. Part A*, vol. 70, pp. 102–110, 2015.
- [163] V. Kostopoulos, A. Baltopoulos, P. Karapappas, A. Vavouliotis, and A. Paipetis, "Impact and after-impact properties of carbon fibre reinforced composites enhanced with multi-wall carbon nanotubes," *Compos. Sci. Technol.*, vol. 70, no. 4, pp. 553–563, 2010.
- [164] B. Ashrafi *et al.*, "Enhancement of mechanical performance of epoxy / carbon fiber laminate composites using single-walled carbon nanotubes," *Compos. Sci. Technol.*, vol. 71, no. 13, pp. 1569–1578, 2011.
- [165] P. Karapappas, A. Vavouliotis, P. Tsoira, V. Kostopoulos, and A. Paipetis, "Enhanced Fracture Properties of Carbon Reinforced Composites by the Addition of Multi-Wall Carbon Nanotubes," *J. Compos. Mater.*, vol. 43, no. 9, pp. 977–985, 2009.
- [166] V. P. Veedu *et al.*, "Multifunctional composites using reinforced laminae with carbon-nanotube forests," *Nat. Mater.*, vol. 5, no. 6, pp. 457–462, 2006.
- [167] E. J. Garcia, B. L. Wardle, and A. John Hart, "Joining prepreg composite interfaces with aligned carbon nanotubes," *Compos. Part A Appl. Sci. Manuf.*, vol. 39, no. 6, pp. 1065–1070, 2008.
- [168] R. Zeiler, C. Kuttner, U. Khalid, M. H. Kothmann, D. Dijkstra, and V. Altstaedt, "The Role of Multi-Walled Carbon Nanotubes in Epoxy Nanocomposites and Resin Transfer Molded Glass Fiber Hybrid Composites: Dispersion, Local Distribution, Thermal, and Fracture/Mechanical Properties," *Polym. Compos.*, 2015.
- [169] K. J. Green, D. R. Dean, U. K. Vaidya, and E. Nyairo, "Multiscale fiber reinforced composites based on a carbon nanofiber / epoxy nanophased polymer matrix:

- Synthesis, mechanical, and thermomechanical behavior," *Compos. Part A*, vol. 40, no. 9, pp. 1470–1475, 2009.
- [170] Y. Zhou, F. Pervin, S. Jeelani, and P. K. Mallick, "Improvement in mechanical properties of carbon fabric – epoxy composite using carbon nanofibers," *J. Mater. Process. Technol.*, vol. 198, pp. 445–453, 2008.
- [171] Q. Chen, L. Zhang, A. Rahman, Z. Zhou, X. Wu, and H. Fong, "Hybrid multi-scale epoxy composite made of conventional carbon fiber fabrics with interlaminar regions containing electrospun carbon nanofiber mats," *Compos. Part A*, vol. 42, no. 12, pp. 2036–2042, 2011.
- [172] Y. Zhu, C. E. Bakis, and J. H. Adair, "Effects of carbon nanofiller functionalization and distribution on interlaminar fracture toughness of multi-scale reinforced polymer composites," *Carbon*, vol. 50, no. 3, pp. 1316–1331, 2012.
- [173] C. Zilg, R. Mülhaupt, and J. Finter, "Morphology and toughness / stiffness balance of nanocomposites based upon anhydride-cured epoxy resins and layered silicates," *Macromol. Chem. Phys.*, vol. 200, pp. 661–670, 1999.
- [174] K. Iqbal, S. Khan, A. Munir, and J. Kim, "Impact damage resistance of CFRP with nanoclay-filled epoxy matrix," *Compos. Sci. Technol.*, vol. 69, no. 11–12, pp. 1949–1957, 2009.
- [175] S. Ullah, A. Munir, R. Hussain, and J. Kim, "Fatigue damage behaviors of carbon fiber-reinforced epoxy composites containing nanoclay," *Compos. Sci. Technol.*, vol. 70, no. 14, pp. 2077–2085, 2010.
- [176] W. L. Bradley, "Understanding the translation of neat resin toughness into delamination toughness in composites," *Key Eng. Mater.*, vol. 37, pp. 161–198, 1989.
- [177] A. J. Russell, "Micromechanisms of interlaminar fracture and fatigue," *Polym. Compos.*, vol. 8, no. 5, pp. 342–351, 1987.
- [178] T. A. Vilgis, G. Heinrich, and M. Klüppel, *Reinforcement of Polymer Nano-Composites. Theory, Experiments and Applications*. Cambridge University Press, 2010.
- [179] M. L. Studebaker, E. W. D. Huffman, A. C. Wolfe, and L. G. Nabors, "Oxygen-Containing Groups on the Surface of Carbon Black," *Ind. Eng. Chem.*, vol. 48, no. 1, pp. 162–166, 1956.
- [180] N. Hu, T. Itoi, T. Akagi, T. Kojima, J. Xue, and C. Yan, "Ultrasensitive strain sensors made from metal-coated carbon nanofiller / epoxy composites," *Carbon*, vol. 51, pp. 202–212, 2013.
- [181] T. Lampke, "Metal-Coated Carbon Fibres for Multifunctional CFRPs," *JOT International Surface Technology*, pp. 44–45, 2014.
- [182] G. Carotenuto, A. Gallo, and L. Nicolais, "Stability of Nickel Coatings on Carbon Fiber Preforms: A SEM Investigation," *Appl. Compos. Mater.*, vol. 1, pp. 231–245, 1994.
- [183] K. J. Lodge and J. Brettle, "Radar Wave Dipole of Copper Coated Carbon Fibers," 4600642, 1986.
- [184] Y. X. Gan, C. Q. Chen, and C. G. Li, "Preparation of Metal-Coated Carbon Fiber

- Reinforced Composites and Their Electromagnetic Properties,” *Mater. Manuf. Process.*, vol. 9, no. 2, pp. 249–262, 2007.
- [185] S. Kushwaha, K. K. Kar, P. S. G. Krishnan, and S. K. Sharma, “Preparation and characterization of nickel coated carbon fiber reinforced polycarbonate composites,” *J. Reinf. Plast. Compos.*, 2011.
- [186] J. Przepiorski, A. W. Morawski, and A. Oya, “Method for Preparation of Copper-Coated Carbon,” *Chem. Mater.*, vol. 15, pp. 862–865, 2003.
- [187] S. S. Kang *et al.*, “Metal-coated carbon fiber for lighter electrical metal wires,” *Synth. Met.*, vol. 222, pp. 180–185, 2016.
- [188] M. Gagné and D. Therriault, “Lightning strike protection of composites,” *Prog. Aerosp. Sci.*, vol. 64, pp. 1–16, 2014.
- [189] E. T. Bannink and G. O. Olson, “Integral Lightning Protection System for Composite Aircraft Skins,” 4502092, 1985.
- [190] S. Geetha, K. K. S. Kumar, C. R. K. Rao, M. Vijayan, and D. C. Trivedi, “EMI Shielding: Methods and Materials — A Review,” *J. Appl. Polym. Sci.*, vol. 112, pp. 2073–2086, 2009.
- [191] B. Pierozynski, “Electrodeposition of Nickel onto 12K Carbon Fibre Tow in a Continuous Manner,” *Croat. Chem. Acta*, vol. 85, no. 1, pp. 1–8, 2012.
- [192] J. M. He and Y. D. Huang, “AFM Characterization of Interphase Properties of Silver-Coated Carbon Fibre Reinforced Epoxy Composites,” *Polym. Polym. Compos.*, vol. 14, no. 2, pp. 123–134, 2006.
- [193] H. Grönbeck, A. Curioni, and W. Andreoni, “Thiols and Disulfides on the Au(111) Surface: The Headgroup-Gold Interaction,” *J. Am. Chem. Soc.*, vol. 122, pp. 3839–3842, 2000.
- [194] C. K. Y. Wong, M. M. F. Yuen, and B. Xu, “Thiol-based self-assembly nanostructures in promoting interfacial adhesion for copper-epoxy joint,” *Appl. Phys. Lett.*, vol. 94, 2009.
- [195] M. A. Neouze and U. Schubert, “Surface Modification and Functionalization of Metal and Metal Oxide Nanoparticles by Organic Ligands,” *Monatsh Chem*, vol. 139, pp. 183–195, 2008.
- [196] L. Srisombat, A. C. Jamison, and T. R. Lee, “Stability: A key issue for self-assembled monolayers on gold as thin-film coatings and nanoparticle protectants,” *Colloids Surfaces A Physicochem. Eng. Asp.*, vol. 390, pp. 1–19, 2011.
- [197] J. C. Love, L. A. Estroff, J. K. Kriebel, R. G. Nuzzo, and G. M. Whitesides, “Self-Assembled Monolayers of Thiolates on Metals as a Form of Nanotechnology,” *Chem. Rev.*, vol. 105, pp. 1103–1169, 2005.
- [198] Y. Xue, X. Li, H. Li, and W. Zhang, “Quantifying thiol–gold interactions towards the efficient strength control,” *Nat. Commun.*, vol. 5, pp. 1–9, 2014.
- [199] M. K. Corbierre, N. S. Cameron, M. Sutton, S. G. J. Mochrie, L. B. Lurio, and A. Rühm, “Polymer-Stabilized Gold Nanoparticles and Their Incorporation into Polymer Matrices,” *J. Am. Chem. Soc.*, vol. 123, pp. 10411–10412, 2001.

9 Supporting Information

In this chapter, a detailed information about the literature summarized in figures 8, 9 and 10 is provided as tables. In addition, C-scans of the used laminates are given.

Table 6. Literature data summarizing the reported electrical conductivity of carbon nanoparticle modified epoxy systems at their threshold particle content. The data are graphically presented in Figure 8 and 9 (Chapter 2.2.1.1.).

Data Point	Research Group	Filler	Epoxy matrix	Threshold concentration	Threshold conductivity
-	-	-	-	wt. %	S/m
1	Sandler et al. [43]	MWCNTs	DGEBA-amine	0.005 wt. %	$2 \cdot 10^{-3}$ S/m
2	Sumfleth et al. [44]	CB	DGEBA-anhydride	0.1 wt. %	$3 \cdot 10^{-6}$ S/m
2	Sumfleth et al. [44]	MWCNTs	DGEBA-anhydride	0.04 wt. %	10^{-6} S/m
3	Gonjy et al. [45]	CB	DGEBA-amine	0.75 wt. %	10^{-5} S/m
3	Gonjy et al. [45]	SWCNTs	DGEBA-amine	0.05 wt. %	$2 \cdot 10^{-5}$ S/m
3	Gonjy et al. [45]	DWCNTs	DGEBA-amine	0.1 wt. %	$5 \cdot 10^{-6}$ S/m
3	Gonjy et al. [45]	MWCNTs	DGEBA-amine	0.1 wt. %	10^{-4} S/m
4	Sandler et al. [46]	MWCNTs	DGEBA-amine	0.06 wt. %	10^{-2} S/m
4	Sandler et al. [46]	CB	DGEBA-amine	1.5 wt. %	10^{-2} S/m
5	Liu et al. [35]	SWCNTs	DGEBF-anhydride	0.075 wt. %	$6 \cdot 10^{-3}$ S/m
6	Schueler et al. [47]	CB	DGEBA-amine	0.1 wt. %	10^{-3} S/m
7	Lonjon et al. [5]	DWCNTs	TGMDA-DDS (M21, Hexcel)	0.4 wt. %	0.12 S/m
8	Guadagno et al. [48]	MWCNTs	TGMDA-DDS	0.32 wt. %	0.03 S/m
9	Vivo et al. [49]	MWCNTs	TGMDA-DDS	0.35 wt. %	10^{-2} S/m

10	Ma et al. [29]	MWCNTs	DGEBA-amine	0.4 wt.%	10^{-2} S/m
10	Ma et al. [29]	CB	DGEBA-amine	1 wt.%	10^{-4} S/m
11	Allaoui et al. [50]	MWCNTs	DGEBA-amine (rubbery)	1 wt.%	10^{-1} S/m
12	Rwei et al. [32]	CB	DGEBA-Anhydride	1 wt.%	$2 \cdot 10^{-3}$ S/m
13	Karippal et al. [51]	CB	DGEBA-amine	11 wt.%	10^{-3} S/m
13	Karippal et al. [51]	MWCNTs	DGEBA-amine	4 wt.%	$5 \cdot 10^{-4}$ S/m
14	Jäger et al. [52]	CB	DGEBA-	6.5 wt.%	10^{-5} S/m
15	Aal et al. [9]	CB	DGEBA-	9 wt.%	$4 \cdot 10^{-3}$ S/m
16	Bryning et al. [53]	SWCNTs	DGEBA-amine	0.00045 wt.%	10^{-4} S/m
17	Zhang et al. [54]	CB with CC	DGEBA-amine	1 wt.%	$5 \cdot 10^{-7}$ S/m
18	Gallego et al. [55]	fGNPs	DGEBA-amine	0.5 wt.%	$5 \cdot 10^{-9}$ S/m
18	Gallego et al. [55]	MWCNTs	DGEBA-amine	0.25 wt.%	$2 \cdot 10^{-4}$ S/m
19	Wei et al. [56]	GNPs	DGEBA-amine	1 wt.%	$1 \cdot 10^{-6}$ S/m
19	Wei et al. [56]	GNPs + CB	DGEBA-amine	0.5 wt.%	$5 \cdot 10^{-6}$ S/m
19	Wei et al. [56]	GNP + CB + CNTs	DGEBA-amine	0.2 wt.%	$7 \cdot 10^{-4}$ S/m
20	Chandrasekaran [57]	GNP	DGEBA-Anhydride	0.3 wt.%	$8 \cdot 10^{-4}$ S/m
21	N. Jovic´ et al. [58]	Extended Graphite	DGEBA	3 wt.%	10^{-6} S/m
22	Monti et al. [59]	GNPs (solvent with DGEBF)	DGEBF-amine	1 wt.%	10^{-6} S/m
22	Monti et al. [59]	GNPs (solvent with amine)	DGEBF-amine	1 wt.%	$7 \cdot 10^{-8}$ S/m

Table 7. Literature data summarizing the maximum reported electrical conductivity of carbon nanoparticle modified epoxy systems at their maximum particle content. The data are graphically presented in Figure 10 (Chapter 2.2.1.1.).

Data Point	Research Group	Filler	Epoxy matrix	Concentration at max. conductivity	Max. reported conductivity
-	-	-	-	wt. %	S/m
1	Sandler et al. [43]	MWCNTs	DGEBA-amine	1 wt. %	2 S/m
2	Sumfleth et al. [44]	CB	DGEBA-anhydride	0.6 wt. %	$3 \cdot 10^{-4}$ S/m
2	Sumfleth et al. [44]	MWCNTs	DGEBA-anhydride	0.6 wt. %	0.03 S/m
3	Gonjy et al. [45]	CB	DGEBA-amine	1.5 wt. %	$3 \cdot 10^{-4}$ S/m
3	Gonjy et al. [45]	SWCNTs	DGEBA-amine	0.3 wt. %	$2 \cdot 10^{-3}$ S/m
3	Gonjy et al. [45]	DWCNTs	DGEBA-amine	0.5 wt. %	0.01 S/m
3	Gonjy et al. [45]	MWCNTs	DGEBA-amine	0.5 wt. %	0.006 S/m
4	Sandler et al. [46]	MWCNTs	DGEBA-amine	0.15 wt. %	0.4 S/m
5	Liu et al. [35]	SWCNTs	DGEBF-anhydride	0.125 wt. %	$6 \cdot 10^{-2}$ S/m
6	Schueler et al. [47]	CB	DGEBA-amine	1.5 wt. %	1 S/m
7	Lonjon et al. [5]	DWCNTs in CF laminate	TGMDA-DDS (M21, Hexcel)	0.4 wt. %	0.1 S/m
8	Guadagno et al. [48]	MWCNTs	TGMDA-DDS	1 wt. %	0.1 S/m
9	Vivo et al. [49]	MWCNTs	TGMDA-DDS	1 wt. %	0.2 S/m
10	Ma et al. [29]	MWCNTs	DGEBA-amine	1 wt. %	0.1 S/m
10	Ma et al. [29]	CB	DGEBA-amine	2 wt. %	$5 \cdot 10^{-3}$ S/m
11	Allaoui et al. [50]	MWCNTs	DGEBA-amine (rubbery)	4 wt. %	10 S/m
12	Rwei et al. [32]	CB	DGEBA-Anhydride	7 wt. %	0.1 S/m
13	Karippal et al. [51]	CB	DGEBA-amine	15 wt. %	$5 \cdot 10^{-3}$ S/m
13	Karippal et al. [51]	MWCNTs	DGEBA-amine	10 wt. %	10^{-2} S/m

14	Jäger et al. [52]	CB	DGEBA-	10 wt.%	10^{-2} S/m
15	Aal et al. [9]	CB	DGEBA-	30 wt.%	6 S/m
16	Bryning et al. [53]	SWCNTs	DGEBA-amine	0.001 wt.%	10^{-2} S/m
17	Zhang et al. [54]	CB with CC in CF laminate	DGEBA-amine	3 wt.%	60 S/m
18	Gallego et al. [55]	fGNPs	DGEBA-amine	1.5 wt.%	10^{-4} S/m
18	Gallego et al. [55]	MWCNTs	DGEBA-amine	0.75 wt.%	$5 \cdot 10^{-3}$ S/m
19	Wei et al. [56]	GNPs	DGEBA-amine	3 wt.%	10^{-5} S/m
19	Wei et al. [56]	GNPs + CB	DGEBA-amine	3 wt.%	10^{-2} S/m
19	We(i) et al. [56]	GNP + CB + CNTs	DGEBA-amine	2 wt.%	1 S/m
20	Chandrasekaran [57]	GNP-sonication	DGEBA-Anhydride	1 wt.%	$1 \cdot 10^{-6}$ S/m
20	Chandrasekaran [57]	GNP-3RM	DGEBA-Anhydride	2.0 wt.%	$5.8 \cdot 10^{-3}$ S/m
21	N. Jovic´ et al. [58]	Extended Graphite	DGEBA	8 wt.%	10^{-1} S/m
22	Monti et al. [59]	GNPs (solvent with DGEBF)	DGEBF-amine	3 wt.%	$9.6 \cdot 10^{-4}$ S/m
22	Monti et al. [59]	GNPs (solvent with amine)	DGEBF-amine	3 wt.%	$5.8 \cdot 10^{-4}$ S/m
23	Gonjy et al. [33]	DWCNT-NH ₂ in glass fiber-epoxy laminate	DGEBA-amine	0.3 wt.%	$4 \cdot 10^{-8}$ S/m

Figure 92 shows the C-scans (as back-wall echo) of the laminates, which are tested via quasi-static fracture mechanical approach. In case that the inhomogeneities observed, they are taken into account during sample preparation and testing.

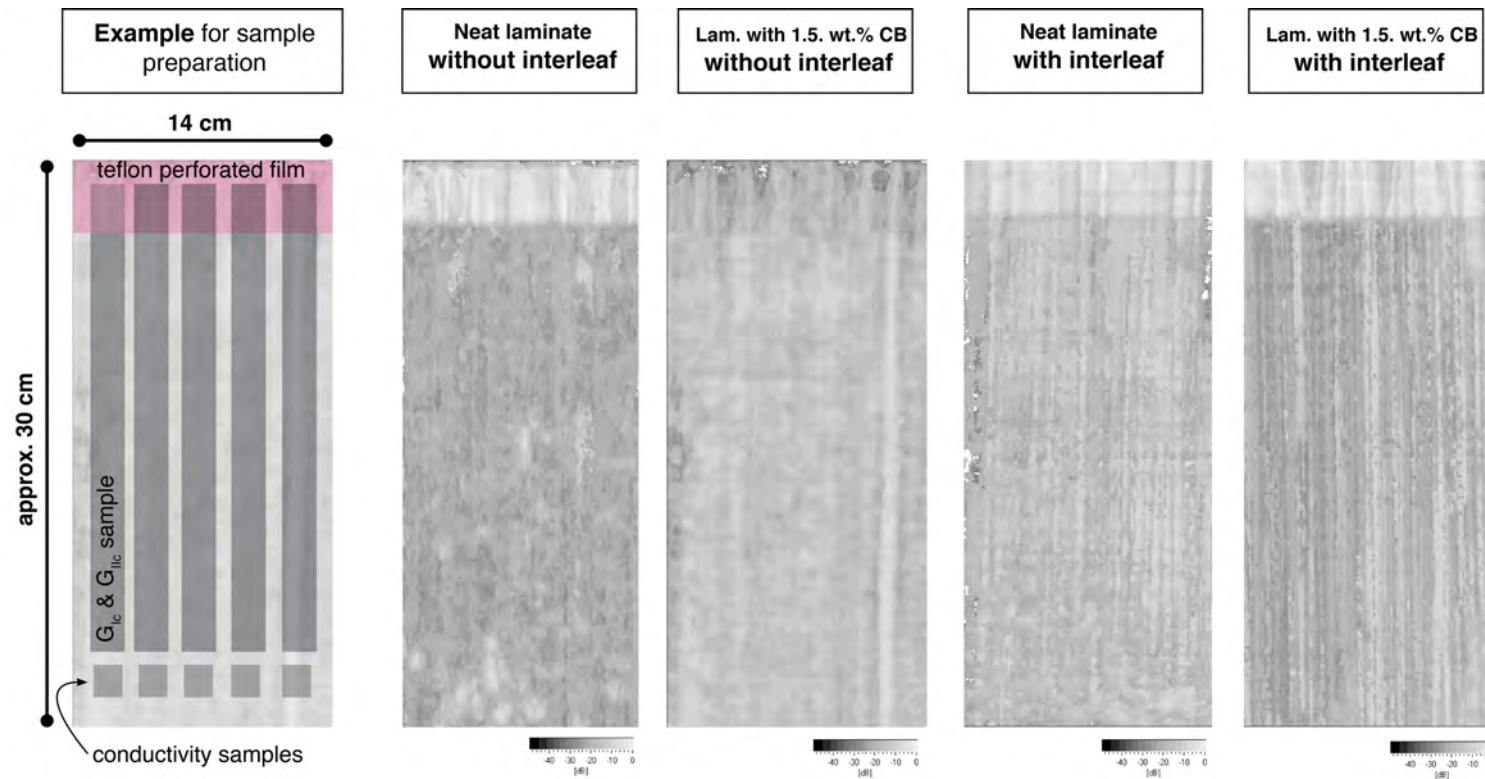


Figure 92. C-scans of the laminates, together with an example schematic to show the positions of the cutted samples for testing.

10 Publications

Submitted and published

Patents

DE102017009661A1, Deutsches Patent- und Markenamt, **2019**
Harzzusammensetzung, Prepregmaterial und Verfahren zur Herstellung einer Harzzusammensetzung

Scientific articles

G. Bakis, M. H. Kothmann, R. Zeiler, A. Brückner, M. Ziadeh, J. Brey, V. Altstädt,
Influence of size, aspect ratio and shear stiffness of nanoclays on the fatigue crack propagation behavior of their epoxy nanocomposites
Polymer, **2018**

M. Häublein, K. Peter, G. Bakis, R. Mäkimieni, V. Altstädt, M. Möller
Investigation on the Flame Retardant Properties and Fracture Toughness of DOPO and Nano-SiO₂ Modified Epoxy Novolac Resin and Evaluation of its Combinational Effects
Materials, **2019**

M. Demleitner, S.A. Sanchez-Vanquez, D. Raps, G. Bakis, T. Pflock, A. Chaloupka, S. Schmölzer, V. Altstädt,
Dielectric Analysis monitoring of thermoset curing with ionic liquids: From modeling to the prediction in the resin transfer molding process
Journal of Polymer Composites, **2019**

Bethke, C., Sanchez-Vazquez, A., Raps, D., Bakis, G., Bard S., Lan Du Ngoc U., Altstädt, V.,
Effect of Resin and Blocked/Unblocked Hardener Mixture on the Production of Epoxy Foams with CO₂ Blocked Hardener in Batch Foaming Process
Polymers, **2019**

M. H. Kothmann, M. Ziadeh, G. Bakis, V. Altstädt, J. Brey,
Analysing the Influence of particle size and stiffness state of the nanofiller on the mechanical properties of epoxy-clay nanocomposites using a novel shear-stiff nanomica
Journal of Material Science, **2015**

Book chapters

M. H. Kothmann, G. Bakis, R. Zeiler, M. Ziadeh, J. Brey, V. Altstädt,

Fatigue crack growth behaviour of Epoxy Nanocomposites. Influence of Particle Geometry

Deformation and Fracture Behaviour of Polymer Materials by W. Grellmann, B. Langer.
ISBN: 978-3-319-41879-7, **2017**

Publications in conference proceedings

G. Bakis, M. Häublein, S. Bard, C. Fischer, A. Aksit, V. Altstädt,

Carbon Black modified epoxy-carbon fiber prepreg laminates. Effect of additives on the z-direction electrical conductivity

ICCM-17 Proceedings, **2017**

C. Pawelski, E. Kang, G. Bakis, V. Altstädt,

Effect of filler type and particle size distribution on thermal properties of bimodal and hybrid-BN/Boehmite-filled EP-Novolac composites

AIP Conference Proceedings 2055, **2019**

Publications in technical magazines

R. Zeiler, G. Bakis, S. Forero, J. Benra, T. Neumeyer, V. Altstädt,

Kleine Beitrag, starke Wirkung

Technische Magazin, Kunststoffe, **2016**

Presentations at national and international conferences

G. Bakis, C. Pawelski, S. Bard, V. Altstädt,

KEYNOTE Presentation

Advancements in thermoset processing and new material developments

15th Innovation DAY – MAGIC MATRIX, CFK Valley, 2017

G. Bakis, M. Häublein, A. Aksit, C. Fischer, A. Lang, A. Brückner, A. Mainz, R. Zeiler, V. Altstädt,

Understanding of electrical conduction mechanisms of nanosized carbon black in epoxy and its prepreg laminates

Innovationsforum Carbon, Nano goes Macro, Nürnberg, Germany, 2017

G. Bakis, A. Aksit, R. Zeiler, C. Fischer, M. Häublein, V. Altstädt

Development of a toughened aerospace grade epoxy resin system. From molecular structure of reactive components to the final cured part properties

5th International Polymeric Composites Symposium and Workshops, Izmir, Turkey, 2017

G. Bakis, M. Häublein, A. Aksit, C. Fischer, S. Bard, V. Altstädt,

Carbon Black modified epoxy – carbon fiber prepreg laminates. Effect of additives on the z-direction electrical conductivity

International Conference of Composite Materials (ICCM)-21, Xian, China, 2017

M. Demleitner, G. Bakis, A. Sanchez, T. Pflock, S. Schmölzer, A. Chaloupka, V. Altstädt,

Dielectric Analysis for In-Situ Cure Monitoring. Correlations to thermal and rheological properties

DEA User Seminar, NETZSCH, Augsburg, Germany, 2017

G. Bakis, R. Zeiler, H. Deutges, C. Fischer, V. Altstädt,

Simultaneously toughened and electrically conductive epoxy resin formulations

17th European Conference on Composite Materials, Munich, Germany, 2016

G. Bakis, A. Brückner, R. Zeiler, H. Deutges, V. Altstädt,

Fatigue crack propagation behaviour of simultaneously toughened and electrically conductive multi-functional epoxy composites

Polymer Processing Society 32, Lyon, France, 2016

G. Bakis, M.H. Kothmann, M. Ziadeh, J. Breu, V. Altstädt,

Influence of size, aspect ratio and shear stiffness of nano-clay on the mechanical properties of epoxy-anhydride

1th Joint Turkey-Germany Workshop on Polymeric Composites, Istanbul, Turkey, 2014

V. Altstädt, M.H. Kothmann, G. Bakis, R. Zeiler, A. Köppel

Ermüdungsrissoausbereitungsverhalten von Epoxid-Nanokompositen. Einfluss der Partikelgeometrie

PolyMerTec, Merseburg, 2014

M. H. Kothmann, G. Bakis, R. Zeiler, M. Ziadeh, A. Köppel, J. Breu, V. Altstädt,
Influence of nanoparticles on the fatigue crack growth behavior of epoxy resins.
European Conference on Composite Materials ECCM 16, Sevilla, Spain, **2014**

V. Altstädt, M. H. Kothmann, G. Bakis, R. Zeiler, A. Köppel,
On the fatigue crack growth behavior of epoxy nanocomposites. Influence of nanoparticle geometry
Polymer Processing Society 2013 Asia Australia Conference, Mumbai, India, **2013**

11 Curriculum Vitae

Personal information

Name: Gökhan Bakis
Birthday/Place: 27.07.1987, Izmir
Civil Status: Married
Nationalty: Turkish



Educational Background

2010-2013 Friedrich Alexander University of Erlangen-Nürnberg (FAU)
Master of Sci. with Honours "Advanced Materials and Processes"
2005-2010 *Technical University of Istanbul (ITU)*
Bachelor of Engineering "Metallurgical and Materials Engineering"
2001-2005 *Izmir Atatürk High School (IAL)*

Scientific Background

2015 – 2018 Group Leader "*Thermosets and fiber reinforced composites*"
Dept. of Polymer Engineering, University of Bayreuth, Germany
2013 – 2015 Scientific Member
Dept. of Polymer Engineering, University of Bayreuth, Germany

Work Experiences

since 2018 Team Leader "Polymer Physics"
BASF Polyurethanes GmbH, Lemförde, Germany